



Provided by the author(s) and University of Galway in accordance with publisher policies. Please cite the published version when available.

Title	On the development of analytical methods for percutaneous transluminal coronary angioplasty catheters and drug eluting stents
Author(s)	McCarthy, James R.
Publication Date	2013-10-07
Item record	http://hdl.handle.net/10379/3977

Downloaded 2024-04-23T07:40:47Z

Some rights reserved. For more information, please see the item record link above.





NUI Galway
OÉ Gaillimh

National University of Ireland, Galway

Thesis for the Degree of Ph. D

On the development of analytical methods for percutaneous transluminal coronary angioplasty catheters and drug eluting stents

Investigation into the formation of everolimus degradation products, measurement of intrinsic particulate matter, and the use of near infrared spectroscopy as an alternative to traditional wet chemistry techniques.

James Raphael McCarthy, BSc, MSc

June 2013

School of Chemistry

Head of School: Prof Paul Murphy

Primary supervisor: Prof Donal Leech

Secondary supervisor: Dr Alan Ryder

Table of contents

Table of Contents

Table of Contents	1
Abstract.....	6
Acknowledgements.....	8
Glossary of abbreviations and acronyms.....	9
Chapter 1.....	11

Thesis overview

1	Introduction	11
1.1	Percutaneous transluminal coronary angioplasty	12
1.1.1	Coronary artery disease	12
1.1.2	Balloon catheters and stents	15
1.1.3	Catheter and guide wire coatings	17
1.1.4	Drug eluting stents.....	19
1.2	Particulate matter analysis for PTCA products	25
1.2.1	What is particulate matter?.....	25
1.2.2	Physiological effects of intravenously administered particles.....	26
1.2.3	Guidance on particulate matter from DES and percutaneous catheters.....	27
1.3	Test methods for analysis of active pharmaceuticals in DES ...	30
1.3.1	Liquid chromatography time of flight mass spectrometry ...	32
1.4	Everolimus degradation pathways	33
1.5	Design of experiment	39
1.5.1	Factorial Designs	41
1.5.2	DoE data analysis	44
1.6	Process analytical technology and quality by design	48
1.6.1	Near infra-red spectroscopy	49
1.6.2	Chemometrics.....	55
1.6.3	Multivariate analysis	56
1.6.4	Selection of spectral ranges	61
1.6.5	Signal pretreatment methods	62
1.6.6	Creation of PLS calibration models	64
1.6.7	Model validation.....	65
1.7	Thesis proposition	66

Table of contents

Chapter 2..... 67

Materials and methods

2	Introduction	67
2.1	Particulate matter methods for PTCA catheters and stents	67
2.1.1	Instrumentation	67
2.1.2	Particulate methods	69
2.1.2.1	Product cleanliness, 2 beaker method for a stent delivery system (SDS)	70
2.1.2.2	Simulated use beaker method	72
2.1.2.3	The baseline particulate test method.....	74
2.1.2.4	RSU particulate test method	74
2.1.2.5	CSU particulate test method	75
2.1.3	Identification of particles.....	78
2.1.3.1	Initial assessment	78
2.1.3.2	Isolation	79
2.1.3.3	Identification	79
2.1.3.4	Pre inspection of devices	79
2.1.3.5	Light microscopy analysis of particles	80
2.2	Investigation into acetonitrile induced degradation of everolimus	83
2.2.1	Instrumentation.....	83
2.2.2	Reagents.	85
2.2.3	Experimental procedure.....	85
2.3	Near infra-red spectroscopy analysis of DES coating solutions	87
2.3.1	Instrumentation.....	87
2.3.2	Reagents	88
2.3.3	Preparation of coating solutions	89
2.3.4	Spectra collection	92

Chapter 3..... 94

The development of in vitro clinically relevant methods for assessment of percutaneous transcatheter angioplasty devices for particulate matter from extrinsic and intrinsic sources.

3	Introduction	94
3.1	Simulated use procedures.....	95
3.2	Results and Discussion.....	97
3.2.1	Particulate matter profile for DES	97
3.3	Particle characterisation	108
3.3.1	Stent coatings.....	108
3.3.2	Leachates	115

Table of contents

3.4	Lubricious coatings	127
3.4.1	Observations related to hydrophilic coating A.....	128
3.4.2	Observations related to hydrophilic coating B	131
3.5	Chapter conclusion	139

Chapter 4..... 142

The use of design of experiment and mass spectrometry to identify a previously uncharacterized drug degradation pathway of everolimus in acetonitrile.

4	Introduction	142
4.1	Description of the problem encountered with everolimus degradation in testing everolimus eluting stents.	143
4.2	Evaluation of acetonitrile used for preparation of everolimus solutions.	146
4.3	Initial DoE carried out to recreate the everolimus degradation products.	151
4.3.1	Peak at RRT 0.58.....	154
4.3.2	Peak at RRT 0.75.....	156
4.3.3	Peak at RRT 0.71.....	158
4.4	Second DoE carried out to increase the concentration of the everolimus degradation products.	159
4.4.1	Identification of the source of base in acetonitrile	165
4.4.2	Mass spectrometry analysis of degradation products.....	167
4.4.2.1	Elucidation of the structure of the product ppearing at RRT 0.58.....	168
4.4.2.2	Elucidation of the structures of the products appearing at RRT 0.71 and RRT 0.75	171
4.5	Chapter conclusion	178

Chapter 5..... 180

The use of near infrared spectroscopy as an alternative to traditional wet chemistry techniques in drug eluting stent process control.

5	Introduction	180
5.1	Results and Discussion.....	181
5.1.1	Experimental design	181
5.1.2	Spectral analysis	182
5.1.2.1	Everolimus coating solutions.....	182
5.1.2.2	Paclitaxel coating solutions	187
5.1.3	Everolimus coating solutions	190

Table of contents

5.1.3.1 Feasibility assessment using laboratory calibration set	191
5.1.3.2 Water variation	202
5.1.3.3 Principal component analysis of the calibration spectra	204
5.1.3.4 Final everolimus coating solution NIR methods.	217
5.1.3.5 Water content analysis	225
5.1.4 Paclitaxel coating solutions	228
5.1.3.4 The application of methods developed to the commercial everolimus eluting stent manufacturing process.....	227
5.1.4.1 Paclitaxel coating solution NIR method development ..	230
5.2 Chapter conclusion	240
6 References	243
Appendix 1	251
The Closed Loop Particulate apparatus from prototype to final design.	
7 Introduction	251
7.1 Early prototypes	255
7.2 Single closed loop particulate apparatus	258
7.3 CLP prototype selection	260
7.4 Comparison between the beaker and CLP methods.....	266
7.5 Tortuosity of artery track fixture	274
7.6 Dual closed loop particulate apparatus.....	276
7.7 Dual loop particulate equipment design.....	277
7.7.1 Water handling and circulation system	279
7.7.2 Sample test fixture	281
7.8 Separation of measurement step.....	284
7.9 Blanking with devices in-situ	288
7.10 Impact of flowing water over the device.....	294
7.11 Length of SDS tested and challenged	294
7.12 Track material	296
7.13 Equipment design to deal with sources of measurement error in light obscuration	297
7.13.1 Air bubbles	298
7.13.2 Environmental contamination	300

Declaration of work ownership

I certify that this Thesis is all my own work and that I have not obtained a degree at NUIG or elsewhere on the basis of any of this work.

Ray (James Raphael) McCarthy

Abstract

This thesis reports on analytical methods required for the development and production of interventional medical devices.

A novel light obscuration method is applied to the measurement of particulate matter during an in vitro clinical procedure in the sub-visible range of 2 to 125 μm . The methodology involves a break from the standard approach of sampling a portion of the rinse solution from a medical device using a flow through syringe sampler, and introduces a closed-loop apparatus. The in-line method developed enables a more rigorous means of measuring particles coming from the devices.

It has been shown that everolimus, an anti-proliferative drug used by drug eluting stents, forms 3 base-induced degradation products when prepared in acetonitrile. The mechanism involved in the degradation pathway has been identified by design of experiment.

Near infra-red transmission spectroscopy was used to determine the in-process concentration of components in different drug eluting stent coating formulations. The results show that near infra-red spectrometry (NIR) is an excellent alternative to traditional wet chemistry analytical techniques for rapid and convenient analysis of these types of samples.

Three different sources of device related, intrinsic particles from medical devices have been discovered using the novel closed-loop method. Light obscuration was successful in providing a fast and accurate particle count and particle size. Further analysis of the particles was carried with the complementary methods of light microscopy, scanning electron microscopy and Raman micro-spectroscopy. Firstly, drug eluting stent coatings were examined. It was discovered that a phosphorylcholine-based stent coating resulted in significantly more particles than coatings based on polymers such as polyvinylidene fluoride-co-hexafluoropropene, and poly-lactic-co-glycolic acid. Particle formation from poly-lactic-co-glycolic acid coatings, when exposed to conditions that promote hydrolysis of the polymer, has also been shown. Secondly the impact of accelerated ageing on Pebax catheters results in the formation of Nylon-12 derived particles. This phenomenon has significant ramifications for medical device manufacturers that wish to speed up device approval through the use of accelerated ageing. Finally, catheter coatings have been shown to contribute significantly to particle counts. Extensive particulate matter evaluation has been carried out on two types of hydrophilic coatings, a cross-linked neopentyl glycol diacrylate with embedded polyethylene oxide, and a cross-linked neopentyl glycol diacrylate with embedded polyvinyl pyrrolidinone. These three examples of intrinsic particle sources have all led to changes in the design of medical devices to improve the particle counts.

The structured experimental approach taken for the investigation into everolimus degradation has shown the power of well-constructed experimental designs. The use of statistical methods proved very successful to help with the identification of the main factors, and with establishing a key interaction involved. This interaction is between alkaline impurities from untreated soda-lime glassware and propionitrile, an impurity related to the manufacture of acetonitrile. Some everolimus degradation prevention measures have been evaluated and shown to be effective, which is hoped will benefit laboratories using this drug and its analogues. Mass spectrometry was used to identify the modified site on the everolimus molecule and structures have been proposed.

Near infra-red transmission spectroscopy was used in combination with partial least squares regression to measure the components in everolimus- and paclitaxel-eluting stent coating formulations. Everolimus coating solutions contained 0.41% w/w everolimus, 2.00% w/w polyvinylidene fluoride-co-hexafluoropropene, 68.3% w/w acetone, and 29.3% w/w cyclohexanone; and the paclitaxel coating solutions contained 1.93% w/w of paclitaxel and poly-lactic acid, and 96.14% w/w n-butyl acetate.

The assay of the paclitaxel coating solution demonstrated that the NIR method of measurement for the drug component at 1.93% w/w matches the accuracy of the established high performance liquid chromatography assay (root mean square error of cross-validation = 0.0318% w/w and root mean square error of prediction = 0.0313 % w/w). Near infra-red technology is not generally used as a trace level technique to provide accurate quantitative analysis < 0.5% w/w, and indeed the NIR method developed for everolimus coating solution demonstrated that the measurement of everolimus at 0.41% w/w does not reach the same level of accuracy as conventional high performance liquid chromatography assays (root mean square errors of cross-validation and prediction = 0.0135 % w/w). Measurement of the polymer, solvent and water components of the coating solutions equalled the performance of the alternative wet chemistry methods.

Acknowledgements

I received tremendous support throughout the years of my Ph. D. study that I would like to acknowledge here.

Foremost, I want to express my sincere gratitude to my supervisor, Prof. Dónal Leech. I am thankful for his agreement to participate in my project after I unexpectedly arrived at his office door 5 years ago with my proposal. What I had not expected then, but which followed, was the much needed and continuous support, advice and mentorship he expertly provided.

Besides my primary supervisor, I would like to thank my co-supervisor Dr Alan Ryder for his expert guidance, insightful comments, and difficult questions. I thank the other faculty members of the School of Chemistry at NUIG, especially Prof. Michael Hynes.

My sincere thanks go to my employer, Boston Scientific for funding the journey. I received support from many colleagues over the years, especially from members of the dedicated team in the Research and Development Department. In particular, I will always be grateful to Dr John Clarke for his initial encouragement of me to pursue a Ph. D. I thank my colleagues past and present for their support and expertise: My management team of Rob Eyers, Chris Frawley and Adrian McNamara, and in the trenches alongside me: Des Coughlan, Patricia Kelly, Philip Bannister, Irene Novak, Shane Sheridan, and Sean O'Connor.

Thank you to my wife, Aoife. I am in the fortunate position of being married to a most determined and smart woman. Her encouragement, counsel and steady bearing ultimately saw me through.

Glossary of abbreviations and acronyms

Glossary of abbreviations and acronyms

Abbreviation	Description
ANOVA	Analysis of variance
BHT	Butylated hydroxyl toluene
BMS	Bare metal stent
BSC	Boston Scientific corporation
CAD	Coronary artery disease
CED	Circular equivalent diameter
CLP	Closed-loop particulate test equipment
CSU	Characterization simulated use particulate method
DES	Drug eluting stent
DLP	Dual-loop particulate test equipment
DoE	Design of experiment
EO	Ethylene oxide
EP	European Pharmacopeia
FDA	Food and Drug Administration
GCMS	Gas chromatography with mass spectrometry detector
GPC	Gel permeation chromatography
HPC	Hydrophilic coating
HPC A	HPC formed through cross-linked neopentyl glycol diacrylate with embedded polyethylene oxide
HPC B	HPC formed through cross-linked neopentyl glycol diacrylate with embedded polyvinyl pyrrolidinone
HPLC	High performance liquid chromatography
LC-ooTOF MS	Liquid chromatography coupled to orthogonal acceleration time of flight mass spectrometry
LM	Light microscopy
LO	Light obscuration
LPW	Low particulate water
MLR	Multiple linear regression
MSC	Multiplicative scatter correction
nBA	n-Butyl acetate
NIR	Near infrared
NPG	Neopentyl glycol diacrylate
OFAT	One-factor-at-a-time
PA	Polyamide
PAT	Process analytical technology
PBMA	Polybutyl methacrylate
PC(A)	Principal component (analysis)
Pebax	Trade name for the family of polymers of the polyether block amide type

Glossary of abbreviations and acronyms

Abbreviation	Description
PEO	Polyethylene oxide
PLA	Poly-lactic acid
PLGA	Poly-lactic-co-glycolic acid
PLS(R)	Partial least squares (regression)
PMA	Pre-market approval
PMS	Particle Measuring Systems
POBA	Plain old balloon angioplasty
PTCA	Percutaneous transluminal coronary angioplasty
PVDF-HFP	Polyvinylidene fluoride-co-hexafluoropropene
PVP	Polyvinyl pyrrolidinone
QbD	Quality by design
RBP	Rated burst pressure (for a balloon catheter)
RMSECV	Root mean square error of cross-validation
RMSEP	Root mean square error of prediction
RRT	Relative retention time
RSM	Response surface model
RSU	Regulatory simulated use particulate method
SDS	Stent delivery systems
SEM	Scanning electron microscopy
SIPN	Semi-interpenetrating polymer network
SLS	Straight line subtraction
USP	United States Pharmacopeia
VN	Vector normalization

Chapter 1

Thesis overview

1 Introduction

The focus of the thesis is in the area of analytical method development for improved quality control and assurance in the development and production of interventional medical devices, with specific focus on quality control of percutaneous transluminal coronary angioplasty (PTCA) catheters and drug eluting stents (DES) used to treat coronary artery disease (CAD). Minimally-invasive medical devices used in the treatment of CAD are of enormous importance and millions of devices are used worldwide every year to improve and prolong the lives of patients. Strict guidelines are issued by regulatory bodies to ensure that the devices used are safe and effective. The burden of proof that manufacturers must commit to providing before the approval of their devices for commercial sale is significant. Proof of safety and effectiveness is usually provided through a combination of technical and clinical data. Technical data comprises laboratory testing of the final device and its components, along with details of the manufacturing process and manufacturing controls. Clinical data is gathered from controlled human clinical evaluations.

The specific focus area for this thesis is on some of the *in vitro* test methods which are used to provide technical data required to develop and gain regulatory approval for interventional coronary devices. Each specific area of advancement in research, presented in chapters 3, 4 and 5 of the thesis, is listed below:

- The development of *in vitro* methods for the assessment of particulate matter from extrinsic and intrinsic sources on percutaneous transluminal coronary angioplasty (PTCA) devices.
- The use of design of experiments (DoE) to identify a previously uncharacterized drug degradation pathway of everolimus in acetonitrile.
- The use of near infrared (NIR) spectroscopy and multivariate analysis for drug formulation control in the production of drug eluting stents.

Chapter 1

While the three research areas are quite different, common to all is their application to contemporary medical device manufacture and development. The review, which follows, will focus only on those aspects which are specifically relevant to the work described in the thesis.

1.1 Percutaneous transluminal coronary angioplasty

1.1.1 Coronary artery disease

Disease of the cardiovascular system is the number one cause of death globally[1]; 17.3 million people die annually from cardiovascular-related diseases, which account for 30% of all global deaths[2]. Making up approximately 40% of this is coronary artery disease (CAD). Two coronary arteries, the right and left, supply oxygenated blood to the heart muscle. The branches of the coronary arteries shown in Figure 1 distribute the blood around the heart. When these blood vessels become damaged, the supply of oxygen to the heart muscle can be reduced.

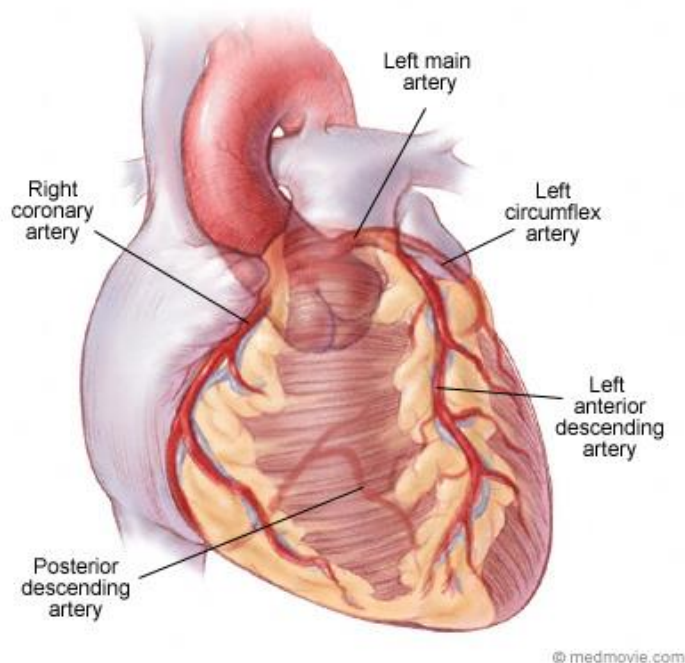


Figure 1 Diagram of the heart showing the left and right coronary arteries and their main branches. Blood enters the coronary arteries at the base of the aorta.

Atherosclerosis is the underlying disease that causes CAD; this is a chronic, systemic and diffuse disease with focal complications in different vascular beds [3]. Atherosclerosis, as shown in Figure 2, is caused by the build-up of cholesterol plaque in

Chapter 1

the walls of arteries. The mechanism for the build-up of the plaque is not fully understood, but plaque itself is a hard, thick substance comprised of cholesterol, calcium, muscle cells and connective tissue. Coronary atherosclerosis is manifested as endothelial dysfunction of the inner layer of the arteries that supply the heart tissue with oxygenated blood. The atherosclerotic plaque can narrow the arteries and thereby restrict blood supply to the heart and, in some cases, the plaque can rupture in an acute event leading to myocardial infarction, otherwise known as a heart attack.

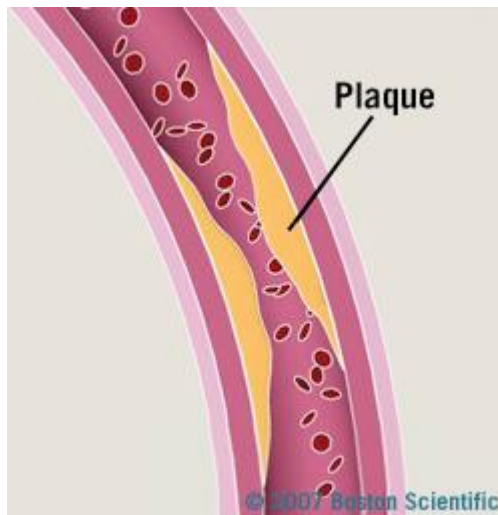


Figure 2 Schematic of cholesterol plaque build-up in a blood vessel.

Treatments for the systemic disease of atherosclerosis involve efforts to lower the lipid levels and changes in lifestyle which slow the progression of the disease [4]. However, it may be necessary to perform surgery at focal points of the arterial system when critical narrowing and blockages are manifested; the coronary arteries are one such focal area. In the past the predominant surgical treatment for diseased coronary arteries was by means of bypass surgery where the affected artery is bypassed, for example by using a vein graft removed from the leg of the patient to divert blood around the blockage [5]. However, this is a major surgery that involves opening the thoracic cage through a sternotomy. Patient recovery time is significant after this surgery and they are left with dramatic scarring. In more recent years, cardiologists are using minimally-invasive medical devices to open up the blocked blood vessels. The minimally-invasive surgical interventions are known as angioplasty, shown in Figure 3, and these procedures are carried out using catheters inserted through the peripheral arteries to gain access to the target area. The term percutaneous transluminal coronary angioplasty (PTCA) is used to describe the procedure [6]. Long, thin catheters are inserted at access points in the

Chapter 1

leg or arm and are guided to the target area through the arteries using X-ray fluoroscopy.

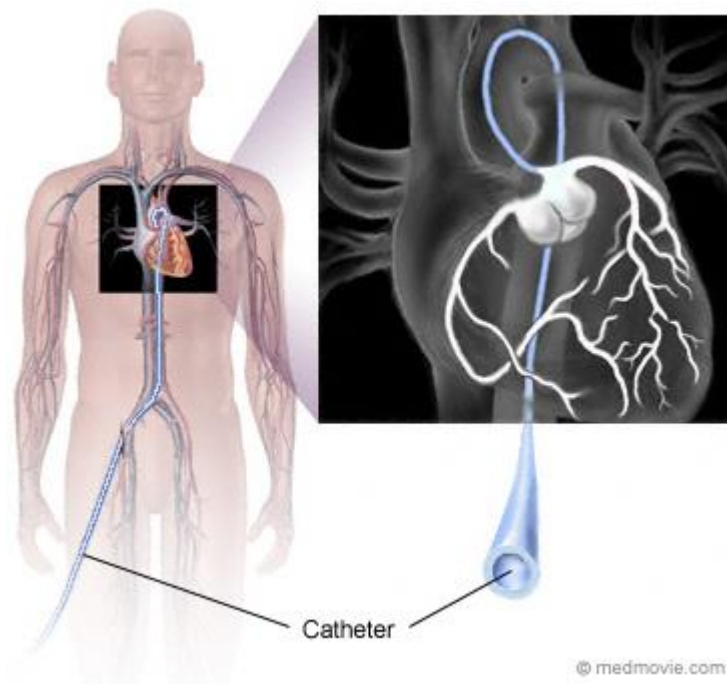


Figure 3 Schematic of an angioplasty procedure. A catheter is introduced to a peripheral artery (the femoral artery in the groin shown here) and is advanced to the coronary arteries through the aorta.

The PTCA procedure shown in Figure 4 demonstrates how balloons at the end of these catheters are placed in the narrowed coronary arteries and inflated to widen the blockage. In many cases a tubular metal mesh known as a stent is permanently implanted to provide additional support to the artery.

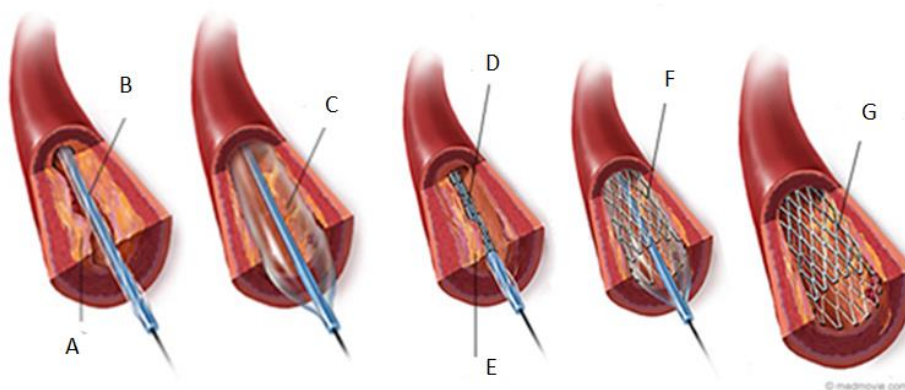


Figure 4 Schematic of a PTCA procedure to unblock and stent an occluded vessel. (A and E) The occluding plaque is traversed with (B) a collapsed balloon at the end of a catheter. (C) The balloon is inflated to push the plaque aside. (D) Alternatively, a collapsed balloon and stent can be placed in the occlusion, (F) the balloon is inflated which expands the stent, and (G) the deployed stent remains behind after the procedure.

Chapter 1

1.1.2 Balloon catheters and stents

Several medical devices are used in PTCA; they fall under the following headings:

1. Introducer sheaths
2. Guide wires
3. Balloon catheters
4. Stent system

Introducer sheaths maintain access at the femoral and radial arteries by dilatation of a puncture site in the leg or arm, respectively. The primary function of the introducer is to protect the other PTCA devices during insertion into the artery. The artery is first located through a surgical incision and then a needle is inserted. A short guidewire is inserted through the needle after which the needle is removed. The sheath is then advanced over the guidewire into the artery. The introducer sheath is left in position as shown in Figure 5 for the full angioplasty procedure. A valve at the sheath's proximal end is used to restrict blood loss while allowing the movement of devices through it.

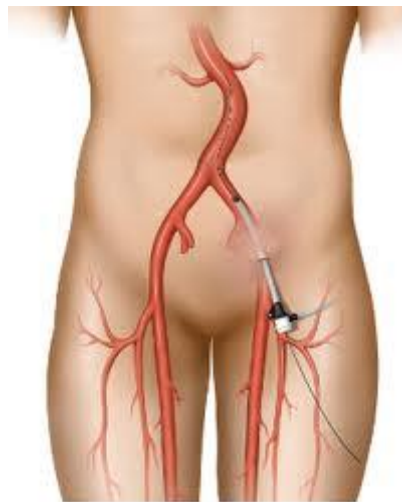


Figure 5 An introducer sheath for accessing the femoral artery in position at the groin.

Guide wires have various functions and they come in many different designs. Primarily they are used to access and cross the blockage in the artery, and then to guide and support subsequent devices used in the angioplasty procedure. Guidewires consist

Chapter 1

of an extremely thin wire of approximately 2 to 3 metres in length with a flexible tip. The wires may be left as bare metal or encapsulated in a polymer sleeve, as with the CHOICE® wire shown in Figure 6. Lubricous coatings are often used on the wires to help them negotiate the tortuous pathways of the arteries and to reduce friction with other devices. The tip of the guide wires may be provided straight or in a pre-bent shape such as a J; wires can also be bent by the physician to aid with steering through the blood vessels.



Figure 6 The distal tip of a CHOICE® Floppy guide wire (Boston Scientific), the tip consists of a 3cm spring coil. The underlying stainless steel core of the device has an overlying polymer sleeve coated with a hydrophilic layer to increase lubricity.

Guide catheters consist of long, flexible, open-ended tubes that are advanced to the ostium (opening to the aorta) of the coronary arteries. This catheter provides the route for the balloon catheters from the peripheral arteries at the insertion site to the coronary arteries. The end of guide catheters come in several shapes which are selected based on the position of the coronary artery that needs to be accessed or the shape of the patient's anatomy; some examples are shown in Figure 7. Strength, shape retention, and kink resistance are important features for guide catheters to reduce friction with the devices delivered through them and to reduce prolapse from the coronary ostium during the angioplasty procedure.



Figure 7 Schematic of a guide catheter in the aorta which is lined up to the ostium of a coronary artery (left hand side); three different tip shapes used for coronary guide catheters (right hand side).

A **balloon catheter** in Figure 8 consists of a cylindrical shaped balloon at the tip of a long catheter shaft. The balloon catheter is threaded over a guide wire to the site of the

Chapter 1

blockage. A mixture of saline and contrast material, which can be seen through X-ray fluoroscopy, is used to inflate the balloon. The pressure of the balloon is gradually increased, sometimes up to 20 atmospheres, compressing the atherosclerotic plaque until the artery lumen is fully opened. Angiographic procedures carried out using these balloon catheters are referred to as plain old balloon angioplasty (POBA) ever since the popular adoption of coronary stenting.

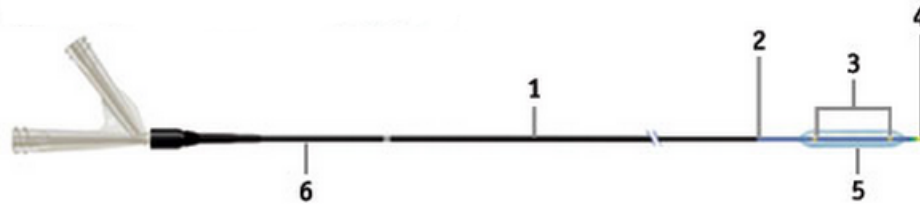


Figure 8 Truncated image of a balloon catheter (Apex™ Over-the-Wire, Boston Scientific), showing (1) the main catheter shaft, (2) the transition point to the balloon, (3) the radiopaque gold marker bands used by the physician to find the position of the balloon using X-ray, (4) the tip of the catheter where the guide wire is inserted, (5) the balloon, and (6) the proximal end of the catheter which remains outside the body; a two port hub is shown which is used to attach a balloon inflation device and provides the exit point for the guide wire.

Intracoronary **stents** are hollow mesh tubes that are implanted as shown in Figure 4 at the site of the blockage to provide mechanical support to the artery. The metal stents are either self-expanding, or most commonly they are delivered over a conventional angioplasty balloon catheter shown in Figure 9. Metal stents reduce the incidence of re-narrowing of the artery after balloon angioplasty. **Drug eluting stents** (DES) are also widely used; these further reduce the recurrence of artery occlusions by releasing a drug over time which disrupts tissue growth.



Figure 9 The PROMUS Element™ Plus (Boston Scientific) everolimus-eluting stent expanded on its balloon catheter.

1.1.3 Catheter and guide wire coatings

Catheters, wires and their accessory devices used for intravascular interventions are often coated with lubricious materials to aid in vascular access and deliverability. These

Chapter 1

coatings are generally accepted to reduce vessel trauma in the form of spasm [7] and aid in device access to target sites in the vasculature. The majority of lubricious coatings used fall into two categories based on their solvation properties; these are 1) hydrophobic coatings, and 2) hydrophilic coatings. Hydrophobic coatings are usually silicone based and hydrophilic coatings consist of hydrogel type polymers such as polyethylene oxide (PEO) and polyvinyl pyrrolidone (PVP) that are hydrated upon immersion in aqueous media. The coefficient of friction for the silicone based coating is relatively high when placed in contact with blood, representing an advantage for the physician if they want to have a better feel for the passage of the device through the vasculature. Some devices, such as POBA catheters may have a combination of a silicone and hydrophilic coating on the same device (Apex™ and Emerge™ PTCA dilatation catheters from Boston Scientific Corp.).

Hydrophilic coatings of various compositions are available, and medical device companies can get external companies to coat their devices or licence the coating process; alternatively they can develop their own coatings. Some hydrophilic coating (HPC) specialist providers are SurModics (Minnesota, USA), Biocoat (Pennsylvania, USA), Bayer (Germany), and Hydromer (New Jersey, USA). Biocoat have issued a white paper that summarizes some important aspects in the development and selection of suitable HPC applications [8]. A predominant consideration for these coatings is their lubricity and durability performance over repeated abrasion cycles [9]. In general the loss in lubricity of the coating is measured as the increase in force required to slide an affixed clamp over the hydrated coating, through repeated cycles. Commercially-available equipment such as OakRiver's DL1000 is available to carry out this type of test. A breakdown in the coating will result in a significant loss in lubricity. There is increased focus from the US Food and Drug Administration (FDA) on the measurement of any associated particle formation from these HPC coatings [10].

Extensive particulate matter evaluation has been carried out on two types of HPC and is reported in this thesis.

1. HPC A; a cross-linked neopentyl glycol diacrylate (NPG) with embedded polyethylene oxide (PEO) [11].
2. HPC B; a cross-linked neopentyl glycol diacrylate (NPG) with embedded polyvinyl pyrrolidone (PVP)[12].

Chapter 1

Both of these coatings can be described as a semi-interpenetrating polymer network (SIPN) [13–16] in which the hydrophilic polymer resides in an insoluble network of cross-linked NPG. SIPNs are described by IUPAC as:

“a polymer comprising one or more networks and one or more linear or branched polymer(s) characterized by the penetration on a molecular scale of at least one of the networks by at least some of the linear or branched macromolecules. Note: Semi-interpenetrating polymer networks are distinguished from interpenetrating polymer networks because the constituent linear or branched polymers can, in principle, be separated from the constituent polymer network(s) without breaking chemical bonds; they are polymer blends [15]”.

Other HPC coatings have been evaluated to a lesser extent; observations from these coatings will also be addressed. However, since specific details of the chemical composition and processing of these coatings was not obtained, a comprehensive discussion of their impact on particulate matter measurements is not possible.

1.1.4 Drug eluting stents

A metal stent acts as a scaffold to support the walls of previously occluded coronary arteries that have been dilated by balloon angioplasty [17–19]; stents typically consist of a narrow metal tube in which the metal is shaped to resemble a wire mesh once it is expanded to a wider diameter in the arteries. Thus the metal stent has a mechanical function in propping the artery open at focal manifestations of atherosclerosis. Drug eluting stents (DES) are stents that contain a drug that is usually embedded in a polymer matrix[20],[21]. The purpose of DES is to treat restenosis (repeat blockage) in a stented artery. The drug component is used to reduce restenosis of the artery following the angioplasty procedure, where restenosis is caused by renewed tissue growth inside the stent that can reduce or block blood flow through the artery.

DES are manufactured by coating metal stents with a drug formulation called a coating solution. Coating solutions are a mixture in which the drug and a polymer are dissolved in a solvent or mixture of solvents; this liquid and the solvent(s) is removed during the manufacturing process. A thin film of drug dispersed in a polymer matrix is left behind on the metal struts of the stent. The drug's therapeutic efficacy requires that it has an extended release period, with this sustained release of drug controlled by the polymer

Chapter 1

component. Several commercial DES products are in the marketplace, and the leading manufacturers are Boston Scientific, Abbott Vascular and Medtronic[20],[21]. Boston Scientific and Cordis (a Johnson and Johnson company which has since left the DES market) are the longest in the market place with their TAXUS (generation 1 and 2, Boston Scientific) and CYPHER (J&J) products having being implanted in millions of patients.

Commercial DES made by all manufacturers fall in to two drug categories, these are paclitaxel eluting stents, and DES that contain sirolimus (rapamycin) and its analogues. Sirolimus, everolimus, zatorolimus, and biolimus are examples of sirolimus analogues used in commercial DES. The structures of paclitaxel, and of sirolimus, with its analogues, are shown in Figure 10 and Figure 11, respectively. These drugs act as anti-proliferative agents that suppress the cell-growth cycle in arterial tissue [22]. This inhibits the healing response after the angioplasty procedure that may result in restenosis. Additional drugs and bioactive agents have been tried on metal stents to improve healing rates and biocompatibility, and several alternative stent materials are under evaluation [23], with however none of these approaches yet successfully adopted beyond animal trials and limited human use.

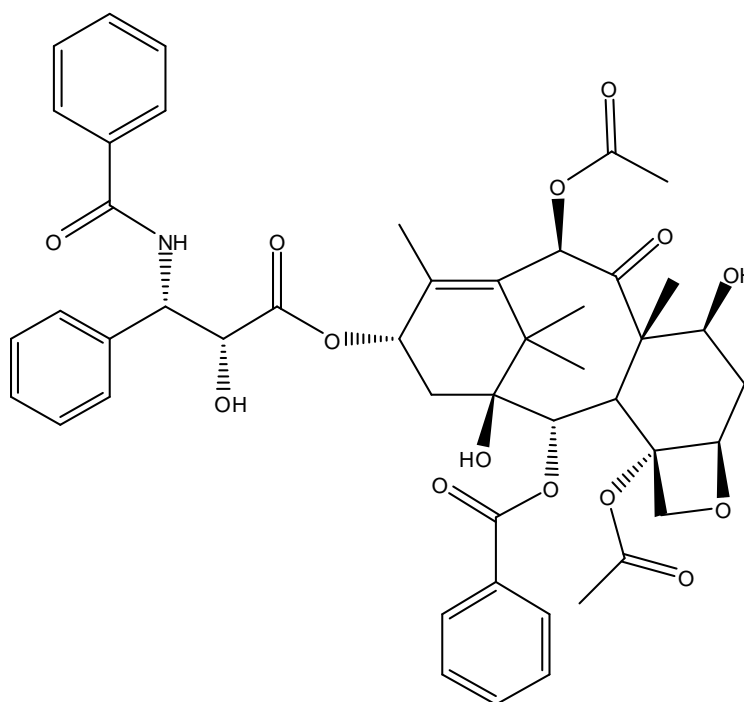


Figure 10 Chemical structure of paclitaxel, chemical formula $C_{47}H_{51}NO_{14}$, exact mass = 853.33.

Chapter 1

Everolimus (Certican®, Novartis Corporation) is an analogue of sirolimus and has been shown to be effective in conjunction with other medications to prevent heart and renal transplant rejection. Everolimus is a powerful anti-proliferative agent that inhibits the growth of proteins involved in the initiation of protein synthesis. Everolimus's cellular actions are carried out through binding to its intracellular receptor, the FK506 binding protein, (FKBP12). Research findings suggest that everolimus forms a complex that binds to and thus interferes with the function of FKBP12-rapamycin associated protein (FRAP)[24], [25]. FRAP is a key regulatory protein which governs cell metabolism, growth, and proliferation. Disabling FRAP function explains the cell cycle arrest caused by everolimus. Animal, and clinical studies have demonstrated that stents coated with everolimus (Xience V, Abbott Vascular Company and PROMUS, Boston Scientific Corp.) have shown a positive effect in the prevention of restenosis[21]. The pharmacological activity of sirolimus results in a high tissue distribution. Due to its chemical structure, everolimus has a less extensive tissue distribution as compared to the parent drug, sirolimus, which is believed to be desirable in terms of local application of anti-proliferative agents via a DES device[26].

Paclitaxel is a natural diterpenoid extracted from the bark, roots, and leaves of several *Taxus* species (Yew tree). The drug is widely used in cancer treatments. Paclitaxel plays a role as a promoter of microtubule assembly responsible for its antitumor activity [27]. The stabilization of microtubule dynamics by paclitaxel can interrupt many cellular processes including cell division, migration, activation, maintenance of cytoskeletal framework, and intracellular as well as trans-membrane protein transport. In the context of restenosis, paclitaxel has been shown to affect development of neointimal hyperplasia in different *in vitro* and animal models of restenosis [20]. Paclitaxel's wide use in the TAXUS DES has shown it to be a successful drug for the treatment of in stent restenosis [28].

Chapter 1

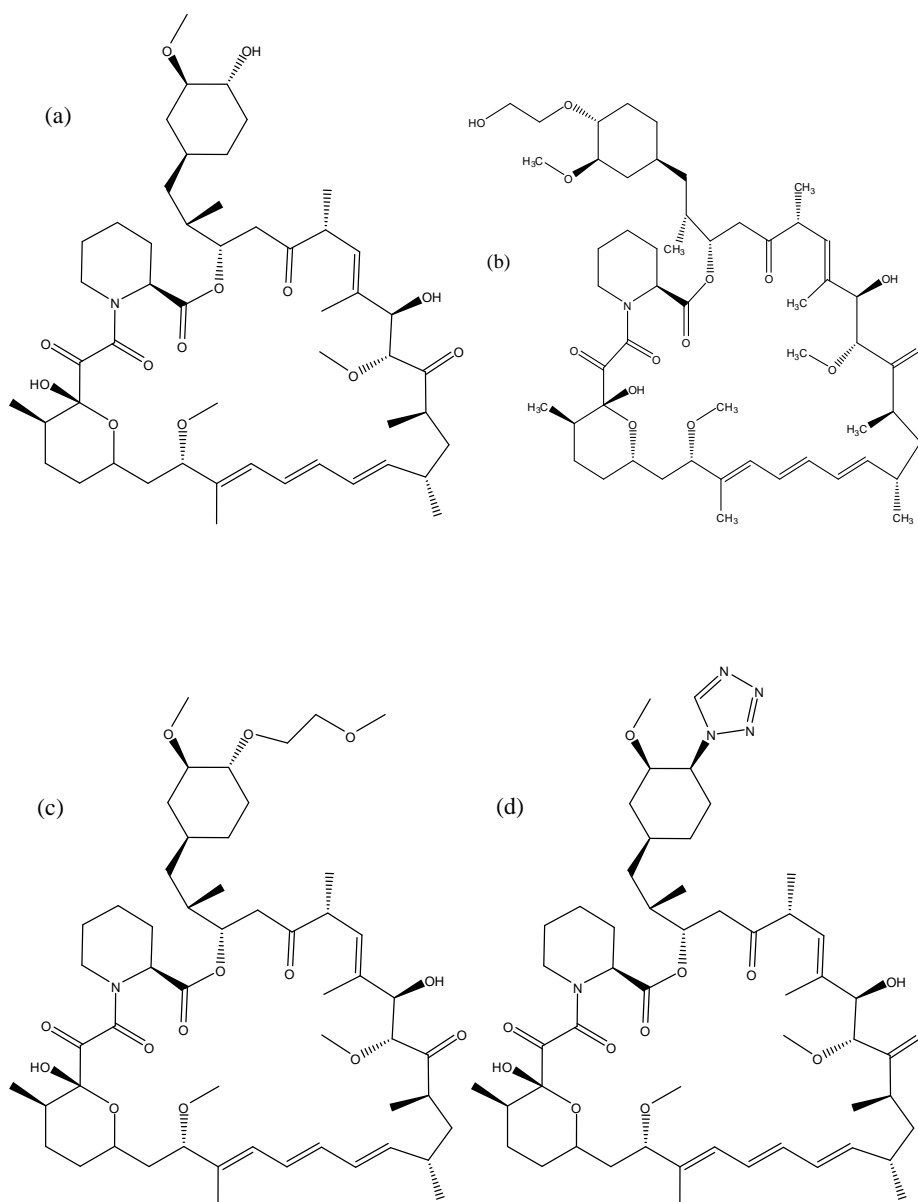


Figure 11 Chemical structures of (a) sirolimus ($C_{15}H_{79}NO_{13}$, exact mass = 913.56), (b) everolimus ($C_{53}H_{83}NO_{14}$, exact mass = 957.58), (c) biolimus ($C_{54}H_{85}NO_{14}$, exact mass = 971.60) and (d) zatorolimus ($C_{52}H_{79}N_5O_{12}$, exact mass = 965.57).

Polymers used in stents are varied in chemical structure and material properties. In general they fall into two categories; indurate polymers and biodegradable polymers. Indurate polymers persist in the body after the drug has been released into the surrounding arterial tissue; as such they are also referred to as bio durable polymers. Two such indurate polymers are used on the everolimus eluting stents manufactured by Abbott Vascular and Boston Scientific, polyvinylidene fluoride-co-hexafluoropropene (PVDF-HFP) and polybutyl methacrylate (PBMA); Figure 12. The former is used as the reservoir for everolimus and controls its release, the latter acts as a tie layer to attach the drug reservoir layer to the metal stent [29]. Common biodegradable polymers used

Chapter 1

on DES are poly-lactic acid (PLA) and poly-lactic-co-glycolic acid (PLGA). These polymers are intended to break down and are fully absorbed by the arterial tissue after the drug has been released; the structures of PLA and PLGA are shown in Figure 13.

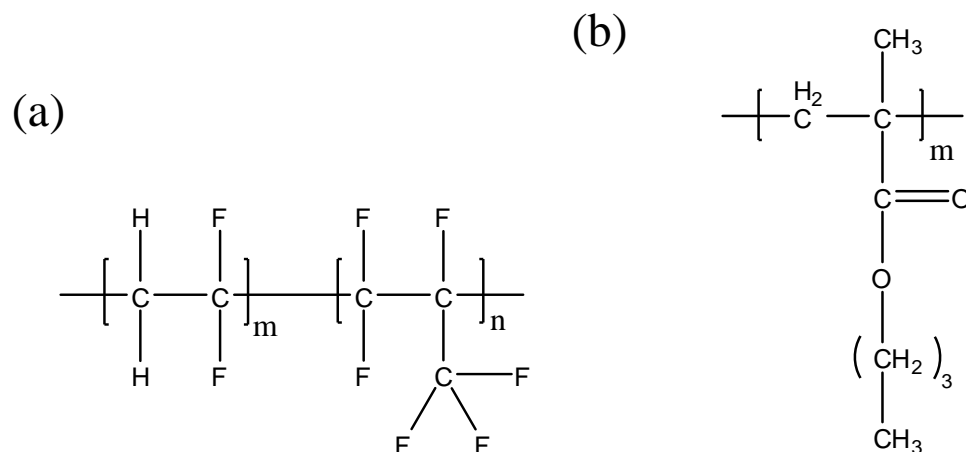


Figure 12 Chemical structures of (a) poly (vinylidene fluoride-co-hexafluoropropylene) (PVDF-HFP) and (b) poly (n-butyl methacrylate) (PBMA).

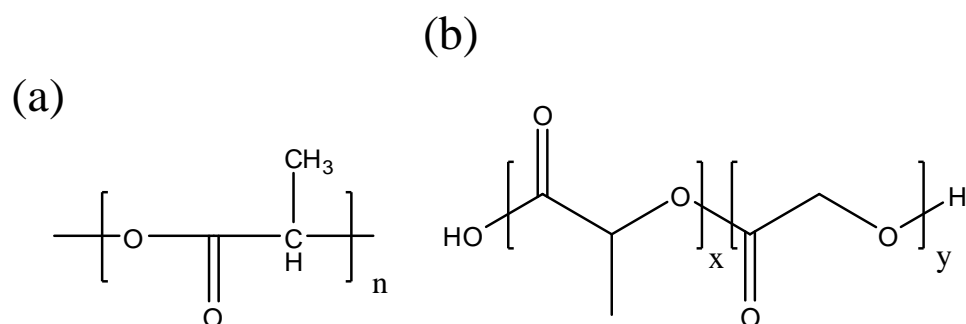


Figure 13 Chemical structures of (a) poly (lactic acid) (PLA) and (b) poly (lactic-co-glycolic acid) (PLGA).

DES are classified as special drug dosage forms that release over an extended period of time *in vivo*, and the rate of the drug release over time is known as the elution profile. The elution profile of the DES is affected by the stent design, the drug and polymer formulation, and the manufacturing process[23].

The formulations used to coat DES (DES coating solutions) consist of polymer and/or drug dissolved in one or more organic solvents. DES coating solutions are formulated by adding the solid and solvent components together and ensuring complete dissolution. Formulations can be kept in one reservoir for use on a single coating apparatus or subdivided for use on multiple coaters. A feed line from these reservoirs to the coater transports the coating solution to the applicator and will be used to coat numerous stents with a thin film of the formulation (film thickness <20 μ m in thickness). DES coating

Chapter 1

solutions are often applied in successive layers to a stent. For example a primer layer of polymer may be applied first and followed by a layer with a polymer and drug mixture. This approach is taken for the Boston Scientific PROMUS stent and the Abbott XIENCE V stent. In these products the base or primer layer consists of PBMA, and a subsequent coating mixture of everolimus and PVDF-HFP, is then applied on top, over the primer layer. Other products use a polymer coat over a layer containing the active pharmaceutical ingredient to control the elution of drug, such as is the case with the CYPHER stent.

Application of the coating solution may be achieved in a number of ways[30]. For example it can be sprayed directly on the stent[31] as shown in Figure 14, or the stent may be dipped or rolled in the solution. Successive layers of the solvent-cast films can be applied in order to build up the coating thickness or to apply a layer with different ingredients. Application of multiple, thin layers can be used to control the drying rate of the coating. The formulations used and the mechanism by which they are applied and dried on the stents have a significant impact on the drug elution from the coating[30], [32].

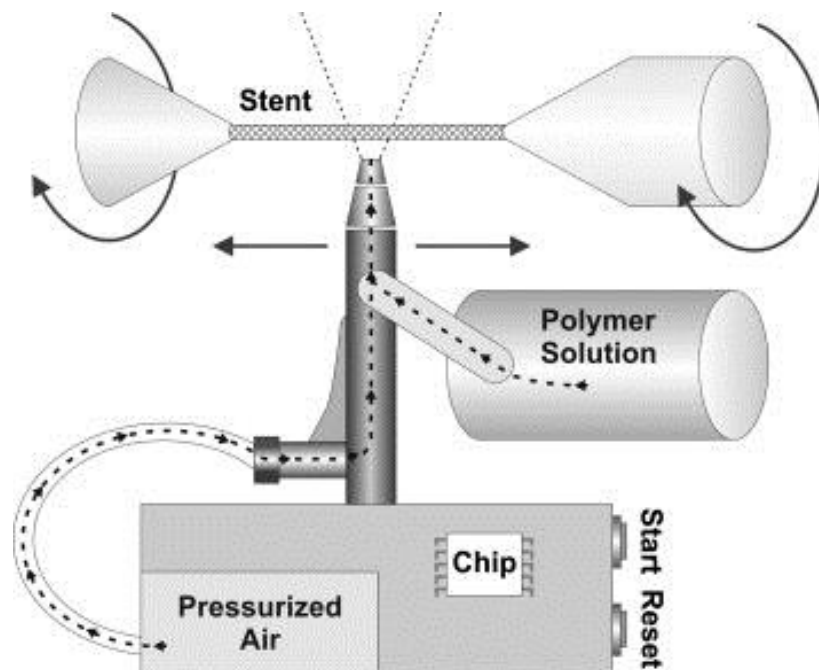


Figure 14 Example of a stent spraying process [31]. The stent is rotated while an aerosolised plume of coating solution is sprayed at it to coat the circumference of the stent; the spray nozzle is moved left to right to coat the length of the stent. The spray nozzle is supplied with coating solution through a feed line from a reservoir.

Chapter 1

1.2 Particulate matter analysis for PTCA products

A medical device is a tool or implant that physicians use to treat a wide range of clinical conditions. It is important that these devices are clean and do not shed harmful amounts of particulate material in the course of their usage or, in the case of implants, over their lifecycle within the body. Particulate matter that may be introduced to the human body via a medical device is of concern to medical device manufacturers, the regulatory agencies that licence them, to the physicians using the devices, and ultimately to the patient in receipt of the device. The onus is on the medical device manufacturer to ensure that all products developed and manufactured by them meet the safety requirements with regard to particulate matter. There are a number of official standards pertaining to evaluation of particulate matter that may be introduced intravenously to the bloodstream[33], [34]. These standards specifically cover the testing of intravenous injections, otherwise known as parenteral solutions. However in the absence of similar standards for the medical device industry the regulatory bodies have adopted these as a starting point for medical devices. In addition the US FDA have published guidelines that build upon the official standard that give specific directions for the particulate testing of certain devices; these devices are DES and coronary catheters[10], [35].

1.2.1 What is particulate matter?

Particulate matter can be classed as any mobile material that is considered small in relation to the system in which it exists. In this definition, a 100 μ m diameter cotton fibre in a 1 L dose of intravenous medicine may be considered as particulate matter, as would a piece of driftwood on the open sea. However, when applied to medical products, particulate matter is generally classed as visible or sub-visible material that is present in or on a product with potential to be administered to a patient during the product's usage. Particulate matter may be extrinsic or intrinsic in nature [34]. Extrinsic particles are usually unrelated to the product, such as a skin flake or piece of wall plaster that has found its way to become attached to the product. These particles have unintentionally become associated with the finished product; however their presence is often unavoidable due to the nature of the manufacturing environment. For example personnel involved in the assembly of the products will contribute some level of particulate matter contamination even with the best efforts employed to prevent this from happening. Intrinsic particles are associated with the product itself, such as

Chapter 1

fragments of the packaging, raw materials, subassembly components or instruments and materials used in the assembly or formulation of the product.

Modern production facilities with clean room technology are capable of producing products with very low levels of extrinsic particulate matter. Sources of extrinsic particles in a manufacturing environment include glove powders, lint and other fibres, paper particles, packaging materials, paint particles, and various other materials[36].

The presence of intrinsic particulate matter is, in some cases an unavoidable consequence of the functionality of the device. For example many medical devices use lubricious coatings that aid in their delivery through tortuous pathways of the vasculature and through tight lesions occluded by the build-up of plaques and calcification. The presence of such coatings greatly improves the deliverability of percutaneous medical devices and reduces trauma to the target vessels, however they are obviously prone to removal from the device. Other coatings such as the polymer and drug coatings present on DES are often made from easily broken up, friable, materials that can be removed from the device either in their delivery or over the lifetime of the implant. In these cases the function, and chemical composition, of the source materials for the particulate matter should be taken into account when evaluating the overall impact of the particulate matter.

1.2.2 Physiological effects of intravenously administered particles

The presence of unintentional particles on medical devices has potential to cause a medical condition, known as thrombophlebitis, when introduced to the body intravenously[36]. This medical condition depends on the size and quantity of these particles. Quality control limits on the size and quantity of particulate matter from the devices are predicted to reduce the potential risk of such adverse effects.

In general, a red blood cell has a diameter of 7-10 μm and can squeeze through a capillary with a diameter of 5 μm . Limits were thus established for various size ranges based on the particle diameter relative to the diameter of red blood cells and capillaries as discussed by Barber[36]. Whilst a body can expel particles of diameter greater than 10 μm up to a certain level or count as detailed below, if the particle load is sufficient then an inflammatory response may occur.

Chapter 1

Particles from intravenous injections typically move towards the right side of the heart, and are then pumped to the lungs. The veins widen as they move towards the heart, therefore there is little likelihood that they will lodge along the way. The arteries get narrower as they move away from the heart and in to the capillary beds, such that there is likelihood that particles moving from the heart will get trapped in the pulmonary artery capillary bed [36]. The lung has mechanisms for passing particles through the capillary wall to be excreted in the sputum or mucus. The extensive circulatory system in the lung means that it would take a substantial amount of particulate matter to cause a physiological response. Larger particles will have a greater impact than small particles due to the potential for occluding larger vessels and the impact of this on the vessels downstream. The physiological effect of such occlusions is determined by the level of collateral blood supply in the tissues. Occlusion in the blood vessels of organs such as the brain, eye, kidney, and heart, which have lesser collateral blood supply than the lungs, may be more likely to have a detrimental result. For medical devices that are used in the arteries, there is potential for particle entrapment in other tissue capillary beds and locations than the lung; therefore when assessing the impact of particulate matter for intravenous, blood-contact medical devices, the site of entry, anatomical route and target site should be considered.

1.2.3 Guidance on particulate matter from DES and percutaneous catheters

USP <788> is the most comprehensive of all particulate matter standards from the compendia and this along with the specific guidance for DES and stent delivery systems (SDS) from the FDA is used as the primary reference. USP <788> describes the analysis of particulate matter from parenteral products, in which one can assume that the particles are unintentionally present in the medical dose. However the FDA have communicated to the medical device industry that they are increasingly concerned with release from coatings on the stent and catheter into the bloodstream during a procedure, and over the lifetime of implants[10], [37], [38]. This concern is not only focused on the good manufacturing practice (GMP) standards of the manufacturing facility with regard to the introduction of extrinsic particles, but is also for the durability and safety of the device with regard to intrinsic particles during clinical interventions.

USP <788> covers the control of particulate matter in parenteral products that cannot be quantified by chemical analysis due to the small amount of material it represents and to

Chapter 1

its heterogeneous composition. Thus tests utilised are physical tests performed to count sub-visible foreign particulates within specific size ranges.

There are two modes of measurement outlined in USP <788>:

- 1) Light obscuration (LO) procedure
- 2) Light microscopic procedure

Both methods are described in detail in USP <1788>[34]. If the test for 1) fails to meet prescribed limits then it must pass 2) with its own sets of limits.

The light obscuration procedure uses a liquid particle counter. Light obscuration particle counters count the shadows cast by backlit particles, this is different to light scattering detectors which measure a particle's scattered light. These types of particle counters use a high-intensity light source in the form of a laser, a controlled liquid flow through a capillary to provide a viewing volume, and a sensitive light gathering photo-detector [36].

The amount of light a particle scatters, or obscures, can vary with several different factors, including the following:

- 1) The shape of the particle: Particles are seldom smooth and spherical like the spherical polystyrene particles used in particle counter calibrations. Often, particles are flakes of skin or jagged fibres. When they float through the viewing volume sideways, they will scatter a different amount of light than if they travel through lengthwise.
- 2) The reflectivity of the particle: Some particles are more reflective (e.g. aluminium) than others, which cause more scattered light onto the photo-detector. The photo-detector produces a larger pulse, and the particle counter measures the particle size larger than its actual size. Conversely, some particles are less reflective (e.g. carbon) and the particle counter records a smaller particle as having passed through the viewing volume.

The liquid particle counter operates on the principle that the light obscured by a particle in a liquid is a direct function of its area. Particles obscure the laser beam during transit through the beam. The pulses produced by electronically detecting the total laser light

Chapter 1

minus the light obscured by the particle are used to size the particle. These pulses are measured by an analogue to digital converter in the sensor. The variation in light caused by the passing of a particle is electronically detected by the photo-detector. This signal is then amplified and converted to its digital equivalent. The value of this digital signal is converted into an equivalent particle size in a microprocessor. The different size particles are counted and stored in the microprocessor and made available for transmission to the data display system.

Light obscuration technology is only used in liquid particle counters that size particles larger than 2.0 μm . The particle sizes are recorded in ranges determined by the instrument used and calibrated with particle counting standards which are typically polystyrene latex spheres of well-defined sizes and concentration. The results are reported as the number of particles at each defined size range.

USP <788> is primarily concerned with intravenous liquid dosage forms, such as intravenous (IV) drug injections, and as a result the product determination is subdivided into two categories of sample preparation depending on dosage volume.

- 1) Small volume injections – volume in container less than 25 mL.
- 2) Large volume injections – volume in container 25 mL or more.

As stent deployment falls under the small volume injection category the USP limits under this category are outlined in Table 1.

Table 1 Particulate limits for small volume injectables

Particle size	Particle count limit
$\geq 10 \mu\text{m}$	6000 per container
$\geq 25 \mu\text{m}$	600 per container

The allowable limits for particle counts do not consider the source of the particulate matter, the shape of the particle, or chemical composition. In addition, care must be taken to ensure that the test environment does not contribute any significant amount of particulate matter, by, for example, use of a laminar flow hood or equivalent with HEPA filtered air (delivering less than 100 particles of 0.5 μm or larger per cubic foot).

Chapter 1

1.3 Test methods for analysis of active pharmaceuticals in DES

DES manufacturers usually adopt in-vitro methods for the quality control of DES coating solutions and the final DES product [37]. Various analytical tests are carried out to ensure that the correct drug content is present, that drug and process impurities do not exceed specified levels[39], and that dissolution of the drug from the DES matches established elution profiles[40–42]. All of these tests involve the removal of the drug from the DES. For coating solutions, an aliquot of the solution is directly dissolved in a suitable analytical solvent. The removal of the process solvent and/or polymer may be required if they are found to interfere with the analysis. High performance liquid chromatography (HPLC) analysis is usually used to quantify the level of drug, drug-degradation products and impurities in these extracted samples. As with many quantitative analytical methods, reference standards with known concentrations of drug, known drug-degradation products, and impurities are used to calculate the levels of these compounds in the samples[43]. In addition, assessment of excipients used with the drug is required, such as polymer molecular weight, drug stabilizer concentration (if applicable), and residual solvent concentration.

In the majority of analyses the stent coating is solubilized in a solvent to make it amenable to analysis[39][44]. Unwanted drug artefacts may be created by the analytical test method which can interfere with the test results. These artefacts may be the product of chemical reactions between components of the sample matrix that are stable in the solid state and only become reactive in solution. Alternatively, test artefacts may arise from interactions with the laboratory reagents and equipment used to prepare and analyse samples.

A common problem encountered by analytical laboratories is the quality of the reagents used in the preparation of test samples. Solvents, both aqueous and organic, are of particular importance in the preparation of drug samples. Buffers, to control the pH of solvents, are used to minimize the degradation of drugs sensitive to acid or base degradation. Everolimus, as will be described, is particularly sensitive to base hydrolysis, so acid is often added to analytical samples to control this degradation. Some organic solvents are hygroscopic and thus, in cases where drugs are sensitive to the presence of water, the solvents may need to be dried before use and kept dry to maintain a practical shelf-life of samples. Water can have various affects, such as

Chapter 1

causing the precipitation of dissolved solids or water may affect the pH of the samples leading to acid or base hydrolysis. Analytical grade acetonitrile used to prepare the everolimus samples described in this thesis is supplied dry; however due to its hygroscopic nature it will quickly absorb water from the ambient environment. Everolimus is also prone to oxidative degradation, so a low concentration of the antioxidant compound butylated hydroxyl toluene (BHT) is mixed with the drug powder and added to analytical solutions to prevent degradation. Solvents can have impurities that lead to the degradation of drugs, these impurities may be a result of the manufacture and purification of the solvent, they may be leached or extracted from the packaging, or they may be introduced from environmental contamination[45].

It is unsurprising that test laboratories may find it a challenge to pinpoint the exact source of drug degradation with this plethora of solvent related impurities and effects. All too often sources of drug degradation are not resolved effectively and preventative measures introduced may offer a temporary solution only leading to recurrence of the problem. Alternatively laboratories may be forced to abide with painfully short sample shelf lives, resulting in inefficient working hours and inability to re-test samples.

For any laboratory the maintenance of stable drug solutions is critical for the laboratory to generate results free from uncontrolled variation or bias. A reasonable time-frame for drug stability in the solutions is needed to carry out pharmaceutical analysis. Experimental run time for a set of samples may take up to 48 hours depending on the type of analysis and number of samples. Laboratory investigations are carried out when unexpected results are generated, re-analysis of the original samples is often the first port of call in these investigations, and therefore sample and reference solutions may be required for up to a week after the original testing has begun. Other events may also occur during analysis that necessitates repeat analysis such as equipment breakdowns, software problems, incorrect experimental set-up, etc.

In chapter 4 it is shown that an investigation that includes a thorough understanding of the properties of the drug and the conditions of its preparation in the laboratory, coupled with a systematic and statistically designed experimental approach can lead to a successful identification of the cause of degradation and the implementation of effective preventative measures.

Chapter 1

1.3.1 Liquid chromatography time of flight mass spectrometry

Analysis of everolimus degradation products by liquid chromatography coupled to orthogonal acceleration time of flight mass spectrometry (LC-*oa*TOF MS) was performed in the work described in this thesis. Mass Spectrometry (MS) is a powerful analytical technique that is used to identify unknown compounds, to quantify known compounds, and to elucidate the structure and chemical properties of molecules[46]. Detection of compounds can be accomplished with very minute quantities (as little as 10^{-12} g, 10^{-15} moles for a compound of mass 1000 Da)[47]. This means that compounds can be identified at very low concentrations (one part in 10^{12}) in chemically complex mixtures.

MS measures the masses of individual molecules that have been converted into ions, i.e., molecules that have been electrically charged. Molecules are so small (mass of hydrogen is 1.66×10^{-24} g) that a convenient unit for the mass of individual molecules is the Dalton (Da) and is defined as follows; 1 Da = 1/12 of the mass of a single atom of the isotope of Carbon 12. The MS detector measures the mass to charge (m/z) ratio of the ions formed from the molecules, when the ions encountered in MS have just one charge ($z = 1$) the m/z is numerically equal to the molecular (ionic) mass in Da. Likewise, when the ions have a charge of 2 ($z = 2$) the m/z is equal to the molecular mass divided by 2.

The process of ionization is aided by the presence of charged molecules like sodium, potassium or ammonium ions. This results in the formation of an ion with a measured mass of the parent molecule plus the charged species, e.g. sodium adduct of everolimus, is 981 Da (everolimus 958 + sodium 23).

The most widely used MS are quadropole based (mass filters and ion traps) and time of flight (TOF) mass analysers[48]. The TOF variants are more sensitive than the quadropole as they produce accurate masses (m/z) compared to the nominal masses produced by the quadropole based instruments[49]. For instance a quadropole based MS producing an ion with a nominal mass (m/z) of 28.0 will make it difficult to ascribe that ion to CO, N₂ or C₂H₄. Conversely, a TOF variant will produce an accurate mass of 27.9949, 28.0061 and 28.0313 Da respectively for the ions.

Chapter 1

1.4 Everolimus degradation pathways

For everolimus eluting stents, acetonitrile is used in the laboratory extensively to prepare solutions of samples and reference standards. Acetonitrile is the preferable solvent for everolimus eluting stents as it solubilizes the active ingredient, everolimus, and the excipient polymer components. However, as will be described in chapter 4 of this thesis, it was observed in some cases that everolimus degraded over time in the samples and reference standards to produce un-identified degradation products. These degradation products were detected using a HPLC method designed to detect known degradation products of everolimus and product specific impurities. The source of the degradation was quickly established not to have originated in the product, thus confirming that laboratory preparations themselves were the source. This was corroborated by the finding that the everolimus reference standards prepared in the laboratory also exhibited the characteristic degradation products.

Everolimus is a 31-membered macrolide lactone with a molecular mass of 957.5814 Da. There are two main isomeric forms of everolimus, the predominant 6-member pyran form and a less dominant 7-member oxepane form (also designated 501-95) shown in Figure 15.

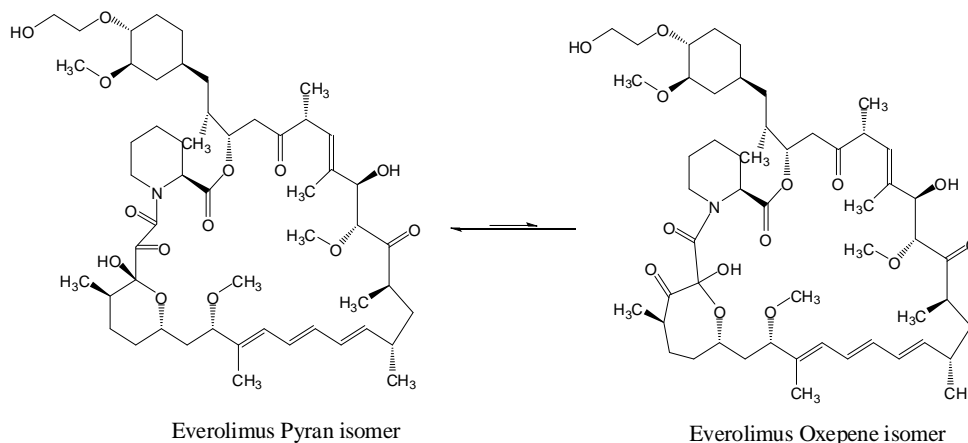


Figure 15 Chemical structures of everolimus isomers, 6-member pyran and 7-member oxepene forms.

The pyran and oxepene isomers are inter-convertible via tautomerisation. Everolimus and its isomer are the active ingredients in Certican™ tablets (Novartis, Basel, Switzerland.), both isomers have the same physiological activity so it is not necessary to isolate one form from the other. Many of the degradation products and impurities of everolimus are also isomers of everolimus, however 501-95 being the only tautomer is

Chapter 1

distinct from the other isomers. For this thesis, reversed phase HPLC was used for the quantification of everolimus and its related substances. The isomers form two fully resolved chromatographic peaks. For quantitative purposes the peak areas of both isomers are summed to establish the overall everolimus quantity.

The UV spectrum (between 200 nm and 320 nm) of everolimus shown in Figure 16 has a characteristic triple peak appearance with a primary peak maximum at 277 nm [50][51] and secondary peak maxima at 268 nm and 289 nm. The characteristic 3 peaked UV spectrum corresponds to the everolimus triene absorption band and proves useful for the identification and structural elucidation of everolimus and its degradation products[52][53]. For everolimus related substances that don't have the triene functional group, a wavelength of 215 nm is used for quantitative purposes. HPLC-UV analysis for everolimus and its related compounds is therefore run using a dual wavelength UV detector set at 215 nm and 277 nm, or alternatively using a diode array detector that encompasses that range.

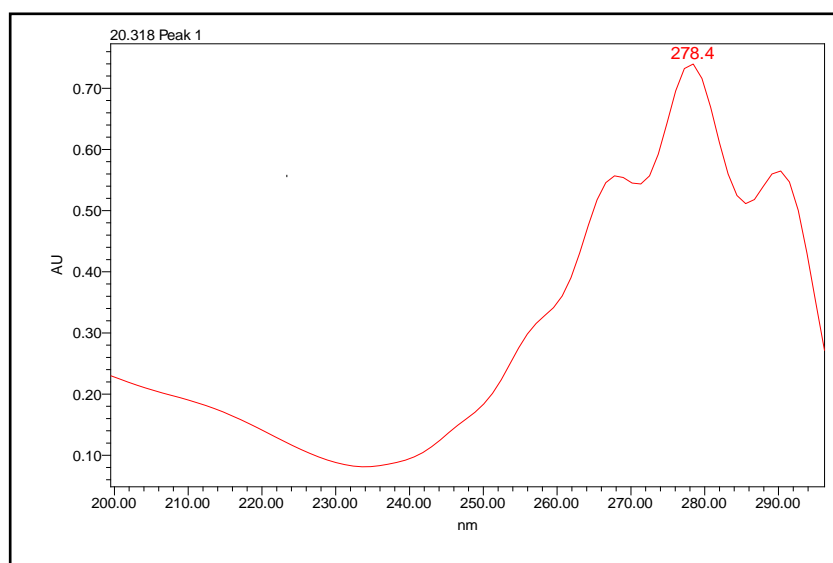


Figure 16 Typical UV spectrum of 500 µg/mL everolimus in acetonitrile .

Degradation pathways of sirolimus and its analogue zatorolimus have been well reported in the literature[39], [52], [54–57]. The major causes of degradation reported are through acid and base catalysis, and oxidation. Consequently, small amounts of butylated hydroxyl toluene (BHT) are commonly added to the drugs; this anti-oxidant protects the drug during production and storage from oxidative degradation[51]. BHT is also added to laboratory reagents used to prepare reference standards and samples for

Chapter 1

analysis. Everolimus, being of a similar structure to sirolimus, is prone to the same type of degradation. Other than metabolic modification of everolimus in-vivo [58] references to the degradation of the drug have not been extensively reported. Characterization of a reference mixture (supplied by Novartis, Basel, Switzerland) created by exposing CerticanTM tablets to stress conditions was used to identify the major degradants of everolimus using HPLC. The mixture contains everolimus, its synthetic impurities, and its degradation products. The chromatogram of the components in the mixture is shown in Figure 17. For the purpose of ease of identification each peak has been labelled with its retention time, and the accompanying Table 2 provides the mass to charge ratio (m/z) for some of the notable peaks. In addition to this reference mixture, the degradation of everolimus in a drug eluting stent has been evaluated by Boston Scientific under various conditions; this data is currently on file with the US FDA in the pre-market approval submission for the PROMUS Element DES (PMA Number P110010).

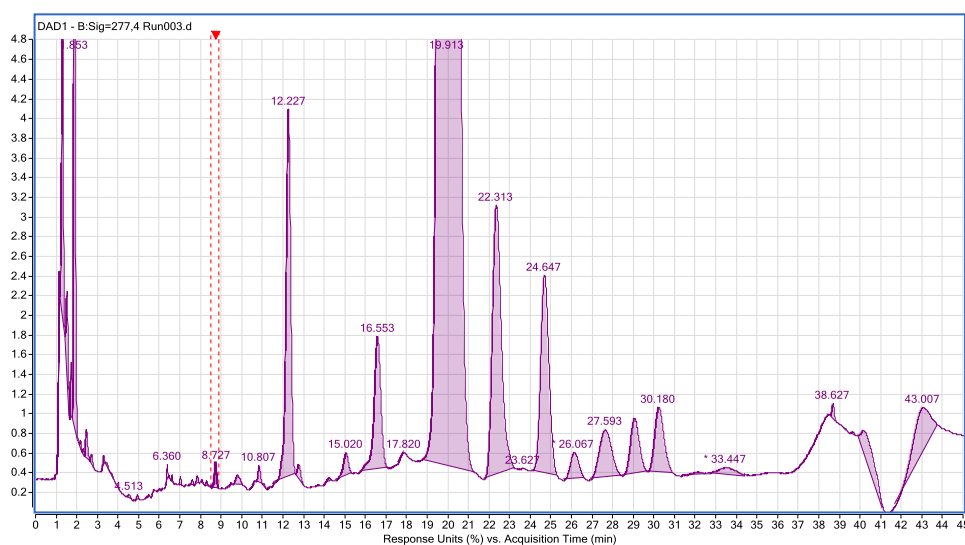


Figure 17 Typical example of chromatography of a degraded everolimus mixture monitored at 277 nm on HPLC with a UV detector.

Chapter 1

Table 2 Summary of LC-UV-MS analysis for degradation products of everolimus.

Novartis nomenclature	RT	RRT	m/z Na⁺ adducts
005-98/211-97	9.8	0.49	966.5551
013-99	12.2	0.61	614.3289
804-95	16.6	0.83	980.5714
009-96	17.8	0.89	980.5697
Everolimus	19.9	1.00	980.5700
Isomer (501-95)	22.3	1.12	980.5731
BHT	24.6	1.24	not analysed
008-96	27.6	1.39	994.5893
012-99	29	1.46	980.5678

It can be surmised from mass to charge values provided in Table 2 that the compounds labelled 804-95, 009-96, and 012-99 may be isomers of everolimus as they have the same mass to charge ratio ($m/z = 980.57$). The degradation product classified as 804-95 is considered a major degradation product of everolimus. The compound, shown in Figure 18 is formed via ester hydrolysis or β elimination reaction of everolimus resulting in a ring opening[58]. A similar ring opened form of sirolimus has been reported after exposure to highly basic conditions [57]. The opening of the macrolide ring results in the formation of a carboxylic acid functionality thereby increasing the polarity of the compound resulting in earlier HPLC elution times. Compound 009-96 has been identified as a synthetic impurity from the manufacture of everolimus. Its structure shown in Figure 18 is proposed by Novartis (data on file with US FDA). Comparison of 009-96 with everolimus highlights the difference being the position of the hydroxyethyl alkylation. The structure of 012-99 shown in Figure 18 is a degradation product of everolimus formed via a retro aldol reaction of everolimus resulting in the opening of the macrolide ring, this form of the open macrolide ring has been shown in sirolimus[59].

Chapter 1

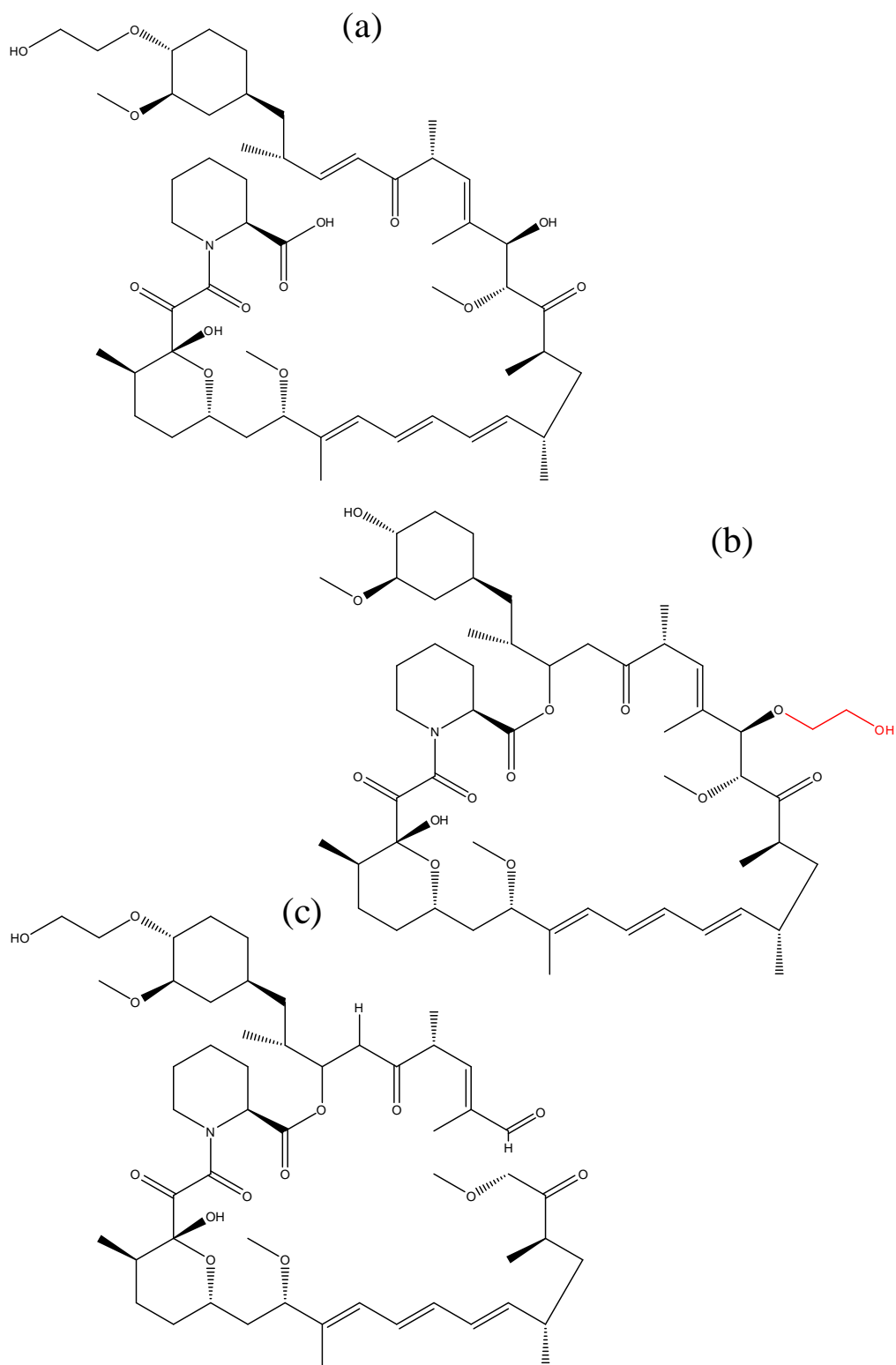


Figure 18 Chemical structures of everolimus related compounds (a) 804-95, (b) 009-96, and (c) 012-99 with mass to charge ratio of $m/z = 980.57$ for their sodium ion adducts. 804-95 is considered a major degradation product of everolimus, formed via ester hydrolysis or β elimination reaction of everolimus resulting in a ring opening. Compound 009-96 has been identified as a synthetic impurity from the manufacture of everolimus, the difference from everolimus being the position of the hydroxyethyl alkylation. The structure of 012-99 is a degradation product of everolimus formed via a retro aldol reaction of everolimus resulting in the opening of the macrolide ring.

Chapter 1

The compound 008-96 in Figure 19 is a methylated variant of everolimus and present as an impurity from the synthetic manufacture of everolimus. As such its sodiated adduct is expected to have a characteristic mass to charge ratio of 994.6 (957.6[everolimus] + 14.0 [-CH₂] + 23.0 [Na⁺]). The compounds in Figure 20 named 211-97 and 005-98 are isomers, each having a molecular weight of 944Da [58]. It can be seen from their structures that these compounds differ in the location of a demethylated group. Demethylation by conversion of a -OCH₃ group to a -OH group has been shown to occur in these macrolide drugs in the presence of acid[39].

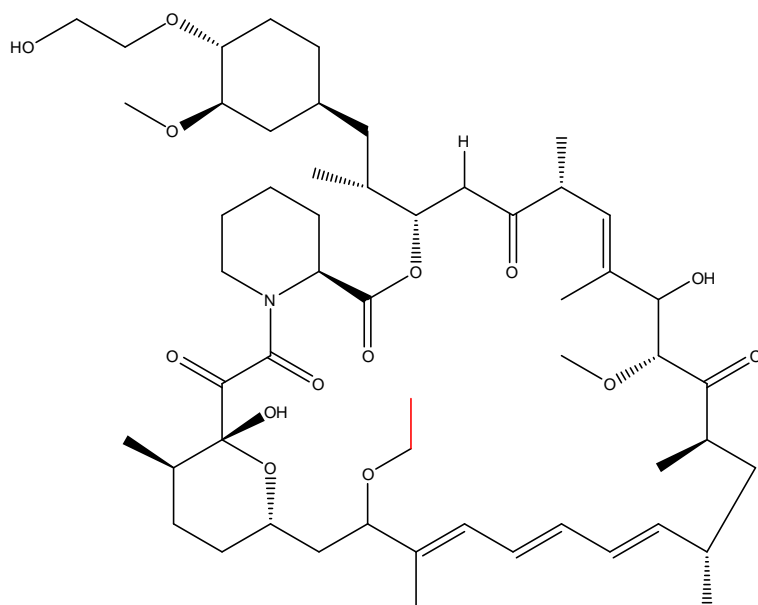


Figure 19 Structure of 008-096, a methylated variant of everolimus.

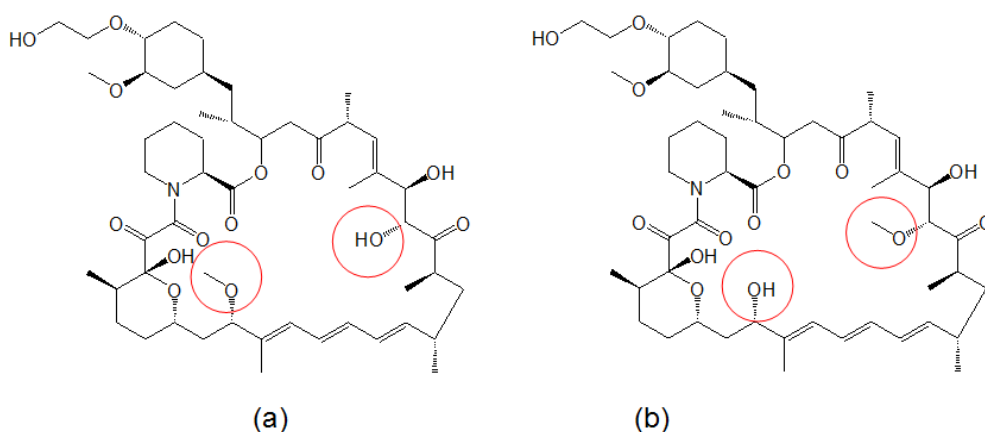


Figure 20 Structures of the demethylated everolimus compounds (a) 211-97 and (b) 005-98.

Chapter 1

The compound shown in Figure 21 (d), named 013-99, is formed from everolimus via a two stage reaction involving a β elimination reaction and a retro-aldol reaction[57]. Figure 21 shows the formation 804-95 (b) via the β elimination or hydrolysis of everolimus (a) resulting in ring opening. 804-95 further undergoes a retro aldol reaction (c) which yields 013-99 (d). It must be noted that while one possible reaction mechanism is demonstrated in Figure 21, it is also feasible to form 013-99 beginning with the retro-aldol reaction. In such a reaction mechanism 012-99 is the intermediate and not 804-95. The reaction kinetics for 013-99 formation will not be addressed in this thesis only to state that typically 013-99 is observed with high levels of 804-95 and 012-99.

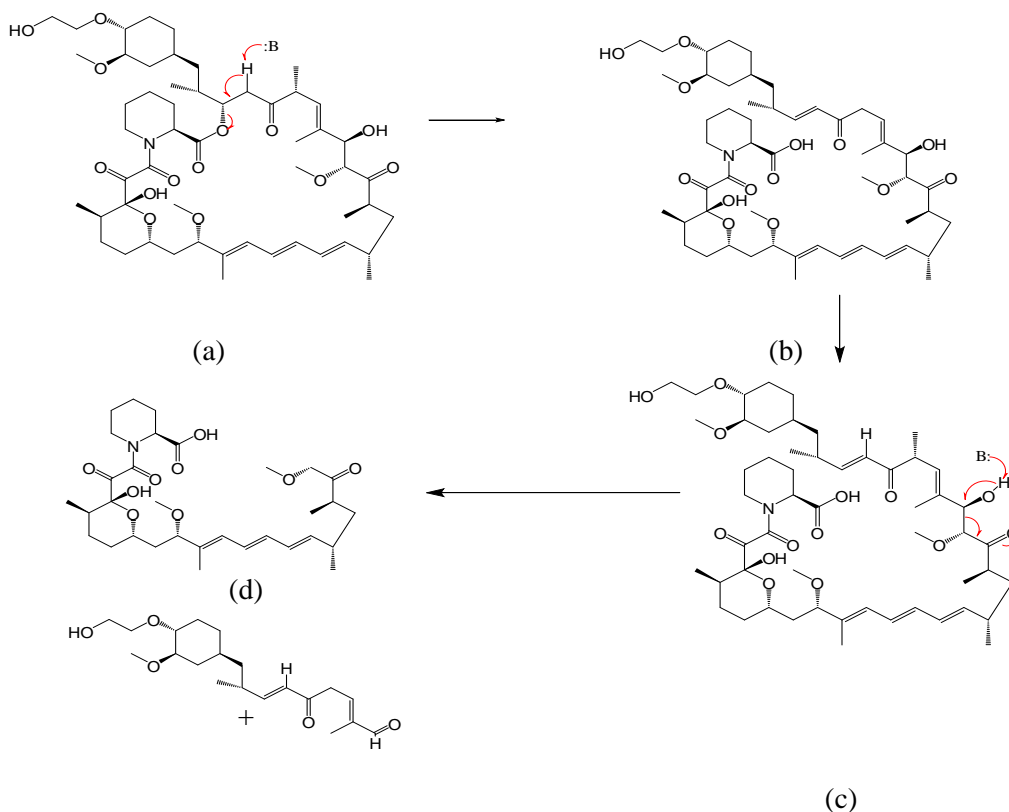


Figure 21 Degradant 013-99 is formed through the degradation of everolimus (a) to 804-95 (b) via β elimination, 804-95 (b) is further degraded as shown in (c) via retro aldol reaction to yield 013-99 (d) and an auxiliary compound (e).

1.5 Design of experiment

Typically experimenters are interested in the effects of more than one factor on their system or process, but often each factor is usually evaluated in isolation; this experimental approach is termed one-factor-at-a-time (OFAT). However, through the

Chapter 1

selection of factorial experimental designs that include all of the factors, a more efficient type of experiment may be carried out. Design of experiment (DoE) is a long established approach that provides a structure to experimental planning and data analysis; the aim of DoE is to extract maximum information from experiments in an efficient manner [60–62]. Cause-and-effect relationships in a process or system, between experimental output and experimental factors, are established after the execution of a purposefully designed experiment. Numerous examples of the application of DoE to solve scientific and engineering problems have been reported [63–65].

The output of every DoE will be a mathematical equation that attempts to fit an empirical model to the data collected in the experiment[60]. The experimental output, y , may be described by this following equation in relation to the experimental factors:

$$y = f(x_1, x_2, \dots, x_n) + \varepsilon$$

Where ε is experimental error, thus implying that the functional relationship between the chosen experimental factors (x_1, x_2, \dots, x_n) and y may not be fully explained.

Figure 22 shows a model of a typical process. The process describes a system, such as a chemical reaction or manufacturing process, with all of its associated variables, for example operators, equipment, procedures, environmental conditions, raw materials and any other variables that changes an input into an output that has one or more observable response variables. Process variables and material properties are either controllable (x_1, x_2, \dots, x_n) , or uncontrollable variables (z_1, z_2, \dots, z_p) .

Chapter 1

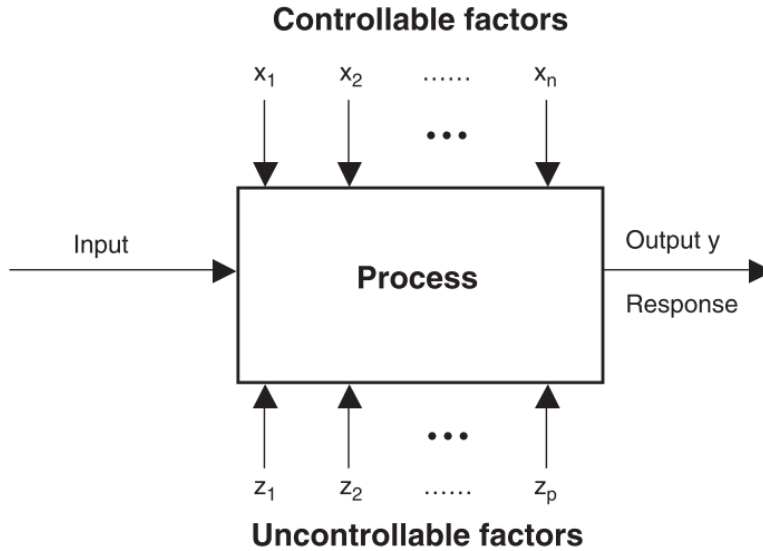


Figure 22 A model of a process or system[60][66].

When designing an experiment, the initial step is recognition of the knowledge gap or problem in the process that needs to be solved; this is commonly described in a problem statement. Following definition of the problem there are three general stages of DoE, these are:

- 1) Selection of the experimental inputs, or factors, and the response variables. Factors are selected on the basis that they may affect the result of an experiment.
- 2) Choosing the design of the experiment and performing the experiment. The experimental values for each factor are organized in a structure that minimizes the effect of uncontrolled factors and allows for meaningful statistical comparisons.
- 3) Analysis of the data using statistics to identify effects associated with the factors and the construction of an experimental design space. Perhaps the most useful aspect of a well-designed and executed DoE is the ability to identify interactions between experimental factors[61].

1.5.1 Factorial Designs

Factorial designs allow for the simultaneous study of the effects that several factors may have on a process. When performing an experiment, varying the levels of the factors simultaneously rather than one at a time is efficient in terms of time and cost, and also

Chapter 1

allows for the study of interactions between the factors. Interactions are the driving force in many processes. Without the use of factorial experiments, important interactions may remain undetected.

In a **full factorial** experiment, responses are measured at all combinations of the experimental factor levels. The combinations of factor levels represent the conditions at which responses will be measured. Each experimental condition is called a run and the response measurement an observation. The entire set of runs is the experimental design.

Figure 23 shows examples of two and three factor designs. The points represent a unique combination of factor levels. For example, in the two-factor design, the point on the lower left corner represents the experimental run when Factor A is set at its low level and Factor B is also set at its low level.

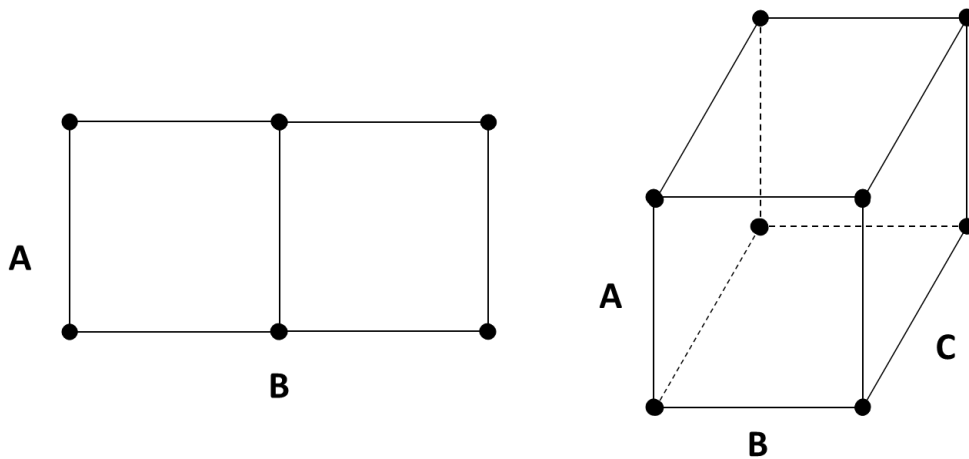


Figure 23 Diagram representing a 2 factor experimental design (left hand side) with 2 levels of factor A and 3 levels of factor B. And, a 3 factor experimental design with 2 levels each of factors A, B and C (right hand side).

In a two-level full factorial design, each experimental factor has only two levels. The experimental runs include all combinations of these factor levels. Although two-level factorial designs are unable to explore fully a wide region in the factor space, they provide useful information for relatively few runs per factor. Because two-level factorials can indicate major trends, they provide direction for further experimentation. For example, to further explore a region where it's believed that optimal settings may exist, factorial designs may be augmented to form a central composite design, as shown in Figure 24. These designs are also referred to as response surface models (RSM).

Chapter 1

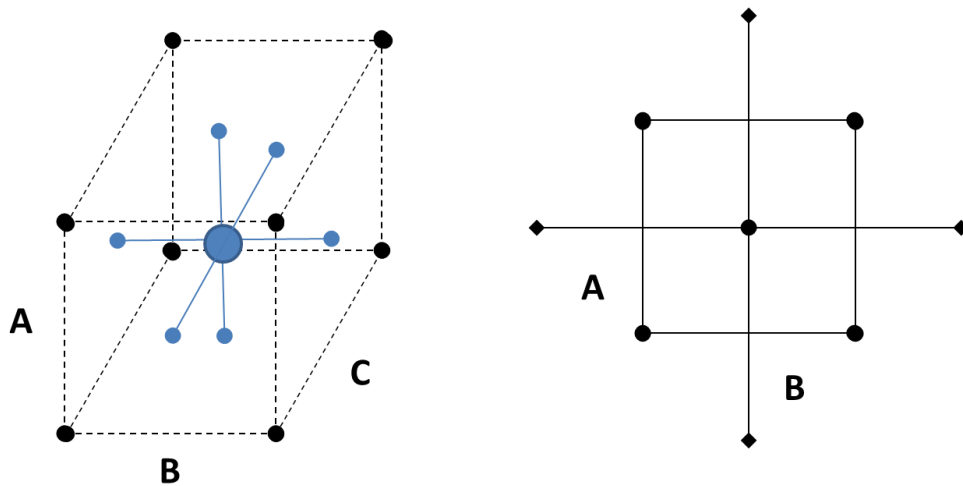


Figure 24 Diagram representing a 3 factor central composite experimental design (left hand side) with 2 levels each of factors A, B and C plus a centre point and points at the centre of each plane. And, a 2 factor central composite design (right hand side) with 5 levels of factors A and B.

In a full factorial experiment, responses are measured at all combinations of the factor levels, which may result in a prohibitive number of runs. For example, a two-level full factorial design with 6 factors requires 64 runs; a design with 9 factors requires 512 runs. To minimize time and cost, designs that exclude some of the factor level combinations can be used. Factorial designs in which one or more level combinations are excluded are called **fractional factorial designs**, an example of these reduced experimental designs is shown in Figure 25.

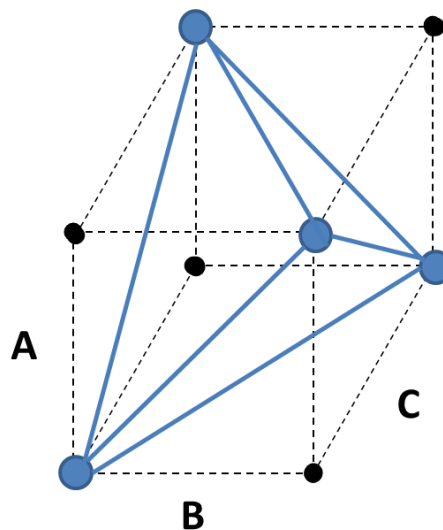


Figure 25 Diagram representing a 3 factor fractional experiment with 2 levels each of factors A, B and C.

Chapter 1

Fractional factorial designs are useful in factor screening because they reduce the number of runs to a manageable size, the equation for calculating the number of runs required for a fractional design is given in Equation 1. The runs that are performed are a selected subset of the full factorial design, the trade-off is that not all factor level combinations will be run; in that case some of the effects will be confounded. Confounded effects cannot be estimated separately and are said to be aliased. Because some effects are confounded and cannot be separated from other effects, the fraction must be carefully chosen to achieve meaningful results. Choosing the best fraction often requires specialized knowledge of the product or process under investigation.

Equation 1 for calculating the number of runs in fractional factorial designs. Where k is the number of factors (i.e. 2^k is a full design) and p is the fraction exponent. If $p = 1$ then the design is cut in half, if $p = 2$ then the design will be a quarter fraction, and so on. A fractional design denoted as 2^{5-1} is a half fraction design for 5 factors, so that the full 2^5 is 32 runs, therefore the half fraction design is 16 runs.

$$2^{k-p} = 2^k \times 2^{-p} = \frac{2^k}{2^p}$$

Several other types of experimental design are available; these will not be described in detail in this thesis. In general, resolution 5 and higher designs will estimate a minimum of all main effects and two-factor interactions. Resolution 4 designs will estimate main effects, but two-factor interactions will be confounded together. Resolution 3 designs will not cleanly estimate any terms. All of these designs estimate only factorial models. If an estimation of curvature is required, then a response surface design is needed.

1.5.2 DoE data analysis

Statistical methods are used in the analysis of the experimental data; this allows identification of significant and insignificant effects and interactions. The experimental output will not be impacted equally by each of the factors. For instance when the level of a factor is changed but its impact on the response is relatively small when compared to the experimental variation due to uncontrollable factors and experimental error (ϵ), then this factor might be insignificant. A factor with a large impact on the response might be a significant factor. At times, two or more factors may interact; in this instance their effects on the output will be more complicated. Analysis of variance (ANOVA) is used to identify significant and insignificant factors in DoE data analysis. ANOVA can identify the relative importance of each factor by giving a numerical score.

Chapter 1

For the purposes of providing a real-world example of a DoE, a particle counting equipment DoE which was used to identify important variables that impact particle count has been used to illustrate the ANOVA output for a 2-level full factorial with 5 factors in Figure 26.

ANOVA for selected factorial model						
Analysis of variance table [Partial sum of squares - Type III]						
Source	Sum of Squares	df	Mean Square	F Value	p-value Prob > F	
Model	1.869E+006	5	3.738E+005	68.62	< 0.0001	significant
A-Flow Rate	1.164E+006	1	1.164E+006	213.76	< 0.0001	
B-System Vol.	6.699E+005	1	6.699E+005	122.99	< 0.0001	
C-Circulation Time	7076.96	1	7076.96	1.30	0.2702	
D-Sample Time	4560.96	1	4560.96	0.84	0.3730	
E-Standard Size	2.666E+005	1	2.666E+005	48.94	< 0.0001	
Residual	92596.48	17	5446.85			
Lack of Fit	70495.51	11	6408.68	1.74	0.2566	not significant
Pure Error	22100.97	6	3683.50			
Cor Total	1.961E+006	22				

Figure 26 ANOVA of a 5 factor, 2 level DoE. In this case factors A, B, and E are significant factors; this is indicated by the corresponding p-values which are < 0.05.

It can happen that none of the experimental factors are found to be significant, and then the experiment is inconclusive which may indicate that important factors were missed. DoE data analysis is able to provide an empirical mathematical model relating the output y to experimental factors. The form of the mathematical model could be linear or polynomial, plus interactions. DoE data analysis can also provide graphical presentations of the mathematical relationship between experimental factors and output, in the form of main-effects charts and interaction charts. The half-normal plot shown in Figure 27 is used to select effects to be included in the model. Large effects (absolute values) appear in the upper-right section of the plot. The lower-left portion of the plot contains effects caused by noise rather than a true effect. In many cases a distinct inflection point or "dogleg" in the noise effects indicates a transition between significant (model) and insignificant (noise) effects.

Chapter 1

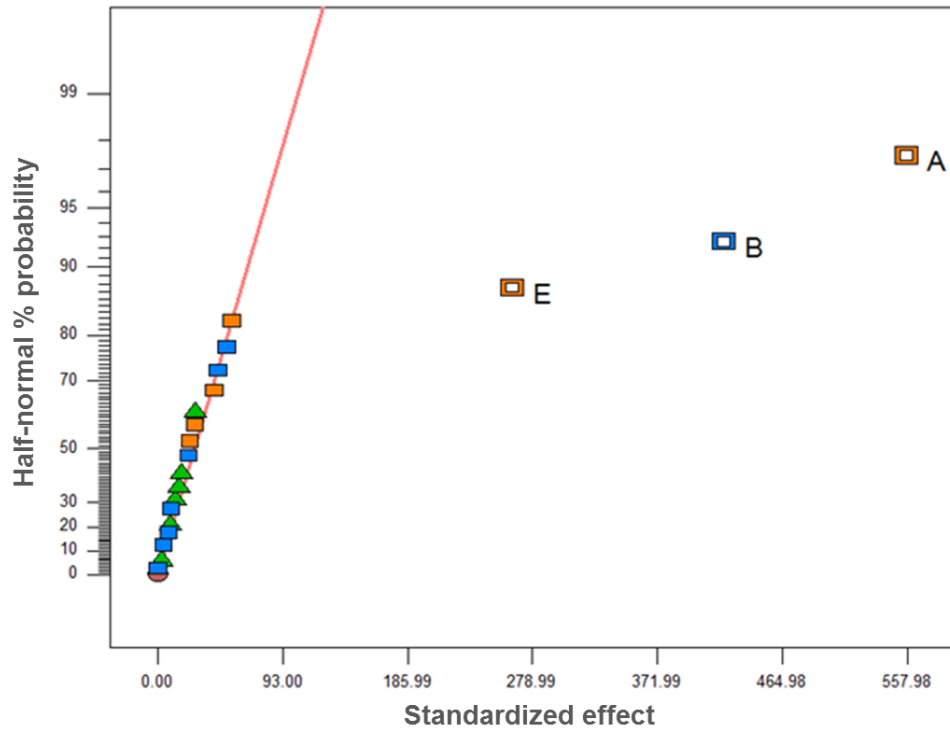


Figure 27 Half-normal plot for a 5 factor DoE, 2 level DoE. Factors A, B and C have shown a significant effect, this is indicated by their presence in the upper right region of the plot and their distance from the points along the guide-line which indicate noise.

An interaction occurs when the response is different depending on the settings of two factors. Plots make it easy to interpret two factor interactions. They will appear with two non-parallel lines, indicating that the effect of one factor depends on the level of the other. Figure 28 shows an interaction plot for the particle counting equipment DoE, in this instance an interaction between the factors does not exist, therefore the lines in the plot are parallel. It is often useful to plot the data from these RSM DoEs in a 3D format such as in Figure 29.

Chapter 1

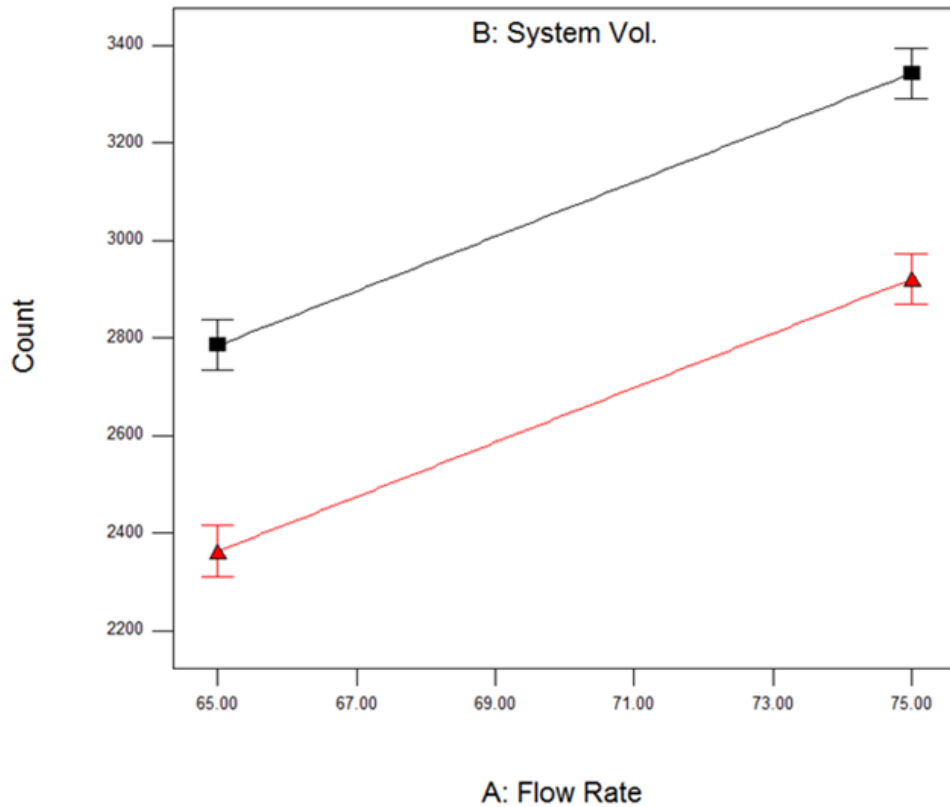


Figure 28 Interaction plot showing the effect of factor A (flow rate) when factor B (system volume) is at level 1 (Black) and at level 2 (Red).

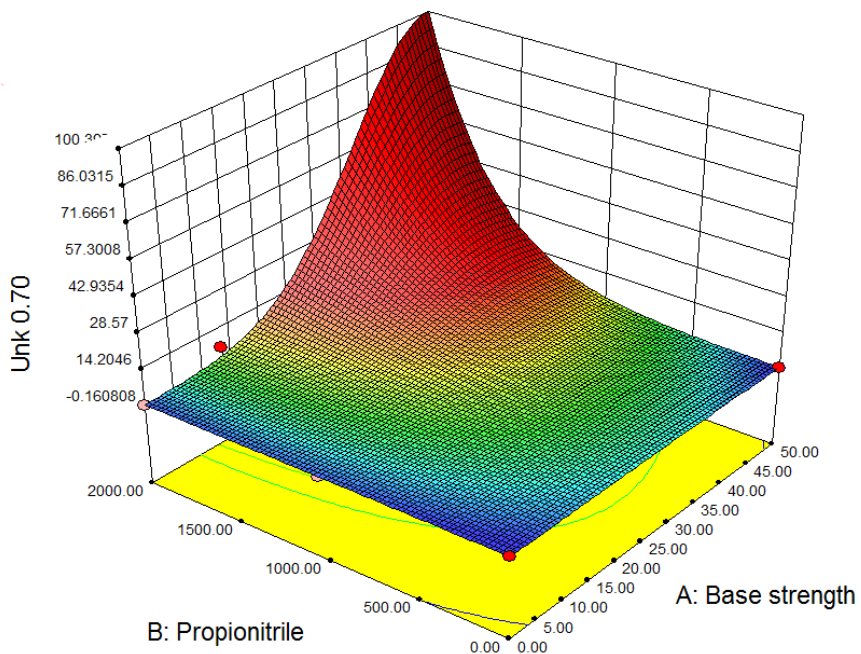


Figure 29 3D plot of two continuous experimental inputs (factors A and B), showing the effect on the output variable (The concentration of Unk 0.70, a drug degradation product).

1.6 Process analytical technology and quality by design

The near infrared spectroscopy (NIR) methods reported in this thesis are intended for making improvements in DES manufacturing processes. The approach taken is based on the pharmaceutical industry best practices of Process Analytical Technology (PAT) and Quality by Design (QbD)[65], [67–69]. The analysis of DES coating solutions by NIR is not reported widely in the literature; however a technical application note [70] from ABB Analytical shows the feasibility of NIR for this area.

In recent years there has been a push towards implementation of the principle of QbD in the pharmaceutical sector, driven by regulatory agencies and the industry itself [71]. It is generally recognized that the pharmaceutical sector lags behind other industries, such as the food industry, in adopting this model of building quality into their processes. The traditional approach of relying on rigid processes, which are dependent upon batch release testing of finished products to control quality, is slowly being recognized as an inefficient manufacturing model[72]. There is an ever increasing number of publications in the scientific literature where examples of technologies capable of real-time process analysis are being applied to make QbD a viable proposition[65], [73]. One of the linchpins of these so called PATs is NIR.

QbD is a systematic approach to development that begins with predefined objectives and emphasises product and process understanding and process control based on sound science and quality risk management. PAT has been described by the US FDA as a system for designing, analysing and controlling manufacturing through timely measurements of critical quality and performance attributes of raw and in-process materials and processes, with the goal of ensuring final product quality[71]. PAT enables the use of real-time data to make decisions. With the combination of both aspects occurring simultaneously, PAT complements QbD by:

- 1) Providing an overall means to minimise variation while improving process understanding.
- 2) Allowing for scale-up to be facilitated.
- 3) Allowing for the monitoring and control of critical processes to achieve product and process robustness.

Chapter 1

Within the principles of QbD and PAT, there is a definite switch of focus from being compliant, for example meeting standards set by FDA, European Pharmacopeia (EP), US Pharmacopeia (USP), etc. to building initial quality in to the process and thereby quality in the product. The best result of using QbD and PAT would be real-time release of quality proven product without the need for the same level of use testing at the end of the process. PAT and QbD can help mitigate the waste on the order of 10s of millions of euro annually by biomedical/pharmaceutical companies because of lack of manufacturing efficiency. Product failures and associated waste account for the majority of these losses. With a functioning QbD approach, all aspects of process understanding gained can be fed back rapidly to process operators, thus allowing for improved process performance. The ultimate goal is that with improved process performance there should be a higher degree of product quality[71].

Possible outcomes of efficient application of PAT can include;

- 1) Reducing product cycle times by accurate in/at-line measurements.
- 2) Reducing or prevent rejects and re-processing.
- 3) Real-time product release.
- 4) Improving energy and materials use, thus increasing production capacity.
- 5) Increasing control of variability.

1.6.1 Near infra-red spectroscopy

In the last 20 years NIR has proved its worth as a powerful tool for research on PAT in agriculture, food, pharmaceutical, chemical, polymer and petroleum industries[74–81]. This lies in the ability of NIR to analyse a wide range of chemical and physical properties of various samples, in a fast, accurate, (due to high penetration of the radiation beam), non-invasive and non-destructive manner, making it well suited for process control testing, particularly for at-line applications.

NIR is a subsection of the IR region included in the electromagnetic spectrum [82]. Infra-red has sub sections of near-, mid- and far- infra-red. The NIR region ranges from 12,500 - 4,000 cm^{-1} (0.780 - 2.5 μm wavelength). NIR spectroscopy employs photon

Chapter 1

energy to promote molecules to excited vibrational states. This energy is higher than required to promote molecules to their lowest excited vibrational state and lower than the typical amount of energy required for electron excitation within molecules.

NIR spectra can provide both qualitative and quantitative information on a sample; this information is gained from the interaction of the NIR electromagnetic waves with the sample constituents. Atom-to-atom bonds within molecules vibrate at certain frequencies. When radiation energy of a specific frequency ($h\nu$) is absorbed by the molecule then these vibrational levels become excited, this is simply illustrated using the diatomic oscillator model in Figure 30.

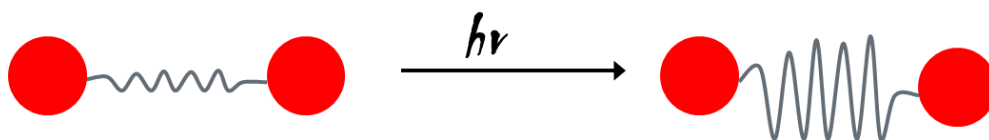


Figure 30. Atom-to-atom bonds within molecules vibrate at certain frequencies. When radiation energy of a specific frequency and wavelength is targeted at the molecule then the vibrational levels become excited.

In the case of an ideal harmonic oscillator in Figure 31 the atoms are excited to one or more higher energy states, which exist at discrete levels. In order for the absorption of radiation to occur, the energy of an excited photon must exactly match the energy difference between the ground state and one of the excited states. As can be seen in Figure 31, these energy levels are equally spaced. Energy transitions from the ground state ($\nu = 0$) to the first energy level ($\nu = 1$) are known as fundamental transitions. These fundamental transitions result in the fundamental absorption bands seen in mid infrared spectra. Other transitions from excited states are also possible, such as $\nu = 1 \rightarrow \nu = 2$, $\nu = 2 \rightarrow \nu = 3$, however the corresponding spectral bands are much weaker than the fundamental absorption[83].

Chapter 1

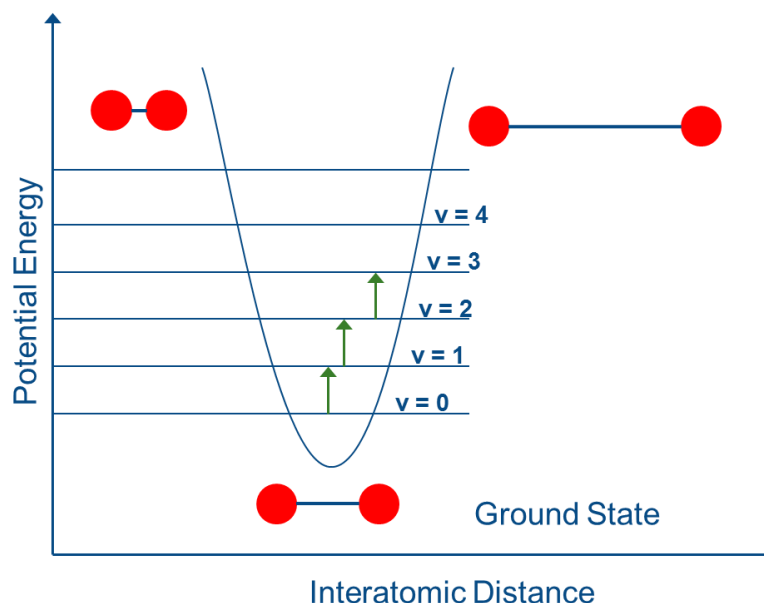


Figure 31 Harmonic energy model for a diatomic oscillator with discrete energy levels ($v = 1, 2, 3, \dots$). Transition from 0 to 1 is a fundamental vibration.

In practice, molecules do not follow the simplistic harmonic oscillator model, instead additional transitions through the energy levels that are not allowed by the harmonic model are observed. The non-ideal nature of molecules at the quantum scale causes the anharmonicity which is observed spectroscopically. Various models then seek to mathematically describe the motions. The anharmonic oscillator model in Figure 32 is required to explain these non-allowed transitions. Molecules are assigned as being anharmonic oscillators for two reasons. Firstly, in an anharmonic oscillator, the vibrational energy levels are no longer equally spaced thus leading to some bands not having the same frequency as the fundamental band. Secondly, transitions referred to as overtones, $v = 0 \rightarrow v = 2, 3, 4$, are allowed. Electrical anharmonicity is responsible for the presence of overtones, these overtones have transitions between energy levels corresponding to two or three vibrational units in the IR spectra. For the anharmonic oscillator it can be seen that the frequencies of the overtones are not exactly 2 or 3 times that of the fundamental absorption. Mechanical anharmonicity causes the frequency of some bands to be less than that of the fundamental transition. Anharmonic motion is described as a vibration; vibration is in essence caused by the rearrangement of electrical charge induced by photon energy absorption. The result of anharmonicity exerts a vibrational energy which contains cross terms which contain vibrational numbers of two or more of the normal vibrations[84].

Chapter 1

As a consequence of the additional energy level transitions explained by the anharmonic model the NIR region contains absorption bands corresponding to overtones and combinations of fundamental transitions. A typical NIR spectrum is shown in

Figure 33. The presence of these transitions and also the observation that the energy levels are not equally spaced implies that in reality the NIR region contains these bands because of the large anharmonicity of the vibrations[82]. The NIR region is dominated by the bands associated with the bonds between hydrogen and larger atoms, such as C-H, O-H and N-H, because of the large anharmonicity of the vibrations involving the light hydrogen atoms. As the overtones and combination bands of C-H, O-H and N-H are much weaker than the fundamental absorption bands, NIR subsequently allows for analysis of samples that are up to several millimetres thick.

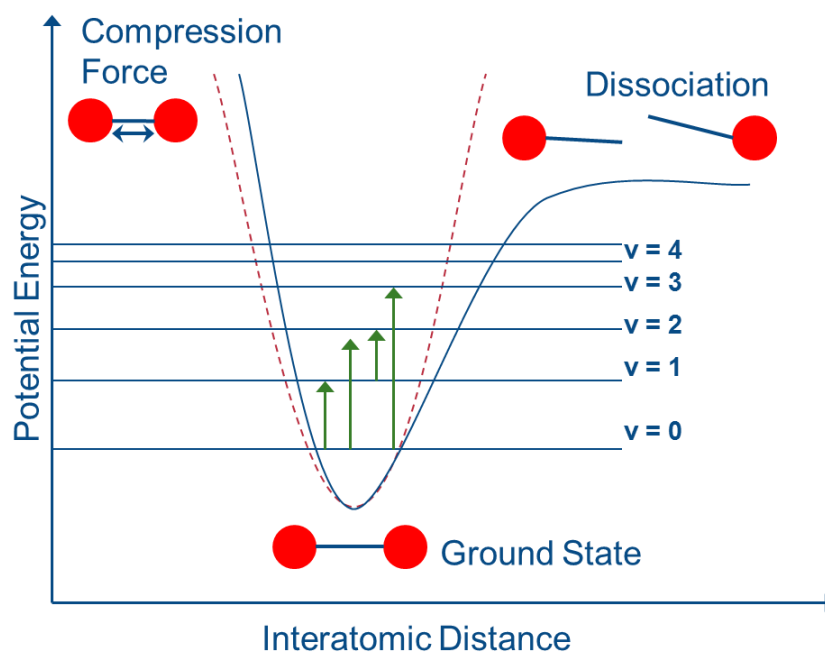


Figure 32 Anharmonic energy model for a diatomic oscillator, overtones ($v = 0$ to $v = 2, 3, \dots$ etc.), Combinations ($v_i = 1$ and $v_j = 1$ simultaneously)

Chapter 1

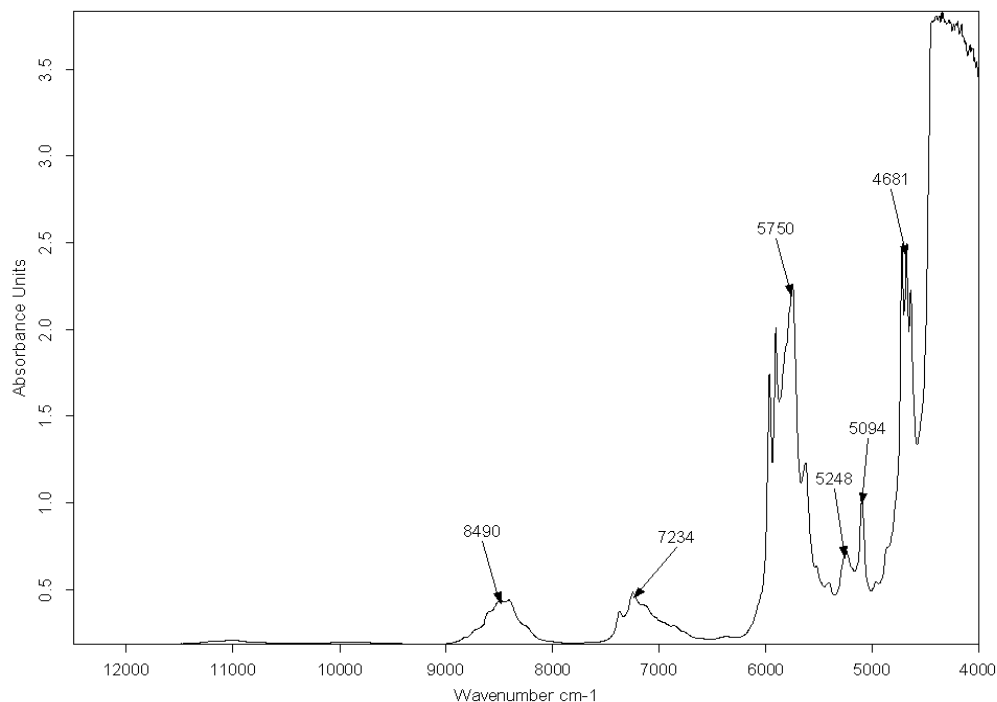


Figure 33 Spectrum of everolimus coating solution collected in transmission mode.

Advantages of NIR[85]:

- 1) Reduced risk of test substance exposure. As glass does not absorb strongly in the NIR spectral region the test substance can be contained in a sealed glass vials or cuvette. the light is not affected greatly by the glass in transmission or reflectance mode, and any effect that may be caused can be removed from the spectrum easily by appropriate background subtraction[86].
- 2) Little or no sample preparation. Analysis using NIR can be done with liquid, powders, slurries, tablets or grain - some of these can be directly analysed with no preparation[81].
- 3) Real-time analysis. With varying methods the analysis time can be within 30-90sec[78].
- 4) NIR analysis can be performed by operators with no NIR analytical skills. Once a calibration design is created and validated to suit a process/design space, an NIR probe can be placed at-line for analysis to create a closed loop feedback process.

Chapter 1

- 5) Cost benefits. Analytical laboratory time, reagents, consumables and equipment costs savings accrue by adoption of NIRS[87].
- 6) Increased process understanding may be acquired through spectra gathered.

Disadvantages of NIR[85]:

- 1) Weak sensitivity to minor constituents due to the relatively low molar absorptivity of adsorption bands in the NIR region (0.01 to $0.1 \text{ mol}^{-1} \text{ cm}^{-1}$)[88].
- 2) Water can present a problem for the use of NIRS in monitoring aqueous solutions, as water has a high absorbance leading to broad peaks that can drown out obscure weaker bands from low concentration analytes. Ingress of environmental water to samples can pose problems for the development of reliable multivariate calibrations[89].
- 3) Broad spectral bands and severe overlap of bands is common, this makes qualitative analysis by classical means problematic[90].
- 4) Reliance on reference methods to construct calibration models[91].

The coating solutions used for DES products are amenable to the application of NIR analysis because they are generally produced using high purity, transparent solvents with one or two non-reactive compounds dissolved in them. In addition to the suitability of the sample matrix, there are many other favourable attributes to this mode of analysis.

Continuous monitoring of these solutions during the DES manufacturing process would prove a valuable tool to ensure the correct ratio of drug to polymer are achieved at formulation stage and that this ratio is maintained from the start to finish of a DES batch production. Continuous monitoring can be used to measure the uptake of atmospheric water which, amongst other things, may impact on the application and drying rate of coatings[92], [93].

Current practices use laboratory based procedures to verify that the correct formulation is achieved. These procedures may be simple and non-specific, such as measurement of the percentage of total solids in solution using gravimetry following evaporation and

Chapter 1

drying-off of the solvents, or they may be based on compound specific methods such as high performance liquid chromatography (HPLC) or gel permeation chromatography (GPC). Some disadvantages of using these laboratory based procedures are that they are time consuming and they are destructive to the sample. Additionally, these tests are carried out on samples taken immediately after formulation and therefore do not account for variations that may creep in over the life cycle of the coating solution. The length of time between sampling and obtaining the results of the analysis adds to the overall manufacturing time. Continuous monitoring of coating solutions gives the opportunity of using the real-time data to identify issues before they impact upon product quality, provides much more data to trend processes with, and may provide additional data that can be used to increase process understanding.

1.6.2 Chemometrics

The use of NIR in tandem with statistical methods allows for qualitative and quantitative information to be obtained from complex NIR spectra. An approach in conjunction with chemometrics is a commonly used method. This approach usually relates physical or chemical properties of the component(s) of interest to the absorption of the radiation in the NIR range. A crucial step in quantification by NIR spectroscopy is to perform a calibration experiment. A reference or calibration set of samples which contain all the expected variations of chemical and physical properties which would occur in the unknown samples are collected. The calibration experiment allows for a mathematical relationship to be established between the NIR spectrum and the properties under investigation. Analysis of the unknown samples is carried out on their NIR spectra by using the built mathematical relationship with reference to the properties of interest.

The application of chemometrics is a key component to successful NIR analysis[91]. One must create a representative design of the process and corresponding product simulations in order to accurately and confidently quantify the same components in an “unknown” sample[94]. In general it can be said that for any quantitative analytical method there is an overall aim of the method to quantitatively determine a system property (or in this case multiple properties), for now named as y , by way of a measured system parameter (or parameters for multi-component systems), x . In order to carry out

Chapter 1

this form of analysis there is a requirement for two main steps, the *calibration* and the *analysis or prediction*[95].

Within the validated and optimised calibration described by Equation 2, the intent is to generate a model allowing prediction of the system property, y from the measured quantity, x . In the instance of analysis or prediction, x is known, y is unknown. After the establishment of a successful calibration procedure described by Equation 3, analysis can be carried out on unknown samples. Determination of the values of these unknown samples involves linking the calibration model to the measured parameter, x (known).

Equation 2 Calibration, building the model

$$x \text{ data} + y \text{ data} \rightarrow \text{Calibration function } b$$

Equation 3 Analysis, prediction of unknown samples

$$x \text{ data} + \text{calibration function } b \rightarrow y \text{ data}$$

To put this in context, within quantitative NIR analysis, the measured value is the absorption spectrum (x values) and the value to determine could be the concentration of analyte in the sample (y values). In this case, a multi-component system is involved. Multivariate calibration methods such as Multiple Linear Regression (MLR) are appropriate in this instance[96]. Multiple regression analysis is the study of how a dependant variable, y is related to two or more independent variables. Information from spectral data is compared to corresponding concentration values. Changes that occur in both data points must be recognised and correlated with each other. For this purpose a large number of samples are required.

1.6.3 Multivariate analysis

Multivariate analysis is used widely for on-line monitoring applications. In most systems, multiple process or product variables can elicit a response on the measured output, such as a spectrum or chromatogram. The responses of these variables are often correlated with one another and are therefore not readily measurable using straightforward univariate calibration techniques[97]. Multivariate methods like principal component regression (PCR) and partial least squares regression (PLSR)[98]

Chapter 1

are suited to building calibration models whereby an output such as a spectrum is used to predict the desired attribute of the sample or system[95], [99–101].

A great deal of process understanding is required before attempting to build a stable multivariate model, as also is the need for good reference measurements. The need for a reference method for multivariate regression is probably the greatest reason why methods that rely on multivariate regressions are not more frequently used in pharmaceutical manufacturing. One has to ask why employ a secondary method to predict the results of an existing procedure? This is an important question with a response that could end up costing or saving significant time and funds for a company. A cost versus benefit analysis looking at the costs required to construct, validate and maintain a multivariate calibration versus the long term benefits of using a method that is capable of real-time measurement needs to be carried out. This usually means that the multivariate approach ends up being adopted for situations where large numbers of samples require analysis and where in-line analysis can improve performance of a process.

Multivariate calibration generally combines a large amount of spectral information with corresponding reference values of the sample. When done correctly, this leads to high accuracy. In this thesis, 3 or more chemical component solutions are analysed using NIR. Taking this in to account plus the information outlined above on regression, it is necessary to carry out a multivariate design in order to achieve the best possible results when analysing or predicting amounts in unknown samples.

Partial least squares regression, a form of MLR, was applied to the pre-treated NIR spectra of DES coating solutions with good success in the work reported in this thesis. PLS can handle multi-co-linearity, many more variables than samples, slight non-linearity and extract factors that are correlated with the predictand[95]. The mathematics of PLS are complex, however many software packages make the selection process for robust PLS models attainable for non-statistician analytical chemists and process engineers who wish to develop calibrations.

Given that the application of these analytical measurements is for the control of pharmaceutical formulations used on devices intended for human use, the level of validation required of these methods is proportionally high. The general method

Chapter 1

followed to establish the coating solution calibrations is described in Figure 34. Details of the main steps involved are provided in the discussion to follow.

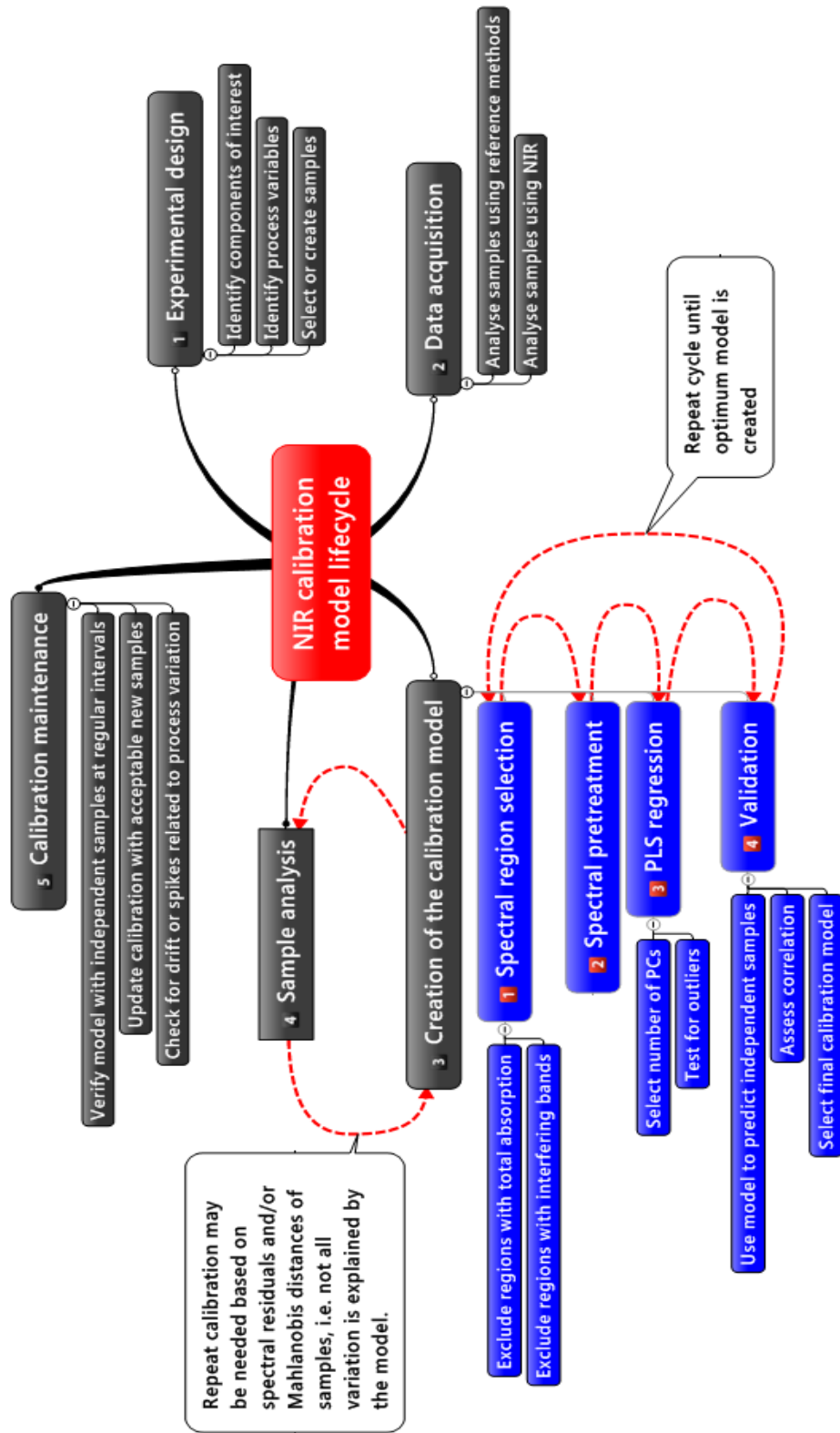


Figure 34 NIR calibration schematic.

Chapter 1

PLS was used for development of calibration models, with a regression step carried out after selection of the loadings. PLS can be used to analyse one chemical component in a mixture at a time, and consists of a process by which the spectral data is decomposed [102]. In order to carry out PLS regression (PLSR) for DES coating solutions, the NIR spectral data is compared to the corresponding concentration values acquired using reference methods. Changes that occur in both data sets must be identified and a correlation between them established. The PLS algorithm consists of a factor analysis method that looks at the full spectral range and changes in this data are used to write down a data point matrix with the corresponding reference data set. The eigenvectors generated from this matrix are called the PLS loadings. The loadings are then used to predict the concentration in the coating solutions instead of the original spectra, as they contain the relevant information necessary for the sample. Furthermore, PLS regression loadings provide a useful mechanism for model interpretation and outlier detection.

PLSR uses both Y (reference values) and X (response variables) to build a calibration for b (component of interest), Equation 4. This allows selection of the best calibration providing that the number of samples used is both large and varied enough. PLS creates concentration dependent loadings vectors from reference values, and in this way a computed scores vector can be compared to the concentrations after each loadings vector is calculated. PLSR was chosen for construction of calibration models in this application because reference methods were already in existence for analysis of the coating solutions. Additionally, preparation of the coating solutions is relatively straightforward and component amounts can be readily varied to desired levels.

$$Y_{Analysis} = X_{Analysis} \times b$$

Equation 4 PLS regression equation. The regression uses both Y (reference values) and X (response variables) to build a calibration for b (component of interest).

In the case of PLS calibrations, the loadings are arranged in descending order; with 1 being the lowest rank and ascending to higher ranks moving away from 1 in whole numbers. In theory the loadings only correspond to concentration variation of each chemical component in the sample. Because the concentration of all components add up to 100%, the number of loadings should equal the number of chemical components minus one[95]. However, in practice more loadings are observed than can be accounted for by the chemical components alone. A common additional loading corresponds to

Chapter 1

light scatter effects or path length differences in the samples. The first loading describes the main changes in the spectrum, and as such has the greatest significance for the calibration model. Conversely the highest loading describes small changes in the spectrum. This is not to say that high ranking loadings do not contain the important information that describes the chemical component of interest. In fact the first few loadings may describe disruptive parts of spectral noise and without inclusion of higher ranking loadings the model will be under-fitted[68]. However, care should also be taken that the highest ranked loadings are not used when they describe spectral noise, as this can lead to over fitting, resulting in unstable calibration models[95]. In practice, as described in chapter 5, the number of chemical components in the coating solutions may be outnumbered by the number of loadings required to obtain good prediction results. This implies that some other effect(s) is (are) explained by these components, such as nonlinear relationships between the chemical concentrations and the spectral measurements.

Once the calibration function, b , is calculated it is then necessary to validate the predictive capability of the calibration model. The validation of the model is achieved by assessing the correlation between the reference data and the spectral data. A good correlation should lead to an accurate and precise prediction of the components of interest in the coating solutions using NIR. The validation of the calibration models is carried out by testing independent samples (independent samples are classified as representative samples that were not used to construct the calibration model) using the chemometric model and comparing them to the concentration values determined by the relevant reference method. Two validation approaches were used in this thesis for assessing the predictive capabilities of calibration models: test set validation, and cross-validation[95].

Test set validation is an example of external validation, where one group of samples is used to construct the calibration model and a completely separate group of samples is used to test the prediction capability of the calibration model[95]. A comparison of the analysis results with the reference method is used to calculate the root mean square error of prediction (RMSEP). The RMSEP is a quantitative measure for the predictive accuracy of the calibration model; the lower the value then the better the model. The main disadvantage of this approach is that many samples are required for the test set,

Chapter 1

and these samples are not available to then use for the construction of the calibration model.

Prediction testing can be used to select the optimum number of loadings to include in the PLS calibration model. A plot of the RMSEP value for each of the loadings typically shows that the RMSEP value decreases over the first few loadings and then begins to increase again[95]. The selection of the number of loadings to include in the calibration model is based on using the first local minimum value for the RMSEP, however when the RMSEP value is approximately the same for a number of loadings then the lowest ranking loading should be selected, this may contain a solution that is more stable over time[103].

Cross-validation is an internal validation approach. Individual samples are taken from the calibration set and the remaining samples are used to construct the calibration model[95]. The calibration model is assessed by predicting the concentration in the individual samples that were previously removed. The removed samples are then returned to the calibration group and different samples are removed, the calibration model is re-established and is used to predict the concentration of the newly removed samples. This process is repeated until all the samples have been removed and analysed once. A comparison of the reference data and the analysis resulting from the calibration model is used to calculate the root mean square error of cross-validation (RMSECV). It is important not to remove too many samples at one time for cross-validation as the calibration model must not vary too much between successive steps. The main advantage of cross-validation is that all samples are used in the construction of the calibration model, making it a more efficient use of samples.

For the coating solution calibration models, the approach taken was to use cross-validation to construct the initial calibration model as fewer samples were available. The models were then independently verified using production samples as they became available. In time, test set validations were made possible as the number of samples increased.

1.6.4 Selection of spectral ranges

PLS and PCA regressions can take into account the full range of spectral data available, but it should not be assumed that the more spectral data points present in the calibration

Chapter 1

model then the better the model will be. There may be good reasons to exclude portions of the spectrum, as inclusion can lead to poorer quality calibration models. In the NIR spectral region most substances have signals that span a wide spectral range thus exclusion of specific regions of the spectrum is acceptable without reducing the quality of the calibration models. The main reasons for excluding regions of the spectral range are due to interference from the absorption bands of some components, and to remove wavelengths that have total absorbance (> 3.5 Absorbance units)[103]. For example, in Figure 132 (Chapter 5) bands showing total absorbance in the region $4,500 - 4,000 \text{ cm}^{-1}$, and in the region $6,000 - 5,500 \text{ cm}^{-1}$ should not be used for calibration model construction. If this were the case the multivariate algorithm would try to account for spectral structures in these regions which do not originate from the component values contributing to deterioration in the analysis.

1.6.5 Signal pre-treatment methods

Pre-processing of NIR spectra prior to calibration is done to maximize analyte signal by reducing the noise from random sources, baseline effects or other spectral interferences. Techniques used to achieve this signal pre-processing are referred to as pre-treatment methods [82]. The purpose is to reduce the number of factors required in the multivariate calibration models by removing spectral variations which do not contain useful information, thereby establishing more robust calibration models in the long run. It may be argued that the multivariate models should be able to handle spectral variations, and this is true to a certain extent. However, the calibration model then needs to include all of these sources of variation, and this can lead to very complex experimental designs. Some common sources of spectral variation are listed below[82], [103], [104]:

- Light scattering from solid samples, slurries or cloudy liquids.
- Pathlength variations.
- Spectral distortions from the spectrometer; baseline drift, wavelength shifts, detector non-linearity or stray light, and noise from the detector.

Spectral variation can therefore be described in terms of external variance (instrument noise, path length variations, etc.) and that variance which is intrinsic to the sample (e.g. scattering, hydrogen bonding etc.). In addition to the generation of less complex

Chapter 1

calibration models, the pre-treatment methods can guard against future unexpected variations in the spectra [95], [103]. Several spectral pre-treatments can be applied to the spectra ahead of PLS regression, as outlined in Table 3. These various pre-treatment options will not be covered in detail here; however, Furukawa describes some of the main techniques in chapter 5 of *Near Infrared Spectroscopy* [82]. First derivatives were the most frequently adopted pre-treatment method of spectral data for the DES coating solutions. These methods are used to emphasize subtle perturbations in otherwise broad and flat NIR absorption bands.

Table 3 Spectral pre-treatment methods.

Pre-treatment method	Description
Straight line subtraction [103], [105]	In each selected frequency range, a straight line is fitted to the spectrum, using the PLS method. The straight line is then subtracted from the respective spectrum. This removes a baseline shift from linear tilt.
First derivative [68], [95], [103]	Calculates the first derivative of the spectrum and is used to remove an additive baseline. Signals with steep edges are emphasized in relation to relatively flat bands. Pronounced, but small spectral features are emphasized compared to broad bands.
Second derivative [75], [95]	Calculates the second derivative of the spectrum and removes a linear baseline. Compared to first derivative, even extremely flat spectral features can be evaluated.
First derivative + straight line subtraction [95], [103]	Combination of first derivative and straight line subtraction.
First derivative + Vector normalization [95], [103]	Combination of first derivative and vector normalization. Vector normalization involves centering the spectra. Then the sum of all squares of all Y-values is calculated, and the respective spectrum is divided by the square root of this sum. The resulting vector norm of the resulting spectrum has a value of 1. This is normally used to eliminate the influence of different optical path lengths.
First derivative + min-max	Combination of first derivative and Min-Max-Normalization. Min-Max-Normalization involves shifting the spectra linearly, so that the minimum Y-value equals zero. The spectra are then expanded, so

Chapter 1

Pre-treatment method	Description
normalization [95], [103]	that the maximum Y-value equals two absorbance units.
First derivative + multiplicative scatter correction[68], [95]	<p>Combination of first derivative and multiplicative scatter correction. Multiplicative scatter correction involves calculating the mean spectrum from all spectra in the calibration set. Then each spectrum (Xi) is transformed according to the following equation:</p> $Xi' = u + v.Xi$ <p>The coefficients u and v are chosen such that the difference between the transformed spectrum Xi' and the mean spectrum has a minimum. This is usually used for diffuse reflectance measurements.</p>

1.6.6 Creation of PLS calibration models

PLS calibration models are created using the recorded concentration values from reference methods and the gathered spectra. After spectra and corresponding concentration values are entered in the modelling program the spectral frequencies that contain areas of total absorbance should be removed. The selection of the appropriate spectral frequency range is the next crucial step for creating a good quality PLS model. Preliminary visual assessment of the spectra is undertaken, examining shifts associated with changes in concentration of the chemical components to identify appropriate frequency ranges. In addition to the pre-treatment methods listed in Table 3, mean centering is done to reduce the absolute changes between samples and to look at the relative changes between samples, which decreases the complexity of the calibration model by reducing the number of PLS factors required[95].

After a spectral frequency range(s) and pre-treatment are selected the calibration development can be carried out. In the case where a test set validation is being carried out, a proportion of the samples are randomly assigned to the test set. Selection of the optimum PLS model is based on the calibration outputs, with the goals being a low RMSEP and/or RMSE of cross-validation (RMSECV) value, a high coefficient of correlation (R^2), a minimum number of outliers, and the lowest number of loadings.

Chapter 1

The process of creating the models is repeated several times to optimize the various settings to improve the final model. During the validation, potential outliers can be detected by principal component analysis (PCA). PCA is generally performed to get an overview of the calibration spectra, to look for outliers and to identify suitable spectra for the calibration set. Similar to PLS regression, PCA is intended to reduce the variation in the data to as few PC factors as possible [95]. For each spectrum a set of scores is calculated, scores contain the information about how the original spectra are described by the PCs. A scatter plot of the scores helps visualise the data as the scores indicate the coordinates of the samples, so that samples that are close to each other or form clusters have similar spectra. These outliers should be double checked for errors and if errors are found then these must be corrected or the outliers removed from the calibration set. After the outliers are removed and the calibration parameters selected, the final PLS model can be created by calculating the scores and loading vectors and thus the calibration function b , Equation 4.

1.6.7 Model validation

The final step in construction of the calibration models is the model deployment which comprises of three steps (in sequence):

- 1) Checking the process spectra for outliers and discarding.
- 2) Checking that the spectra collected in the process are the same as those generated in the laboratory, this can be done through PCA.
- 3) Predicting the unknown samples and comparing the results with the in-house QC data.

There are many reasons that outliers may occur, such as sample mix-up and instrument error. Both of these will result in spectral differences, x variables, that are significantly different from the normal population of samples. Outliers may also occur in the y variables, which can be caused by transcription errors or problems with the reference method. A common way of detecting outliers is through analysis of the spectral residues [95]. The individual spectra are compared to the theoretical spectrum that is created after factor analysis of the calibration set. Large differences between an

Chapter 1

individual spectrum and its theoretical spectrum should prompt an investigation into the legitimacy of that sample.

1.7 Thesis proposition

Each specific area presented in chapters 3, 4 and 5 of the thesis deals with advancement in research for *in vitro* test methods used in PTCA and DES development and manufacture. Chapter 2 provides the materials and methods used; in addition an in depth description of the development of the particulate test methods is provided in Appendix 1 at the back of the thesis. Chapter 3 covers the development of *in vitro* methods for the assessment of particulate matter from extrinsic and intrinsic sources on PTCA devices. Chapter 4 describes the use of DoE to identify a previously uncharacterized drug degradation pathway of everolimus in acetonitrile. Finally, chapter 5 proposes an alternative to traditional wet chemistry test methods for the control of DES coating solution formulations by the use of NIR and multivariate analysis.

Chapter 2

Materials and methods

2 Introduction

All analysis, unless otherwise stated, was carried out in the R&D laboratories at Boston Scientific, Galway.

2.1 Particulate matter methods for PTCA catheters and stents

Development of methods for the evaluation of particulate matter from stent delivery systems has proven to be a complex undertaking. The mode of measurement is critical. The regulatory bodies, in particular the FDA, have indicated that USP <788> should be used as a basis for any methods developed[33]. However, this USP standard is intended for use in the testing of parenteral solutions and not medical devices; it does however contain details of the test equipment, sampling regimes and acceptable controls that should be applied to particulate matter detection in general. The challenge was to adapt this standard intended for liquid solutions to medical devices. Much of the equipment used for collection of particle counts from PTCA catheters and stents was custom built. Significant effort has been expended in the development of this equipment and rather than put all of this detail in the materials and method section of this thesis, the equipment and method development studies have been captured in the Appendix, section 7, of this thesis.

2.1.1 Instrumentation

Light obscuration (LO) counters from Particle Measuring Systems (Boulder, CO, USA), Liquilaz volumetric spectrometer run with SamplerSight Pharma software, was predominantly used for the collection of particle counts. The laser source for the Liquilaz sensor is a laser diode, and the dynamic range is 2 to 125 μm . The Liquilaz E20 laser was used with a syringe sampler in some of the early studies, operated at 20mL/min, however most work was carried out with a customised Liquilaz sensor calibrated at 70mL/min with samples delivered through an Ecoline CC-280, 2-roller

Chapter 2

peristaltic pump from Ismatec (Glattbrugg, Switzerland). A HIAC 9703 LO particle counter (HACH, Oregon, USA) was also utilized, with a dynamic range of 2 – 150 μm , operated with PharmSpec 2.0 software. Customized glassware was fabricated by AGB Dublin (A VWR International company), and test apparatus frames were fabricated by Caulfield Industrial, Galway, Ireland.

Light Microscopy analysis was carried out using a selection of manually operated light microscopes (Leica) at various magnifications. Automated light microscopy was carried out using a Morphologi G3 (Malvern Instruments Ltd., Worcestershire, UK), with a Nikon CFI 60 bightfield/darkfield optical system; illumination is via white light, brightfield diasopic and episcopic, or darkfield episcopic, and the detector is a 5M pixel 2592 x 1944 colour CCD array, with pixel size 2.78 mm x 2.78 mm.

Scanning electron microscopy was carried out using a Zeiss 1540XB CrosBeam Ion Beam field emission SEM.

Raman micro spectroscopy was carried out at RapID Particle Systems GmbH (Berlin, Germany), using their proprietary Single Particle Explorer® system. Samples were collected after particulate testing in particle free amber bottles using a syringe and filtered within 24 hrs. through a 5 μm gold coated polycarbonate filter. At RapID, samples were imaged for particle size, shape and location using dark field spectroscopy on an X,Y stage with 0.1 mm resolution. Once the particle images were taken, spectra for the particles on the filter were gathered using Raman spectroscopy. The light source used for Raman is a frequency doubled neodymium-doped yttrium aluminium garnet (NdYAG) laser that generates laser light at 532 nm (i.e. excitation wavelength of 532 nm). The Raman exposure time to particles was 20 sec. After filter scanning, spectral matching software, APSys-Central-Control-Center-Unit (ACCU), was used to identify scanned particles. The Raman spectrum for a particle was compared to library reference spectra using a correlation algorithm, the Pearson algorithm was used to compare reference and particle spectrum, and the background was subtracted using an algorithm called Detrending.

Infra-red micro-spectroscopy was carried out on a ReFlachromat™ FTIR 32x microscope objective used on a Thermo Nicolet FTIR using a LN2 cooled MCT detector. 400 scans were signal averaged for both the background and the sample.

Chapter 2

Water and carbon dioxide correction was used on some but not all of the scans. The method passes the IR beam through the sample, it reflects off the underlying gold substrate, then on to the detector so it is essentially like transmission mode with a path length of 2x the sample thickness.

Filtration of particles for light microscopy was carried out using vacuum filtration through 47 mm polycarbonate track etched filters (Sartorius part number 23006/47/N). The vacuum was supplied through an electronic pump called the Microsart eJet pump from Sartorius. Particle samples were collected on the filters by placing the filter in disposable 250 mL funnels (Micro Sart funnels from Sartorius), through which the water was pulled. The funnels were immediately capped and dried for 24 hours at 40°C in a convection oven. The filtration of particles for Raman and FTIR spectroscopic analysis was also carried out using vacuum filtration, but the particles were collected on gold coated polycarbonate track etched filters, supplied by RapID (Germany). In order to avoid agglomeration, the filters were analysed during the filtration process using a light microscope to ensure that the particles did not overload the filter. The particles were concentrated on a circular area of 4mm in diameter using a customized funnel, the filter was removed to a capped petri-slide until analysed.

Low particulate water (LPW) was generated by filtering analytical grade water through a 0.2 µm filter (Sartolab Plus from Sartorius). The specification for low particulate water is: not more than 1 particle per mL ≥ 10 µm, and not more than 0.2 particles per mL ≥ 25 µm as measured by light obscuration. LPW was stored for up to 24 hours in 2 L or 5 L in clear borosilicate glass bottles.

2.1.2 Particulate methods

Both categories of particulate matter test method, described in USP <788>, light obscuration (LO) and light microscopy (LM) have been evaluated for application to medical devices. However as LO has significant time saving advantages and better analytical precision over LM it was decided that LO would be the preferred measurement technique for routine quality control testing purposes. However, LM has an advantage over LO in relation to the qualitative measurement of particles, and depending on the particle type, LM may be the only option for particulate matter measurement in certain cases.

Chapter 2

Off the shelf LO particle counters are typically integrated with syringe pumps that pull a liquid through the detector from a parenteral container, beaker or similar vessel. These are adequate systems for the sampling of liquids such as parenteral solutions and offer a relatively straight forward approach for validation as reference standards can be obtained in solution and can be tested in an almost identical manner to test samples. A difficulty with particulate tests of medical devices is that test samples are comprised of solid components that need to be washed to remove particles prior to analysis, and the test samples may have to be preconditioned to obtain a suspension of particles in solution. Preconditioning of the medical devices presents a significant challenge. The clinical use of the device, the test environment, and integration with the particle measurement system are key factors to be considered when devising a pre-conditioning procedure.

The methods described in this thesis range from simple pre-conditioning procedures carried out by placing a medical device in a beaker of water to more complex procedures that required bespoke equipment design. Thus, preconditioning of the devices required the fabrication of several arterial models of various shapes and sizes. The following sections describe these methods and equipment designs. A comprehensive description of the development and validation of these methods is given in Section 7.

2.1.2.1 Product cleanliness, 2 beaker method for a stent delivery system

This is a very straight forward method for assessment of particulate matter contamination of a stent delivery system (SDS), and is widely used in medical device manufacturing to test several types of devices or device components for particulate matter contamination. The method does not stray far from the USP <788> LO method. Variants of this type of method are described by Barber in relation to other medical device types[36].

Two 600 mL beakers with 200mL of low particulate water (LPW) in each are used to collect particles removed from a catheter. One beaker is for the stent and the other for the remainder of device. The distal section of the catheter, which contains a stent crimped on an expandable balloon, is first immersed in beaker 1 (Figure 35), and the stent deployed using an inflation device. Once the balloon is deflated the stent comes away from the catheter and remains in beaker 1. The removed catheter is then

Chapter 2

suspended over beaker 2, and initially flushed through its guide wire lumen with 20mL of LPW in to the beaker and then hand coiled up and submerged under the level of the water in the beaker. Both beakers are then agitated on an orbital shaker for 5 minutes to remove and suspend particles. Five separate sequential measurements of particulate matter are sampled by a liquid laser particulate counter (HIAC 9703) from solutions drawn from each beaker through a 10mL auto syringe sampler. The first two measurements are discarded and the average obtained for the final three measurements. The particulate count is determined and reported as per USP <788> requirements in the ≥ 10 and $25 \mu\text{m}$ particle size brackets. The particulate count from the full SDS is the average of the three measurements from beaker 1 added to the average of the three measurements from beaker 2.

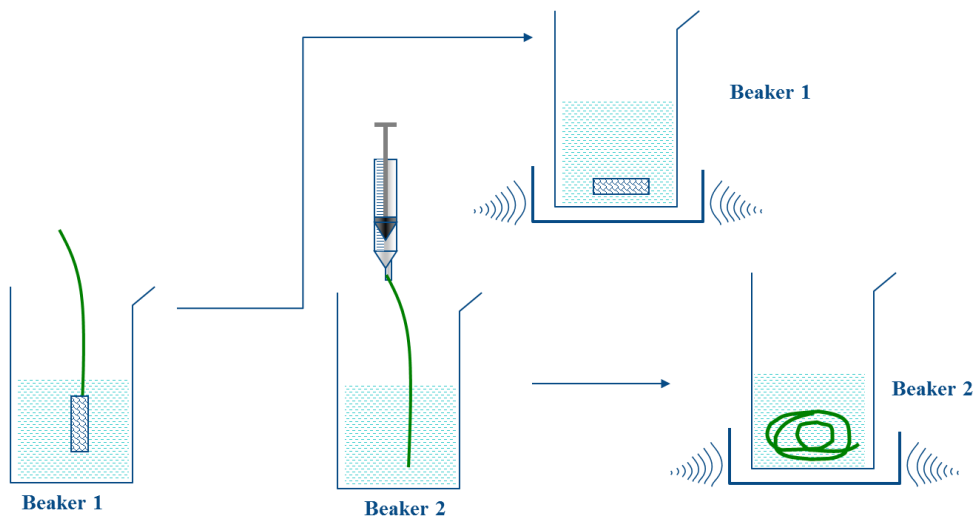


Figure 35 Schematic of the steps involved in the 2-beaker product cleanliness method for a stent delivery system. Step 1: The distal end of the catheter, where the balloon and crimped-on stent are located, is placed in Beaker 1 and deployed by inflating the balloon. Step 2: The deflated balloon catheter is suspended over beaker 2 and water is flushed into the beaker, through the catheter guide wire lumen using a syringe. Step 3: After flushing, the catheter is coiled into beaker 2. Step 4: Beaker 1 and 2 are agitated on an orbital shaker for 5 minutes. Step 5: Samples from each beaker are taken for particle counting using a light obscuration particle counter.

Chapter 2

2.1.2.2 Simulated use beaker method

This method operates by deploying stents in a beaker of LPW after tracking the distal end of the catheter through a PTFE-lined arterial model, this shown in schematic form in Figure 36. The starting volume of LPW in the beaker is 350 mL. Twenty (20) mL of the beaker solution is used to flush out the arterial model using a syringe and particle count measurements taken (Measure 1), in the same way as described for the 2 beaker method. Measure 1 is the blank and limits have been set for the maximum number of ≥ 10 and $25 \mu\text{m}$ particles, these limits are < 600 and < 70 particles respectively. Following this an un-deployed stent is immersed in the same beaker alongside the arterial model, and the measurement sequence repeated (Measure 2). Finally the distal section of the catheter, which contains a stent crimped on an expandable balloon, is tracked twice through the arterial model, with the stent deployed at the end of the second tracking, the catheter removed, and the measurement sequence repeated (Measure 3). The particle count from the full SDS is the sum of measure 2 and measure 3 less measure 1. The particle count for pre-track is calculated by subtracting measure 1 from measure 2. The particle count for post-track and deploy is calculated by subtracting measure 1 and measure 2 from measure 3. Measure 1, measure 2, and measure 3 are obtained from 5x10mL samples, by discarding the initial 2 particulate measurements and calculating the average of the remaining three particle measurements as described for the 2 beaker method.

Chapter 2

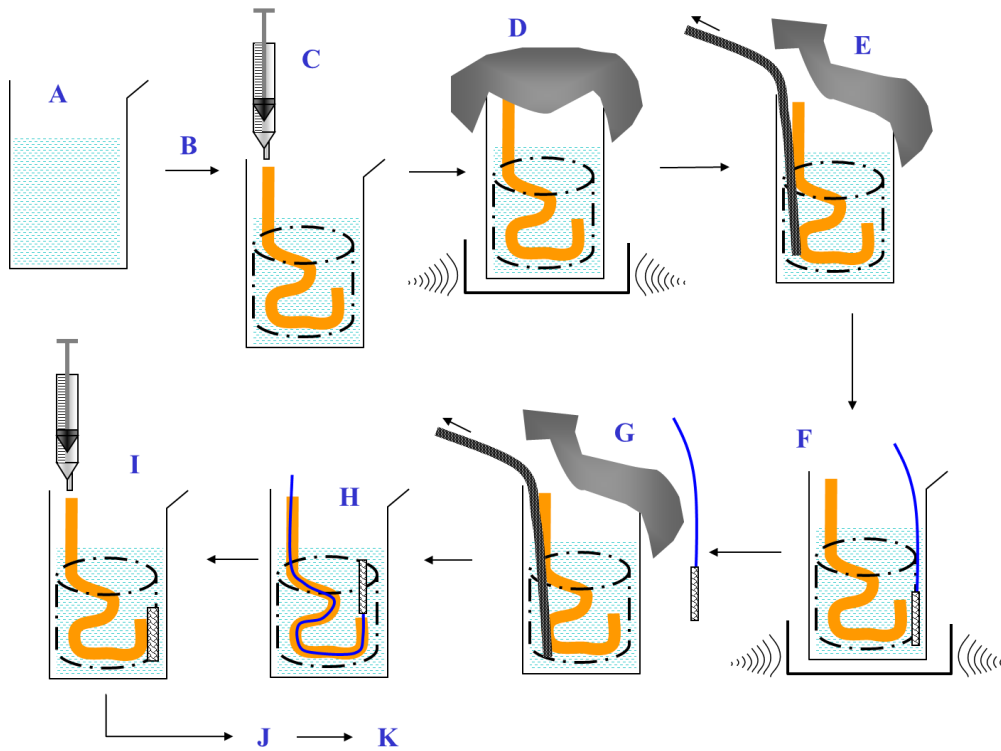


Figure 36 Schematic of the steps involved in the simulated use beaker method for measurement of particulate matter released from stent delivery catheters. (A) Fill the beaker with 350 mL of LPW, (B) add the arterial model, (C) rinse the lumen of the PTFE tube with 20mL of water from the beaker, (D) cover the beaker with aluminium foil and shake on orbital shaker for 5 minutes at 150 rpm, (E) remove beaker from the orbital shaker and sample 5x10mL aliquots using the LO detector (discard the 1st and 2nd measurements). This is the blank measurement, the $\geq 10 \mu\text{m}$ particle count should be ≤ 600 , and $\geq 25 \mu\text{m}$ particle count should be ≤ 70 . (F) Remove the aluminium foil and set aside. Take the catheter from its packaging and place the distal portion (stent and balloon) in the beaker alongside the arterial model. Shake on the orbital shaker for 5 minutes at 150 rpm. (G) Remove the catheter and replace the aluminium foil. Take 5 x 10 mL aliquots using the LO detector (discard the 1st and 2nd measurements), this is the pre-tracking and pre-deployment measurement. (H) Remove the aluminium foil and track the catheter through the artery until the stent exits the PTFE tube, withdraw the catheter and repeat the tracking and withdrawal step once more. Deploy the stent in the beaker and discard the deployed catheter. (I) Rinse the PTFE tube of the arterial model with 20 mL of water from the beaker. (J) Cover the beaker with the aluminium foil and shake on the orbital shaker for 5 minutes at 150 rpm. (K) Remove the beaker from the orbital shaker and take 5 x 10 mL aliquots using the LO detector (discard the 1st and 2nd measurements). This is the post-tracking and post-deployment measurement.

Chapter 2

2.1.2.3 The baseline particulate test method

The baseline test method evaluates a DES device for particulate matter that may be released from the DES without pre-conditioning. The device is not tracked prior to stent deployment. Testing is performed using the baseline test apparatus as illustrated in Figure 37. The stent delivery system (SDS) is inserted into the apparatus until the stent is positioned within the deployment chamber. The stent is deployed to rated burst pressure and the balloon deflated. A measurement is taken for unconstrained rated burst pressure deployment of the stent.

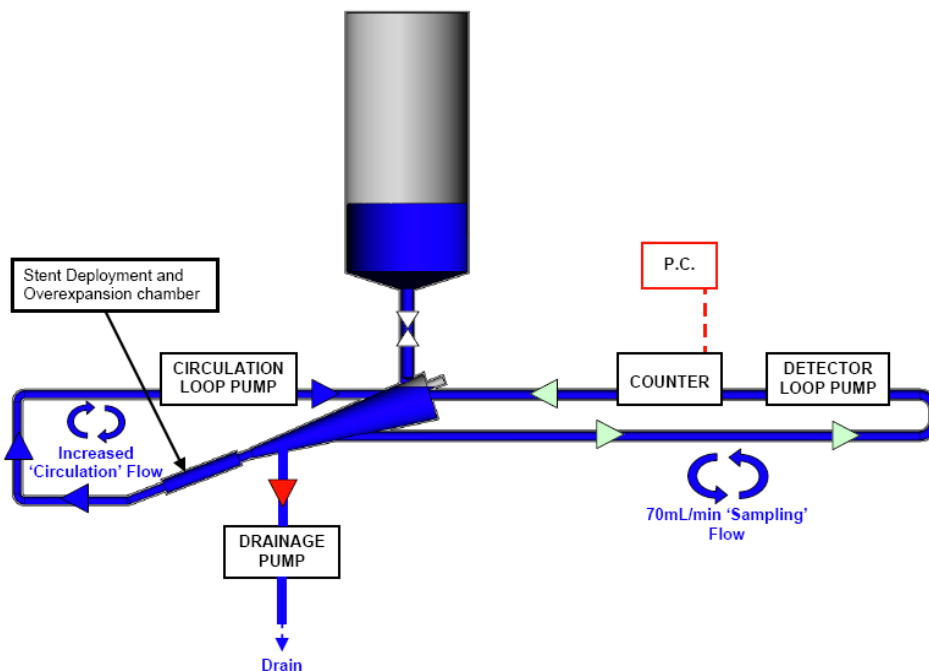


Figure 37 Baseline particulate apparatus.

2.1.2.4 Regulatory simulated use particulate test method

The regulatory simulated use (RSU) test method simulates the particulate matter released into the patient's systemic circulation due to device tracking and deployment. Medical device manufacturing facilities use this method for the regulatory purposes of batch release testing and stability testing for DES products[37]. Simulated clinical use in this test is carried out by tracking a device through an aortic arch and a tortuous artery model specified by ASTM F2394, this artery model is shown in Figure 38 integrated into the bespoke CLP equipment. The artery track model consists of glass tubing and the constrained deployment tube is made from silicone. The device is

Chapter 2

tracked over non-shedding guide wire into the closed loop apparatus until the DES is positioned within the deployment tubing. The stent is then deployed to rated burst pressure (RBP). Following deflation of the balloon, the catheter is then retracted from the apparatus, leaving the deployed stent in the silicone deployment tube. A measurement for particulate matter is then taken to give the total particulate matter level.

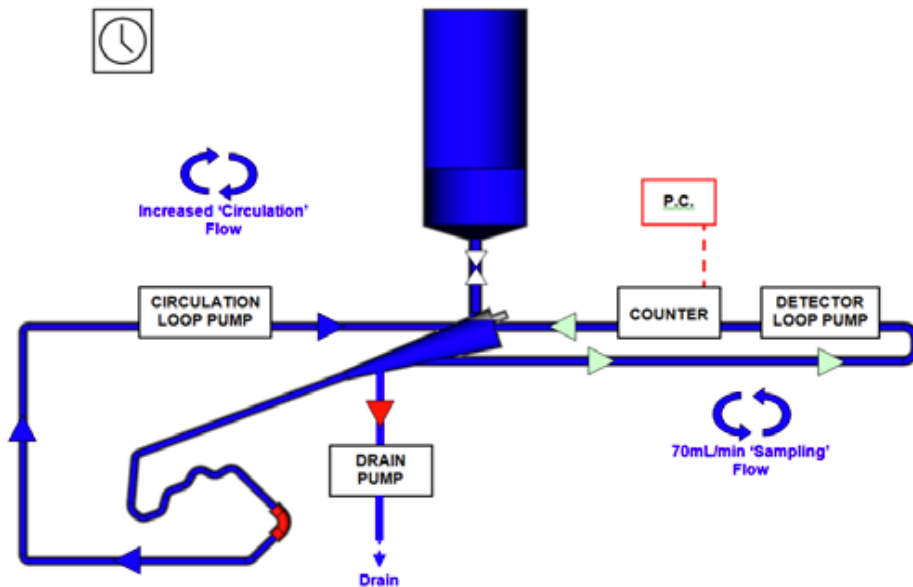


Figure 38 Schematic of the RSU test apparatus.

2.1.2.5 CSU particulate test method

The characterization simulated use particulate method (CSU), is used to measure the particles removed from 2 SDSs after they are tracked through a clinically relevant track model, deployed constrained in an overlapping configuration on a curve, and then over expanded to their maximum labelled diameter. The two devices are advanced over a commercially available guide wire, and through a commercially available guide catheter.

The CSU test apparatus, shown in Figure 39, is similar to the RSU test apparatus. The difference between the two is the diameter of the capillary where the guide catheter is placed and the use of an overexpansion gauge located at the point of stent deployment for the CSU method. In the CSU method the diameter of the proximal section of the track model is wider to accommodate a guide catheter, the diameter of the glass capillary is 3.5mm for the CSU method versus 2.0mm for the RSU method. The

Chapter 2

portion of the track model that has a wider diameter for the CSU method corresponds to the section coloured in green shown in Figure 39. For the measurement of stent overexpansion, the CSU method incorporates a sliding block which moves a gauge to indicate when the stents have reached the desired diameter. The RSU method has a rigid fixture in which the stents are deployed. Seven particle count measurements are taken at different points during the CSU test, and the test procedure this consists of multiple steps, illustrated in

Figure 40.

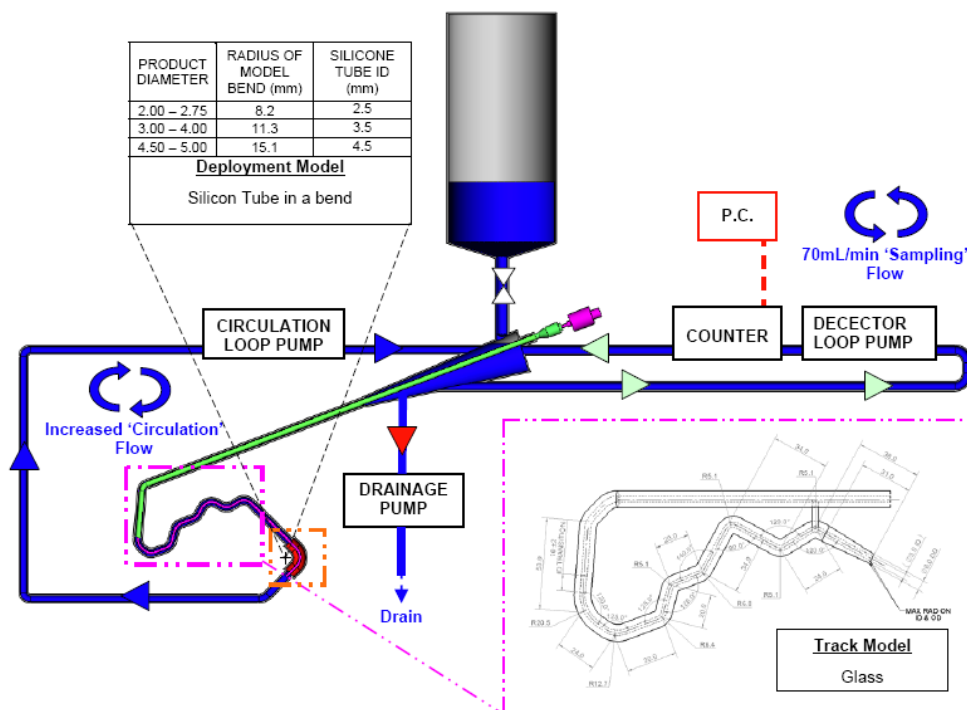


Figure 39 CSU particulate test apparatus. The guide catheter is marked in green.

Chapter 2

2.1.3 Identification of particles

Following the enumeration of particulate matter via LO, the identification of these particles is the next logical step. LO is an indiscriminate technique, and whilst it is fast and repeatable, it does not provide any information about the morphology, and identity of the particles it counts and sizes. Positive identification of particulate contamination is necessary for various reasons:

- 1) To ascertain if the particles could lead to an adverse effect when introduced to the body.
- 2) To identify if the presence of such particles indicate a stability issue for the device.
- 3) Identification of the contaminant particles is necessary to provide means of removing the source from the manufacturing process if possible.

There are two general types of contaminants, product related and foreign material. Product related contaminants may be from the stent coating or its component parts (e.g. drug and polymer), particles may originate from the delivery system, product container or packaging material (e.g. Teflon, graphite, glass, rubber, metals, plastics, silicone and paper). Contamination can also result during manufacture of the product (e.g. charred materials, detergents and lubricant oils), metal particulates may originate from metal corrosion or wear. Environmental contaminants such as fibres and skin flakes may also be found.

2.1.3.1 Initial assessment

The first thing that must be considered is the state the sample will be in when analysed e.g. solution, solid, etc. As the main concern of the test procedures described in this thesis is to analyse particulate matter that may be released when a device is tracked through an arterial model and then upon device performance (e.g. stent deployment), a washing step is required, therefore the sample will be most likely suspended in water. However, pre-inspection of the device prior to the test is a good initial step. This should quickly show if any relatively large contaminants are present and are clearly distinguishable from the rest of the product. It will also establish a baseline for the device appearance prior to simulated use, images taken before and after may indicate where intrinsic particles may have come from on the device.

Chapter 2

2.1.3.2 Isolation

Isolation of particles viewed optically may be possible by manual means using a tungsten needle to directly remove them from the surface of the device. However, as the devices are deployed in solution, filtration is the most practical technique to isolate any particles from the rinse solution. Polycarbonate track etched membrane filters were chosen as they have a smooth surface from which to observe and pick particles. Common membrane filters contain interlinked pores formed through the criss-crossing of the membrane material, thus particles can be captured not only on the surface but also throughout the depth of the membrane. Particles are then unavailable for observation on the surface by LM and SEM (FE-SEM: Zeiss Supra 40 VP). Polycarbonate track etch filters contain uniform, cylindrical pores, thus allowing for an even distribution of a collected sample in one plane across the entire exposed membrane surface.

2.1.3.3 Identification

After the particles are isolated a suitable mode of analysis must be selected; this will depend on the particle type. Particles can be grouped into basic categories of different particle type by optical means, such as organic, inorganic, fibrous, crystalline, etc. Optical examination of the sample may be sufficient in characterizing the contamination. However additional techniques are usually required to establish the identity of most particles. A range of other micro-analytical techniques were utilised for material characterisation in this thesis. The particle characterization techniques used were light microscopy (LM), scanning electron microscopy (SEM), and Raman microspectroscopy. Raman is suited for the analysis of particles that appear to be organic during optical examination. Raman is a complementary method to infrared spectroscopy and is particularly suited to the analysis of particles because of its high spatial resolution (<1 μ m in diameter). Raman spectra are unique for every organic molecule, when compared to the spectra of a known material qualitative identification can be made for contaminant particles. Organic particles commonly found in these manufacturing processes include polymeric material, pharmaceuticals and their degradants, hydrocarbons, etc.

2.1.3.4 Pre inspection of devices

The most widely used technique to examine medical devices for particulate matter is LM. Light microscopes are generally employed in the processing of medical devices to

Chapter 2

inspect the device for defects as well as foreign matter. The technique is not destructive and is typically used for 100% inspection of devices prior to final packaging. This ensures that any relatively large visible particles and fibres can be identified and removed from the device. However for characterization of devices in the sub visible range (1 – 150 μm) the light microscope is not as useful as the scanning electronic microscope (SEM).

SEM can be used to inspect for the presence of product defects and the physical appearance of the device. It is a widely used tool for the inspection of various mechanical properties and visual aspects of prototype devices during product development. However outside R&D, SEM is not used for 100% inspection because it is a destructive technique. In the manufacturing environment, SEM may be used to examine a representative sample from a batch of product. Due to the relatively narrow field of view which would lead to impractical analysis time, the entire device is rarely examined under SEM, instead regions of particular interest may be inspected, or representative sections of the overall device. Of particular interest to drug eluting stent manufacturers is the integrity of the stent coating, it is common practice to analyse the stent coating from representative samples of every batch of DES prior to commercial release. For this thesis LM and SEM were used to inspect devices prior to and post simulated use to establish if specific particles could be attributed to intrinsic components of the test device.

2.1.3.5 Light microscopy analysis of particles

Analysis of particles by LM is a very time consuming technique, it is also open to operator subjectivity. To reduce the burden of analysis, an automated light microscope may be used; the Morphologi G3 from Malvern was used to gather particle data for this thesis. The instrument uses a robotic stage to move a mounted filter membrane under the microscope, a camera records images of the field of view. These images are analysed using Malvern's proprietary software to separate particles from the filter background. The threshold and light settings used to differentiate particles from the filter membrane background are pre-selected and programmed into the software prior to analysis. Each particle is saved as an individual image file by the software along with a list of quantitative descriptors of the particles, such as circular equivalent diameter,

Chapter 2

length, aspect ratio, etc. (Figure 41). Each frame is also stitched together to provide an overall image of the analysed area (Figure 42).

Primarily, LM enables the morphological analysis of particles as well as overcoming some of the other disadvantages of light obscuration (LO). The main disadvantages of LO encountered by this author are the interferences by false particles of immiscible liquids and air bubbles, both of which are detected as particles via LO, and non-detection or under sizing of some particle types. Other drawbacks of the LM method include:

- 1) Greater variation caused by operator subjectivity.
- 2) Agglomeration of particles.
- 3) Increased analysis time.

These aside, LM as a qualitative technique is a valuable tool to the medical device designer and manufacturer for the identification of particles. In this context LM is used to further the understanding of medical device particle formation and contamination, and is essential for the accurate determination of a devices performance in a simulated clinical use setting.

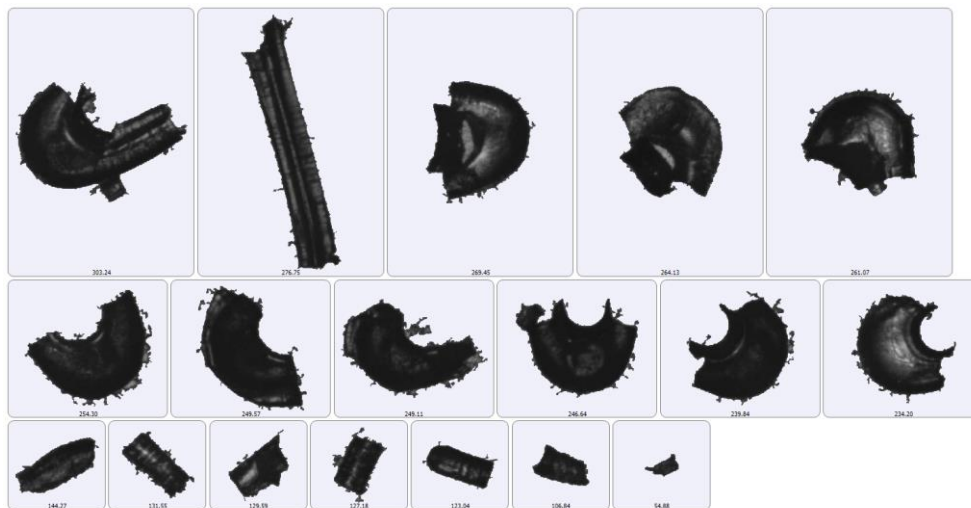


Figure 41 Individual images of particles from a biodegradable drug eluting stent which was processed to instigate coating mechanical degradation.

Chapter 2

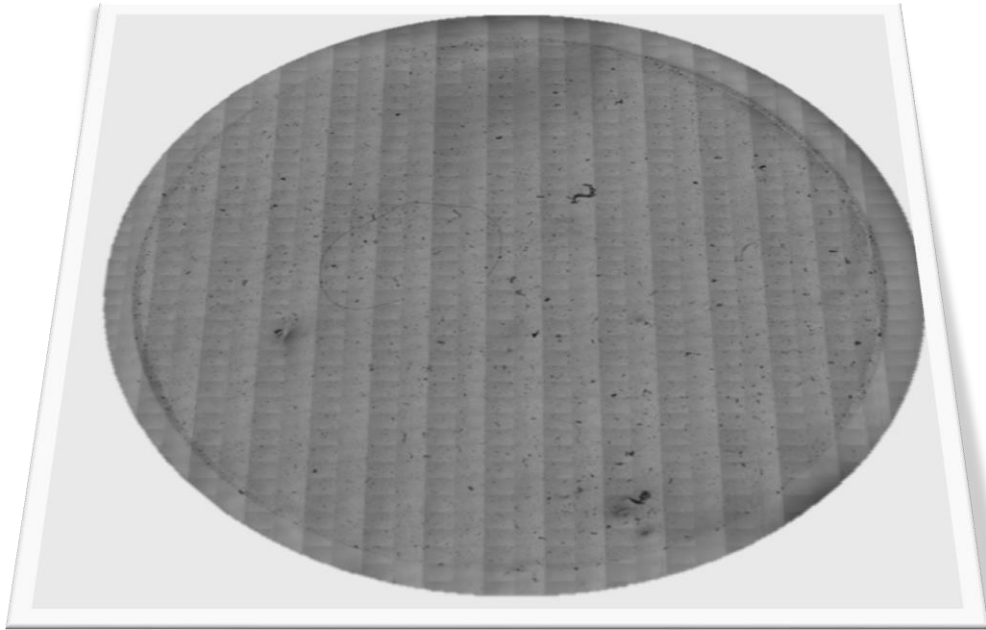


Figure 42 Image of a 47mm diameter filter which has been stitched together from each image frame taken by the Morphologi G3 microscope. The sample is from a stent delivery system after been tracked through a simulated arterial model.

Chapter 2

2.2 Investigation into acetonitrile induced degradation of everolimus

2.2.1 Instrumentation

High-performance liquid chromatography (HPLC) analysis was performed on a Waters 2695 Alliance separations module with Waters 2996 Photo Diode Array (PDA) detector. Quantitation was performed with Waters Empower 2 (version 4.0) software by the external standard calibration method. Everolimus assay in coating solutions and for DES was carried out via HPLC analysis on a Waters 2690 or 2695 Alliance Separations Module, with Waters 2487 Dual λ absorbance UV Detector, on a Waters XBridge C18 column (3 x 150 mm) with C18 bonded silica stationary phase, particle size 3.5 μm . Everolimus impurities and related substances analysis was carried out via HPLC on a Waters 2690 or 2695 Alliance Separations module, with a waters 996 or 2996 UV photo diode array (PDA) detector, on a Thermo-Hyersil-Keystone BDS column (3 x 250 mm) with C18 stationary phase, particle size 5 μm . The mobile phase consisted of water in reservoir A and acetonitrile in reservoir B. HPLC operating conditions were as follows: 1.1 mL/min flow rate at 65% A for 1min, followed by a linear gradient to 46% A over 6.5 min, continue a linear gradient to 41% A over 22.5 min. A linear gradient to 10% A over 5 min is followed by 10% A maintained for 5 min to wash the system and re-equilibration for the next injection is achieved by maintaining 65% A over 7 min following a 1 min linear gradient to 65% A. The column was maintained at 50°C. The sample injection volume was 30 μL .

Liquid chromatography mass spectrometry (LCMS) was carried out using an Agilent modular 1200 SL system with a Diode Array Detector and QToF model 6520 fitted with Electrospray ionization source. Liquid chromatography was carried out using an X-bridge C18 column, 3.5 μm particle size with 2.1 x 150mm column. Flow rate was 0.3 ml/min at 50 °C with a 10 μL injection. UV absorption detector was used to collect data at 215 nm and 277 nm. The mobile phase consisted of water in reservoir A and acetonitrile in reservoir B. HPLC operating conditions were as follows: 65% A for 1 min, followed by a linear gradient to 40% A over 4 min, followed by a 34 min hold at 40% A, then a linear gradient to 65% A over 2 min. A linear gradient to 15% A over 2 min is followed by 15% A maintained for 4 min to wash the system. Settings for the QToF detector are listed in Table 4, and MassHunter© software was used for data analysis.

Chapter 2

Table 4 Mass spectroscopic settings for QToF.

Parameter	Setting
Ionisation Mode	Positive
Fragmentor Voltage	150 V
Skimmer Voltage	65 V
Oct 1 RF Vpp	750 V
V Cap	4000 V
Gas Temp	350 °C
Drying Gas	10 L / min
Nebuliser	40 psig
Mass Range	30-1500 m/z
Rate	1 spectra / s
Time	1000 ms / spectra
Reference Mass (1)	149.02332
Reference Mass (2)	922.00980

Gas chromatography mass spectrometry analysis was carried out using an Agilent 6890N GC with a 5975 series MS detector. Quantification was performed using Agilent's MSD ChemStation software. The chromatography column was a HP-INNOWax capillary with polyethylene glycol stationary phase (60 m long, with 0.25 mm bore and 0.5 μ m stationary phase). Direct solvent injections of 1 μ L using an auto syringe were added in split mode, injector temperature was 240 °C with a split ratio of 50:1. Carrier gas was helium in constant flow at 1mL/min. Gas outlet from the GC column was to the MSD through a transfer line set at 250 °C. Total run time was 29 min, starting at a temperature of 40°C, with a 5°C/min ramp rate up to 80 °C followed by a 10°C/min ramp rate up to 40 °C and a 5 minute final hold time. The detector ionisation setting was 70 eV, and the resultant spectra were compared to an NIST reference library.

Gel permeation chromatography (GPC) was used to measure paclitaxel and PLA content in the coating solutions on a Waters 2695 LC with refractive index detector (Waters 410). Two PLgel 5 μ m mini-mixed-D columns (250 mm long x 4.6 mm diameter) were used in series, at 25 °C. Mobile phase was tetrahydrofuran at a flow rate of 0.3 mL/min, with an overall run time of 23 minutes. Quantification was performed with Waters Empower 2 (version 4.0) software by the external standard calibration method

Chapter 2

Distillation of Acetonitrile was carried out in two ways. Quick distillation using a Buchi R-210, rotary evaporator at 50 °C was used to distil relatively large quantities, 5 litres, at a time. Fractionation distillation using a 600 mm Vigreux column was used to achieve higher levels of acetonitrile purity.

2.2.2 Reagents

Organic solvents used for liquid chromatography were LiChrosolv® grade (Merck); other chemicals used Sodium Azide (Fluka); Potassium Dihydrogen Phosphate, ACS reagent puriss grade (Sigma Aldrich); Butylated Hydroxy Toluene (BHT) GC grade, (Aldrich); Everolimus (Certican®, Novartis Corporation, Switzerland) and SST2 mixture (Novartis Corporation); Propionitrile (Fluka); Sodium Hydroxide (BDH); Ammonium Hydroxide (Fluka).

2.2.3 Experimental procedure

Two planned experiments were carried out using design of experiment (DoE), referred to here as DoE#1 and DoE#2. These experiments were designed and analysed using the commercially available software Design-Expert® from Stat-Ease Inc. (Minneapolis, MN, USA).

Six (6) factors were chosen for evaluation in DoE#1; these are listed in Table 5. DoE#1 was a response surface type study with a central composite design, in total 29 everolimus solutions were made up in vendor A's acetonitrile to a concentration of 500 µg/mL, each of the 29 solutions had varying concentrations of the 6 factors listed in Table 5. Table 6 lists the experimental conditions for the 29 solutions. The order of the experiment was fully randomised; the preparation and analysis followed this random run order listed in the run order column of Table 6. Analysis of the solutions for degradation products of everolimus was carried out by HPLC.

Table 5 Experimental inputs for DoE#1

Factor	Name	Units	Factor type	1.565	1	0	-1	-1.565
A	Hydrochloric acid	ppm	Numeric	0.5	0.41	0.25	0.09	0
B	Sodium hydroxide	ppm	Numeric	0.5	0.41	0.25	0.09	0
C	Ammonium hydroxide	ppm	Numeric	30	24.6	15	5.4	0
D	Acetic acid	ppm	Numeric	30	24.6	15	5.4	0
E	Water	ppm	Numeric	1000	819	500	181	0
F	Propionitrile	ppm	Numeric	1000	819	500	181	0

Chapter 2

Table 6 DoE#1 experimental runs

Study order	Run order	A	B	C	D	E	F
26	1	0	0	0	0	1.565	0
5	2	-1	1	-1	1	1	1
24	3	0	0	0	1.565	0	0
20	4	0	1.565	0	0	0	0
17	5	-1.565	0	0	0	0	0
14	6	-1	-1	1	1	1	1
4	7	1	-1	1	-1	1	1
12	8	1	-1	-1	-1	1	-1
13	9	-1	-1	-1	1	1	-1
7	10	-1	1	1	-1	-1	-1
29	11	0	0	0	0	0	0
6	12	1	-1	1	1	-1	1
2	13	1	1	1	-1	1	-1
27	14	0	0	0	0	0	-1.565
9	15	1	-1	-1	1	-1	-1
19	16	0	-1.565	0	0	0	0
8	17	1	1	-1	-1	1	1
11	18	-1	1	-1	-1	-1	1
16	19	-1	-1	-1	-1	-1	-1
21	20	0	0	-1.565	0	0	0
10	21	-1	-1	1	-1	-1	1
28	22	0	0	0	0	0	1.565
3	23	1	1	-1	1	-1	1
23	24	0	0	0	-1.565	0	0
22	25	0	0	1.565	0	0	0
18	26	1.565	0	0	0	0	0
25	27	0	0	0	0	-1.565	0
1	28	1	1	1	1	-1	-1
15	29	-1	1	1	1	1	-1

Four (4) factors were chosen for evaluation in DoE#2; these are listed in Table 7. DoE#2 was a response surface type study with a D-optimal design, in total 24 everolimus solutions were made up in acetonitrile to a concentration of 5µg/mL, each of the 24 solutions had varying concentrations of base and propionitrile, in two vendor's solvents, B and C, using either strong or weak base. The experimental factors and the levels chosen are listed in Table 7. Vendor C's solvent was classed as 'good' acetonitrile as everolimus does not degrade in it, vendor B's solvent was classed as 'bad' solvent as it caused the degradation of everolimus. Table 8 lists the experimental conditions for the 24 solutions. The order of the experiment was fully randomised; the preparation and analysis followed this random run order listed in the run order column of Table 8. Analysis of the solutions for degradation products of everolimus was carried out by HPLC.

Chapter 2

Table 7 DoE#2 experimental inputs

Factor	Name	Factor type	-1	-0.5	0	0.5	1
A	Base strength	Numeric (ppm)	0	12.5 (NaOH) & 125 (NH ₄ OH)	25 (NaOH) & 250 (NH ₄ OH)	37.5 (NaOH) & 375 (NH ₄ OH)	50 (NaOH) & 500 (NH ₄ OH)
B	Propionitrile	Numeric (ppm)	0	500	1000.00	1500	2000
C	Base type	Categoric	NaOH	-	-	-	NH ₄ OH
D	Solvent	Categoric	Vendor C	-	-	-	Vendor B

Table 8 DoE#2 experimental runs

Study order	Run order	A:Base strength	B:Propionitrile	C:Base type	D:Solvent Vendor
17	1	1	-1	{ 1 }	{ -1 }
13	2	-1	-1	{ 1 }	{ 1 }
23	3	-1	0	{ -1 }	{ -1 }
2	4	1	0	{ 1 }	{ 1 }
14	5	-1	1	{ -1 }	{ -1 }
16	6	0	1	{ 1 }	{ 1 }
9	7	1	1	{ 1 }	{ 1 }
8	8	1	0	{ -1 }	{ 1 }
15	9	-0.5	1	{ 1 }	{ -1 }
10	10	1	-0.5	{ 1 }	{ 1 }
4	11	0	-1	{ 1 }	{ 1 }
1	12	1	-1	{ 1 }	{ -1 }
22	13	-1	-1	{ -1 }	{ -1 }
7	14	1	0	{ -1 }	{ -1 }
24	15	0.5	-0.5	{ 1 }	{ -1 }
3	16	0	0	{ -1 }	{ -1 }
5	17	-1	-1	{ 1 }	{ 1 }
19	18	1	1	{ -1 }	{ 1 }
21	19	-1	-1	{ -1 }	{ 1 }
11	20	0	1	{ 1 }	{ 1 }
12	21	0.5	-1	{ -1 }	{ 1 }
18	22	0	-0.5	{ -1 }	{ -1 }
20	23	-1	1	{ -1 }	{ -1 }
6	24	-1	0	{ -1 }	{ -1 }

2.3 Near infra-red spectroscopy analysis of DES coating solutions

2.3.1 Instrumentation

Spectrometry. NIR Spectra were collected in transmission mode using a Bruker Multi-Purpose Analyser (MPA) Fourier Transform Near Infra-Red Spectrometer, with an InGaAs detector in the spectral range 12,800 – 4,000 cm⁻¹. The acquisition and

Chapter 2

deciphering of the FT-NIR spectra was performed using Bruker's OPUS™ software package. Everolimus coating solutions were placed in 7 mm borosilicate disposable vials supplied by Bruker optics. Paclitaxel coating solutions were placed in borosilicate vials with an 18 mm path length. The resolution used was 4cm^{-1} .

Chromatography. Quantitation was performed with Waters Empower 2 (version 4.0) software by the external standard calibration method. Paclitaxel and PLA Gel Permeation Chromatography (GPC) assay was carried out on a Waters 2690 or 2695 Alliance separations module, with a Waters 2410 refractive index detector. Two columns in series, PLgel (4.6×250 mm) Mini-Mixed-D stationary phase, with particle size of $5 \mu\text{m}$. Mobile phase was 100% HPLC grade tetrahydrofuran.

Water analysis. Karl Fischer titrimetric analysis was carried out using a Metrohm 756 KF Coulometer.

Gravimetry. For the preparation of coating solutions in the laboratory a Mettler Toledo AX 205 analytical balance, with 4 places of decimal accuracy, was used.

2.3.2 Reagents

Everolimus Certican®, Novartis Corporation, Switzerland, PVDF-HFP with a ratio 85:15 PVDF:HFP from Solvay Mw 600,000 Da, PBMA from Aldrich (USA) Mw 337,000 Da. Acetone, analytical grade from Burdock and Jackson or Sigma/Aldrich. Cyclohexanone, analytical grade from Burdock and Jackson or Sigma/Aldrich.

Paclitaxel from Indena® (Milan, Italy), Poly (DL-lactide) (PLA) from Boehringer-Ingelheim (Germany) Resomer® R 202 S, n-Butyl Acetate from Burdock and Jackson.

Water was from Fisher Scientific or equivalent grade from a Milli-Q water purification system with resistivity $> 5 \text{M}\Omega\text{cm}$. Acetonitrile, HPLC Grade, Fisher Scientific. Potassium dihydrogen phosphate (KH_2PO_4), Sigma/Aldrich, ACS grade. Hydranal Coulomat AK reagent for KF in ketones (anolyte solution), and Hydranal Coulomat AK reagent for KF in ketones (catholyte solution).

Chapter 2

2.3.3 Preparation of coating solutions

Coating solutions were formulated gravimetrically by weighing out each component individually, and then mixing. Everolimus coating solutions contained varied levels of everolimus, PVDF-HFP, acetone, and cyclohexanone, and paclitaxel containing coating solutions contained varied levels of paclitaxel, PLA, and n-butyl acetate (nBA). The normal concentration for the everolimus coating solutions is 0.41% w/w everolimus, 2.00% w/w PVDF-HFP, 68.3% w/w acetone, and 29.3% w/w cyclohexanone. The normal concentration for the paclitaxel coating solution is 1.93% w/w for both paclitaxel and PLA, and 96.14% w/w nBA. The resulting solutions were agitated on an orbital shaker until all the solid constituents had dissolved. Laboratory scale coating solutions were made up to a total mass of 20, 50 or 100 g. Process solutions total mass were in the order of 2 or 4 kg for everolimus containing formulations and approximately 100 g for paclitaxel containing formulations. Samples were analysed within 24 hours and then stored between 2 – 8 °C in a dark refrigerator. Where re-analysis was carried out on the samples, they were brought to ambient temperature prior to analysis.

The calibration sets were created from a mixture of laboratory prepared formulations and from batches sourced directly from the manufacturing floor. Fortunately, the development of the calibration sets coincided with the R&D phase for both the PROMUS everolimus-eluting stent and a non-commercialized paclitaxel-eluting stents. At this early stage in the development cycle of a DES device several different combinations of the drug, polymer and solvents were still being explored to better understand the design and process, and this generated a wide range of formulation concentrations for NIR assessment. This provided a wider concentration range of manufacturing batches than would be normal for a commercial product. However, the range of concentrations from these batches was not ideal for building complete calibrations, thus supplementation of the manufacturing batches was achieved by formulating additional samples in the laboratory using a scaled down version of the manufacturing process.

The calibration sets were formulated according to an experimental design created in the OPUS software. This feature of the software creates a mixture DoE where the components in each solution add up to 100%. To create the calibration design a range of concentrations was selected for each constituent, this range was centred on the

Chapter 2

concentrations required for the normal process. The calibrated range is wider than the range of concentrations expected of the tests samples. As such, robustness of the calibration model for component values lying at the limits of accepted process tolerances is assured. This is crucial, so that a reliable analysis of failing batches from the manufacturing process is attained.

The advantage of incorporating a synthetic set of samples allows for creation of an even distribution of concentration over the concentration range. It is not good practice to incorporate samples into the calibration data set if the concentration lies significantly outside the normal range as this can lead to unreliable analysis[95]. In addition to this even concentration distribution within the normal range, it is also important that co-linearity of the individual component concentrations is avoided[95]. Co-linearity means that the concentrations of the individual components increase or decrease equally across the samples. In this situation the multivariate analysis may be unable to assign the individual spectral bands accurately to the respective component values. Therefore, through the DoE calibration design format, co-linearity between components of the coating solutions used in the calibration set may be avoided. The following tables list the mass of the individual components used in the calibration designs.

Table 9 Laboratory calibration samples for everolimus coating solutions, without water. The measurement error for each of the components is $\pm 0.005\%$ w/w.

Sample Number	everolimus (%w/w)	PVDF-HFP (%w/w)	Acetone (%w/w)	Cyclohexanone (%w/w)
1	0.36	2.09	66.68	30.87
2	0.62	2.25	67.35	29.78
3	0.17	2.42	67.65	29.76
4	0.11	1.56	72.11	26.22
5	0.23	2.31	64.30	33.16
6	0.39	1.85	68.73	29.03
7	0.41	1.61	65.40	32.59
8	0.53	1.55	70.55	27.36
9	0.43	1.58	72.64	25.35
10	0.63	2.49	64.00	32.88
11	0.12	1.89	68.07	29.92
12	0.47	2.47	69.69	27.37
13	0.25	1.99	68.03	29.73
14	0.68	1.92	64.82	32.59
15	0.15	2.41	70.80	26.64

Chapter 2

Table 10 Laboratory calibration samples for everolimus coating solutions with water. The measurement error for each of the components is $\pm 0.005\%$ w/w.

Sample No.	everolimus (%w/w)	PVDF-HFP(%w/w)	Water (%w/v)	Acetone (%w/w)	Cyclohexanone (%w/w)
1	0.27	2.44	0.39	67.23	29.88
2	0.29	2.02	0.45	69.95	27.48
3	0.42	1.90	0.47	69.72	27.67
4	0.50	1.57	0.28	68.24	29.63
5	0.42	2.15	0.32	67.11	30.22
6	0.31	2.38	0.29	69.90	27.35
7	0.47	2.43	0.34	66.77	30.20
8	0.36	1.80	0.37	68.40	29.25
9	0.50	1.93	0.47	69.96	27.32
10	0.43	1.62	0.45	68.89	28.80
11	0.40	2.16	0.50	68.82	28.30
12	0.41	2.26	0.41	67.87	29.26
13	0.31	2.18	0.38	66.51	30.82
14	0.47	1.73	0.24	68.93	28.86
15	0.45	2.41	0.36	67.06	29.91
16	0.45	1.77	0.45	69.33	28.21
17	0.35	1.99	0.30	69.80	27.77
18	0.43	2.04	0.24	68.32	29.20
19	0.42	2.41	0.49	67.39	29.48
20	0.52	1.73	0.42	66.80	30.71

Table 11 Summary table of the 69 process calibration samples for everolimus coating solutions. The measurement error for each of the components is $\pm 0.005\%$ w/w.

Number of samples	everolimus (%w/w)	PVDF-HFP (%w/w)	Acetone (%w/w)	Cyclohexanone (%w/w)
69	Min = 0.397	Min = 1.992	Min = 68.23	Min = 29.17
	Max = 0.409	Max = 2.006	Max = 68.42	Max = 29.35
	Mean= 0.407	Mean =1.999	Mean =68.32	Mean = 29.27

Chapter 2

Table 12 Laboratory (1-25) and process 26- 30 calibration samples for paclitaxel coating solutions. The measurement error for each of the components is $\pm 0.005\%$ w/w.

Sample Number	Paclitaxel (%w/w)	D,L-PLA (%w/w)	n-butyl acetate (%w/w)	%w/w Water
1	1.91	1.60	96.44	0.05
2	1.18	1.04	97.74	0.04
3	1.66	1.78	96.51	0.06
4	2.20	2.41	95.33	0.05
5	2.10	1.09	96.74	0.07
6	1.48	1.34	97.13	0.05
7	1.27	1.60	97.07	0.06
8	1.90	2.24	95.80	0.06
9	1.49	2.31	96.14	0.05
10	1.73	1.12	97.08	0.07
11	2.46	2.23	95.25	0.06
12	1.95	1.75	96.25	0.05
13	2.37	2.15	95.43	0.05
14	2.23	2.11	95.61	0.05
15	1.67	1.57	96.71	0.05
16	1.03	1.04	97.44	0.25
17	1.78	1.76	95.88	0.30
18	2.43	2.39	94.96	0.13
19	1.11	1.11	97.38	0.22
20	2.35	2.33	95.00	0.21
21	1.14	1.03	97.25	0.35
22	1.66	1.76	95.77	0.52
23	2.19	2.39	94.84	0.49
24	2.06	1.12	96.31	0.37
25	2.46	2.35	94.93	0.23
26	1.86	1.84	96.30	0.24
27	1.92	1.92	96.15	0.21
28	1.93	1.93	96.15	0.13
29	1.73	2.13	96.14	0.22
30	2.12	1.74	96.14	0.22

2.3.4 Spectra collection

Each solution was scanned using an FT-NIR spectrometer 3 or 5 times for everolimus and paclitaxel coating solutions, respectively. Borosilicate glass vials of 7 mm (obtained from Bruker Optics) in diameter were used for the everolimus samples, and borosilicate glass vials of 18 mm in diameter were used for paclitaxel. Vials were filled using a Pasteur pipette and capped to make airtight immediately. An ambient air spectrum was used as a background measurement. For NIR, the water vapour in the air can generate an appreciable signal in the spectrum. In the region of approximately 7,500

Chapter 2

- $6,700\text{ cm}^{-1}$ and $5,800 - 5,000\text{ cm}^{-1}$ sharp spectral structures associated with the humidity are visible in the spectrum gathered in ambient air[103], Figure 43. Background measurements were taken at least every day to compensate for any ambient influences in the test environment or the equipment, but where analysis stretched over a long period of the day a background was collected every hour. Coating solutions for individual components with higher concentrations were also scanned to help identify spectral features associated with these compounds; in these cases a solvent background was collected in addition to ambient air.

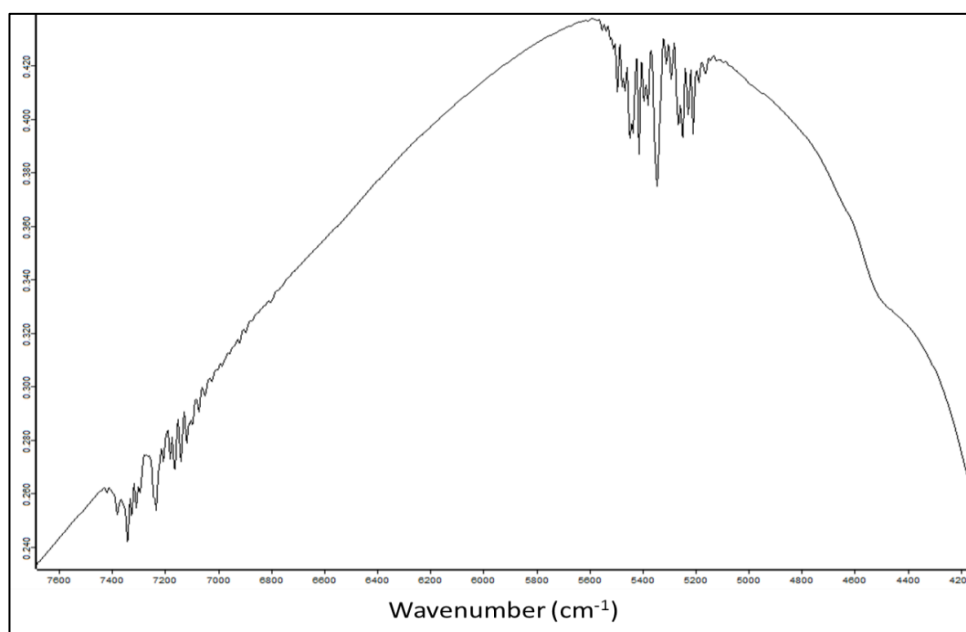


Figure 43 NIR spectrum of ambient air showing sharp features associated with humidity.

Chapter 3

The development of in vitro clinically relevant methods for the assessment of percutaneous transcatheter angioplasty devices for particulate matter from extrinsic and intrinsic sources.

3 Introduction

The FDA has asked SDS and plain old balloon angioplasty (POBA) manufacturers to simulate the clinical use of their devices and measure the particulate matter that is released[10], [37]. This is not an easy request to fulfil, as the use of these device types involves a complicated clinical procedure. Current standards provide only limited guidance for particulate testing of medical devices, primarily because of the sheer number of different medical devices available. Standards that are in existence deal with uncomplicated devices, and the particulate assessment consists of simple flushes or immersion in water. For example, one medical device manufacturer, Boston Scientific, has historically used the simple 2-beaker product cleanliness method described in section 2.1.2.1 to measure particle contamination on their devices. However, particulate matter that may be removed from medical devices using the 2-beaker method may not adequately reflect particulate matter removal during actual use in a percutaneous procedure. A method similar to the 2 beaker method was thus developed at the outset of this thesis work, by incorporation of a simulated artery tracking fixture through which the device is preconditioned before use; the simulated use beaker method (section 0). This method was used for an interim period in Boston Scientific until better test methods could be developed. The design and development of the improved methods using bespoke equipment and validation of the new methods are described in greater detail in Appendix 1.

The sequence in which the closed loop particulate (CLP) and dual loop particulate (DLP) apparatuses were developed reflects the changes in regulatory landscape that has occurred between 2004 and 2012. The CLP apparatus was first developed in response

Chapter 3

to a requirement for a more accurate and repeatable method than the beaker style methods. Subsequently whilst the basic principle of the CLP apparatus remained the same the arterial models and simulated use steps changed in response to more detailed regulatory requirements. These changes involved introduction of the ASTM F2394 arterial model, the constrained deployment of stents in a tube and their overexpansion, and introduction of a baseline test that evaluates the unconstrained deployment of stents without tracking them first. Requirements for particulate matter evaluation from stent delivery systems were recently modified when the FDA added a requirement for the counting of particles $\geq 50 \mu\text{m}$, which necessitated a change in the CLP apparatus design. The DLP apparatus, evaluated in prototype form at the outset, was re-visited in response to these changing requirements. The final DLP system presented here permits the counting of particles $\geq 50 \mu\text{m}$, but also has improved upon other aspects of the earlier CLP apparatus. Throughout this development process the understanding of factors that impact particulate matter release from medical devices has grown and opportunities to improve device performance in this regard have been implemented where appropriate.

3.1 Simulated use procedures

Since the initial development of the CLP apparatus and the more recent DLP apparatus, several simulated use procedures have been used to support product approval submissions by Boston Scientific. Initially, procedures were discussed through one-to-one communications with regulatory bodies. In general, simulated use conditions have become more complex over time under request of the regulatory agencies and these requests have in the main come from the FDA. Specific guidance on these simulated use procedures has now been provided by the FDA for DES and other SDS devices[10], [37]. Relevant excerpts from these guidance documents are given below.

Guidance for Industry: Coronary Drug-Eluting Stents— Nonclinical and Clinical Studies [37].

“FDA recommends measurement of particulate matter generated by breakdown of the coating or from the stent platform, stent delivery system, and product packaging both at release and after aging. Particulate matter testing serves multiple purposes: (1) it provides an indirect evaluation of the coating integrity of the finished product and (2) it

Chapter 3

establishes the number of particles that can potentially be introduced systemically using the stent system. FDA believes that the main purpose in particulate matter testing for DESs is to provide a level of assurance of patient safety in terms of total particulate matter introduced into the bloodstream. Therefore, since the concern applies to the total number of particles released into the bloodstream, the test should apply to the entire stent delivery system, not just the stent.”

“Simulated use (e.g., during tracking and deployment):.....This testing should be performed with use of an in vitro model....It is recommended that deployment be simulated in an in vitro model intended to mimic in vivo physiologic and anatomic conditions (e.g., tortuous path, aqueous environment). The stent should be in direct contact with the simulated vessel without the use of other coatings, lubricants, sheaths, or protective wraps between the stent and simulated vessel.....Note that physiologically relevant worst-case conditions should be applied. To ensure measurement of the total number of particles that could be potentially introduced into the bloodstream, the stent delivery system should be inserted into the test fixture to the point at which it would be inserted in clinical use.....This testing should involve expansion of the stent to the maximum diameter allowed.....In the event that an accessory device (e.g., embolic protection, atherectomy) is intended to be used in conjunction with a DES, the sponsor should provide appropriate supportive engineering performance test data to ensure that the integrity of the coating is maintained.”

Non-Clinical Engineering Tests and Recommended Labelling for Intravascular Stents and Associated Delivery Systems [10].

“We recommend using an in vitro model intended to mimic in vivo physiologic and anatomic worst-case conditions (e.g., tortuous path, aqueous environment) to evaluate particulates. For coronary indications, FDA recommends the tortuous path described by Figure X2.4 of ASTM F239412. If you expect your stents may be deployed in an overlapped configuration during clinical procedures, we recommend that you measure particulates generated during deployment of two overlapping stents in a mock vessel. For coronary stents, the mock vessel should be bent to a clinically relevant radius of curvature as.....Additionally, any accessory devices required for the placement of the product should be used in this evaluation. The total number of particulates including those from the stent, delivery system, and accessory devices should be reported in each

Chapter 3

of three size ranges: $\geq 10\mu\text{m}$, $\geq 25\mu\text{m}$, and at the largest size for which validation yields $\geq 75\%$ recovery. At a minimum, the largest size should be $\geq 50\mu\text{m}$. Appropriate precautions should be implemented to ensure that the particles are suspended during sampling for particle counting and sizing to minimize artefacts from the test system.”

The purpose of this guidance from the FDA is to create a particulate matter profile of the candidate product[10]. This profile is intended to evaluate how the product might perform under physiological conditions and through interaction with ancillary devices used during a clinical procedure. Three methods have been developed, and described in this thesis, to construct this profile for a DES. These are the baseline, regulatory simulated use (RSU), and characterisation simulated use (CSU) test methods.

3.2 Results and Discussion

3.2.1 Particulate matter profile for DES

As an example of the application of the methods developed, a particulate matter profile of a DES device, currently under development in Boston Scientific, was created and is presented in the following sections. The stent has a biodegradable polymer and everolimus coating and a polyethylene oxide (PEO) and neopentyl glycol diacrylate (NPG) based hydrophilic catheter coating. To examine the validity of the Baseline and RSU methods 80 devices were tested. The devices tested included 10 each from 8 batches of different size stent, ranging from 2.25 to 4.0 mm in diameter and 8 to 38mm in length. For evaluation of the CSU method 120 devices were tested, with 10 devices (5 pairs) each from 12 batches of different product size stent ranging from 2.25 to 4.0 mm in diameter and 8 to 38mm in length. The CSU method involves 5 different devices (2 SDS, a post dilation catheter (POBA), a guide wire, and a guide catheter). The results from the particulate matter in Figure 44 clearly show that the number of particles created using the average of the size categories, from this DES device, during stent deployment without pre-conditioning or interaction with other devices (Baseline) is relatively small when compared to the number of particles created through tracking alone (RSU), or the number of particles from a complete simulated procedure (CSU), described in chapter 2.

Chapter 3

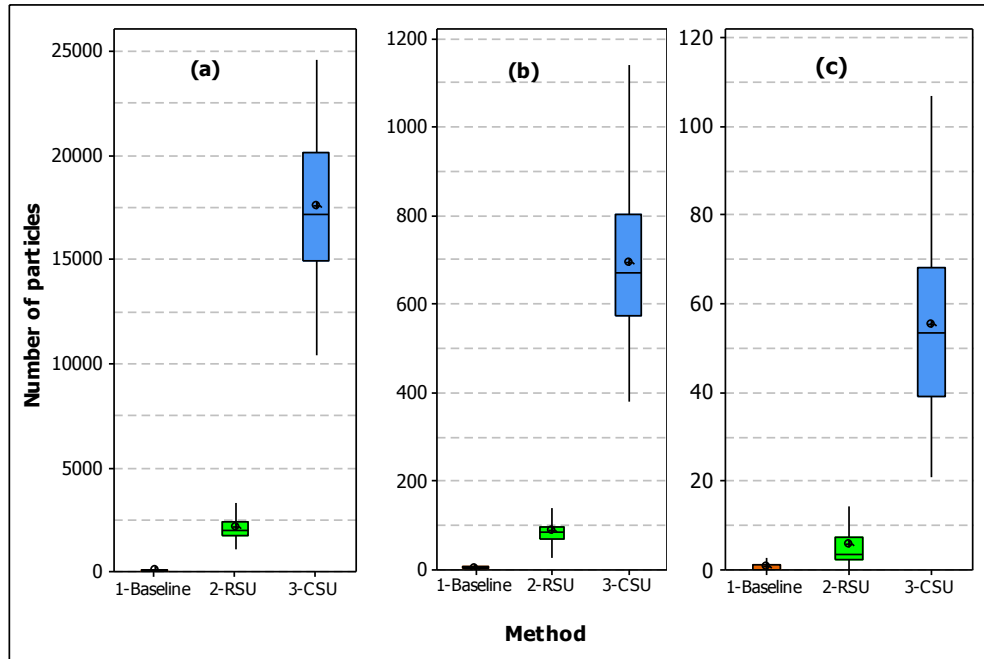


Figure 44 The number of particles of (a) $\geq 10 \mu\text{m}$, (b) $\geq 25 \mu\text{m}$ and (c) $\geq 50 \mu\text{m}$ created from a DES device during stent deployment without pre-conditioning or interaction with other devices (Baseline) compared to the number of particles created through tracking alone (RSU), and the number of particles from a complete simulated procedure (CSU).[†]

To better understand the origin of the particulate matter, released during CSU, the results from this method are expanded upon in Figure 45, Figure 46, and Figure 47, by plotting cumulative particle counts (A) and the differential particle counts (B) across the seven steps of the CSU method. It is evident that every step contributes some particles. The number of particles from stent deployment, constrained in a silicone tube, after tracking (measurement 3) is relatively low compared to other steps. Although the particle counts are marginally higher than those seen during the baseline method, this

[†] Box and whisker plots of this format are used throughout this chapter. These provide a graphical summary of the distribution of a sample that shows its shape, central tendency, and variability. The upper whisker extends to the maximum data point within 1.5 box heights from the top of the box. The lower whisker extends to the minimum data point within 1.5 box heights from the bottom of the box. The interquartile range box represents the middle 50% of the data. The top line (third quartile) marks where 75% of the data are less than or equal to this value. The middle line (median) marks where 50% of the data are less than or equal to this value. The bottom line (first quartile) marks where 25% of the data are less than or equal to this value. The symbol representing the mean value is represented by a circle enclosing a cross.

Chapter 3

indicates that the stent coating is not prone to significant particle formation after tracking and during constrained deployment.

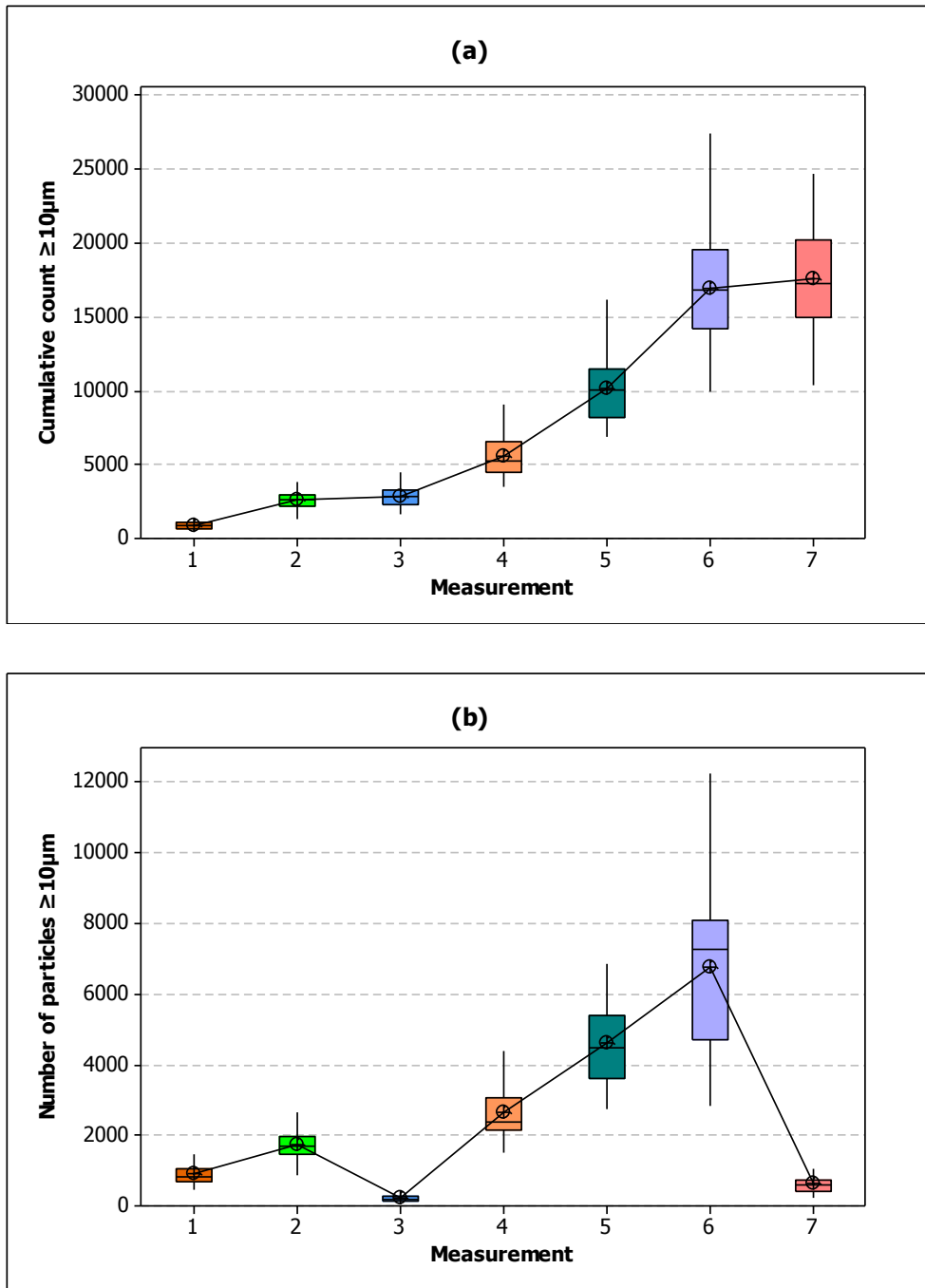


Figure 45 Plot of the $\geq 10 \mu\text{m}$ cumulative particle counts (a) and the differential particle counts (b) across the seven steps of the CSU method.

Chapter 3

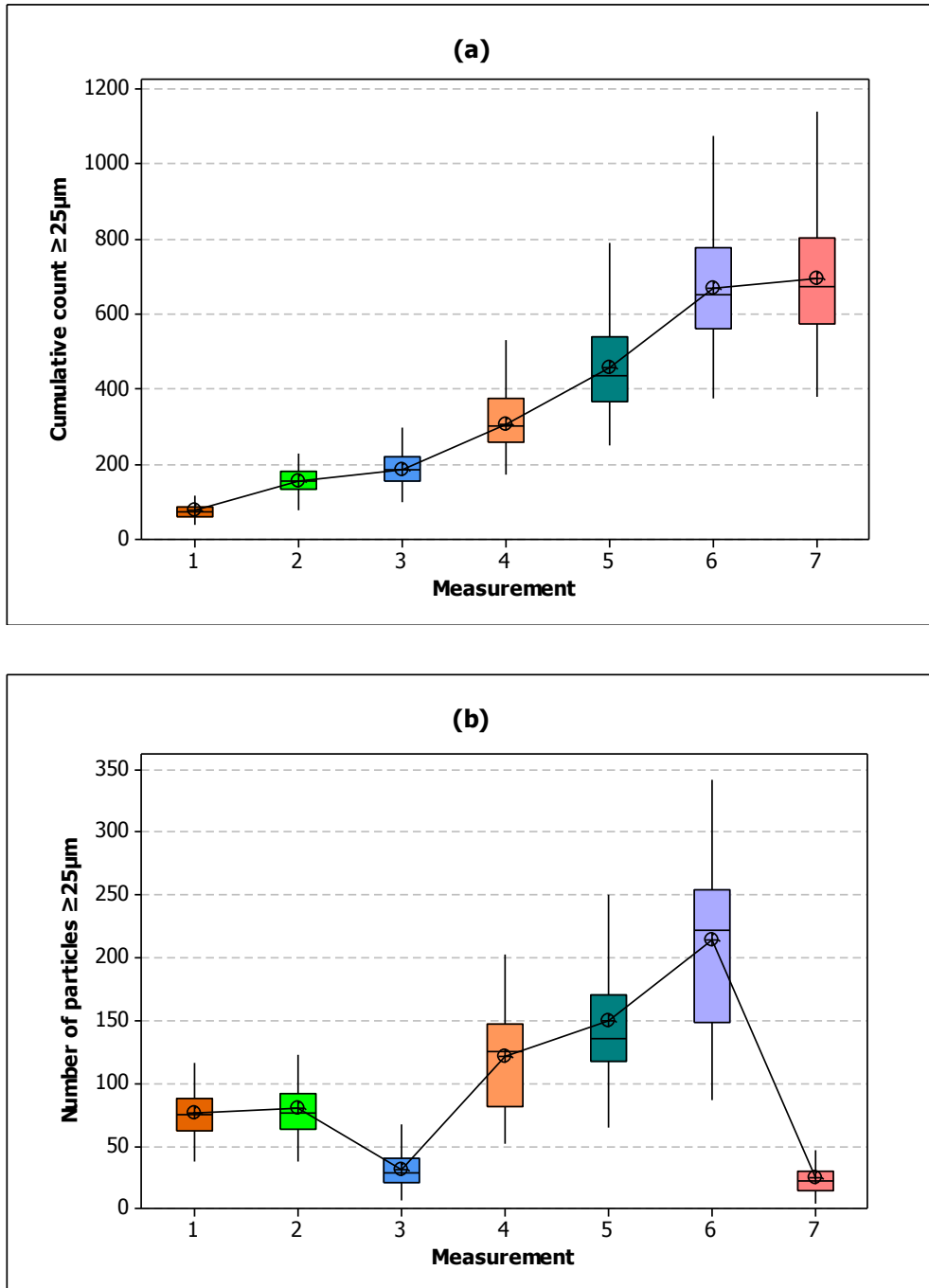


Figure 46 Plot of the $\geq 25 \mu\text{m}$ cumulative particle counts (a) and the differential particle counts (b) across the seven steps of the CSU method.

Chapter 3

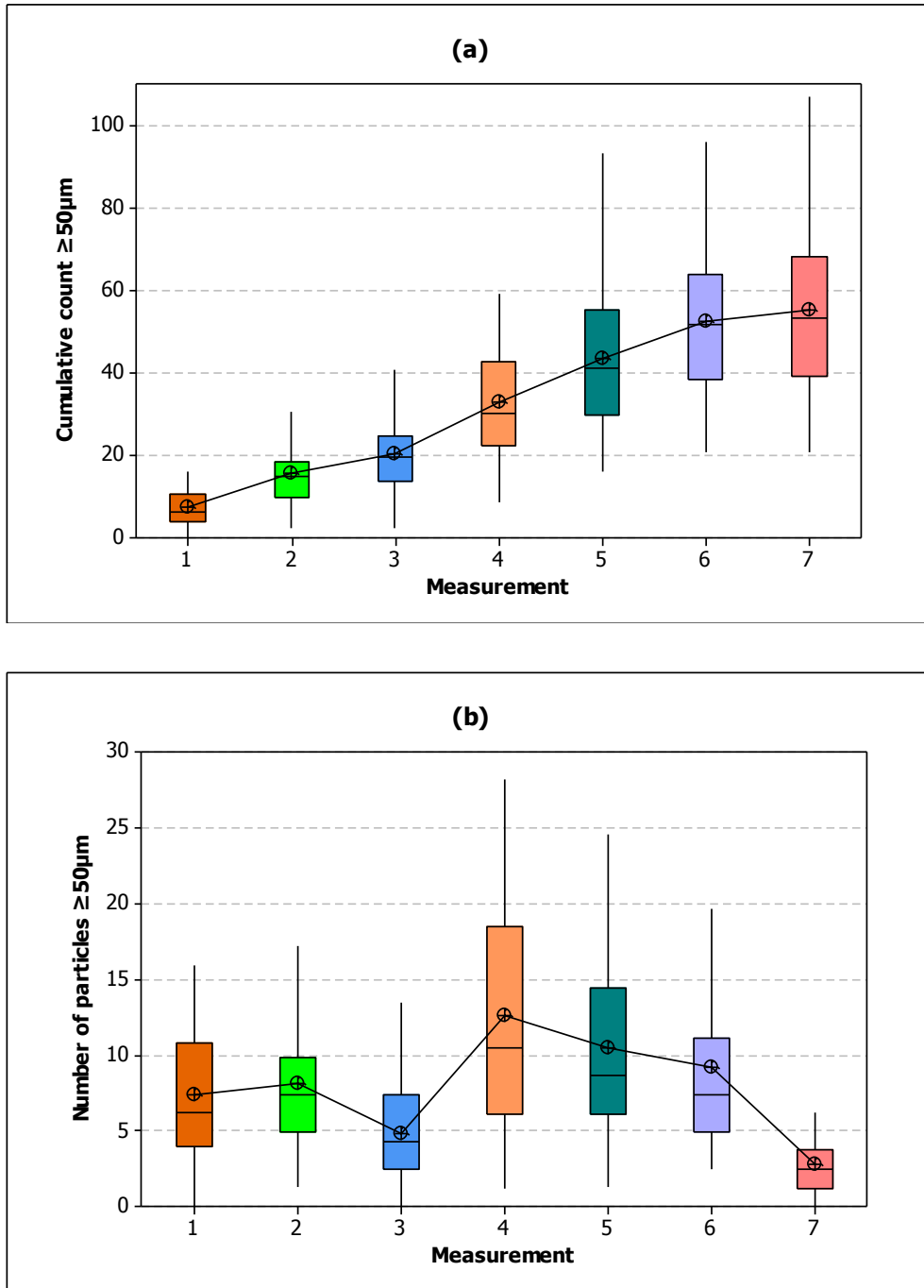


Figure 47 Plot of the $\geq 50 \mu\text{m}$ cumulative particle counts (a) and the differential particle counts (b) across the seven steps of the CSU method.

Chapter 3

The tracking, deployment and retraction of the SDSs in the CSU method contribute significantly higher particle counts than the RSU method, as shown in Figure 48 where CSU1 and CSU2, correspond to the first and second device tested, respectively. The guide wire used in the CSU test is coated with a hydrophilic polymer coating (HPC). However, the RSU test does not use a coated wire. The contribution of the HPC is suspected to account for the difference in particulate matter between methods. If this is the case, the coating on the wires is removed by successive SDSs, and the particle counts will decrease, explaining why the ≥ 25 and $50 \mu\text{m}$ particle counts are lower for the second SDS tracked on the CSU method. A second interaction between the SDS balloon and the guide catheter can occur. Following deflation of the balloon the profile is greater than before removal of the stent, thus on retraction of the SDS catheter in to the guide catheter particles may be sheared from the balloon. This effect may not be very significant for SDS balloons because no lubricious coating is applied to the balloon in order to ensure stent securement[‡]. However for POBA devices lubricious coatings are typically applied to the balloons to improve deliverability and to make lesion crossing easier. These coatings can shear off the balloon as particles upon balloon withdrawal into the guide catheter.

[‡] Dislodgment of the stent prior to deployment can result in stent embolization in the blood vessels; as such stent securement on the balloon is essential. Stents without sheaths may dislodge if they catch on tortuous anatomy, guide catheters, or other devices[10].

Chapter 3

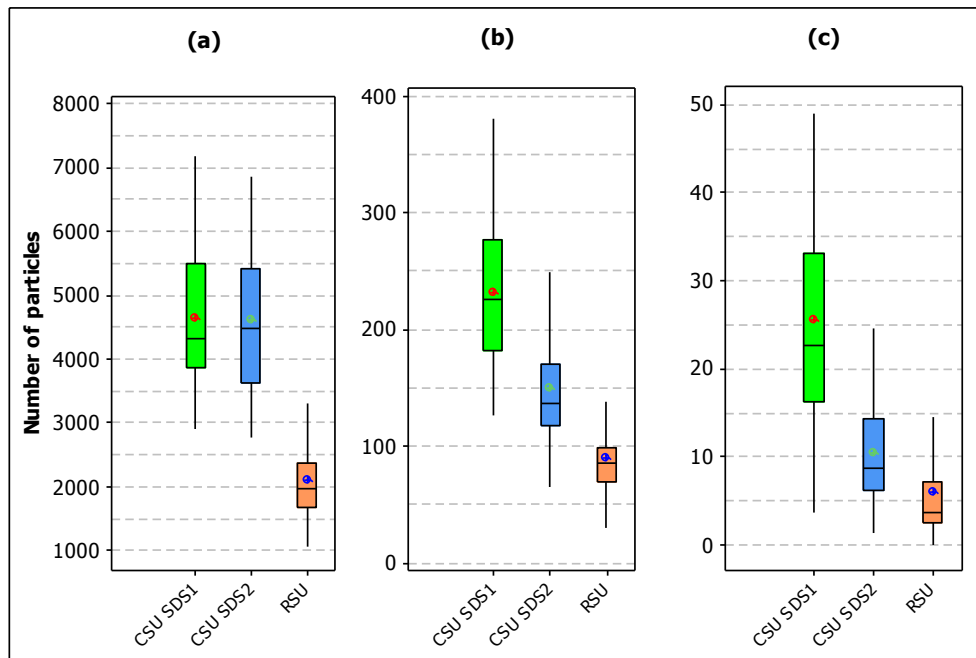


Figure 48 Shown in this figure are the particle counts for (a) $\geq 10 \mu\text{m}$, (b) $\geq 25 \mu\text{m}$ and (c) $\geq 50 \mu\text{m}$, comparing the tracking, deployment and retraction of the SDSs in the CSU method which contribute significantly higher particle counts than the RSU method. Where CSU1 and CSU2, correspond to the first and second SDS device tested, respectively.

The particulate profiling of this DES provides an indication of how the product might behave in a clinical procedure, and it also establishes a performance level by which the manufacturer can monitor the device throughout its lifecycle. Deviation from the particulate matter profile established during initial manufacture may indicate that something has changed in the manufacturing process. Manufacturers may also compare candidate products to similar approved products to help them and regulatory agencies to determine if any harmful physiological effects may be expected of the proposed new product. However, regulatory agencies may want to see improvement over existing products, so matching the performance of legacy devices may not be good enough to achieve an approval. The absence of standard procedures across the biomedical device industry at present makes it difficult to establish general acceptance criteria for particulate matter on PTCA devices, so each manufacturer proposes their own particulate matter specification on a case-by-case basis. In many instances the potential risk of creation of particles from devices may be outweighed by the beneficial effect of the design feature that creates them, such as a DES or a lubricious coating.

Ultimately, in order for the manufacturer to demonstrate device safety has to provide evidence of both a stable, repeatable manufacturing process and product stability over

Chapter 3

the expected shelf-life. The approval to carry out human clinical trials relies on in vitro particulate testing, amongst many other tests, to satisfy the approving body that the manufacturer has a stable process and product. However, as so many factors can influence particle counts, not least of which is the test method used, interpretation of the data is critical. As an example of a comparison, testing was carried out to estimate particulate matter using the RSU method released from different devices currently on the market with results displayed in Figure 49, Figure 50, and Figure 51, with Table 13 providing a key to the plots. These plots provide a snapshot of the LO defined particle counts from PTCA devices provided by different manufacturers (Boston Scientific, Medtronic, Abbot Vascular, and Biosensors) using the same test method and preconditioning technique, with however the names of the specific devices not supplied.

Apart from wire 0 and POBA 0, all of the devices tested are commercially available products. Wire 0 and POBA 0 are a nitinol wire and a dilatation balloon catheter, respectively, without any lubricious coatings. These non-coated devices are included to explore the effect of lubricious coatings on particle counts. Fewer particles are created by tracking POBA 0 over wire 0 compared to the same device tracked over wire 1 and wire 2 (rectangular dashed box). Similarly fewer particles are created by tracking POBA 1 and POBA 2 over the wire 0 compared to the same device tracked over wire 1. Whilst the particle counts from the 4 SDS devices (BMS 1 and DES 1-3) produce a wide range, it is not possible using LO alone to determine if the particles are from the coated stent or catheter. Section 2.1.3 lists some techniques used to identify the source of these particles.

Chapter 3

Table 13 A descriptive list of different devices currently on the market.

NAME	DEVICE TYPE	LUBRICOUS COATING
BMS 1	SDS with bare metal stent	Yes
DES 1	SDS with drug eluting stent	Yes
DES 2	SDS with drug eluting stent	Yes
DES 3	SDS with drug eluting stent	Yes
Wire 0	Nitinol guide wire	No
Wire 1	Interventional cardiology guide wire	Yes
Wire 2	Interventional cardiology guide wire	Yes
POBA 0	Interventional cardiology dilatation balloon catheter	No
POBA 1	Interventional cardiology dilatation balloon catheter	Yes
POBA 2	Interventional cardiology dilatation balloon catheter	Yes
POBA 3	Interventional cardiology dilatation balloon catheter	Yes
POBA 4	Interventional cardiology dilatation balloon catheter	Yes
POBA 5	Interventional cardiology dilatation balloon catheter	Yes

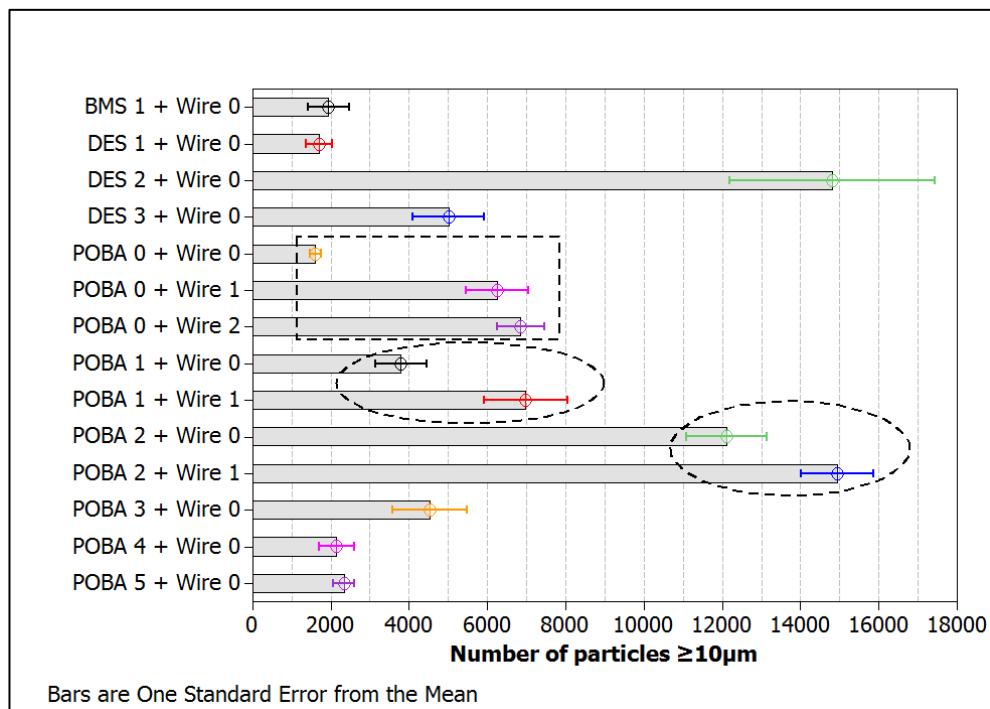


Figure 49 Comparative RSU testing, showing $\geq 10 \mu\text{m}$ particle counts, carried out to estimate particulate matter released from different devices currently on the market.

Chapter 3

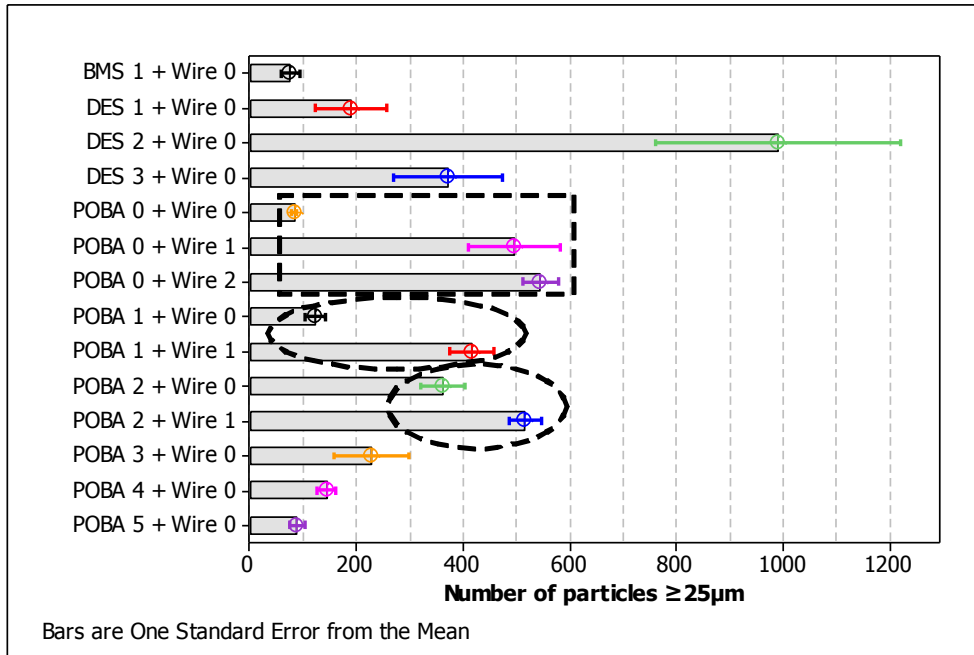


Figure 50 Comparative RSU testing, showing $\geq 25 \mu\text{m}$ particle counts, carried out to estimate particulate matter released from different devices currently on the market.

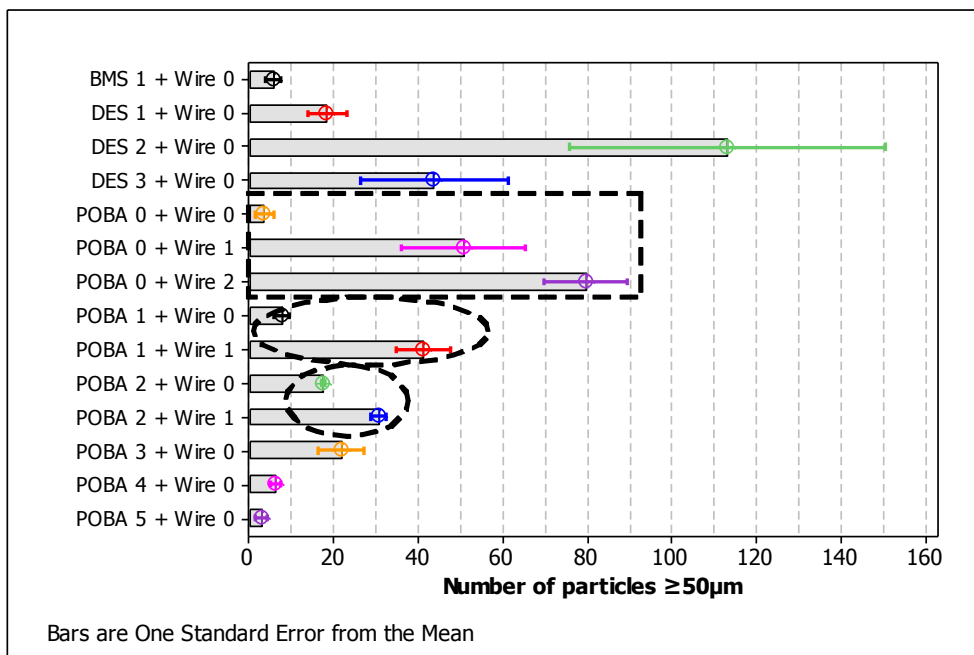


Figure 51 Comparative RSU testing, showing $\geq 50 \mu\text{m}$ particle counts, carried out to estimate particulate matter released from different devices currently on the market.

Chapter 3

The comparison of particle counts from these PTCA devices highlights the variation that exists between commercial products. Ancillary devices[§] selected to carry out the tests also play an important role. The FDA has specifically asked for commercially available ancillary devices to be used in simulated use tests[10]. Often, ancillary devices used are manufactured by other companies and, aside from the significant expense associated with acquiring these devices for testing, important information about the product design is not usually available to the testing laboratory. This can make interpretation of the data difficult. Thus, where possible, it is recommended that the same batch and age of ancillary devices should be selected for CSU testing. For example, work for this thesis has revealed that provisional testing carried out using non particle shedding ancillary devices (e.g. uncoated guide wires and guide catheters rinsed with low particulate water) have lower particle counts when compared to testing carried out with commercially available ancillary devices. Up front efforts made to determine the factors that can influence particle creation from the sample device saves time, reduces variation, and facilitates data interpretation. These factors can then be incorporated in the preconditioning steps to ensure that the test method is adequate. For the reasons outlined above, based on the data above it is recommended that test methods selected for batch release and stability testing should **not** use commercially available ancillary products, as this could mask significant changes in the test sample.

[§] Ancillary devices are devices that are used during a simulated intervention along with the test device. For example, guide catheters, guide wires, introducer sheaths, and pre- and post-dilatation catheters are ancillary devices that may be used in the delivery of DES.

3.3 Particle characterisation

The results from section 3.2.1 demonstrate that simulated use of PTCA devices results in release of particles associated with abrasion in the arterial track models, interaction with ancillary devices, and after stent deployment. The orthogonal methods of light microscopy (LM), scanning electron microscopy (SEM) and Raman micro-spectroscopy were examined in this section to better elucidate the identity and source of these particles.

3.3.1 Stent coatings

The function of the drug carriers used in DES is to bind the drug to the stent and control its release. These carriers can be made from indurate polymers such as PVDF-HFP and PBMA used in the PROMUS and Xience V products, friable phosphorylcholine (PC) containing coatings used in the Endeavor Sprint product, or biodegradable polymer coatings such as poly lactic acid (PLA) used in the Biomatrix product. In this section LO test results are presented for these types of coated stents. It will be shown that clearly different particle counts are associated with procedural steps involving stent deployment for each product. For example, stents coated with indurate polymers and biodegradable polymers released significantly fewer particles than PC coated devices and that exposure to elevated humidity and temperature of biodegradable coatings outside their hermetically sealed packaging resulted in increased particle counts for these products. Variation in stent surface pre-treatments also contributes to increased stent coating particle formation from PLGA coated stents.

To explore the particle counts, and their characterisation, released from a range of DES with indurate polymer coatings, TAXUS (Boston Scientific) and CYPHER (Johnson & Johnson), were tested alongside a PC coated stent, ENDEAVOUR SPRINT (Medtronic), and its uncoated bare metal stent (BMS) version, DRIVER (Medtronic), on the CLP apparatus. The devices were tracked once through the curved section of the arterial model, a measurement was taken at this point, and then the stent was deployed to rated burst pressure (RBP) unconstrained followed by a second measurement. The SDS tracking and deployment particle counts for each DES are shown in Figure 52.

The particle count for tracking and deploying the PC coated stent are much greater than for the stents coated with indurate polymers and the DRIVER BMS. LO does not allow for differentiation of catheter derived particles from stent coating particles; however the

Chapter 3

number of particles associated with stent deployment of the ENDEAVOUR SPRINT DES would indicate that coating particles have been created. The deployed stents were analysed after the test using SEM to examine the integrity of the stent coating remaining. Images of the deployed TAXUS and ENDEAVOUR DES are shown in Figure 53 and Figure 54, respectively. Whilst the TAXUS stents do show some coating displacement, there is no evidence of coating removal as particles because the coating covers the entire stent surface. The ENDEAVOUR stents showed evidence of coating removal on the inner (a) and outer surfaces (b) of the stent. Stent coating removal from the outer walls of the stent is caused from tracking the device through the arterial model, this occurs where the outer wall of the stent is scraped against the glass as it negotiates the bends. Removal of the stent coating is also seen from the inner walls during stent expansion. Balloon inflation creates a strain on the stent coating as the metal stent expands, cracking it and leading to particle formation. Close magnification of the stent coating (c) illustrates its friable nature. The relatively high LO particle counts acquired from tracking and deploying the ENDEAVOUR stent indicates that this stent coating is more prone to particle formation than the other DES tested.

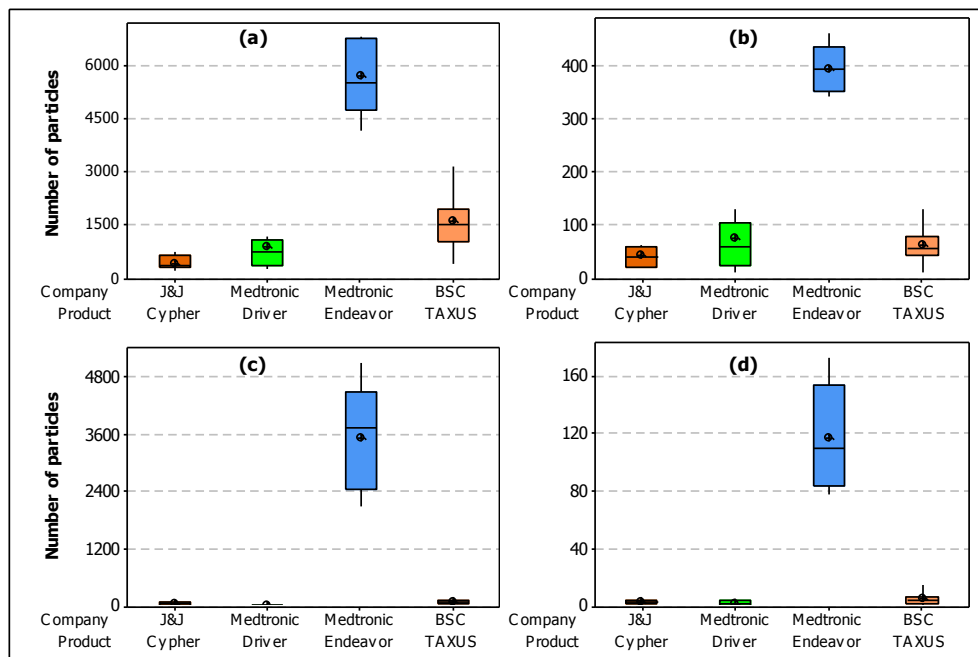


Figure 52 Plots showing the particle counts after SDS tracking, (a) $\geq 10 \mu\text{m}$ and (b) $\geq 25 \mu\text{m}$; and after stent deployment (c) $\geq 10 \mu\text{m}$ and (d) $\geq 25 \mu\text{m}$ from a range of DES with durable polymer coatings, TAXUS (Boston Scientific) and CYPHER (Johnson & Johnson), ENDEAVOUR SPRINT (Medtronic), and its uncoated bare metal stent (BMS) version, DRIVER (Medtronic), on the CLP apparatus. The devices were tracked once through the curved section of the arterial model, a measurement was taken at this point, and then the stent was deployed to RBP unconstrained followed by a second measurement.

Chapter 3

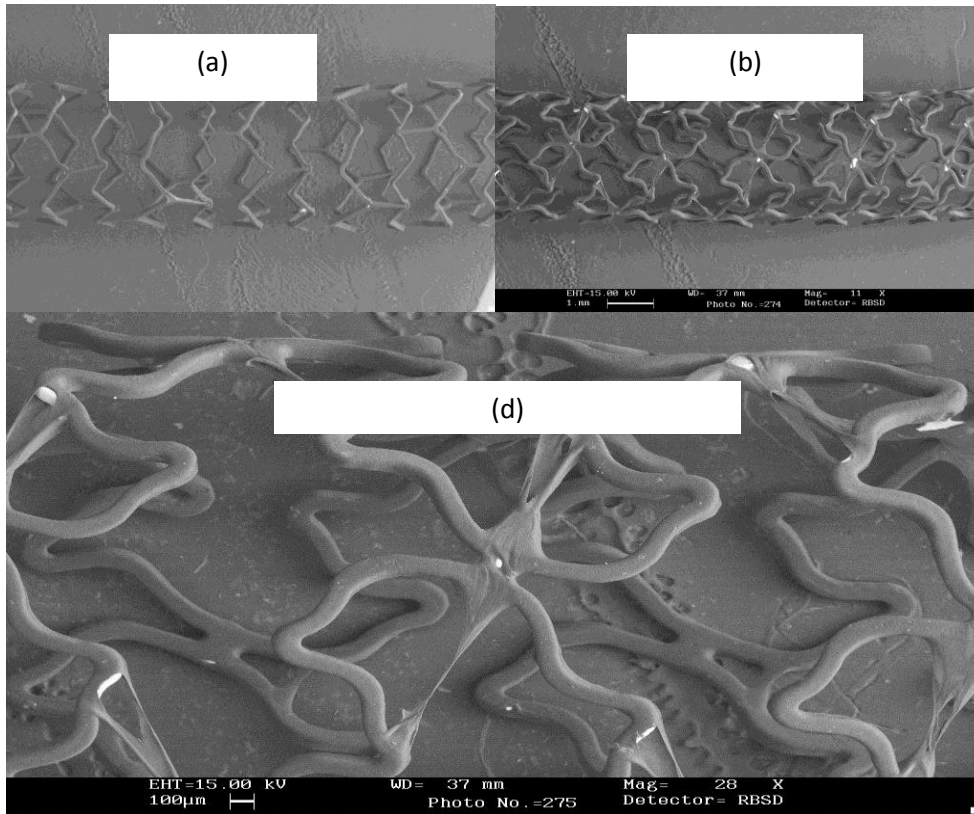


Figure 53 A deployed TAXUS Express² DES is shown in image (a) and a TAXUS Liberté DES is shown in image (b). A close up magnification of the deployed TAXUS Liberté DES with coating displacement is shown in image (d), there is no evidence of coating removal.

Chapter 3

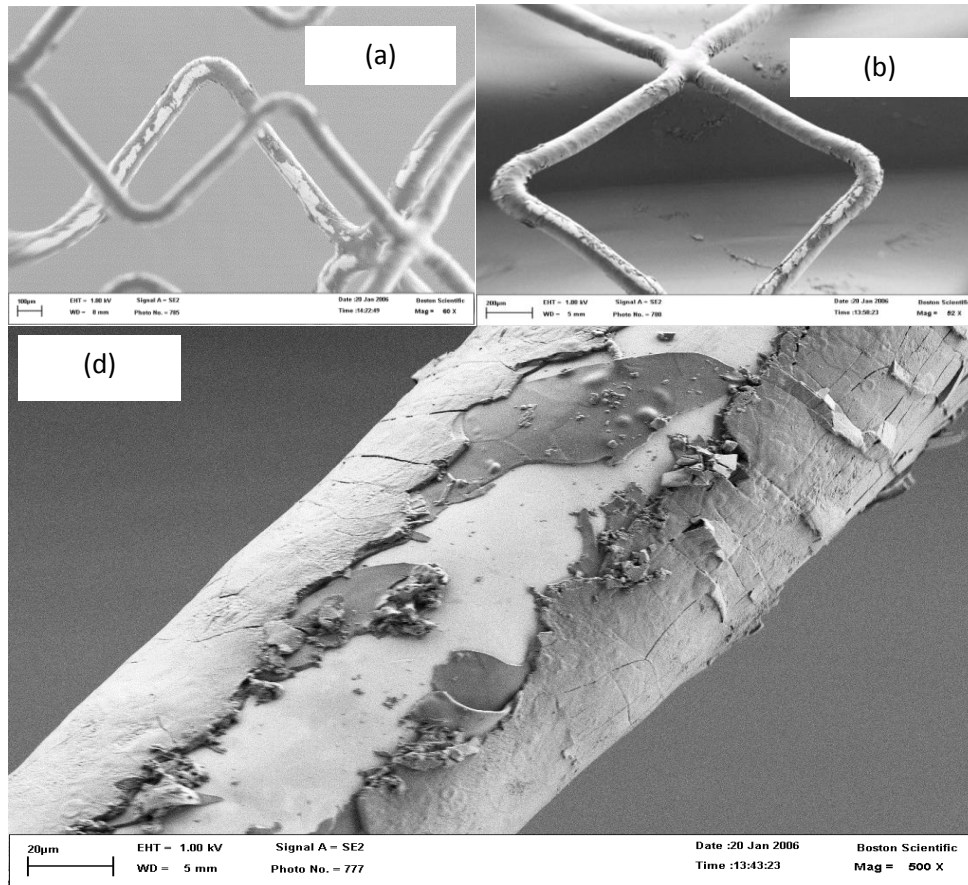


Figure 54 Deployed ENDEAVOUR DES stent after simulated use testing showing evidence of coating removal on the inner (a) and outer surfaces (b) of the stent. Close magnification of the stent coating (c) illustrates its friable nature.

DES coated with the biodegradable polymer poly(lactic-co-glycolic acid) (PLGA) and poly-lactic acid (PLA) are relatively new to the market, and none have been commercialised in the US to date. These biodegradable, biocompatible polymers are broken down by hydrolysis in the body to leave the bare stent behind. A DES with a coating of PLGA and everolimus, applied to its abluminal surface, was investigated for its susceptibility to form particles using the DLP apparatus. Particle testing of this DES has been extensively reported in section 3.2.1, the data shows low particle counts from the stent coating. A hermetic environment is created for this device by using an outer package of water tight foil and inclusion of a desiccant. The purpose of the foil pouch is twofold, first to prevent drug degradation, and second to prevent polymer hydrolysis. An investigation was carried out to ascertain if a failure in the package would result in polymer hydrolysis thereby creating coating particles.

The devices were removed from their foil pouches and stored at 40°C/75% RH for a period of 3, 7 and 8 weeks, and tested using the RSU method on the DLP apparatus.

Chapter 3

The rinse solution was filtered for automated LM analysis. Figure 55 shows the LO particle counts ≥ 10 , 25 and 50 μm and the number of particles identified as stent coating, with a circular equivalent diameter (CED) greater than 50 μm . The particle count increased over the 8 week storage period. Measurement of the molecular weight of the polymer over the same time period showed a reduction in molecular weight as a function of storage time, thus confirming that hydrolysis had occurred - Figure 56. Molecular weight measurements were obtained using gel permeation chromatography (GPC), by dissolving the polymer from the devices and then injecting the samples on the GPC system. Some images of the coating particles gathered on the filters are shown in Figure 57. The presence of these coating particles not only justifies the use of a foil pouch and desiccant for storing this particular DES, but it also provides confidence that the particulate matter methods are capable of detecting changes in the stent's coating integrity. It should be noted that this device was also tested after storage in foil pouches under accelerated ageing conditions to an equivalent of 18 months and to 12 months at ambient conditions with no adverse impact on the coating.

For particles that are easily recognisable using light microscopy, for example stent coating particles may be in the shape of the stent struts from which they have been removed (Figure 57); images can be used to positively identify the particle composition and source. In contrast to LO, which can only express particles in one dimension, i.e. the drop in electrical signal equivalent to a polystyrene sphere, the images for particles shown in Figure 57 can be described in various ways, such as by circular equivalent diameter (CED) and aspect ratio as shown in Figure 58. For the examination of particle release as a function of humidity and storage, described above, the mean aspect ratio and CED remained the same over the eight week period.

Chapter 3

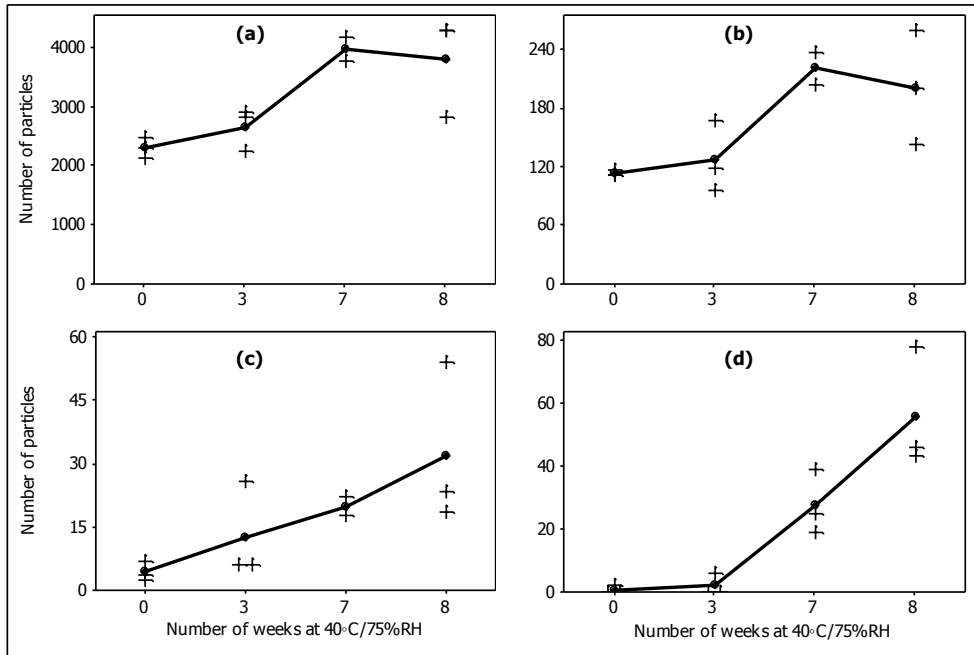


Figure 55 LO particle counts $\geq 10 \mu\text{m}$ (a), $\geq 25 \mu\text{m}$ (b) and $\geq 50 \mu\text{m}$ (c) and the number of particles identified as stent coating using LM, with a circular equivalent diameter (CED) greater than $50 \mu\text{m}$ (d). The graphs show that the particle count increased over the 8 week storage period at $40^\circ\text{C}/75\% \text{RH}$.

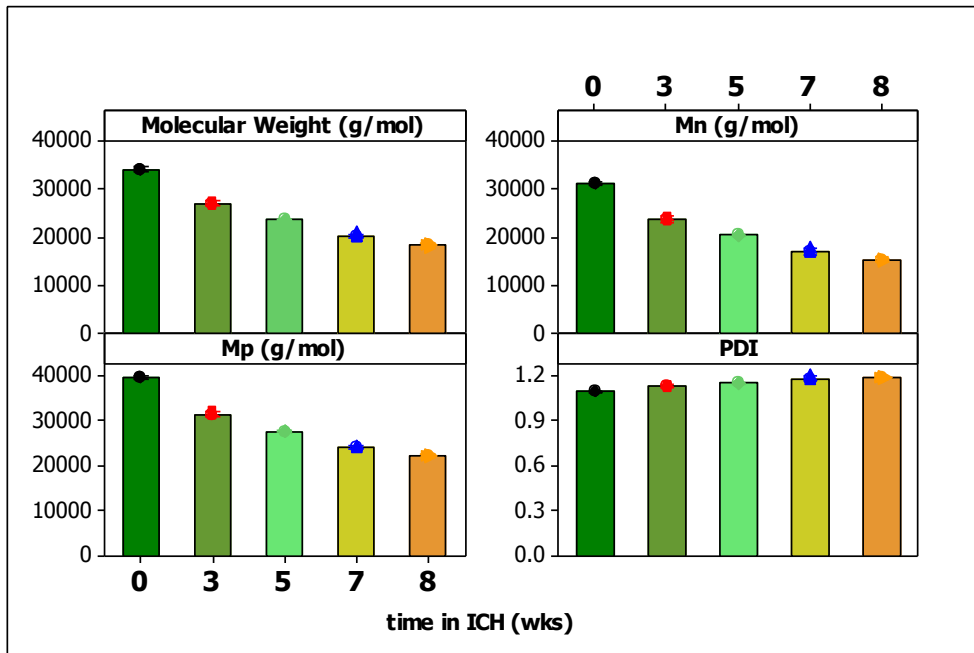
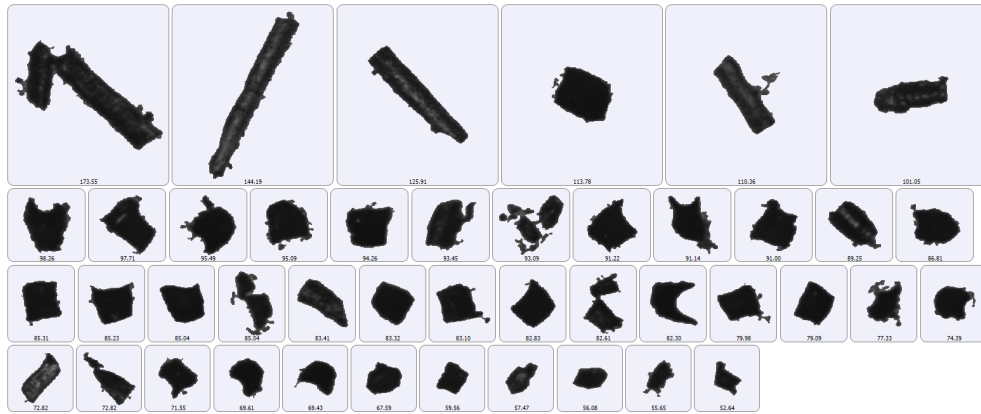


Figure 56 Measurement of the molecular weight of the PLGA polymer over an 8 week period showed a reduction in molecular weight as a function of storage time.

Chapter 3



Measurement: Req No 18702 Study_vmes, Record: 50 - RE-RUN 14501518-038(5) 23-Jan-12 STENT COATING

Figure 57 Images of stent coating particles gathered on a polycarbonate filter and viewed by light microscopy.

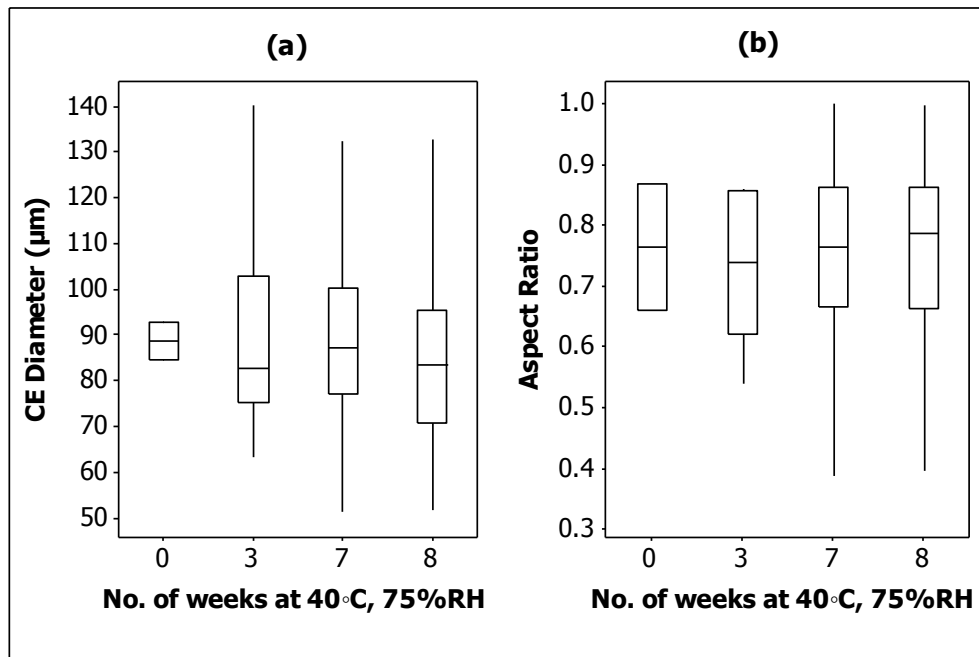


Figure 58 Circular equivalent diameter (a) and aspect ratio (b) of stent coating particles over an 8 week period.

As shown in this section, the particle count associated with DES coatings can vary significantly based on the material used and the environmental conditions to which they are exposed. LO can be used to provide a quick assessment of the propensity for the DES coating to produce particles, however complimentary techniques such as LM and SEM are required to confirm that the particles have been removed from the stent and to provide a morphological assessment of the particles.

Chapter 3

3.3.2 Leachates

Particle counts collected via LO on the CLP method showed evidence that the quantity of particles increased over time as TAXUS devices aged in their packaging. Figure 59 displays the particle count distribution for the ≥ 10 and $25\mu\text{m}$ particles from products of different age; 0 - 3, 3 - 12, 12 - 18, and 18 - 30 months. The number of particles is seen to increase as the product ages.

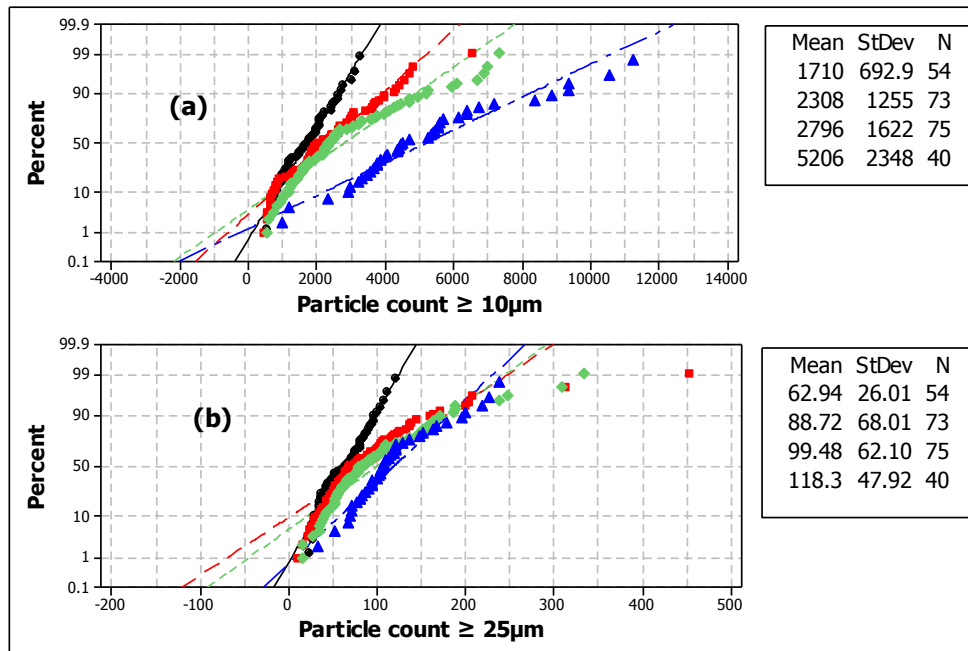


Figure 59 Probability plots showing the impact of product age on the number of particles $\geq 10 \mu\text{m}$ (a) and $25 \mu\text{m}$ (b). The 4 age brackets displayed are 0 - 3 months (black), 3 - 12 months (red), 12 - 18 months (green) and 18 - 30 months (blue). The mean particle count, standard deviation and sample size (N) are also provided for each particle size, these descriptive statistics are provided in descending order of age, e.g. the values corresponding to the newest devices at the top and the oldest devices at the bottom of the inset panels.

Particle count data was collected from TAXUS Express² and TAXUS Liberté devices that were exposed to different levels of temperature and relative humidity. The ageing conditions are specified by ICH (international conference on harmonization) nominal, intermediate and accelerated aging storage conditions, which are $25^{\circ}\text{C}/60\%\text{RH}$, $30^{\circ}\text{C}/60\%\text{RH}$ and $40^{\circ}\text{C}/75\%\text{RH}$ respectively. Measurements were taken after tracking the SDS through a simulated artery model and after the stent had been deployed at rated

Chapter 3

burst pressure (RBP). Total particle counts were calculated as the sum of SDS and stent measurements^{**}.

The devices were stored for 18 months at nominal, 12 months at intermediate, and 6 months at accelerated conditions. The accelerated and intermediate conditions resulted in increased particle counts compared to nominally stored devices. The accelerated, intermediate, and nominal storage conditions had mean values of 6.2×10^5 , 4.9×10^5 , and 4.5×10^4 particles $\geq 2 \mu\text{m}$ respectively, refer to Figure 60. The number of particles of larger size also increased however the distribution appears to change between the different conditions. It was observed that the increased particle count at forced age conditions is a phenomenon of the SDS and not the stent. Particle counts from the stents are comparable between storage conditions and do not show the same level of particle increase as seen for the SDS, refer to Figure 61.

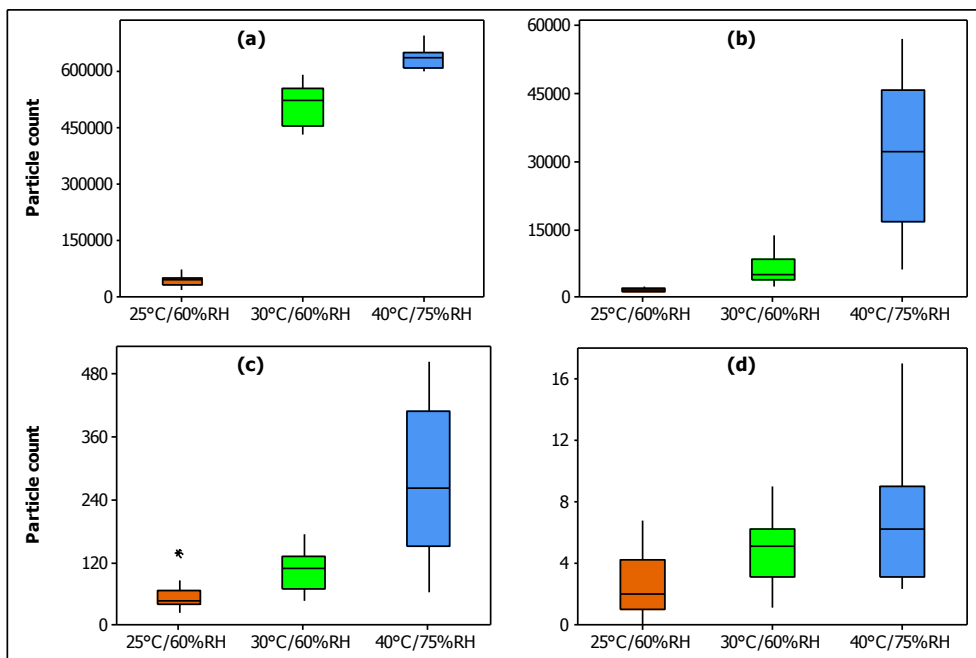


Figure 60 Box plots for particle counts from the SDS + stent $\geq 2 \mu\text{m}$ (a), $\geq 10 \mu\text{m}$ (b), $\geq 25 \mu\text{m}$ (c) and $\geq 50 \mu\text{m}$ (d) from nominal (25 °C/60% RH), intermediate (30 °C/60% RH), and accelerated (40 °C/75% RH) aged devices.

^{**} The operational range of the Liquilaz particle counter is from 2 μm to 125 μm ; to gather size distribution of particles within this range particle counts from 15 size bins were recorded. The size bins selected were $\geq 2, 3, 4, 5, 7.5, 10, 12.5, 15, 20, 25, 35, 50, 75, 100$ and 125 μm .

Chapter 3

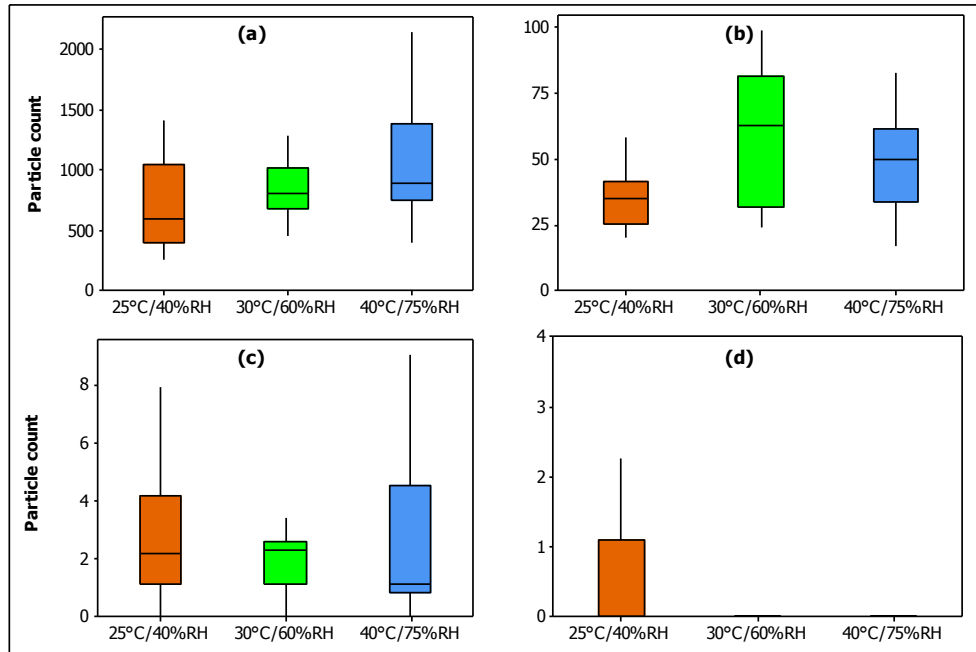


Figure 61 Box plots for particle counts from the stent $\geq 2 \mu\text{m}$ (a), $\geq 10 \mu\text{m}$ (b), $\geq 25 \mu\text{m}$ (c) and $\geq 50 \mu\text{m}$ (d) from nominal (25°C/60%RH), intermediate (30 °C/60% RH), and accelerated (40 °C/75% RH) aged devices

Typically, foreign material suspended in liquids have a characteristic exponential particle size distribution[36], [106], [107]. As may be expected, particle counts increase as particle size decreases. Foreign particulate matter (FM) follows this relationship when suspended in liquid such as water. Figure 62 shows the exponential increase in particle count as particle size decreases. If plotted on a log-log graph, the data will approximately yield a straight line. Figure 63 shows the log-log plot for particle counts from devices for accelerated, intermediate, and nominal aging conditions.

Chapter 3

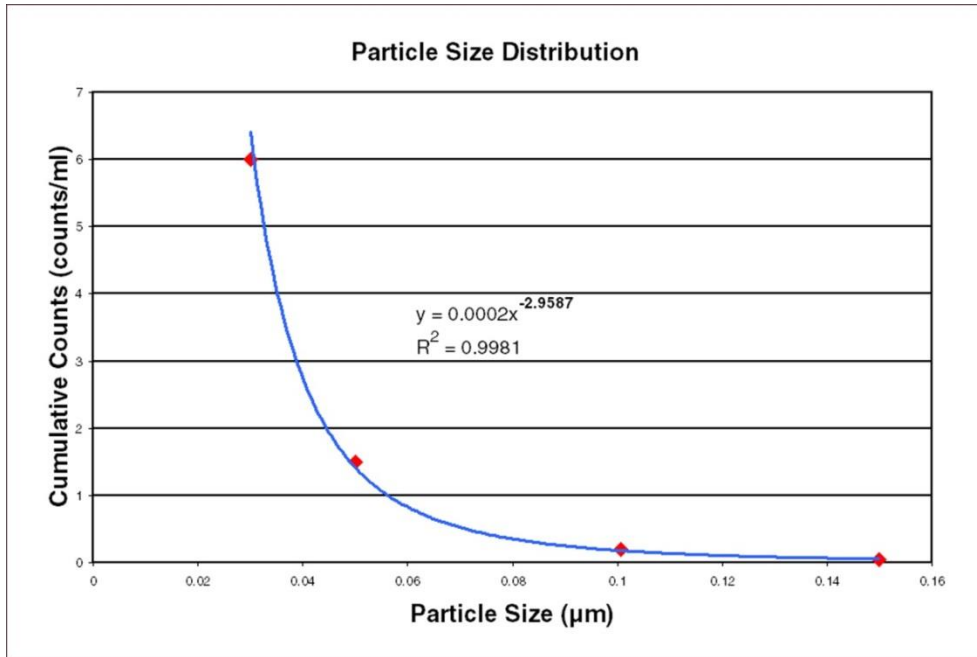


Figure 62 Normal particle size distribution in liquid (courtesy of Particle Measuring Systems Ltd., Colorado, US)

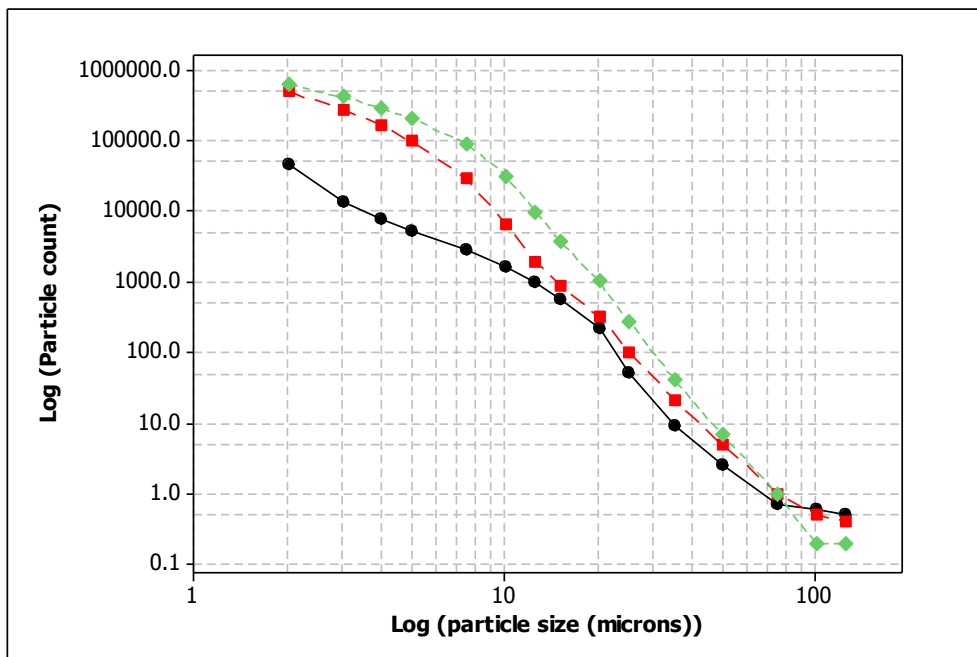


Figure 63 Overlaid particle size distribution log-log curves for nominal (black), intermediate (red) and accelerated (green) storage conditions.

More information can be gathered by taking a closer look at particle distribution by using probability plots, refer to Figure 64. Firstly, comparing the probability plots of the cumulative particle count $\geq 2 \mu\text{m}$ to the cumulative particle count $\geq 10 \mu\text{m}$, the ratio between the accelerated and nominal devices remains the same over this range,

Chapter 3

approximately 30:1, whilst the ratio between the intermediate and nominal devices decreases from approximately 20:1 to 3:1. So by the stage that the particle counts for intermediate devices reach the particle size of 10 μm it is significantly closer to the nominal device particle count than accelerated devices.

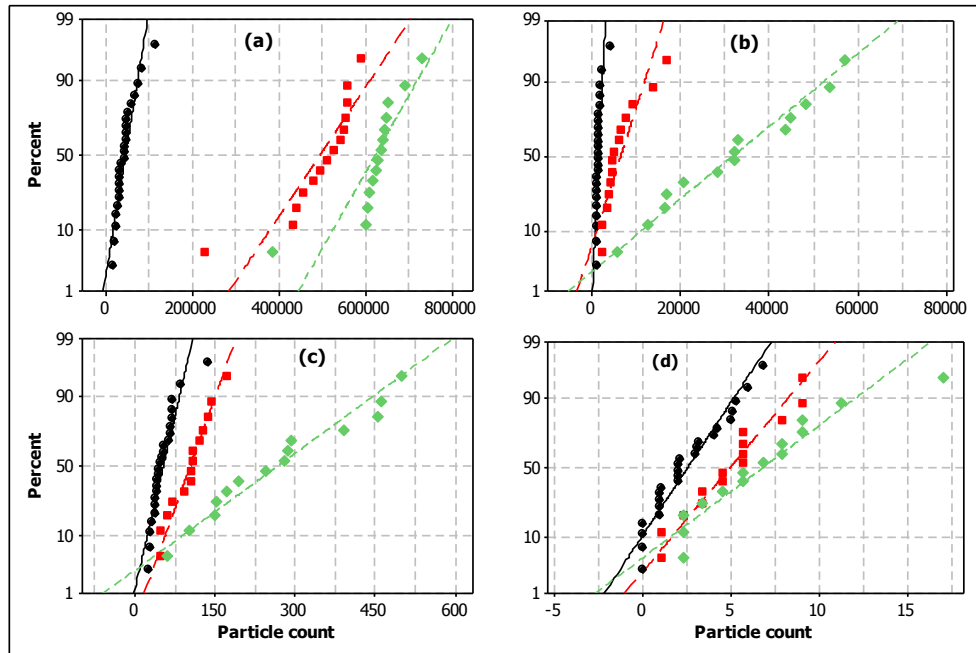


Figure 64 Probability plots for particle counts from the SDS and stent $\geq 2 \mu\text{m}$ (a), $\geq 10 \mu\text{m}$ (b), $\geq 25 \mu\text{m}$ (c) and $\geq 50 \mu\text{m}$ (d) from nominal – 25 $^{\circ}\text{C}/60\% \text{RH}$ (black), intermediate – 30 $^{\circ}\text{C}/60\% \text{RH}$ (red), and accelerated – 40 $^{\circ}\text{C}/75\% \text{RH}$ (green) aged devices

In general there is a convergence of the particle counts from all 3 storage conditions as the particle size increases. Although the intermediate and accelerated devices start out with a similar magnitude of particle counts $\geq 2 \mu\text{m}$, there is a greater proportion of larger particles in the accelerated aged devices when compared to intermediate devices.

The catheters that are used for the TAXUS catheters are made from polyether block amide polymers, which go by the trade name Pebax. Polyether block amide or ester-linked polyether-polyamide copolymer materials have a structure as shown in Figure 65.

Chapter 3

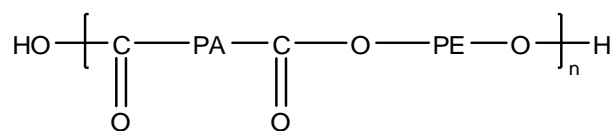


Figure 65 Chemical structure of Pebax.

Where PA is a polyamide such as nylon 12, PE is a polyether such as polytetramethylene oxide (PTMO), and n is an integer greater than 1 which represents the number of blocks of copolymer molecular units within the molecular formula of the copolymer[108]. Pebax is a thermoplastic elastomer consisting of hard PA and soft PE domains in the polymer. Catheters require a material such as this to impart them with high kink resistance, high flexibility associated with maximum tensile strength and good tear resistance. The nature of the link between the hard and soft segments depends on the nature of their functional end-groups. In the case of esters this will have an impact on the thermal and hydrolysis resistance of the final polymer[108].

It was observed by SEM that a powdery deposit of micron-sized, needle-like material developed over time on the distal section of the Pebax catheter shaft after exposure to increased temperature and humidity. An SEM image of the catheter shaft is shown in Figure 66 and Figure 67 at magnifications of 100X and 1,000X respectively. When the catheters were tested under simulated use conditions, the needle-like particles were also observed on filters of the rinses when viewed under SEM, refer to Figure 68. Leachate from Pebax in the form of lactam containing material was found to be the contributor to the increased particle numbers observed, using FTIR and Raman spectroscopy. The presence of unreacted monomers or the formation of low molecular weight oligomers of lactam during polymerization is the source of this leachate. Another potential source of the leachate is from hydrolysis of the polymer. Polyesteretheramides such as Pebax are physically cross-linked using ester linkages that are prone to hydrolysis. It is thought that the hydrolysis of these ester linkages may contribute significantly to a particle blooming phenomenon (shown in Figure 67) which is generally exhibited on the surface of these materials[11], [12], [109].

Raman micro spectroscopy identified these particles as containing Nylon 12 through matching the spectra to a reference spectrum shown in Figure 69 and Figure 70. Nylon 12 is one of the building blocks of the Pebax polymer. Laurolactam is the precursor for Nylon 12, its chemical structure is given in Figure 71. The Raman method used collects

Chapter 3

a very low resolution Raman spectra and as such may not be the best for discriminating between Nylon 12 and lauro lactam. The migration of lauro lactam and other related lactams to the surface of Nylon 12 polymers under accelerated aging conditions has been reported on by Chernev *et al*[110]. The SEM images published by Chernev are very similar in appearance to those seen on the surface of the Pebax catheters shown in Figure 66 and Figure 67.

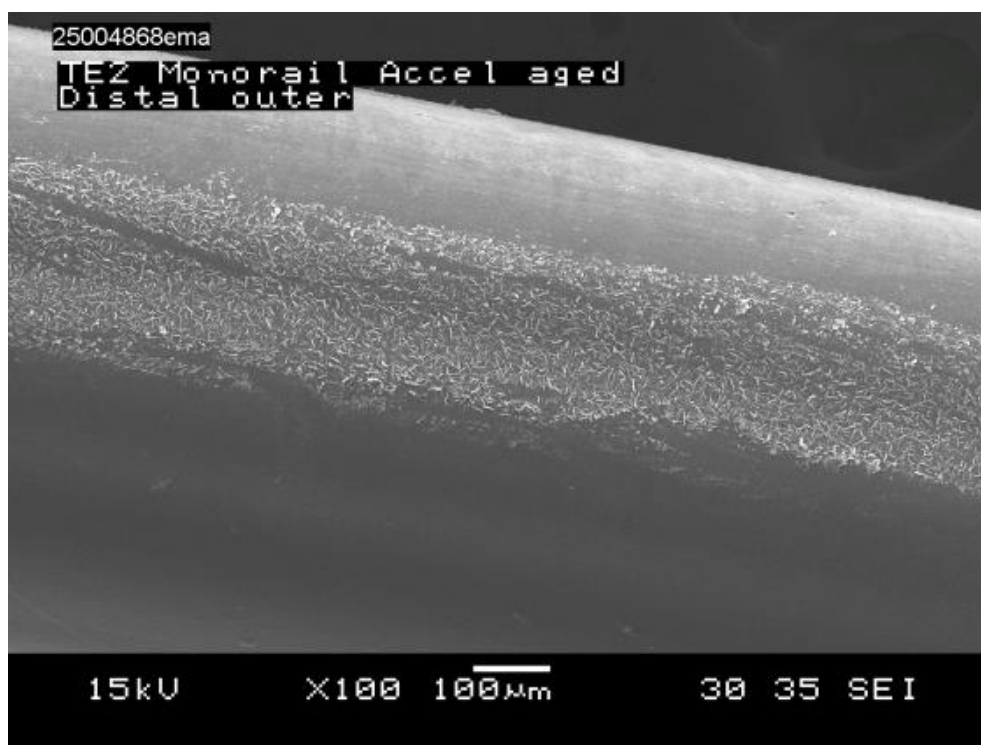


Figure 66 SEM image of a Pebax catheter shaft exposed to accelerated aging conditions for 6 months, a powdery residue is visible in the middle ground; Magnification = 100X

Chapter 3



Figure 67 SEM image of a Pebax catheter shaft exposed to accelerated aging conditions for 6 months, the needle-like shape of the residue is visible; Magnification = 1000X

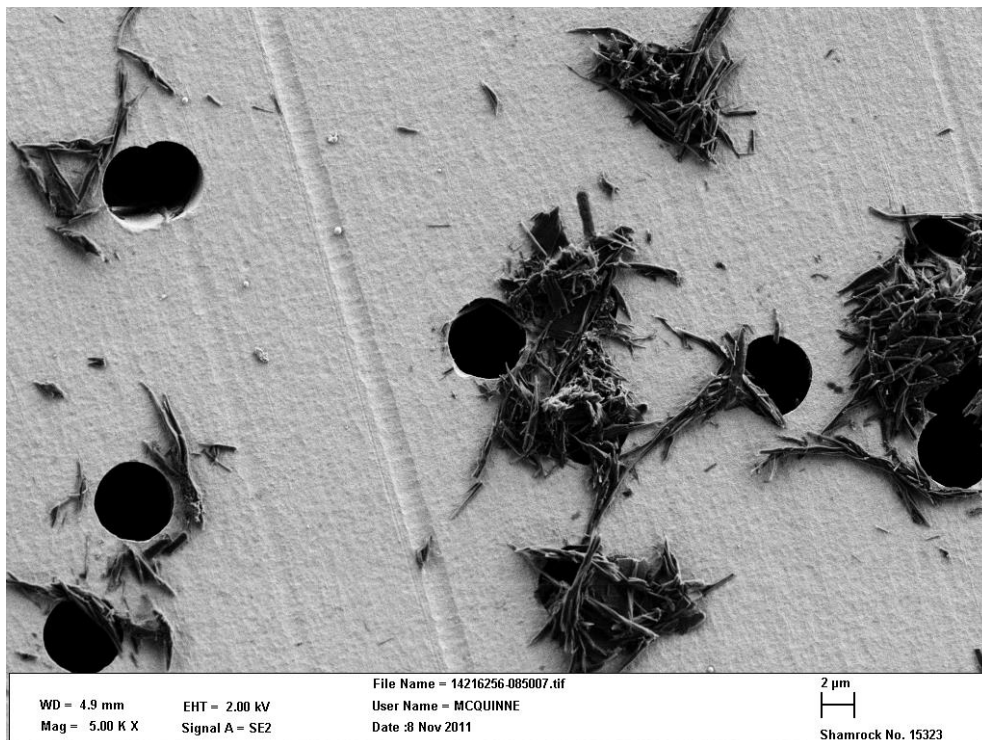


Figure 68 SEM image of the needle-like particles of Lauro lactam on the surface of a 5µm pore size, gold coated, polycarbonate, and track-etched filter membrane. The 5µm pores are visible as black circles; Magnification 5,000X.

Chapter 3

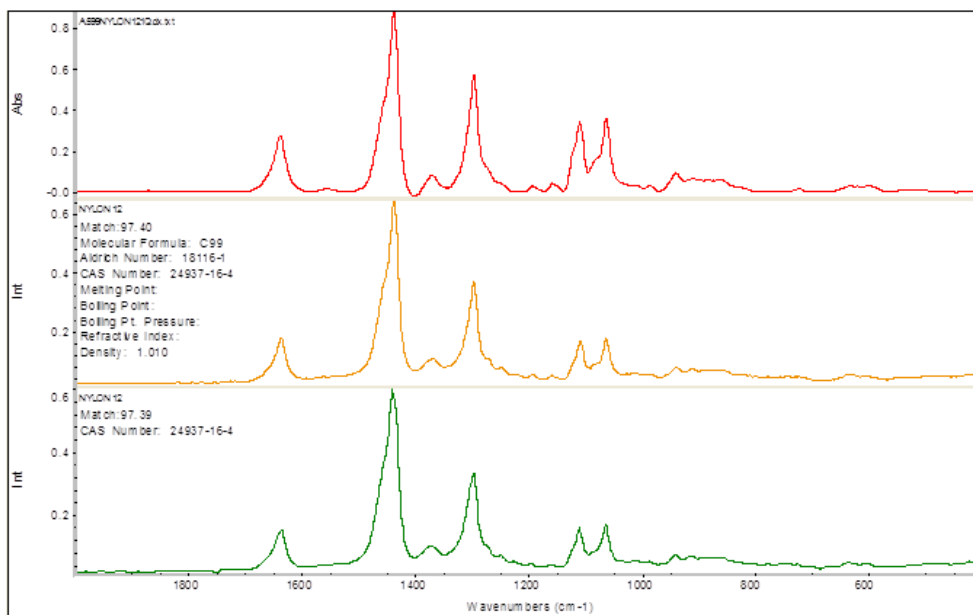
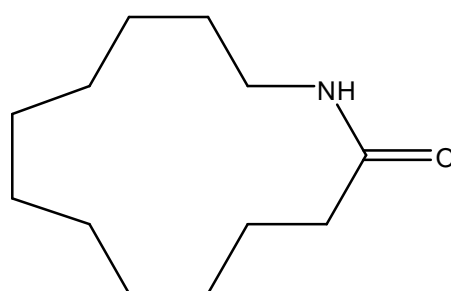


Figure 69 Raman spectrum of crystals compared to library spectrum of Nylon 12 (middle and lower spectrum) compared to the spectrum of the needle like particles recovered from the Pebax catheters.

Index	Match	Compound Name	Library Name
1	13715	97.40 NYLON 12	HR Aldrich Raman
2	2717	97.39 NYLON 12	Nicolet Standard Collection of Raman Spectra
3	2724	93.37 NYLON 11	Nicolet Standard Collection of Raman Spectra
4	13714	93.12 NYLON 11	HR Aldrich Raman
5	12	87.29 Ethylene/Vinyl Acetate Copolymer 72/28	Raman Sample Library
6	2716	86.94 NYLON 6/12	Nicolet Standard Collection of Raman Spectra
7	2744	86.51 POLY(ETHYLENE-CO-METHACRYLIC ACID), SC	Nicolet Standard Collection of Raman Spectra
8	1799	86.38 1,12-DIBROMODODECANE, TECH	Nicolet Standard Collection of Raman Spectra
9	1800	86.16 12-BROMO-1-DODECANOL, 99%	Nicolet Standard Collection of Raman Spectra
10	2788	85.09 NYLON 6/9	Nicolet Standard Collection of Raman Spectra

Figure 70 Library matching for Raman spectrum of needle-like particles. The light source used for Raman is a frequency doubled neodymium-doped yttrium aluminium garnet (NdYAG) laser that generates laser light at 532 nm.



lauro lactam

Chemical Formula: $C_{12}H_{23}NO$

Figure 71 The structure of lauro lactam, the building block for the Nylon 12 polyamide block of Pebax.

It was noted that the deposit was concentrated in the location of the Pebax shaft that had been coated with hydrophilic polymer coating (HPC). The HPC consists of a cross-linked vinyl polymer in which a non-cross linked hydrogel polymer is retained, as

Chapter 3

described by Buscemi and Slaikeu[9]. The specific coating used on the TAXUS catheters consists of cross-linked neopentyl glycol diacrylate (NPG) with embedded polyethylene oxide (PEO), designated as HPC A. It appears that HPC A facilitates the passage of Nylon 12 from the Pebax to the surface of the catheter where they bloom into needle shaped particles. Polyamides are immiscible with PEO, hence the Nylon 12 particles grow on the surface of the HPC and don't appear to reside in the HPC matrix.

The TAXUS devices are packaged in gas permeable pouches made from Tyvek[®]; and this facilitates use of ethylene oxide (EO) sterilization of the devices. The packaging provides a barrier to prevent microbial contamination but does not prevent water vapour or EO ingress to the product. EO sterilization is carried out under vacuum and in the presence of steam; with the microbes killed by the delivery of a lethal dose of EO gas. Water which will build up in the hydrophilic coating under atmospheric conditions is thought to accelerate the migration process and this may be the reason for the increased particle counts observed under nominal and accelerated aging conditions. One solution to this effect is to prevent water vapour access by placing the Tyvek pouch inside a water impermeable foil pouch after product sterilization.

DES for which foil pouches are used to prevent drug or polymer degradation of the stent coating demonstrate that particle formation in the presence of HPC A is suppressed under normal aging conditions, and much reduced under accelerated aging conditions, Figure 72. The $\geq 10 \mu\text{m}$ particle count on the devices aged for 6 months under accelerated conditions in a foil pouch had a mean of 5,715 particles compared to a mean of 31,801 particles without a foil pouch (Figure 60). It should be noted that Nylon 12 derived particles don't pose a risk to the patient with respect to the toxicity, as extensive biocompatibility studies have been carried out (internal information to Boston Scientific). In addition the particles don't reach sizes that may illicit an adverse physiological response, based on animal studies and clinical data in which particles of known size were introduced to the vasculature and physiological responses measured[36].

The use of extra foil packaging adds to manufacturing costs, and in a commercial enterprise this is a significant factor in the development of any new products. Another factor that impacts new product development and the speed-to-market of medical devices is the establishment of product shelf life. Product approvals can be facilitated

Chapter 3

by providing interim shelf life test data to regulatory agencies on products which have been aged under accelerated conditions. Projections on test data can be made using an Arrhenius type relation for product stability to extrapolate the product's performance over the proposed shelf life by the manufacturer. This data is not a substitute to actual testing carried out on the device aged under nominal conditions, but it can be used to speed up the product approval process significantly. However, particulate matter evaluation of medical devices is one of the tests used to establish if the product is stable over the proposed shelf life, thus the fact that increasing particle counts related to Nylon-12 derived leachate are observed provide an unwelcome interference.

Alternative hydrophilic coatings have been examined in an attempt to suppress the formation of lactam particles for these SDS devices, such as the polyvinylpyrrolidone (PVP) based coating patented by Nazarova *et al*[12] (HPC B). The particulate matter data reported in support of this US granted patent was generated using the CLP test method. The data comparing HPC A to HPC B packaged in Tyvek® pouches are not repeated here but the determination of particle counts released upon storage within foil pouches for the two types of hydrophilic coatings are shown in Figure 72 to Figure 74. The use of the HPC B coating resulted in an improvement over use of HPC A coating only when devices were aged under accelerated conditions for $\geq 10 \mu\text{m}$ particle counts (Figure 72). This result shows that the foil pouch inhibits formation of particles regardless of the HPC coating under normal storage conditions. However HPC B performs better under accelerated conditions. Thus manufacturers could use HPC B to speed up collection of product ageing data by using accelerated ageing conditions without increasing the number of intrinsic particles formed.

Chapter 3

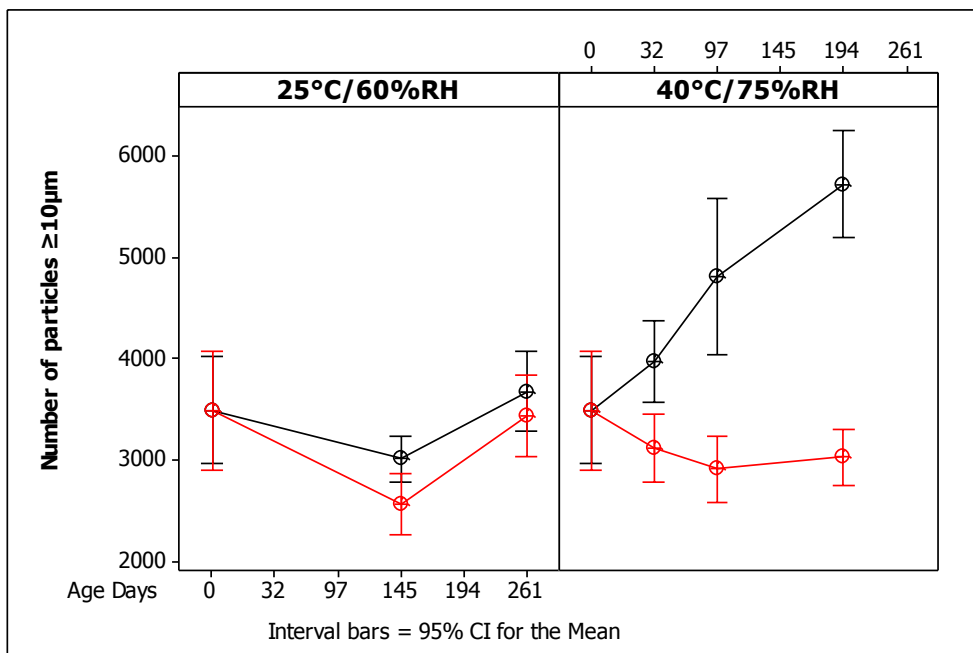


Figure 72 LO $\geq 10 \mu\text{m}$ particle counts from devices coated with HPC A (black) and HPC B (red). The devices were packaged in foil pouches to create a moisture free environment for the device. The products were aged under nominal conditions (left plot) and accelerated conditions (right plot), particle counts were obtained at time intervals displayed on the x-axis.

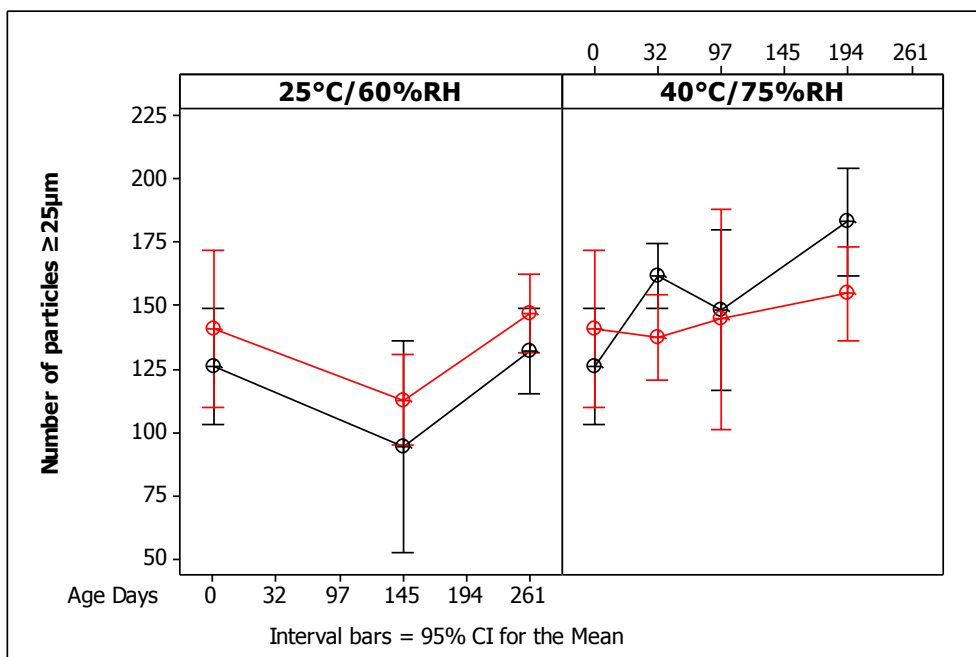


Figure 73 LO $\geq 25 \mu\text{m}$ particle counts from devices coated with HPC A (black) and HPC B (red). The devices were packaged in foil pouches to create a moisture free environment for the device. The products were aged under nominal conditions (left plot) and accelerated conditions (right plot), particle counts were obtained at time intervals displayed on the x-axis.

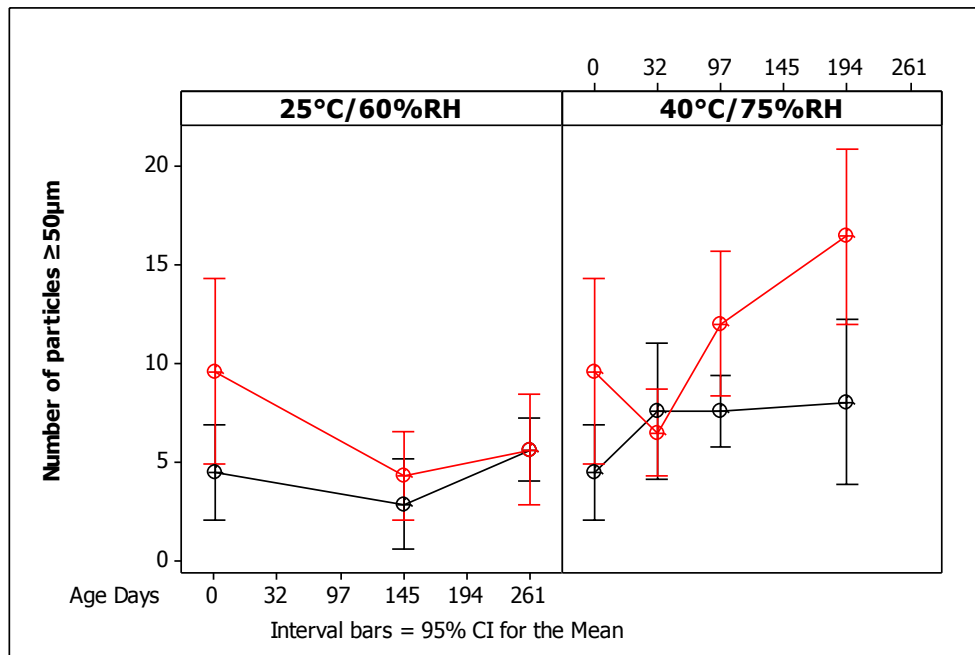


Figure 74 LO $\geq 50 \mu\text{m}$ particle counts from devices coated with HPC A (black) and HPC B (red). The devices were packaged in foil pouches to create a moisture free environment for the device. The products were aged under nominal conditions (left plot) and accelerated conditions (right plot), particle counts were obtained at time intervals displayed on the x-axis.

3.4 Lubricious coatings

The lubricious coatings used on a device can have a significant impact on particulate matter release. As already mentioned, HPC may act as a conduit for lactam leachates from Pebax. However the HPC coatings themselves may also be a source of particles. Silicone is a liquid, and as such is not considered a particle[36]. But silicone is immiscible with water, thereby forming spherical droplets when removed from devices in aqueous media. Silicone has a different refractive index to that of water and will be detected as a particle using LO. This phenomenon is well understood and has been extensively reported on with respect to parenteral particulate matter measurements[36].

The impact of silicone on LO particle counts can easily be assessed by filtering the device rinse solutions to collect any particles. The silicone, being a liquid, will pass through the filter pores leaving no particles to observe via LM, this has been confirmed through experiments. When POBA devices were coated with different quantities of a silicone lubricious coating and were analysed for particle release using LO on the RSU method a marked increase in apparent particle counts was observed compared to counterparts with the silicone coating omitted and as a function of the length of the catheter coated with silicone, Figure 75. The significance of this result for the industry is that LO measurements alone on devices coated with silicone may produce an

Chapter 3

inaccurate determination of the number of particles present. LM should be considered as an alternative in these cases.

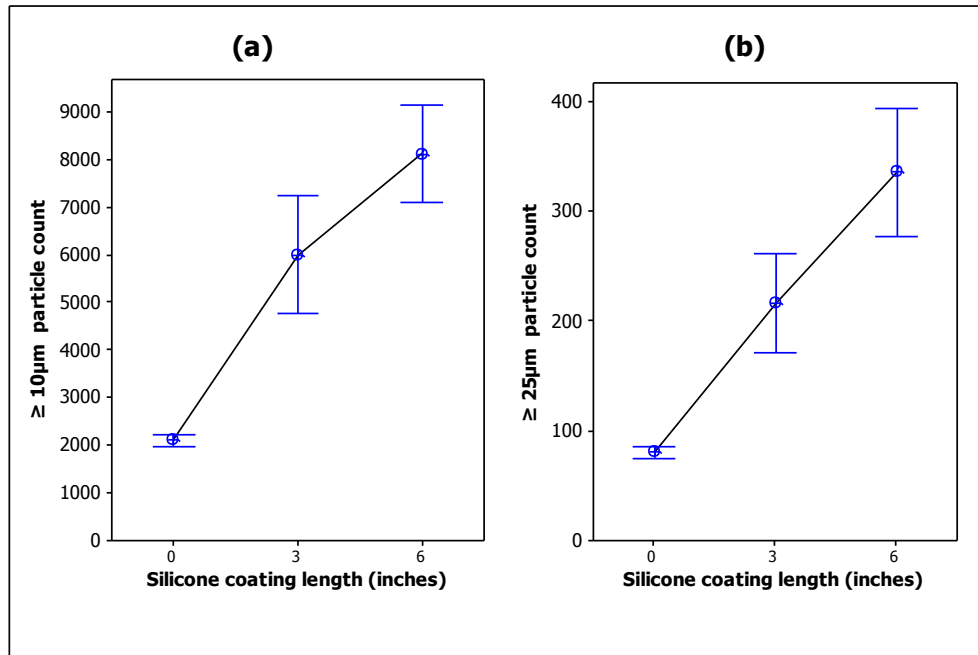


Figure 75 Number of particles $\geq 10 \mu\text{m}$ (a), and $\geq 25 \mu\text{m}$ (b) counted by LO based on the length of catheter coated. One standard error from the mean is indicated by the bars.

3.4.1 Observations related to hydrophilic coating A (HPC A)

The functional component of HPC A is the water soluble polymer PEO[111]. The tendency for Nylon12 derived particles to migrate to the surface of this coating from the underlying Pebax catheter shaft has already been discussed in section 3.3.2. This leachate phenomenon was of special consideration when trying to evaluate the impact of the particulate matter contribution from HPC A caused by Nylon 12 derived particles. As such, products being evaluated were tested within a short period of manufacture or were packaged in foil pouches in order to limit the growth of the lactam particles.

Initial assessments were carried out by a straight-forward comparison of HPC coated catheters with non-coated catheters using the DLP method (Figure 76). After one track through the simulated artery, the counts for the HPC A coated devices were higher than the non-coated catheters, although this was only significant in the $\geq 2 \mu\text{m}$ particle counts. However after multiple tracks (5) the number of particles created using the coated catheters increased markedly compared with the non-coated catheter in the larger particle size categories too. This showed that the HPC A coating is removed from the device by abrasion. This is not unexpected as lubricity and durability testing showed

Chapter 3

that the coating, like other similar coatings, loses lubricity after multiple cycles. This suggests that the coating or at least the PEO component is removed through abrasion.

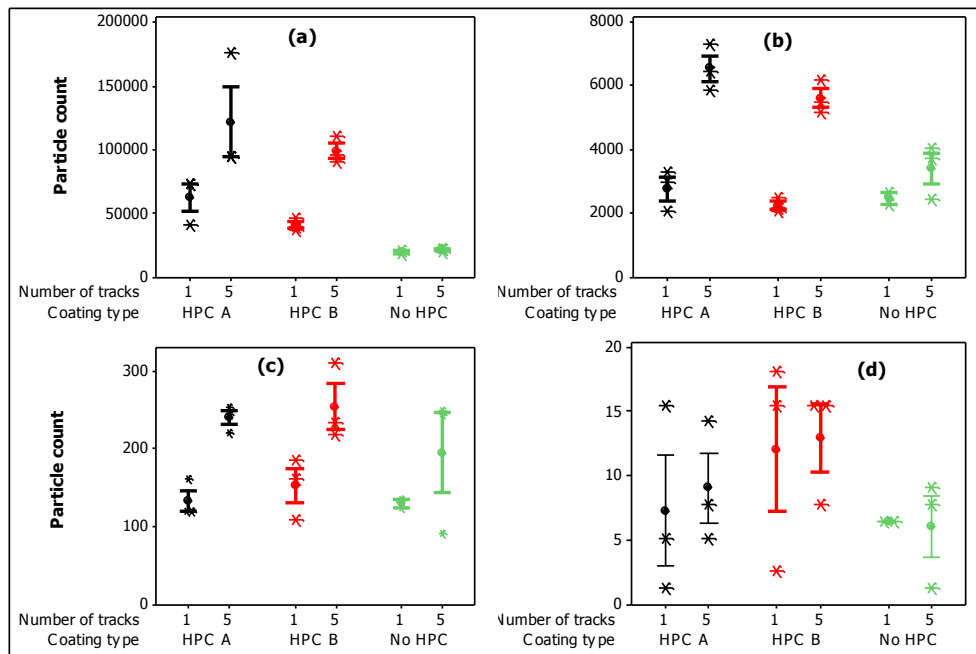


Figure 76 Particle counts $\geq 2 \mu\text{m}$ (a), $\geq 10 \mu\text{m}$ (b), $\geq 25 \mu\text{m}$ (c) and $50 \mu\text{m}$ (d) for non-coated catheters (green), and catheters coated with HPC A (black) and HPC B (Red). Catheters were tracked once or five times through the simulated artery. Particle counts with sizes ≥ 2 , 10, 25 and $50 \mu\text{m}$ are shown respectively, moving clockwise from the top left of the figure. The interval bars on the plot mark one standard error from the mean.

When the rinse solution was filtered, no visible particles were seen (Figure 77). Filters were acquired from devices coated with HPC A that had been accelerated aged. From a macroscopic look at the composite images of the filter membranes in Figure 78, it was evident that the images of the accelerated aged membranes were darker. Figure 79 shows that at higher magnification, the filters exhibited domains that were featureless (no particles), surrounded by darker regions which appear to consist of fine particulate matter. The fine particles can be attributed to the presence of Nylon-12 that leaches from the catheter under accelerated ageing. The Nylon-12 derived particles act to highlight the areas with no particles present, but why aren't the particles homogeneously distributed? The presence of the particle-less domains suggests that they are an artefact from hydrogel particles of HPC A. The needle-like particles are not present in these domains because Nylon-12 is immiscible with PEO; as discussed, Nylon-12 migrates through HPC A to precipitate on its surface.

A number of mechanisms may explain why no HPC particles are seen on the filter surface.

Chapter 3

- 1) PEO is water soluble and under vacuum filtration solubilises and passes through the membrane leaving behind an area free from particles.
- 2) The desolvated hydrogels leave behind small quantities of PEO that are not visible by LM.
- 3) The HPC particles may break apart under the vacuum pressure at the filter surface and then pass through the filter pores.

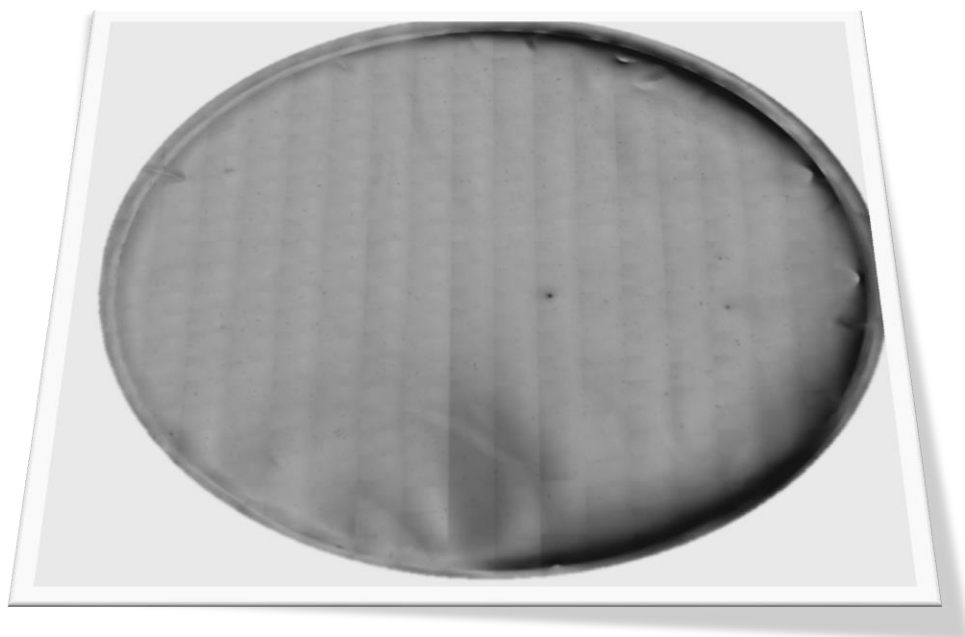


Figure 77 Image of a filter taken from non-aged devices coated with HPC A.

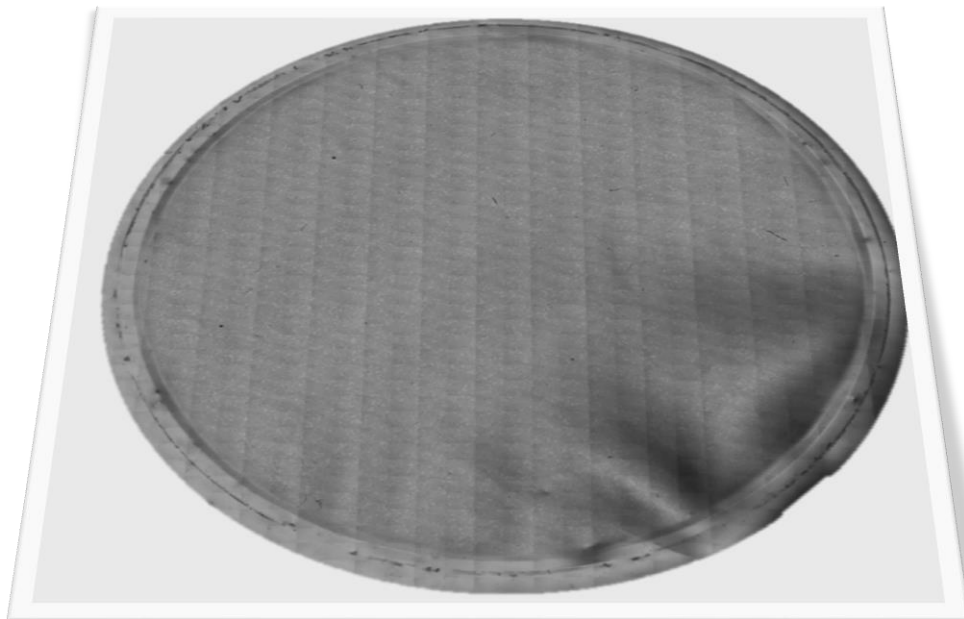


Figure 78 Image of a filter taken from aged devices coated with HPC A.

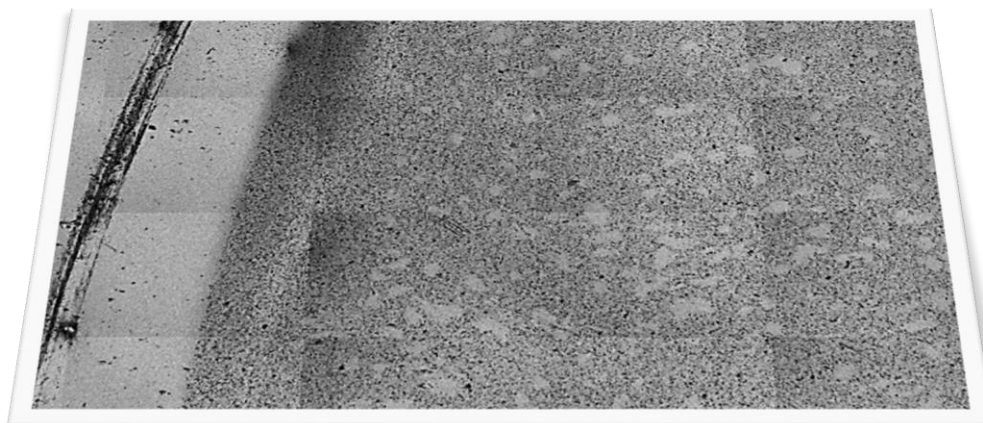


Figure 79 Increased magnification image of a filter taken from aged devices coated with HPC A, shown in Figure 78.

3.4.2 Observations related to hydrophilic coating B (HPC B)

The functional component of HPC B is the water soluble polymer PVP. One of the goals in developing this coating was to suppress the formation of particles created by migration of Nylon 12 derived compounds to the surface from the underlying Pebax

Chapter 3

catheter shaft[12]. To this end HPC B is successful; LO particle counts did not increase when devices were aged. HPC B showed an improvement over HPC A even when devices were packaged in a moisture impermeable package and aged under accelerated conditions - Figure 76. However, HPC B behaves in a similar manner to HPC A when particle counts are monitored over repeated tracks through the DLP method and compared to non HPC coated catheters. This showed that the HPC B coating is also removed from the device by abrasion. The observation is not unexpected as lubricity and durability testing show that this coating loses lubricity after multiple cycles too. The same conclusion was arrived at with respect to HPC B as with HPC A, the coating is removed as particles through abrasion. However when the rinse solutions were filtered in the case of HPC B, there was a clear difference observed between the coatings.

The initial observation from vacuum filtering, even before the particles were looked at by microscopy, is that filtration took longer based on the number of tracks performed. Five (5) devices were tracked through the DLP track model a different number of times; ranging from 0 to 10 times (5 devices tracked at each level). The time taken to filter the 175 mL rinse solution through a 47 mm diameter, 0.45 μ m pore size, and track etched polycarbonate filter membrane was recorded. Figure 80 shows the results from this experiment; for comparison purposes the data is expressed as a mean percentage of the total number of particles or filtration time recorded from the five devices tested at each challenge level. The number of particles \geq 10, 25, and 50 μ m all increased with the number of times the devices were threaded through the tortuous section of the track model. Filtration took considerably longer when the devices were tracked 5 and 10 times through the model compared to no track (0), half a track (0.5, this entailed just inserting the device once through the curves), and one track (1, this entailed inserting and retracting the device once through the curves). No observations related to the length of time taken to filter the rinse solution were observed from HPC A coated devices, regardless of the number of tracks.

Chapter 3

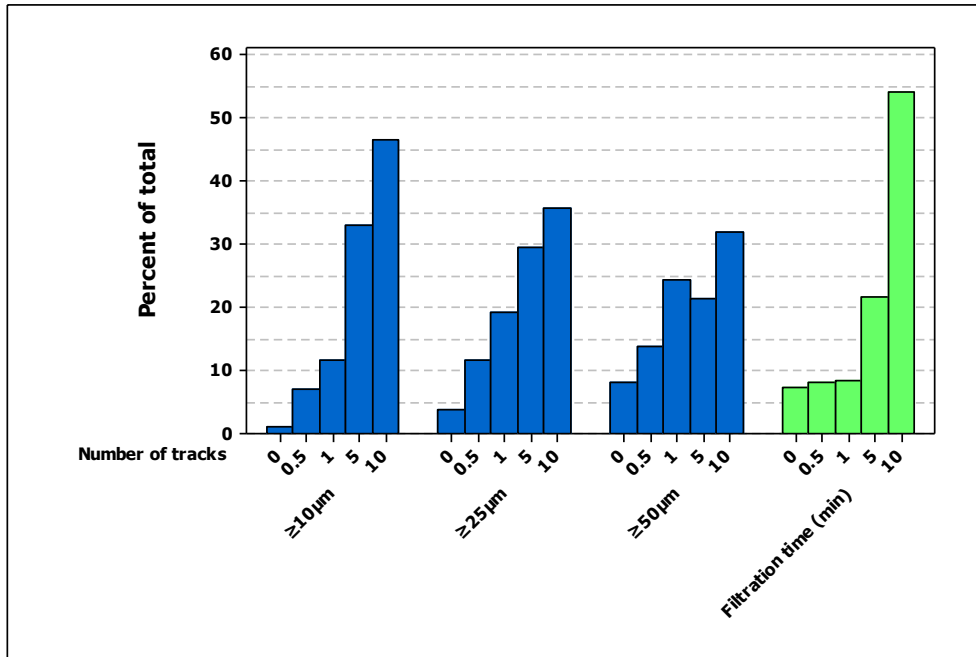


Figure 80 The number of particles observed when devices coated with HPC B were challenged in the simulated track model (blue bars), expressed as the percentage of the sum of all particles removed at each condition. The challenge to the device is expressed as the number of times it was tracked through the tortuous curves (in and out) in the track model. The bars in green show the length of time, expressed in percentage, taken to filter the rinse solution from each of the five challenge conditions.

The macroscopic view of the filters showed the presence of relatively large particles, Figure 81. These particles were not visible for the 0 track challenge level, but they were visible after tracking the device through the curved section of the model just once (the 0.5 level). At higher magnifications too, the membrane surface was shown to have a predominance of very faint particles, with less defined edges than the larger particles visible at higher magnifications. SEM analysis of separate gold coated filters with $5\mu\text{m}$ pores, Figure 82, showed that these particles appeared to be relatively thin and it was evident that the vacuum filtration had stretched them out between the filter pores ($5\mu\text{m}$ pore size). On close inspection smaller particles resembling the Nylon-12 derived need-like structures that were seen on Pebax catheters coated with HPC A were observed (Figure 83).

Chapter 3

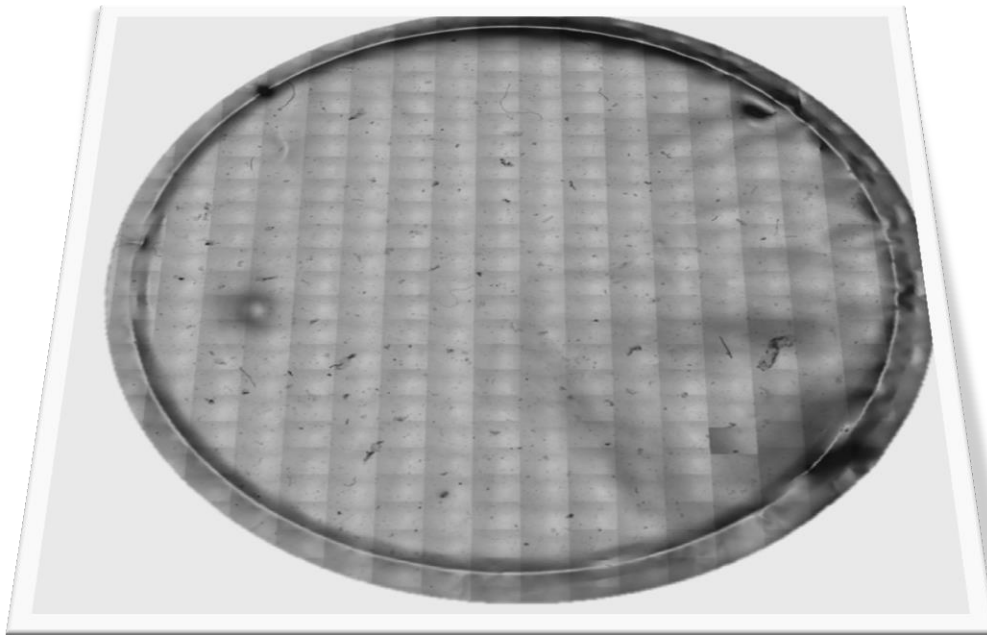


Figure 81 Light microscope image of a filter with particles observed when devices coated with HPC B were challenged in the simulated track model.

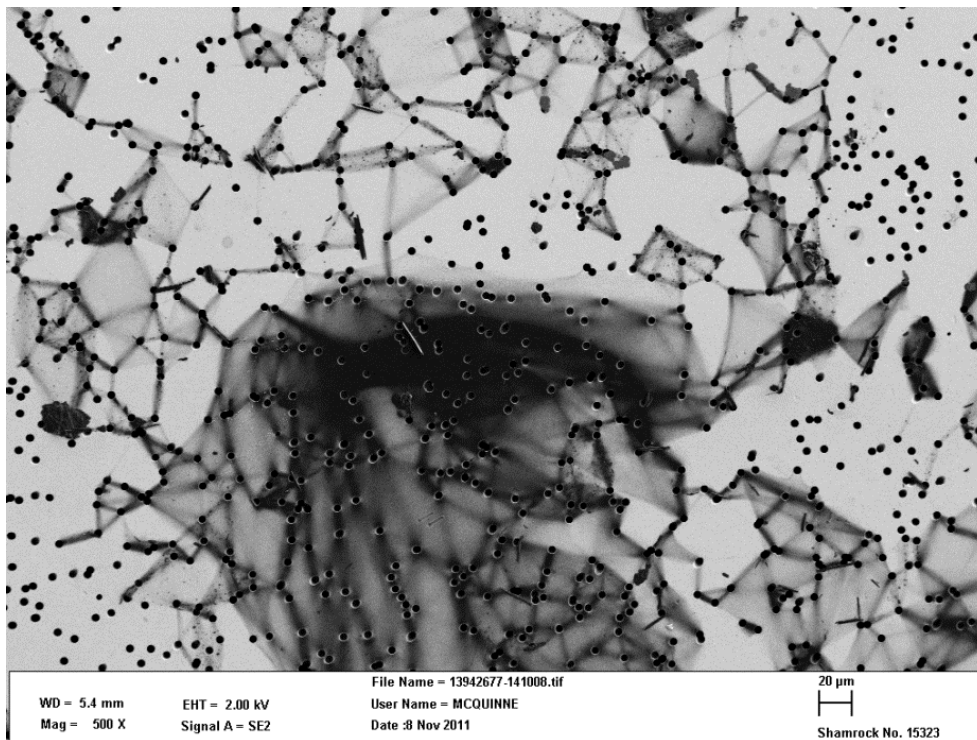


Figure 82 SEM image (500X) of a filter with particles observed when devices coated with HPC B were challenged in the simulated track model.

Chapter 3

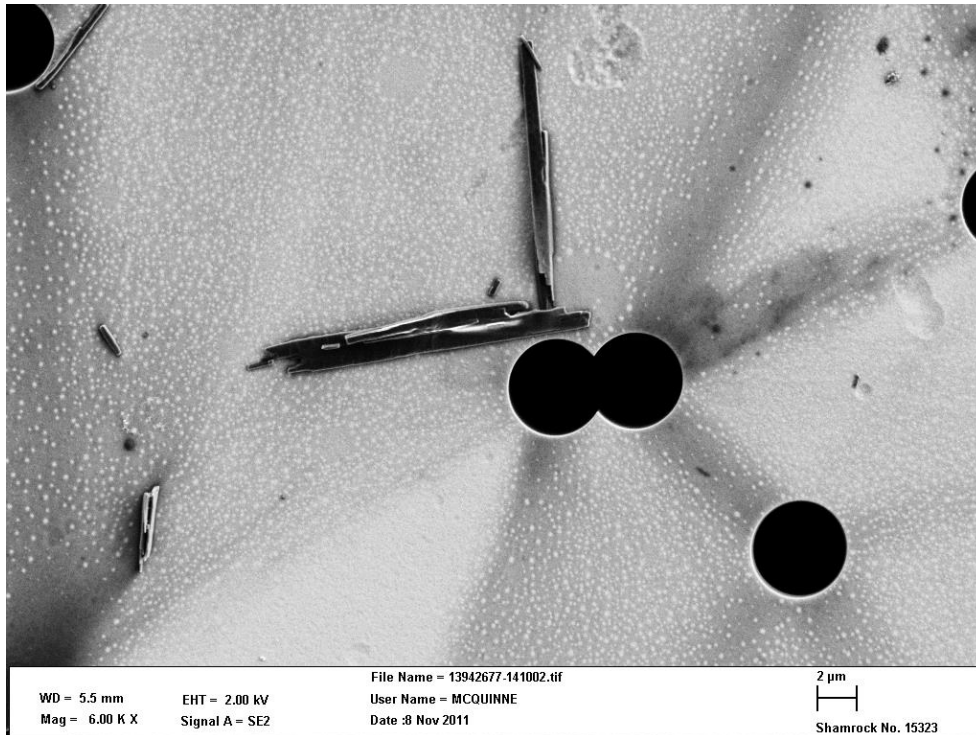


Figure 83 SEM image (6,000X) of a filter with needle-like particles observed when devices coated with HPC B were challenged in the simulated track model.

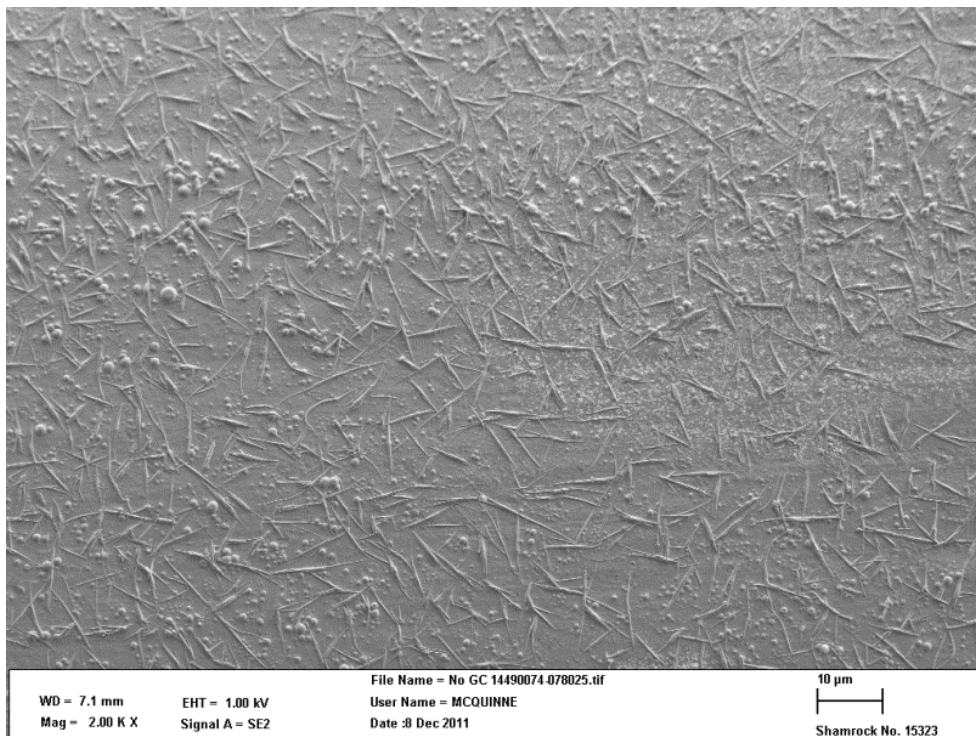


Figure 84 SEM image (2,000X) of a catheter with needle-like particles observed on devices coated with HPC B

The majority of HPC B particles have a relatively small mass when desolvated. Comparing dry filters using a light microscope to the same filters when still wet, the wet filters have a greater particle count than the same filter when dry. As the particles dry

Chapter 3

out, they appear to get smaller or disappear, and it is difficult to establish a defined edge to them. They appear relatively large in size on a filter when viewed under a microscope (circular equivalent diameter $> 50 \mu\text{m}$), but they are quite thin and diffuse, much like a stain or residue left on the filter surface. In solution these particles are a hydrogel with liquid properties, hence when they are vacuum filtered and dried they flatten out and have very little depth in the z-axis. Under SEM the HPC B particles are little more than a stain on the surface, they appear like marks made with a marker on a whiteboard. However a small population of HPC B particles are larger, these have a defined edge, they are ribbon shaped and film like, sometimes they can be up to 5mm in length.

It was observed that the rinse solution from some batches of product coated with HPC B can be significantly slower to filter than others even after just one track. Counter intuitively, these batches appeared to have fewer visible HPC B particles. An experiment was designed to establish if variation in the coating process could have led to this. The HPC B coating is applied as a solution to the catheter, this is followed by a curing step intended to crosslink the NPG polymer to form the SIPN^{††}. The speed at which the coater operates determines the thickness of the coating and the coat weight applied to the catheter. In the experiment, the coating speed was set at 0.5 inches/second to achieve a thin coat of HPC B and at 4.5 inches/second to obtain a thicker layer. The devices were then tested on the DLP method, they were tracked once and then the rinse solution was filtered. The results of this experiment are displayed in Figure 85.

It was to be expected that higher particle counts would be obtained when more of the coating was applied to the catheters. The number of particles $\geq 10, 25, \text{ and } 50 \mu\text{m}$ were all elevated for the catheters coated at the higher speed setting. The UV exposure times had the effect of increasing the particle count based upon the length of exposure for the number of particles ≥ 10 and $25 \mu\text{m}$. The filtration times were significantly impacted by the UV curing time, with just 20 seconds of exposure the filtration times were very

^{††} Crosslinking is initiated by photo-polymerization using UV lamps. The normal UV exposure time is 40 seconds. In the experiment the length of time that the samples were exposed to the UV lamps was 20 or 60 seconds, amounting to approximately 120 and 370 mJ/cm^2 of UV dosage respectively.

Chapter 3

long compared to 60 seconds of UV exposure. Therefore the observations of some batches which had rinse solutions that were slow to filter can be linked to an inadequate UV cure of the HPC B coating.

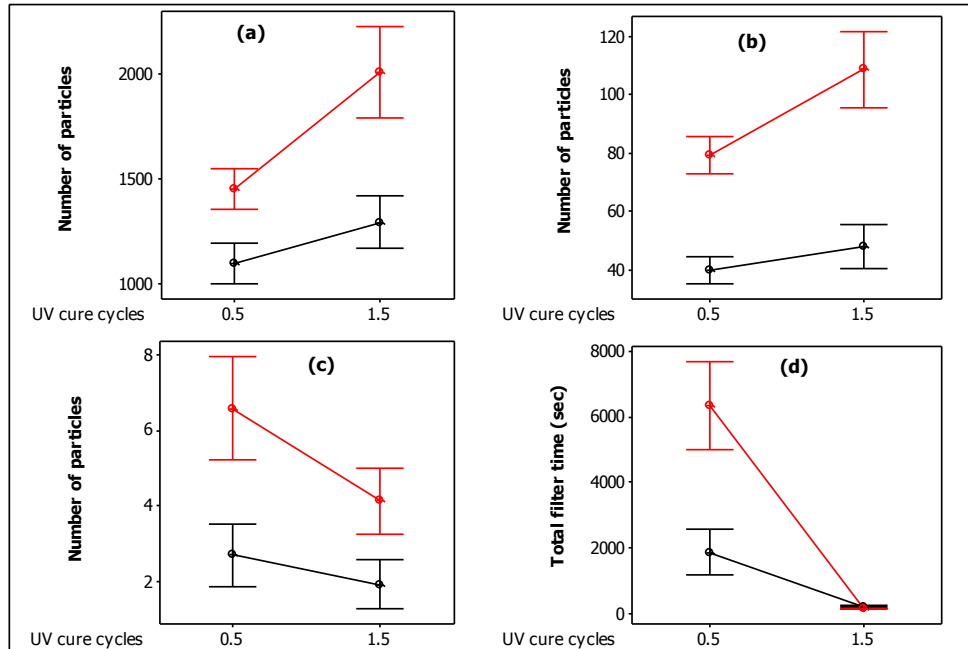


Figure 85 Process experiment to determine the effect on 10 μm (a), 25 μm (b) and 50 μm (c) particle counts and filtration time (d) of applying different amounts of HPC B as determined by coating speeds of 0.5 (black) and 4.5 (red) inches/second to catheters, and the different exposure time to UV lamps (x-axis). Interval bars mark one standard error from the mean.

Solubility studies in water were carried out using films of HPC B and its two polymer components PVP and NPG. The results showed that the HPC B films and NPG are not water soluble, whilst PVP is water soluble[112]; this confirms the reported properties of these two materials. The solubility study was extended to NPG and PVP components exposed to UV radiation at the same wavelength range used in the HPC process for curing. UV curing at the selected wavelength range initiated crosslinking in both polymers that resulted in water insoluble material. The formation of cross-linked, insoluble PVP was not the intent for the SIPN design of HPC B. The intent was for the PVP to remain unchanged within the NPG network of cross-linked polymer chains. Short UV exposure times initiated cross linking of PVP which results in the formation of small insoluble particles under simulated use, and at longer UV exposure times the formation of larger insoluble particles was the result. Looking at particles with LM gives a perspective of the HPC B particles in relation to their shape and structure that one cannot achieve using LO alone. LO measurements cannot provide specificity

Chapter 3

between different particle types and particle shapes; however one gets a more reliable particle count.

Extensive CSU particulate testing was carried out comparing HPC A to HPC B. Light obscuration particle counts $\geq 10, 25$ and $50 \mu\text{m}$, comparing devices coated with HPC A to devices coated with HPC B are shown in Figure 86, Figure 87, and Figure 88 respectively. Sixty pairs of DES devices from each HPC group were tested, 5 pairs from 12 different size devices. The results clearly show that HPC B results in a larger number of ≥ 25 and $50 \mu\text{m}$ particles than HPC A.

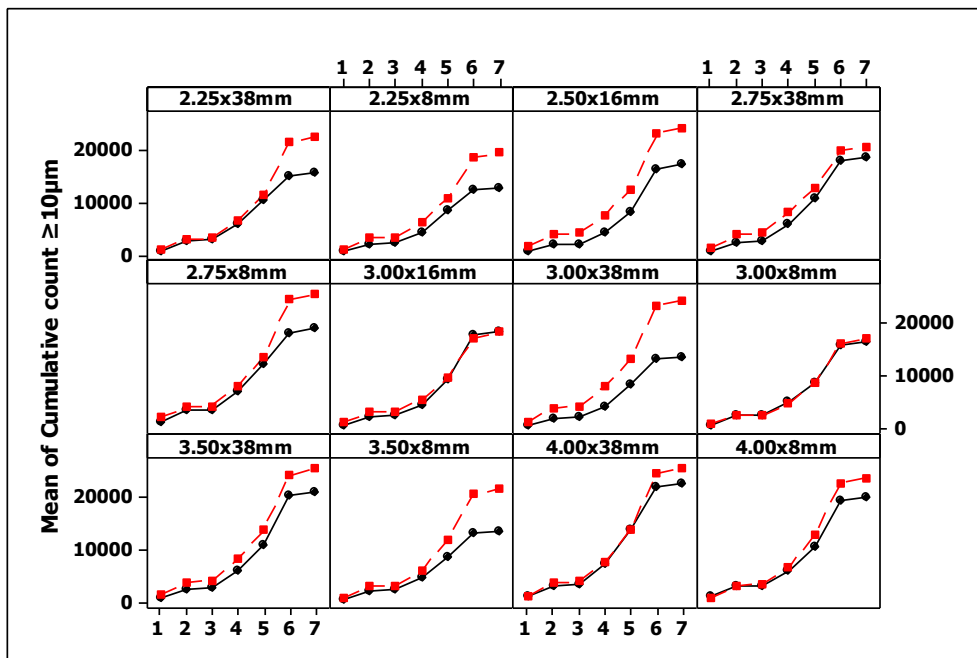


Figure 86 Light obscuration counts $\geq 10 \mu\text{m}$, comparing devices coated with HPC A (black) to devices coated with HPC B (red) tested on the CSU particulate method. Each of the 12 panels contains the data from a different size device (indicated by balloon diameter and length, D x L mm). Each line represents the mean cumulative particle count from 5 pairs of devices across steps 1 to 7 of the CSU test.

Chapter 3

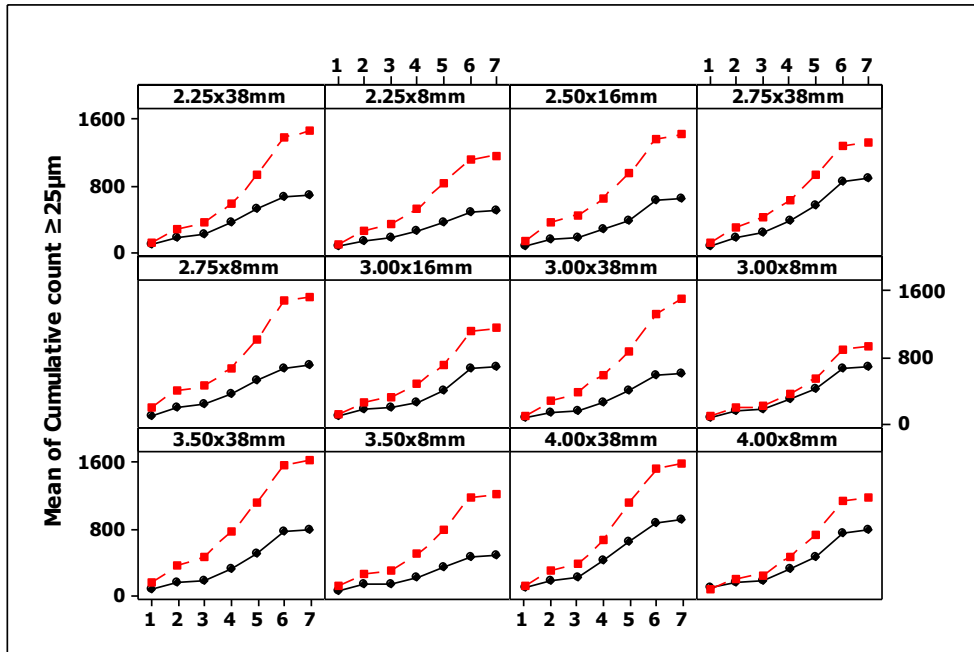


Figure 87 Light obscuration counts $\geq 25 \mu\text{m}$, comparing devices coated with HPC A (black) to devices coated with HPC B (red) tested on the CSU particulate method. Each of the 12 panels contains the data from a different size device (indicated by balloon diameter and length, D x L mm). Each line represents the mean cumulative particle count from 5 pairs of devices across steps 1 to 7 of the CSU test.

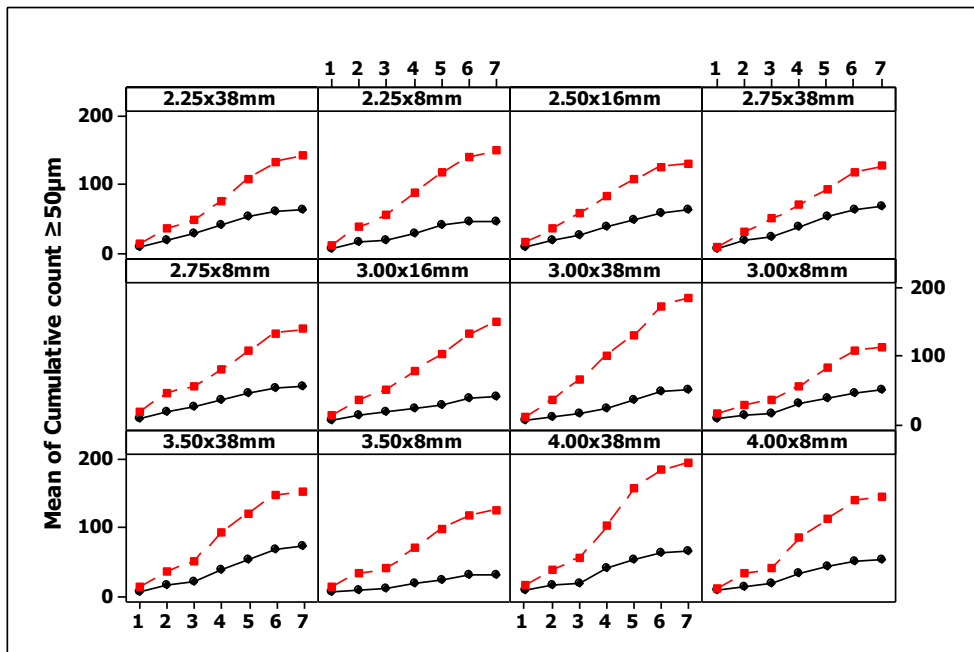


Figure 88 Light obscuration counts $\geq 50 \mu\text{m}$, comparing devices coated with HPC A (black) to devices coated with HPC B (red) tested on the CSU particulate method. Each of the 12 panels contains the data from a different size device (indicated by balloon diameter and length, D x L mm). Each line represents the mean cumulative particle count from 5 pairs of devices across steps 1 to 7 of the CSU test.

3.5 Chapter conclusion

The focus of the research presented in this chapter is on some of the findings that have been encountered through the particulate matter analysis of PTCA devices. Device

Chapter 3

design and functional attributes that impact the source of particulate matter has been explored using the novel LO methods developed.

The use of LO testing on parenteral solutions for particulate matter is the industry standard when it comes to the quality control of intravenous injections [36]. LO application to medical devices is less straightforward, as medical devices come in an abundance of designs with very different intended uses. This chapter introduced a novel method for the quality control and characterization of particles associated with percutaneous catheters and their accessory devices. The methodology, described in detail in Appendix 1, involves a break from the standard approach of sampling a portion of the rinse solution from a medical device using a flow through syringe sampler, and introduces a closed-loop apparatus that enables continuous sampling of the rinse solutions.

The closed loop methodology has been shown to be more repeatable and reproducible than the open vessel, flow through approach, enabling the better assessment of different PTCA medical devices through its unique design and adaptability. Thus, the closed loop apparatus is a powerful tool for the characterization of devices in a simulated clinical use procedure. The in-vitro test gives the medical device manufacturer the ability to evaluate the robustness of the design prior to clinical use and can be used to provide a quality control assessment of production batches prior to commercial release. The in-line particle counter facilitates a more rigorous means of ensuring that the water in which the device is rinsed is free from contamination prior to device testing, the same water used for blanking is used to rinse the device, thus ensuring that the particles coming from the device are accurately counted without test method interference.

Three different potential sources of device related, intrinsic particles from PTCA devices have been provided. Firstly the stent-coating on various DES devices has been assessed for durability under simulated use conditions. The results show that the properties of the coating can have a significant impact on whether the stent coating is prone to removal as particulate matter. For example, phosphorylcholine based DES coating resulted in significantly more particles than polymers such as PVDF-HFP, and PLGA. The methods have proved effective at detecting the breakdown of bio-degradable polymer DES coatings, e.g. PLGA, when exposed to conditions that promote hydrolysis of the polymer, thus providing an effective means of establishing

Chapter 3

stability over the device's shelf-life. Secondly the impact of accelerated-ageing on Pebax catheters has been shown to promote the formation of Nylon-12 derived particles. This phenomenon has significant ramifications for medical device manufacturers that wish to speed up device approval through the use of accelerated ageing. Finally, lubricious coatings have been shown to contribute significantly to particle counts, the simulated use methods are an effective way of determining the durability of these catheter coatings however orthogonal methods such as LM and SEM should be used to determine whether the particles are real, especially when using silicone-based coatings.

The three examples of intrinsic particle sources described have all led to changes in design of the medical devices to improve the particle counts. Significant changes have been undertaken by the medical device industry to provide assurances that the particles released do not pose a safety concern, and it looks like the regulatory bodies will continue to look for more assurances in this vein for the foreseeable future. The US FDA have been asking for similar testing to be carried out on ever more devices, not just PTCA catheters but also peripheral intervention devices, and structural heart devices such as trans catheter aortic valve replacement systems.

Importantly the work presented clearly demonstrates that a holistic approach should be taken when assessing the particulate matter associated with medical devices. Manufacturers need to be mindful of the intended use of the device so that appropriate simulated use procedures can be developed. This awareness must include the impact of the particular anatomy the device must pass through as well as the intended target, and also the ancillary devices that are utilised. The material properties of devices, including stability over the device's shelf life must be considered when designing devices. It is apparent that one particulate counting method will not suffice for gaining an understanding of particulate matter associated with candidate medical devices, but the manufacturer must also identify the type of particles present so that their origin can be determined.

Chapter 4

The use of design of experiment and mass spectrometry to identify a previously uncharacterized drug degradation pathway of everolimus in acetonitrile

4 Chapter introduction

Everolimus degradation products observed during the testing of everolimus eluting stents is the focus of the work reported in this chapter. DES play an important role in the reduction of neointimal hyperplasia in the treatment of coronary artery disease. The stents are coated using solutions prepared in organic solvents, and it is important to understand any potential interactions that may lead to drug degradation in solution. Instances of everolimus degradation were first observed in the laboratory sporadically during the HPLC-UV analysis of everolimus in coating solutions prepared for drug eluting stents. It was quickly discovered that the test methods used to measure everolimus from the DES were also affected by everolimus degradation. This chapter describes the approach taken to discover the cause of the everolimus degradation.

Whilst testing everolimus eluting stents and coating solutions in our laboratory, the presence of additional chromatographic peaks were observed in the HPLC drug content assay, and in the impurities and related substances test method described in section 2.2.1. It will be shown that these peaks correspond to previously unknown degradation products of everolimus as distinct from the known degradation products described in the introduction section of this thesis. Initial investigations established that the peaks were potentially everolimus related because they had a characteristic 3-peak UV spectrum indicative of everolimus. Troubleshooting of the issue quickly established that a laboratory reagent, acetonitrile, as the most likely cause of everolimus degradation. However degradation of everolimus did not occur in all of the acetonitrile batches sourced by the laboratory, pointing towards the presence of an unknown,

Chapter 4

intermittent occurrence of the cause of degradation. The work reported here points to an interaction between base and propionitrile contamination of acetonitrile as a root cause of everolimus instability. Design of experiment used in aid to the investigation was effectively used to decipher this interaction.

4.1 Description of the problem encountered with everolimus degradation in testing everolimus eluting stents.

Figure 89 (a) shows a typical chromatogram for everolimus using a HPLC assay to quantify everolimus in DES coating solutions, methods described in section 2.2.1. The main peak in the chromatogram with a retention time of 10 min has been identified by reference standards as the pyran isomer of everolimus and the second, later eluting, smaller peak, with a retention time of 12 min, corresponds to the oxepene isomer of everolimus. The chromatogram in Figure 89 (b) on the other hand is of an everolimus sample exhibiting degradation, as evidenced by the group of early eluting peaks in the chromatogram between 4 and 6 min. The formation of these additional peaks corresponds to a reduction in the everolimus peak area, indicating that the peaks are degradation products of the parent everolimus molecule.

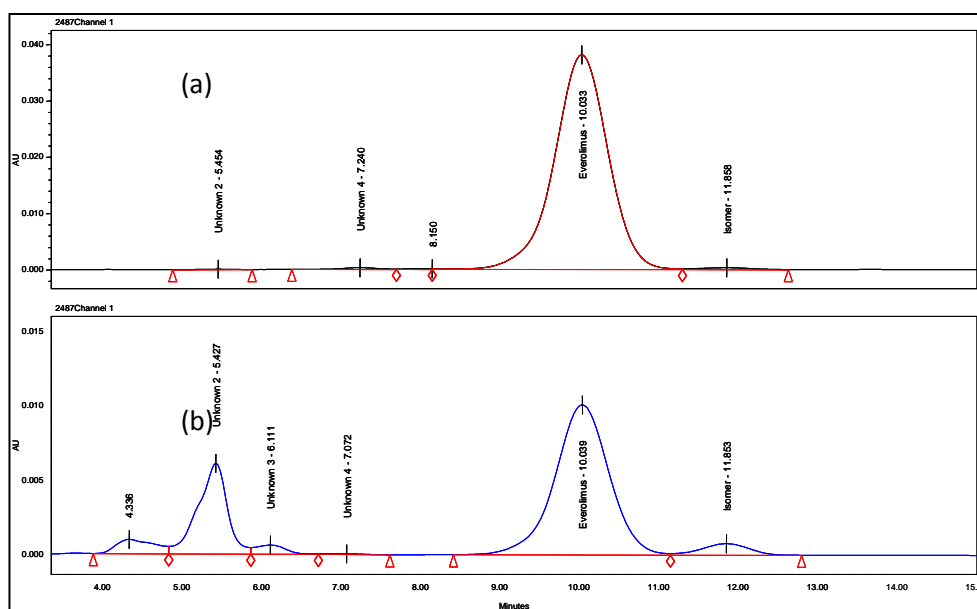


Figure 89 Typical Chromatogram of everolimus sample (a) without degradation and (b) with degradation. This chromatogram was obtained using the everolimus assay described in section 2.2.1.

The everolimus impurities and related substances method previously described in section 2.2.1 was used to acquire separation of these degradation products which could

Chapter 4

then be compared to the known everolimus degradation products. This chromatogram is shown in Figure 90, the peaks have relative retention times (RRT) of 0.58, 0.71 and 0.75 which established that they represent different compounds than the known everolimus impurities and related substances[39], [54]. UV spectra of the three peaks were collected using a photo diode array detector - Figure 91 to Figure 93. The characteristic 3 peaked triene absorption band with λ_{max} at 277 nm is present for all three degradation products, as such providing additional supporting evidence that the peaks are everolimus-related compounds. The chromatogram does not show an increased level of the base related degradation products 013-99, 804-95, so the well reported base degradation pathway of everolimus[57] and other related macrolides[39], [54] was not considered the obvious cause for these unidentified compounds. The three new peaks appeared sporadically and their occurrence was linked to particular batches of acetonitrile used to prepare samples and standard solutions of everolimus, shown in Figure 94.

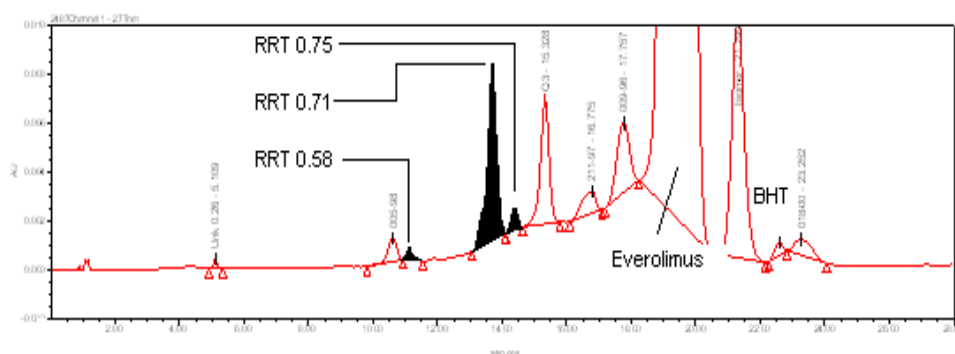


Figure 90. Acetonitrile induced degradation products relative to the retention time of everolimus by HPLC

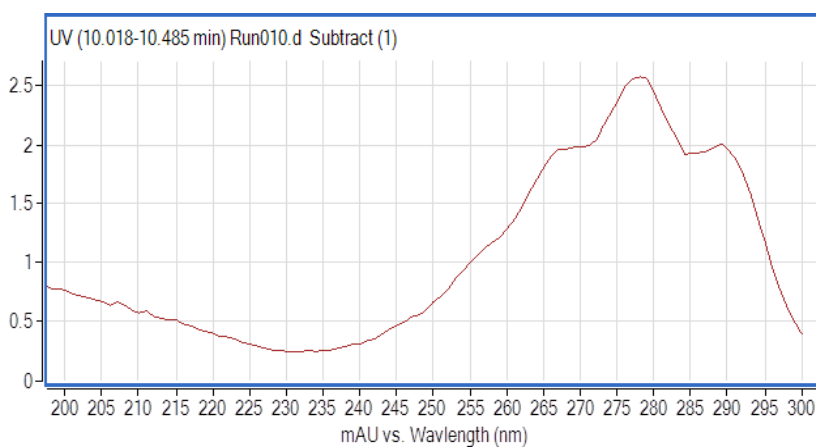


Figure 91 Three peak shaped UV spectrum characteristic of the triene functional group of everolimus, here seen on the degradant product appearing at RRT 0.58.

Chapter 4

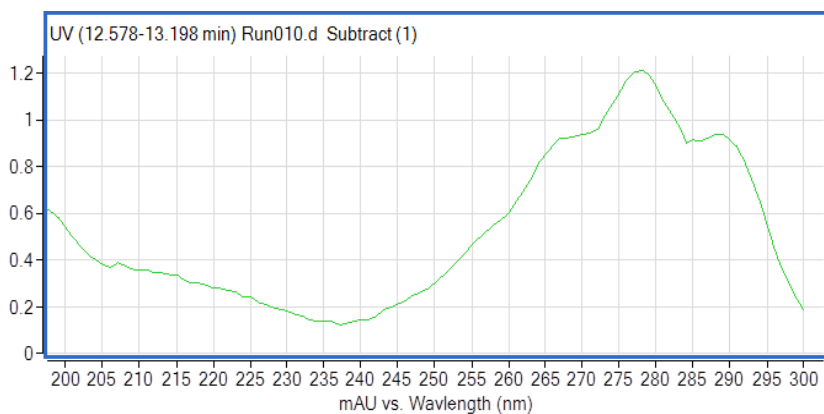


Figure 92 Three peak shaped UV spectrum characteristic of the triene functional group of everolimus, here seen on the degradant product appearing at RRT 0.71.

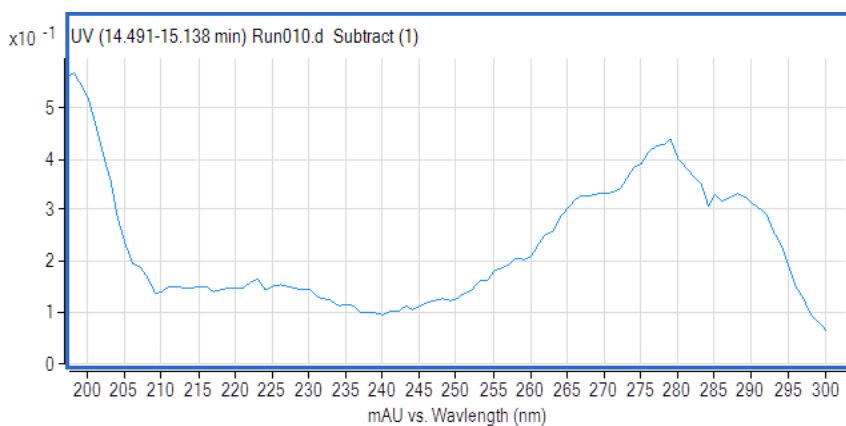


Figure 93 Three peak shaped UV spectrum characteristic of the triene functional group of everolimus, here seen on the degradant product appearing at RRT 0.75.

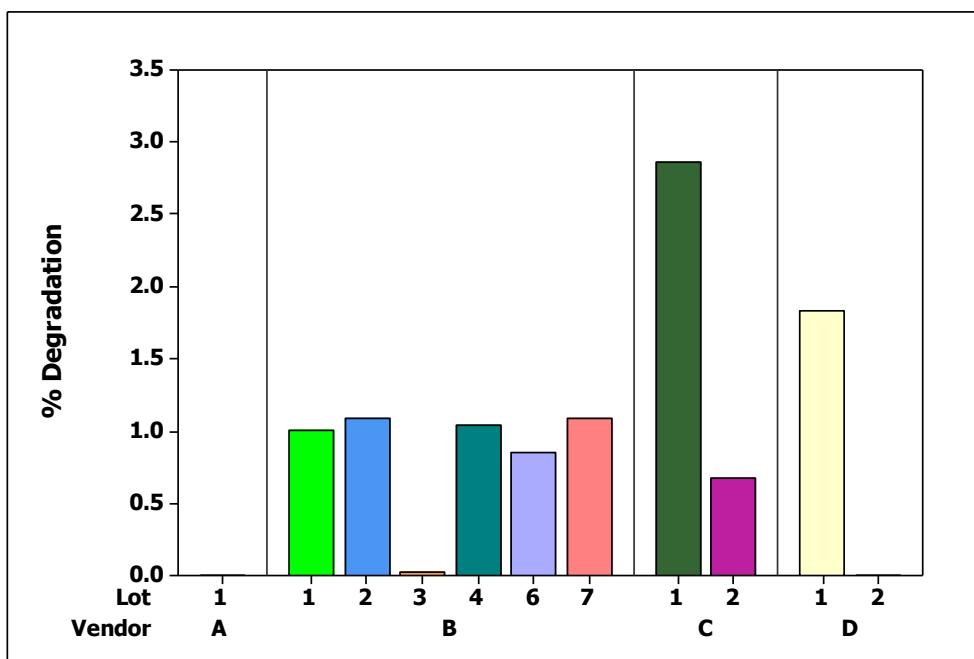


Figure 94 Plot of the % everolimus degradation in a 5 µg/mL everolimus solution attributed to the 3 degradation products appearing at RRT 0.58, 0.71, and 0.75. The plot shows the sum of the 3 products in acetonitrile in different manufacturing lots from 4 vendors (A, B, C, and D).

4.2 Evaluation of acetonitrile used for preparation of everolimus solutions.

Acetonitrile is obtained as a by-product of the manufacture of acrylonitrile, a chemical mostly produced by ammoxidation of propylene [113]. The acetonitrile by-product is purified by the solvent suppliers to remove impurities and bring the acetonitrile to an acceptable grade for use as chemical reagent[114]. The potential contaminants from this process are acid, base, various nitriles and water. Acetonitrile sourced from various vendors was therefore analysed for the presence of these, and other possible contaminants. The gas chromatography method described in section 2.2.1, with mass spectrometric detection (GC-MS) was developed for this purpose. The GC-MS method identified water and propionitrile in acetonitrile samples. It was found that acetonitrile had little or no water present when received from the manufacturers. But water levels increased upon opening bottles and handling the solvent in the laboratory, as shown in the chromatogram presented in Figure 95. The figure shows that while the level of propionitrile remains constant, the water level increases when the acetonitrile is used to make up an everolimus standard, and it increases further when the acetonitrile is distilled using vacuum filtration in a rotary evaporator.

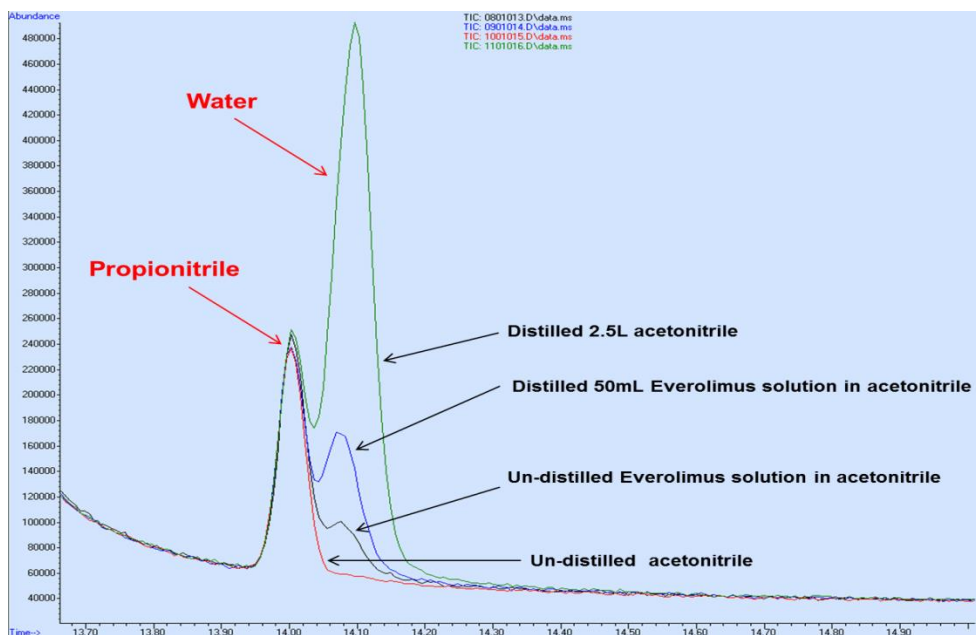


Figure 95 Gas chromatograph of acetonitrile showing the water and propionitrile peaks in vacuum distilled and un-distilled acetonitrile solutions, with and without everolimus present.

Propionitrile is a by-product of acrylonitrile production along with acetonitrile[113]. Levels of propionitrile in acetonitrile varied in samples of the solvent sourced from different vendors, and indeed from batch to batch of the same vendor's material. Typical propionitrile levels ranged from approximately < 1 ppm up to 200 ppm, as determined by GC-MS. Distillation of acetonitrile can reduce the level of propionitrile, but complete removal of this impurity was not achieved, with instead a reduction of the level by approximately 30% by fractionation distillation.

Aqueous titration for acid and base in acetonitrile was attempted using the American Chemical Society (ACS) standard methods for determination of titratable acid and base in acetonitrile [115]. The concentration of the ACS titrants was also decreased from 0.01M to 0.001M in an effort to improve sensitivity. Figure 96 shows that no trend was observed between the levels of acid and base measured in the acetonitrile solvents and the level of everolimus degradation products assayed by HPLC. It was observed in Figure 97 that distilled acetonitrile was marginally more acidic than un-distilled acetonitrile by the same titration method.

Chapter 4

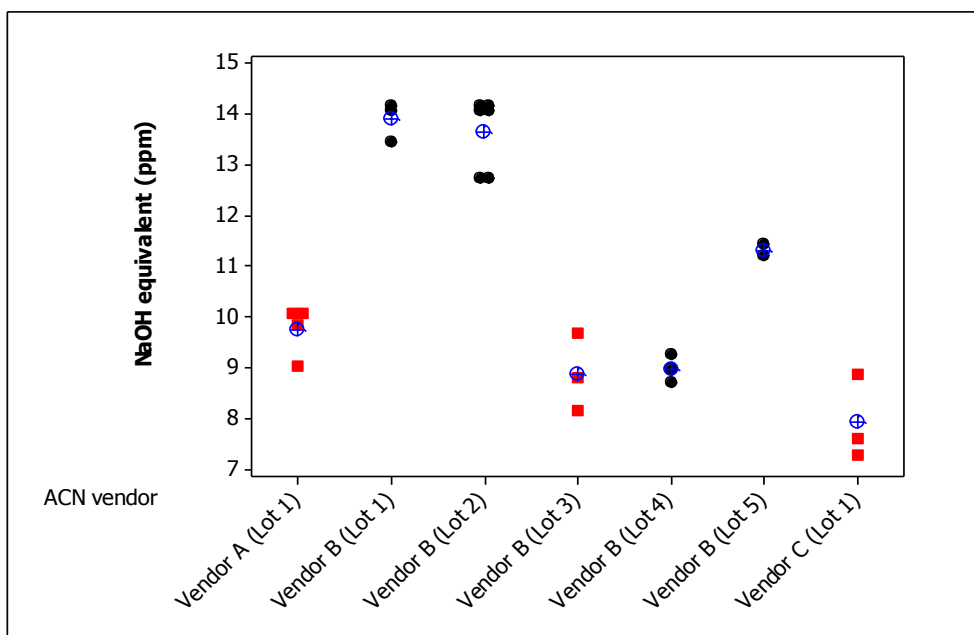


Figure 96 Graph showing the results of aqueous titration for acid and base in acetonitrile using the American Chemical Society (ACS) standard methods for determination of titratable acid and base (in black) for acetonitrile where everolimus degradation products appeared compared (in red) to acetonitrile in which everolimus was free from degradation.

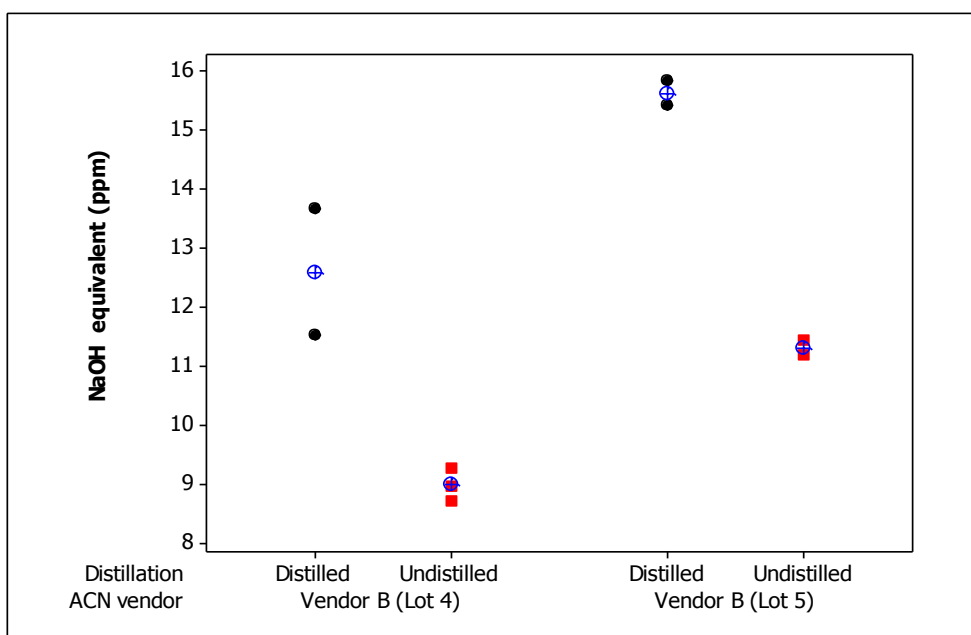


Figure 97 Graph showing the results of aqueous titration for acid and base in acetonitrile using the American Chemical Society (ACS) standard methods for determination of titratable acid and base (in black) for distilled acetonitrile which was marginally more acidic than (in red) un-distilled acetonitrile by the same titration method.

Distillation of acetonitrile resulted in a reduction in the formation of the degradation products. For example, Figure 98 (a) shows HPLC assays for the degradation profile in 5 $\mu\text{g/mL}$ everolimus solutions prepared using solvent sourced from vendor B. In Figure 98 (b) and (c) the chromatograms for the everolimus degradation products are shown

Chapter 4

after the solvent has been distilled prior to use for solution preparation. Peaks for the degradation products at RRT 0.58 and RRT 0.75 are eliminated when using the distilled solvent and the peak area at RRT 0.75 has been reduced significantly. In contrast, after the removal by distillation of 66% of the initial solvent volume the peak area of RRT 0.71 has remained at the same level as that observed for the solutions using never-distilled acetonitrile. However peak areas for RRT 0.58 and RRT 0.75 have increased significantly compared to those using never-distilled acetonitrile. Thus, it is probable that the contaminant that causes the formation of the everolimus degradation products appearing at RRT 0.58 and RRT 0.75 is less volatile than acetonitrile and is thus concentrated in the fraction remaining upon distillation.

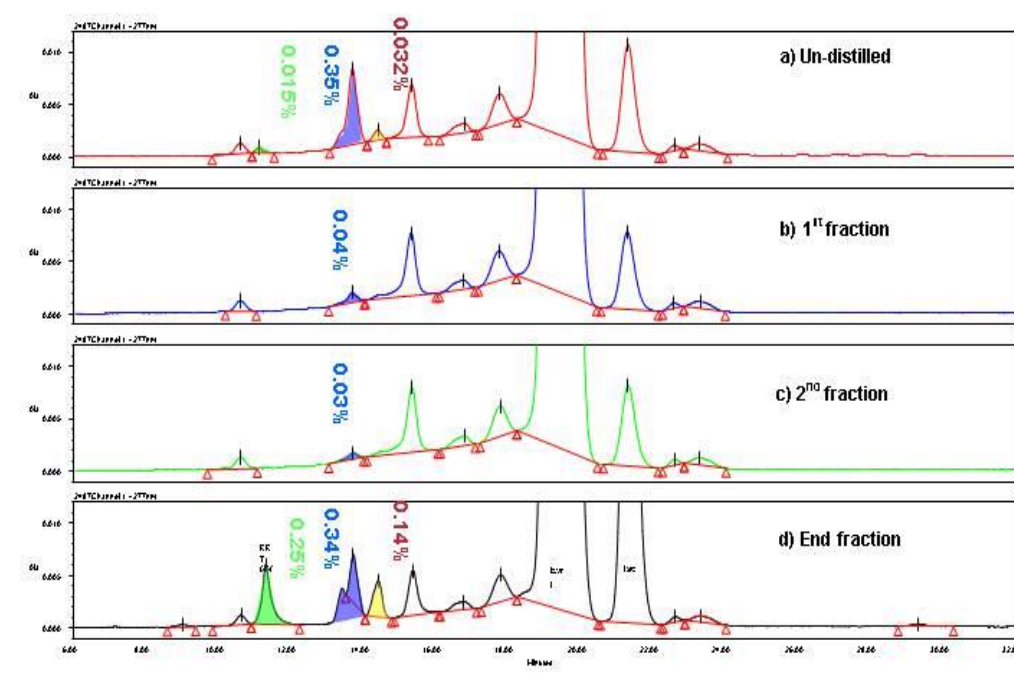


Figure 98 HPLC chromatogram for everolimus dissolved in acetonitrile (vendor B) that (a) solvent prior to distillation or never-distilled acetonitrile, (b) and (c) the 1st and 2nd distilled solvent fractions, respectively, and (d) solvent that was remaining after distilling 66% (Fraction 1 and 2) off.

The concentration of the degradation products was evaluated in 5 $\mu\text{g/mL}$ everolimus solutions. The solutions were prepared in distilled and never-distilled acetonitrile from vendor A (1 Lot) and B (6 Lots) over a 17 day period. The level of degradation shown in Figure 99 was measured at day 0, day 7 and day 17. Interestingly, never-distilled acetonitrile that showed no initial degradation (Vendor A, Lot 1 and Vendor B, Lot 3) remained stable over the 17 days. Acetonitrile that exhibited degradation at day 0 continued to degrade over time, albeit at a much reduced level in distilled acetonitrile.

Chapter 4

The levels of water and propionitrile in different batches of acetonitrile were measured, and compared in Figure 100 to the amount of everolimus degradation in 5 $\mu\text{g/mL}$ everolimus solutions prepared in the same batches of solvent. No trend between the extent of degradation and the levels of water and propionitrile was apparent.

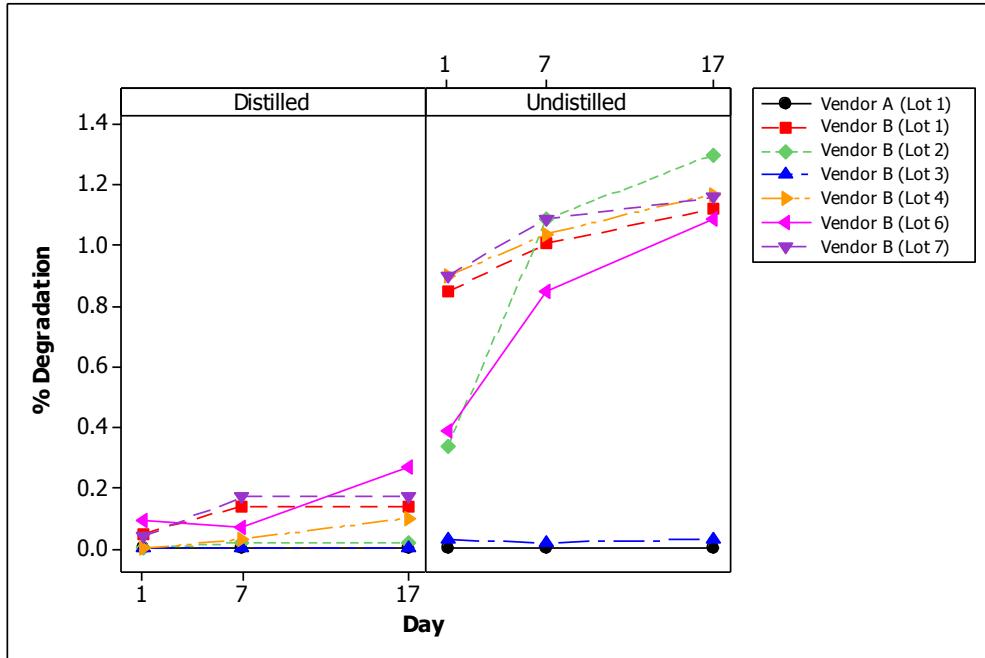


Figure 99 Plot showing the concentration of the degradation products in 5 $\mu\text{g/mL}$ everolimus solutions prepared in distilled and undistilled acetonitrile from vendor A (1 Lot) and B (6 Lots) over a 17 day period.

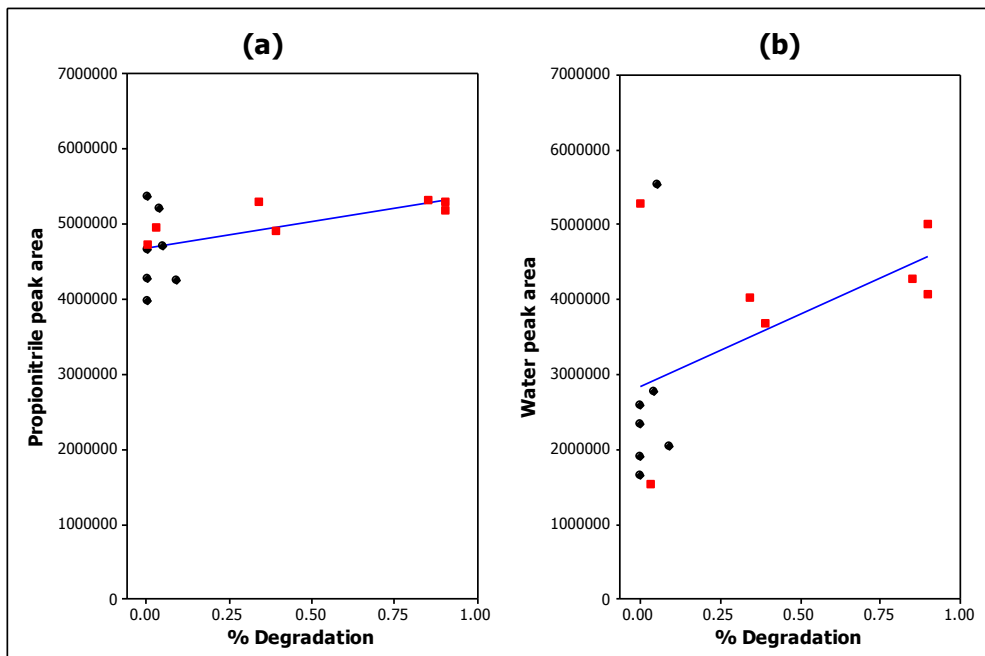


Figure 100 Plot showing the levels of water (b) and propionitrile (a) in different batches of acetonitrile (never distilled in red, and distilled in black) compared to the cumulative amount of everolimus degradation from the three unknown compounds in 5 $\mu\text{g/mL}$ everolimus solutions.

Chapter 4

In another attempt to recreate the characteristic degradation products, direct addition of propionitrile, water, acid and base to everolimus in acetonitrile was undertaken. The components were added one at a time at levels that were near the levels measured in batches of acetonitrile. These simple, one-factor-at-a-time (OFAT) experiments did not result in the appearance of the three distinctive degradation products at RRT 0.58, RRT 0.71 and RRT 0.75 in the everolimus HPLC assay. Rather than eliminate these compounds from the investigation, and potentially miss an unknown interaction between them, the next step was to use the DoE approach to look for interactions. DoE was used to plan a series of experiments that involved the addition of mixtures of the compounds to everolimus in acetonitrile solutions. HPLC was used to analyse the solutions for evidence of the degradation of everolimus.

4.3 Initial DoE carried out to recreate the everolimus degradation products.

The initial DoE, termed DoE 1, involved the addition of different levels of strong acid and base, weak acid and base, propionitrile, and water to acetonitrile that was previously determined not to cause everolimus degradation after distillation. This solvent was supplied by Vendor A, the solutions were prepared as described in section 2.2.3, Table 5 and Table 6. Everolimus was prepared in these solutions to a concentration of 500 µg/mL. Concentrations of the degradation products were calculated from their peak areas and expressed as a percentage of the peak area of everolimus in non-degraded samples using Equation 5.

Equation 5 Calculation of the % concentration of degradation products of everolimus from the peak areas of their chromatographic peaks. This equation is for samples where the concentration of everolimus in the degraded and non-degraded samples are the same, for instances when the concentration was different then this was accounted for in the calculation.

$$\% \text{ Conc. of degradation product} = \frac{\text{Peak area of degradation product}}{\text{Peak area of everolimus in undegraded sample}} \times 100$$

The presence of two peaks corresponding to known degradation products 804-95 and 005-98 were monitored to check the validity of the experiment; these peaks are seen at 9.2 and 11.7 minutes in Figure 101. These particular peaks were selected as they are known to be everolimus base and acid degradation products, respectively. The

Chapter 4

occurrence of these compounds in the samples provided an internal means of evaluating the degradation processes involved.

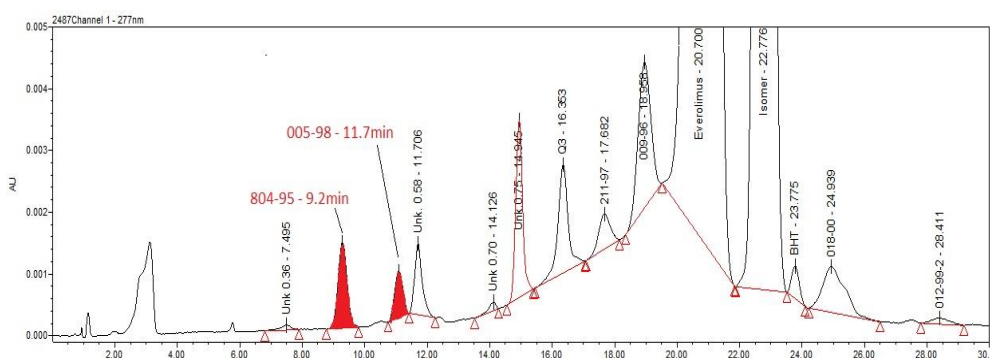


Figure 101 A chromatogram showing two peaks corresponding to known degradation products 804-95 and 005-98 seen at 9.2 and 11.7 minutes.

Figure 102 and Figure 103 show the behaviour of the % peak area in the chromatograms for 005-98 and 804-95. The peak for the base-induced degradation product, 804-95, increases with the amount of ammonium hydroxide present, and is eliminated in the presence of high levels of hydrochloric acid. The % peak area of the acid induced degradation product, 005-98, has an opposite behaviour; increasing with the acid content and is eliminated in the presence of sodium hydroxide. This confirmed that expected everolimus degradation behaviour was achieved in the experiment.

Chapter 4

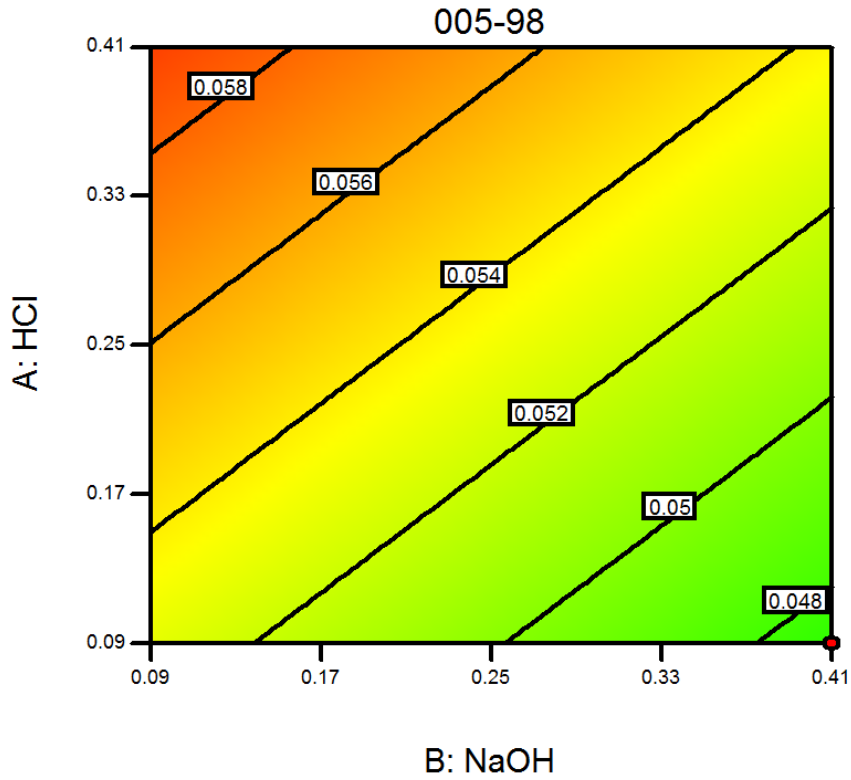


Figure 102 Plot showing the increase in 005-98, a known acid induced everolimus degradation product. Blue/green colouring indicates low concentration and red/yellow colouring indicates high concentration.

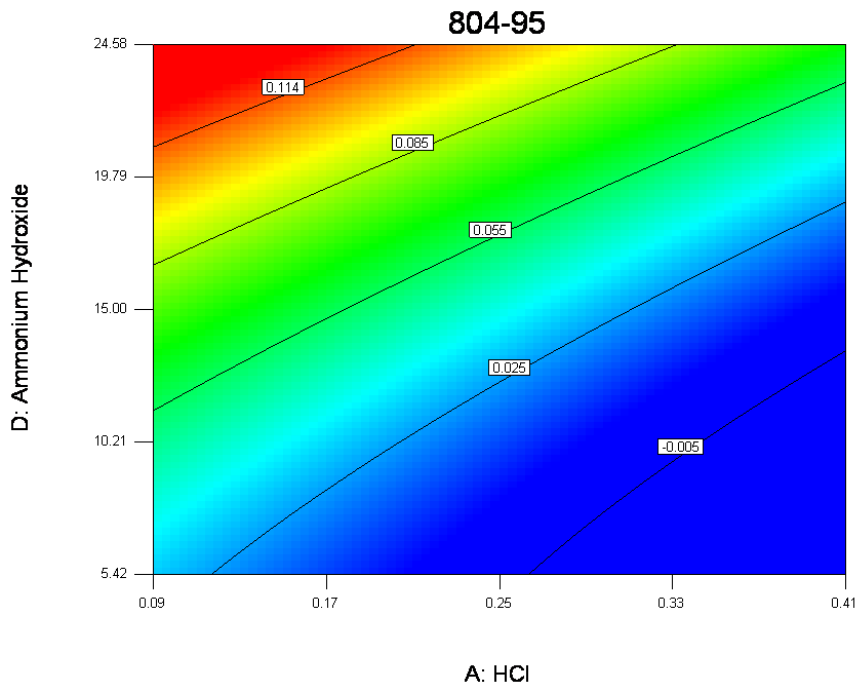


Figure 103 Plot showing the increase 804-95, a known base induced everolimus degradation product. Blue/green colouring indicates low concentration and red/yellow colouring indicates high concentration.

Chapter 4

The new degradation products were detected in some, but not all of the solutions prepared. The peak areas of the unknown degradation products with RRT of 0.58, 0.71 and 0.75 decreased with increasing acid present, which points towards a base catalysed degradation mechanism that is prevented in the presence of acid. Indeed, a relationship was found between the concentration of base and the peak areas at RRT 0.58 and, 0.71 and 0.75. Furthermore, it was established that an interaction between propionitrile and base leads to the highest peak areas of RRT 0.58 and 0.75.

4.3.1 Peak at RRT 0.58

The peak at RRT 0.58 was not created regardless of the level of water or propionitrile present in solutions with relatively high acid concentration (0.5 ppm hydrochloric acid, and 30 ppm acetic acid). However, under basic conditions low levels of the peak at RRT 0.58 were created. Figure 104 and Figure 105 show the concentration of the peak at RRT 0.58 formed in solutions with 0 and 1000 ppm of water respectively, and with no acid present. These plots show the concentration of the degradation product at RRT 0.58 created in the range of 0.09 to 0.41 ppm of NaOH and 180 to 819 ppm propionitrile. Blue colouring indicates low concentration (< 0.01%) of the degradation product at RRT 0.58 and red colouring indicates higher concentration (> 0.025%) of the degradation product at RRT 0.58. The plots show that the level of this degradation product increased proportionally with increasing levels of propionitrile and base. More of the degradation product at RRT 0.58 is formed in the presence of 1000 ppm of water than with no water added, thus providing evidence that water provides favourable conditions for the degradation of everolimus to yield the peak at RRT 0.58.

Chapter 4

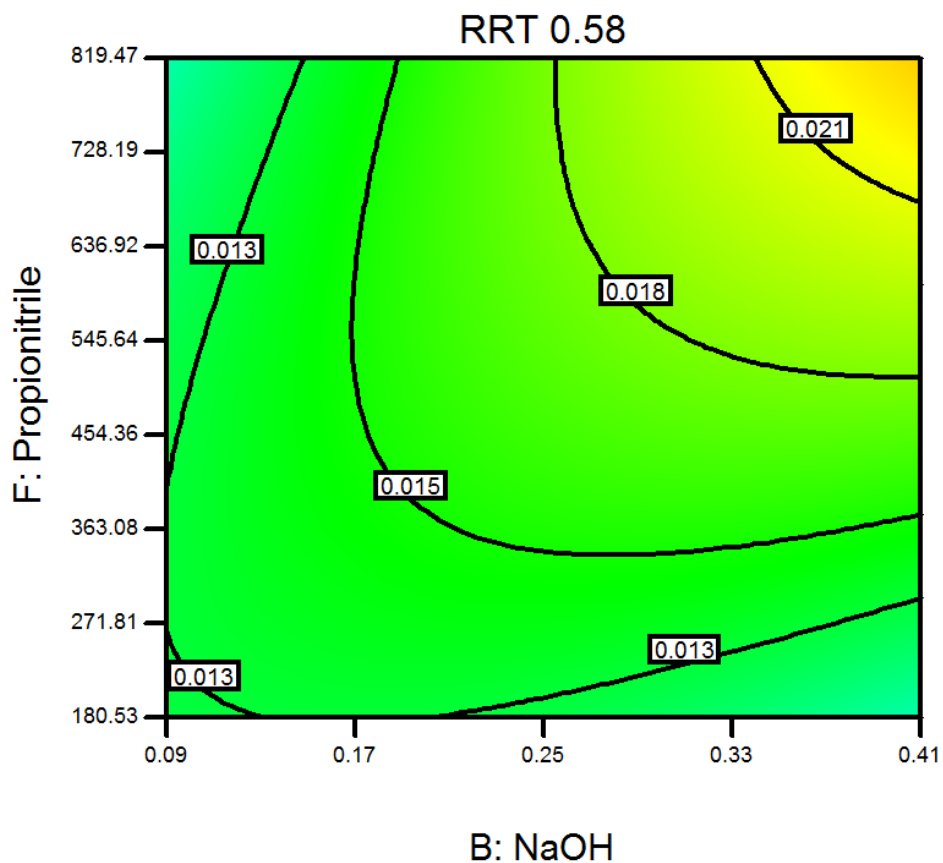


Figure 104 Plot showing the % concentration of degradation product RRT 0.58 in low acid and water conditions and in the range of 0 to 0.5 ppm sodium hydroxide (x-axis) and 0 to 1000ppm propionitrile (y-axis). Green colouring indicates relatively low concentration of RRT 0.58 and yellow colouring indicates higher concentration of RRT 0.58.

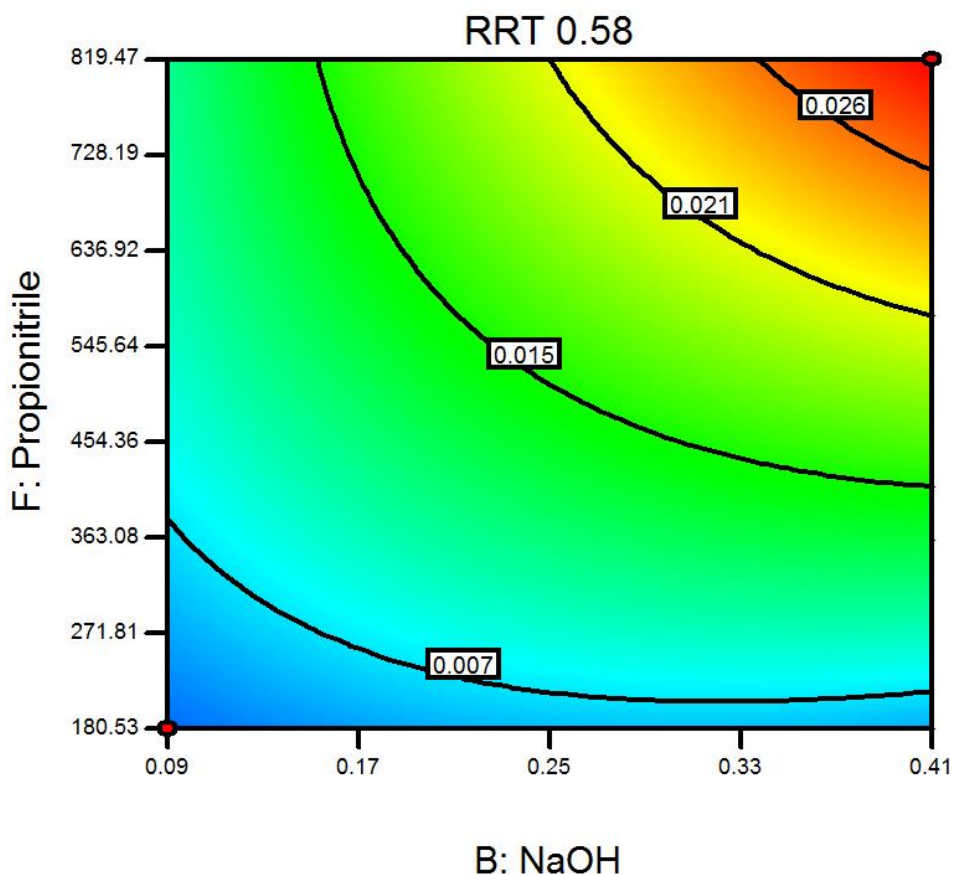


Figure 105 Plot showing the % concentration of degradation product RRT 0.58 in low acid and high water (10000 ppm) conditions and in the range of 0 to 0.5 ppm sodium hydroxide (x-axis) and 0 to 1000 ppm propionitrile (y-axis). Blue colouring indicates low concentration of RRT 0.58 and red colouring indicates high concentration of RRT 0.58.

4.3.2 Peak at RRT 0.75

Figure 106 and Figure 107 show plots for the degradation product at RRT 0.75 as a function of sodium hydroxide and propionitrile concentration in solutions with no added acid and with 0 and 1000 ppm water added, respectively. As with the peak at RRT 0.58 the degradation product does not form in the presence of acid, thus basic conditions favour the formation of the peak at RRT 0.75 too. Except in the presence of water and the absence of acid (Figure 107), no trend was observed for the formation of the peak at RRT 0.75 with increasing levels of propionitrile and base (Figure 107). These data points towards the formation of the degradation product appearing at RRT 0.75 being more dependent on the presence of water than that for the peak at RRT 0.58.

Chapter 4

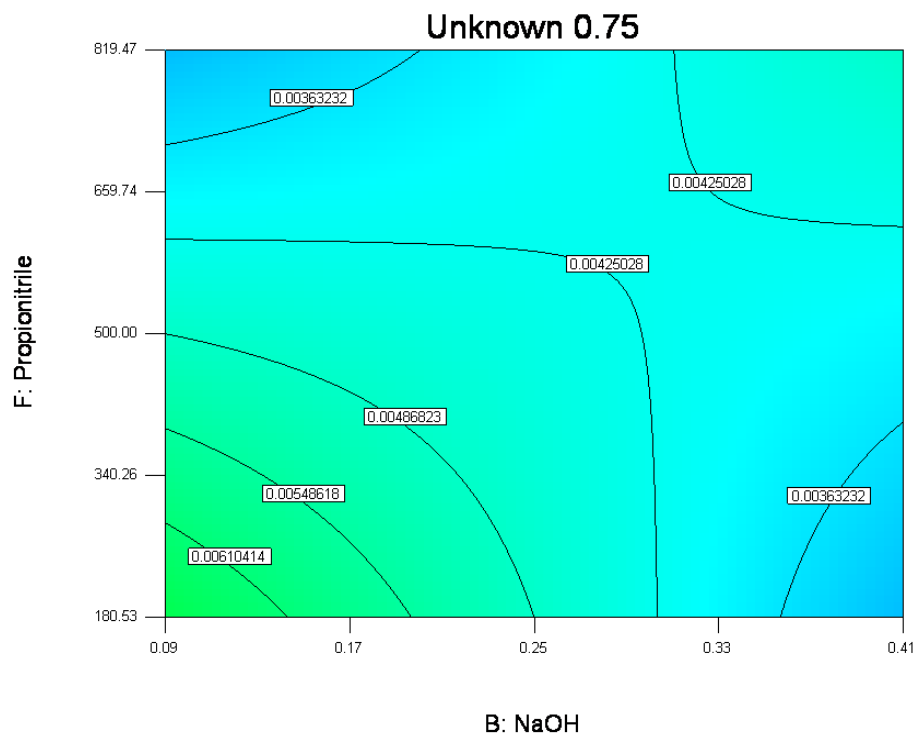


Figure 106 Plot showing the % concentration of degradation product RRT 0.75 in low acid and low water conditions and in the range of 0 to 0.5 ppm sodium hydroxide (x-axis) and 0 to 1000 ppm propionitrile (y-axis). Blue colouring indicates low concentration of RRT 0.75 and green colouring indicates higher concentration of RRT 0.75.

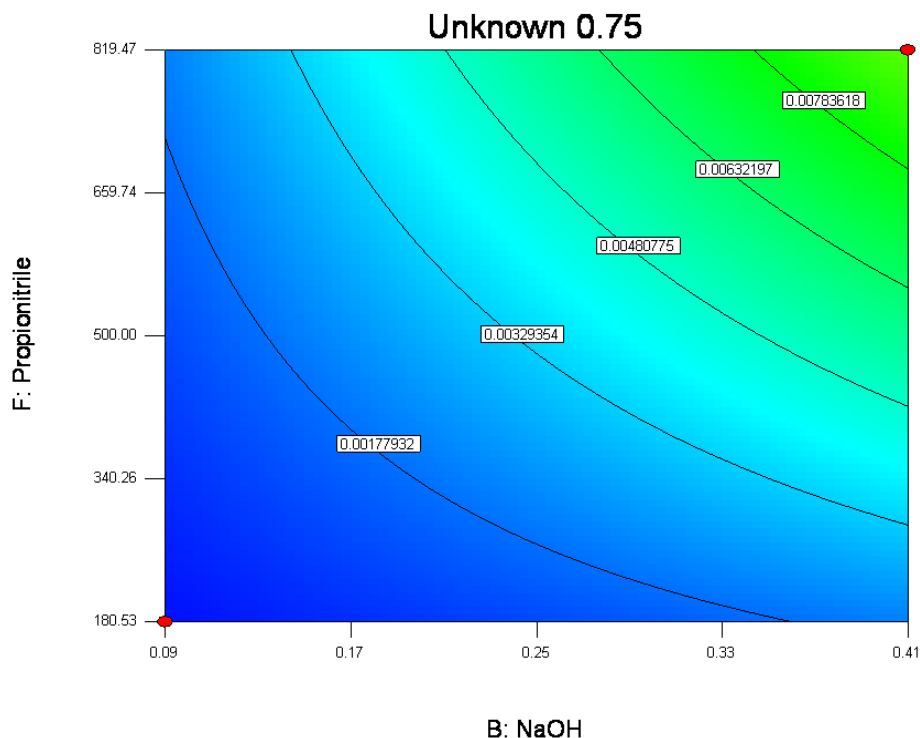


Figure 107 Plot showing the % concentration of degradation product RRT 0.75 in low acid and 1000 ppm water conditions and in the range of 0 to 0.5 ppm sodium hydroxide (x-axis) and 0 to 1000 ppm propionitrile (y-axis). Blue colouring indicates low concentration of RRT 0.75 and green colouring indicates higher concentration of RRT 0.75.

Chapter 4

4.3.3 The peak at RRT 0.71

The appearance of a peak associated with a degradation product at RRT 0.71 did not occur in many of the prepared solutions. Like the other two degradation products, its formation is inhibited by the presence of acid. The peak was observed in only 4 out of 29 solutions, yet its presence seemed correlated to increased propionitrile concentration as observed from the plot in Figure 108. The occurrence of the peak at RRT 0.71 does not appear to be linked to the amount of water present, and this may indicate that the product at RRT 0.71 can form under dry solvent conditions, however with so little data from the appearance of the peak at RRT 0.75 acquired from this experiment it cannot be stated with confidence.

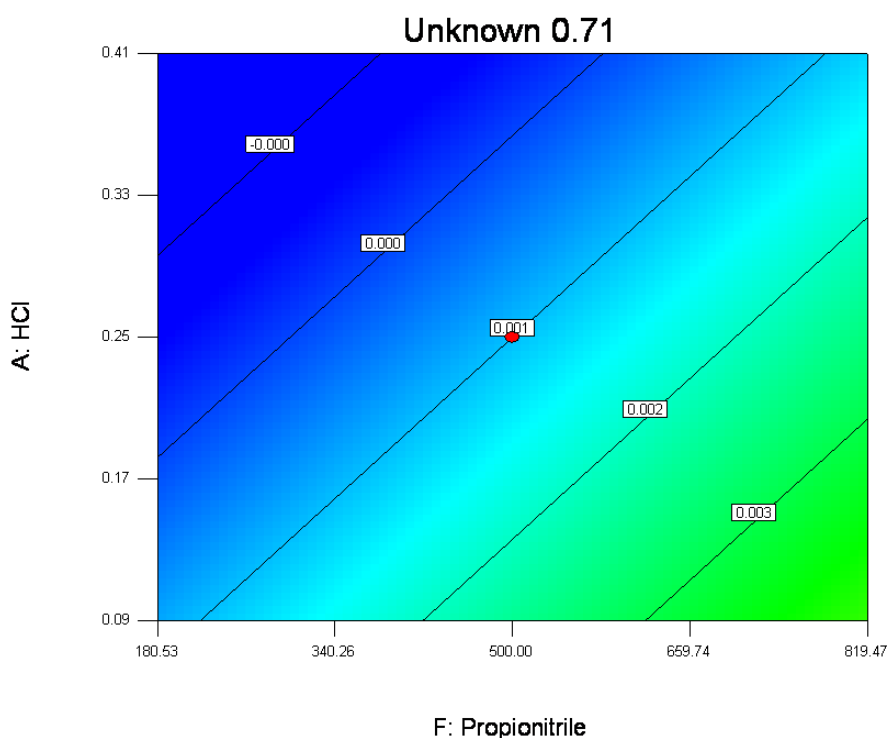


Figure 108 Plot showing the effect of propionitrile and HCl concentration on the formation of the everolimus degradation products RRT 0.71.

Although the initial DoE was successful at identifying factors that caused the degradation products, the level of each degradation product produced was extremely low, thus pushing the 0.005% limit of detection for the HPLC method. The low levels of degradation achieved (0.003 to 0.05%) were about 100 to 1000 times lower than the typical concentration of the degradation products routinely seen in samples and

Chapter 4

standards. Therefore, having identified base and propionitrile as the causes of the degradation, the concentration of each of these was increased in a second DoE to increase the concentration of the degradation products.

4.4 Second DoE carried out to increase the concentration of the everolimus degradation products.

DoE 2 was carried out to increase the level of everolimus degradation and to confirm that the correct degradation products were being created. Acid was not included this time as its effect on reducing the occurrence of the degradation products was proven. Water was not deliberately added in this experiment, to explore further the observation in the first DoE where little of the peak at RRT 0.71 was produced compared to that at RRT 0.75. Water was limited by using dry solvents, so it was hoped in this experiment the formation of the peak at RRT 0.71 would be encouraged in preference to that at RRT 0.75. Acetonitrile from vendor B that had previously resulted in the formation of the 3 everolimus degradation products and acetonitrile from vendor C that didn't cause degradation were included as a control. By comparing the chromatography it was confirmed that vendor B's acetonitrile increased the concentration of the 3 degradation products, and it was confirmed that the same 3 degradation products formed in vendor C solvent. The experimental plan for DoE 2 is provided in Section 2.2.3, Table 7 and Table 8.

The DoE 2 experiment was successful at increasing the peak area of the everolimus degradation products significantly, as observed from the plots in Figure 109 and Figure 110 of the overall percentage of everolimus degradation. The percentage of everolimus degradation was calculated by comparing the peak area of everolimus to the peak area of a non-degraded reference standard.

Chapter 4

Equation 6 Calculation of the % concentration of everolimus degradation from the peak area (PA) of the everolimus chromatographic peak. This equation is for samples where the concentration of everolimus in the degraded and non-degraded samples are the same, for instances when the concentration was different then this was accounted for in the calculation.

$$\% \text{ Conc. of everolimus degradation} = 100 - \frac{\text{PA everolimus in degraded sample}}{\text{PA everolimus in undegraded sample}} \times 100$$

Relatively high levels (50 ppm) of the strong base, sodium hydroxide, results in complete degradation of everolimus, but the 3 degradation products were not observed under these aggressive conditions. It is probable that any degradation products formed were not stable for sufficient time prior to analysis, similar to the reported behaviour of sirolimus in strong base conditions[57]. Four (4) out of the 24 preparations showed degradation of all of the everolimus to compounds that were not detectable using the HPLC method, and these were at a high concentration of NaOH. Fortunately, even though high levels of everolimus degradation occurred in the presence of ammonium hydroxide, the degradation products appearing at RRT 0.58, RRT 0.71 and RRT 0.75 persisted in the resultant solutions. The concentration of the degradation products was higher in vendor B's acetonitrile (Figure 109) than in vendor C's solvent (Figure 110). It is expected that vendor B's solvent would result in higher levels of degradation because of the residual levels of degradation that already occur in this solvent without any additives.

Although all three degradation products appeared in some of the 24 preparations there was very little of the product at RRT 0.75 observed compared with those at RRT 0.58 and RRT 0.71. Just 3 out of the 24 preparations contained the peak at RRT 0.75, and all were below 1.0% w/w; compared to 12/24 containing the peak at RRT 0.71 and 16/24 containing the peak at RRT 0.58, with the highest recorded concentrations of 17% and 57%, respectively. The low quantities of the degradation product at RRT 0.75 are consistent with the observation that formation is favoured under conditions of high water content.

Chapter 4

Design-Expert® Software
 Factor Coding: Actual
 Original Scale
 (median estimates)
 Overall Degradation

X1 = A: Base strength
 X2 = C: Base type

Actual Factors
 B: Propionitrile = 918.92
 D: Solvent = Vendor B

■ C1 NaOH
 ▲ C2 NH4OH

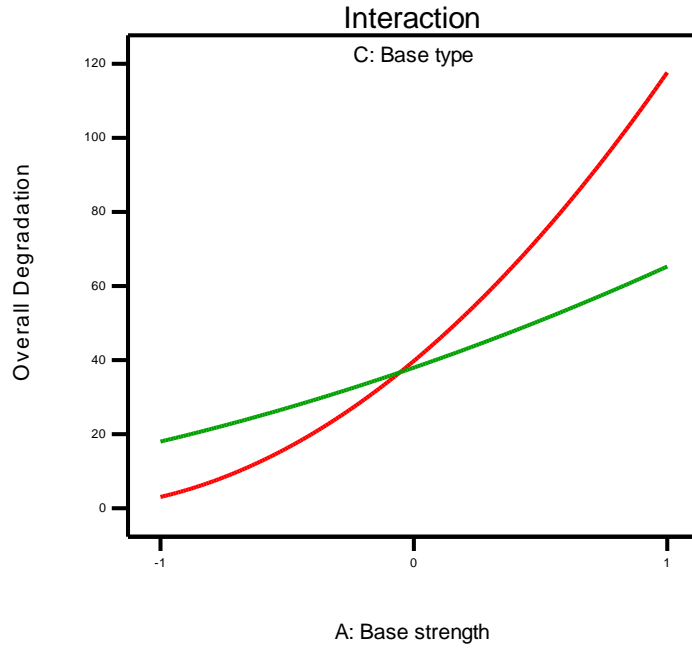


Figure 109 Plot of the overall percentage of everolimus degradation (y-axis) in relation to the concentration of base in solution (x-axis) and the type of base present. Sodium hydroxide is represented by the red line and ammonium hydroxide is represented by the green line. This plot shows the results when using vendor B's acetonitrile.

Design-Expert® Software
 Factor Coding: Actual
 Original Scale
 (median estimates)
 Overall Degradation

X1 = A: Base strength
 X2 = C: Base type

Actual Factors
 B: Propionitrile = 918.92
 D: Solvent = Vendor C

■ C1 NaOH
 ▲ C2 NH4OH

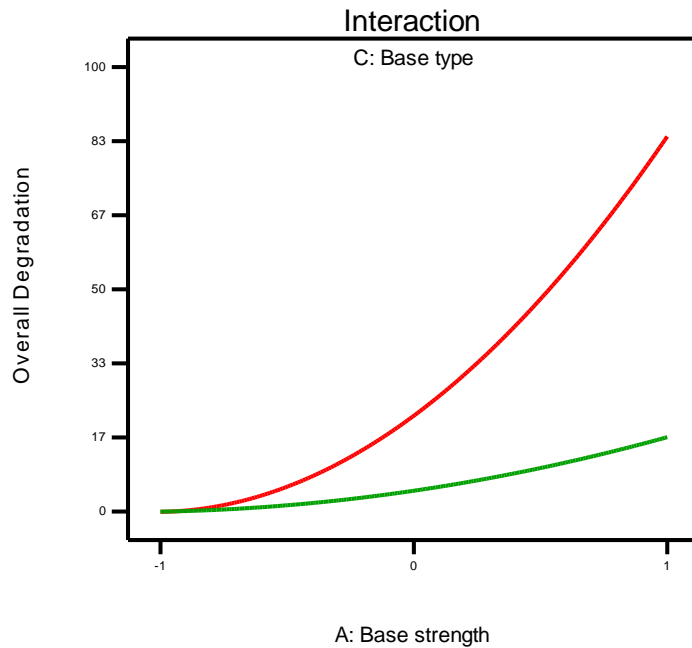


Figure 110 Plots of the overall percentage of everolimus degradation (y-axis) in relation to the concentration of base in solution (x-axis) and the type of base present. Sodium hydroxide is represented by the red line and ammonium hydroxide is represented by the black line. This plot shows the results when using vendor C's acetonitrile.

Chapter 4

Formation of the degradation product appearing at RRT 0.58 demonstrates a strong link to the interaction between the concentration of base and propionitrile, as evidenced in Figure 111 and Figure 112. Higher levels of the product are present in vendor B's solvent, (Figure 112), than that from vendor C, (Figure 112), this is presumably a consequence of the prerequisite conditions being present in vendor B's acetonitrile before adding any additional compounds. The presence of propionitrile alone is not sufficient to cause degradation to produce the peak at RRT 0.58. However when propionitrile is present in basic conditions it favours the conversion of everolimus to produce the peak at RRT 0.58.

For degradation product appearing at RRT 0.71 a similar trend is observed, and Figure 113 and Figure 114 display the interaction plots. Once again vendor B's solvent (Figure 113) causes formation of a peak at RRT 0.71 without any addition of base or propionitrile, highlighting that these are already present at sufficient levels to promote degradation of everolimus to form these products. The shape of the contours in Figure 113 shows that the level of the degradation product appearing at RRT 0.71 remains constant in Vendor B's acetonitrile when there is approximately a 4:1 ratio between the propionitrile and ammonium hydroxide concentration. When the ratio of propionitrile to base is lower, then less of the product appearing at RRT 0.71 is formed. This is probably due to a greater quantity of everolimus degradation to form the peak at RRT 0.58 under these conditions. In Figure 114 base and propionitrile was added to vendor C's acetonitrile. This acetonitrile did not cause formation of the degradation products without addition of base or propionitrile. The addition of base or propionitrile alone does not cause the formation of the product at RRT 0.71, establishing that both components are required to affect the formation of a degradation product that appears at RRT 0.71. In this respect the peak at RRT 0.71 differs from that at RRT 0.58 as that peak forms in the presence of base without requiring propionitrile to be present.

Chapter 4

Design-Expert® Software
 Factor Coding: Actual
 Original Scale
 (median estimates)
 RRT 0.58

● Design Points
 57.36
 0

X1 = A: Base strength
 X2 = B: Propionitrile

Actual Factors
 C: Base type = NH4OH
 D: Solvent = Vendor C

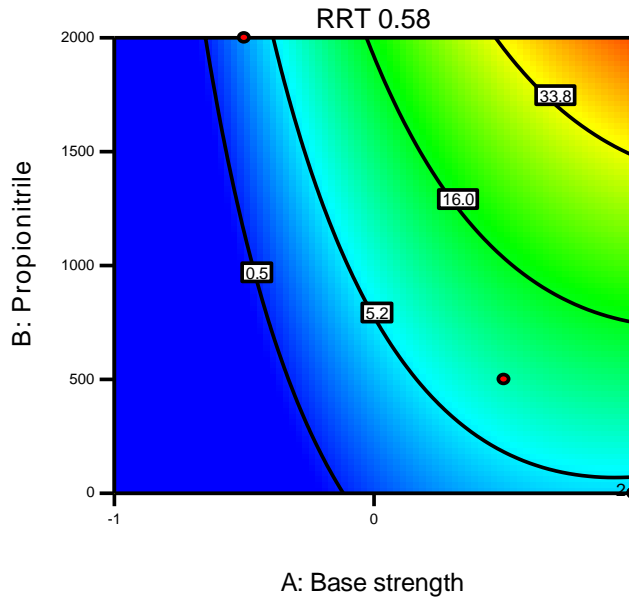


Figure 111 Plots showing the concentration of RRT 0.58 in relation to the concentration of base used (x-axis) and the concentration of propionitrile (y-axis). This plot represents the data with ammonium hydroxide and solvent from vendor B.

Design-Expert® Software
 Factor Coding: Actual
 Original Scale
 (median estimates)
 RRT 0.58

● Design Points
 57.36
 0

X1 = A: Base strength
 X2 = B: Propionitrile

Actual Factors
 C: Base type = NH4OH
 D: Solvent = Vendor B

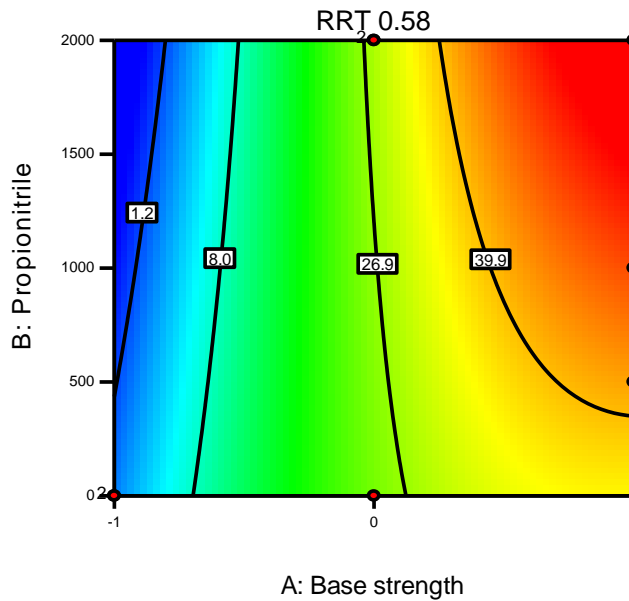


Figure 112 Plots showing the concentration of RRT 0.58 in relation to the concentration of base used (x-axis) and the concentration of propionitrile (y-axis). This plot represents the data with ammonium hydroxide and solvent from vendor C.

Chapter 4

Design-Expert® Software
 Factor Coding: Actual
 Original Scale
 (median estimates)
 Unk 0.71
 ● Design Points
 16.7
 0.0

X1 = A: Base strength
 X2 = B: Propionitrile

Actual Factors
 C: Base type = NH4OH
 D: Solvent = Vendor B

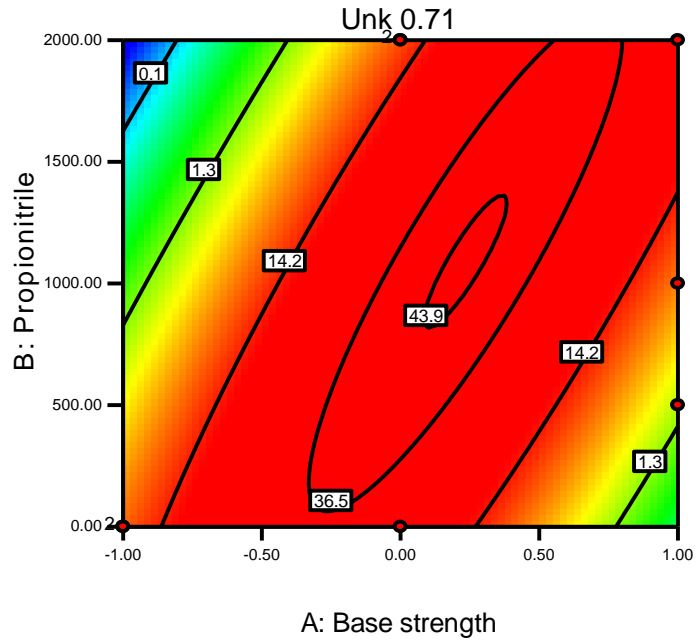


Figure 113 Plots showing the concentration of RRT 0.71 in relation to the concentration of base used (x-axis) and the concentration of propionitrile (y-axis). This plot represents the data with ammonium hydroxide and solvent from vendor B.

Design-Expert® Software
 Factor Coding: Actual
 Original Scale
 (median estimates)
 Unk 0.71
 ● Design Points
 16.7
 0.0

X1 = A: Base strength
 X2 = B: Propionitrile

Actual Factors
 C: Base type = NH4OH
 D: Solvent = Vendor C

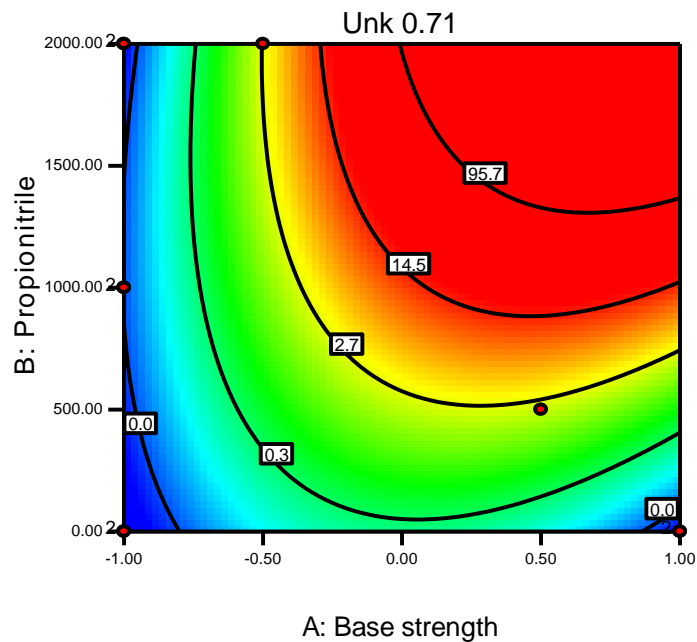


Figure 114 Plots showing the concentration of RRT 0.71 in relation to the concentration of base used (x-axis) and the concentration of propionitrile (y-axis). This plot represents the data with ammonium hydroxide and solvent from vendor C.

Chapter 4

4.4.1 Identification of the source of base in acetonitrile

In the planning stages for DoE2 it was noted that vendor C acetonitrile, which consistently resulted in no degradation of everolimus when used as a solvent, did cause degradation when that solvent had been rebottled. The bottles used to rebottle the acetonitrile were 1L, amber, soda-lime bottles bought specifically for air transport of solvents. The bottles were certified as clean by the supplier, therefore the bottles were just rinsed with a small volume of acetonitrile prior to filling them without any additional cleaning of the bottles. A review of the type of glass used by various solvent suppliers revealed that different grades of glass are utilized. The grade of glassware typically used is untreated soda-lime. However vendor C used a pre-treatment with fluorine to reduce chemical reactivity of their glass[116]. To test whether use of the soda-lime glass was the source of base in acetonitrile, some of vendor C acetonitrile was tested using a non-aqueous titration based on a Metrohm instrument procedure[117]. Vendor C's acetonitrile showed no detectable base when sampled directly from the fluorine-treated bottle, but when it was re-bottled in untreated soda-lime glassware 0.24 ppm equivalents of NaOH was detected. Displacement of Na⁺ ions from the glass can be a source of formation of NaOH [116], and as demonstrated in this thesis NaOH can cause the identified degradation products of everolimus.

An evaluation of different containers was therefore undertaken to identify a suitable transport and storage vessel for the solvent. Whilst fluorinated soda-lime glass is a suitable container material, it was not possible to find a European supplier that used this for their solvent vessels. For an effective resolution to this problem a European supplier was needed, as it is not always practicable or cost effective to ship solvent from the USA for a DES manufacturing plant such as Boston Scientific Galway.

To attempt to address this, the Vendor C acetonitrile was exposed to different container material and everolimus solutions were prepared from this solvent. Vendor B acetonitrile, and vendor C acetonitrile that had been spiked (adulterated) with 200 ppm of propionitrile and allowed to stand in soda lime glass for 5 days was included as a control. The materials assessed for storage were stainless steel, borosilicate glass and soda-lime glass. Unsurprisingly Vendor B and the adulterated Vendor C acetonitrile resulted in the everolimus degradation products in all three container types, as evidenced from the data in Figure 115. However use of the acetonitrile from vendor C

Chapter 4

stored in borosilicate glassware and stainless steel did not result in degradation. Use of acetonitrile from vendor C stored in soda-lime glassware did however result in everolimus degradation.

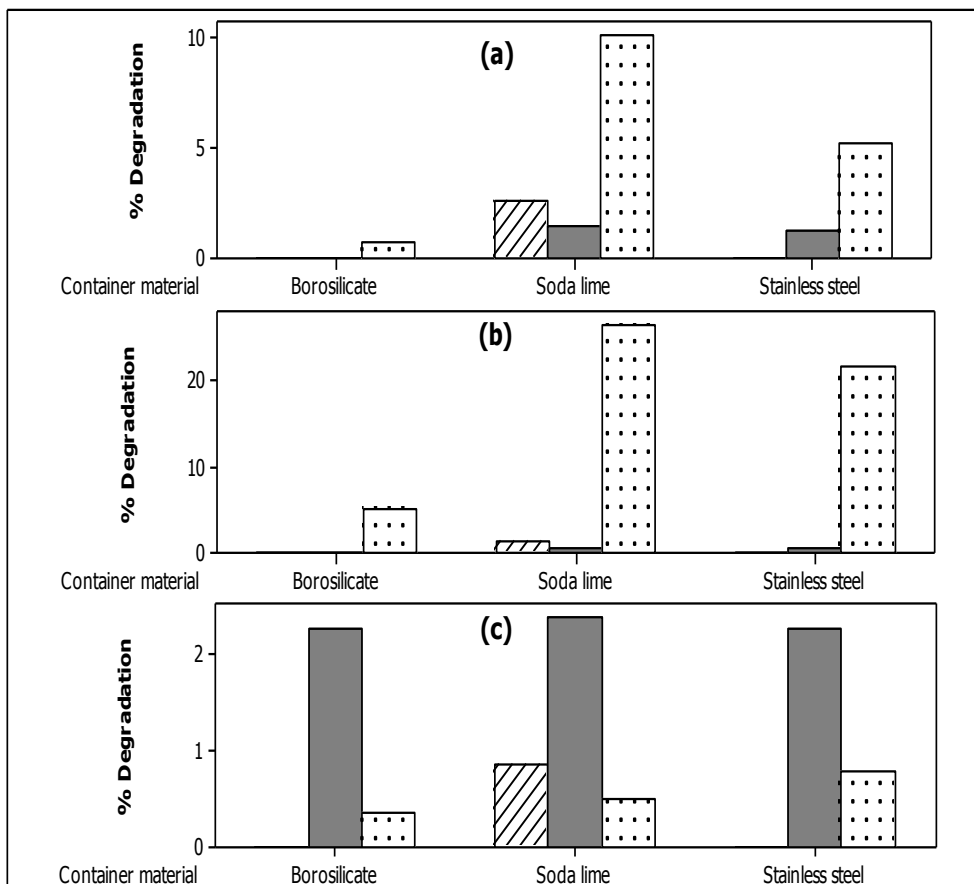


Figure 115 Graphs showing the levels of (a) RRT 0.58 , (b) RRT 0.71, and (c) RRT 0.75 when everolimus solutions were prepared in vendor C acetonitrile (diagonal lines), vendor C acetonitrile spiked with 200 ppm propionitrile and placed in soda lime glass (dots), and unadulterated vendor C acetonitrile (solid grey). The three solvent types had previously been stored in borosilicate glass, soda lime glass or stainless steel.

Chapter 4

4.4.2 Mass spectrometry analysis of degradation products

In the previous sections the observation of base-induced degradation products of everolimus that can occur in acetonitrile solution was described. The causative agents for this degradation are 1) base, from soda-lime glass, and 2) propionitrile, an impurity in acetonitrile that is associated with the manufacturing process. In this section the use of LC-MS/MS is undertaken to attempt to identify these degradation products. Structures for these degradation products, from their mass fragmentation analysis, are proposed.

The primary degradation products of everolimus produced under basic conditions are 804-95 ($m/z = 980$), the ring-opened isomer of everolimus resulting from ester hydrolysis/dehydration or β -elimination, 013-99 ($m/z = 614$) and an increase in the main everolimus pyran isomer, as discussed in chapter 1. However, in this special case of base/propionitrile induced degradation a different degradation signature is seen. Table 14 lists the 3 degradation products that have been identified, by their relative retention times (RRT). The 3 degradation products were isolated by LC-MS and their mass to charge ratios (m/z) obtained, Table 14 lists the corresponding m/z values for each degradation product. To carry out the LCMS analysis, the HPLC-UV method was adjusted, principally, by reducing the flow rate by more than 50%. This reduction in flow rate is necessary to ensure sufficient ionization of the molecules by the electrospray set in positive mode. This change in flow rate expectedly increases the retention times of the components on the HPLC UV detection prior to MS.

Table 14 Major acetonitrile induced degradation products relative to the retention time of everolimus by HPLC

Peak	Relative Retention Time	Name	m/z
1	0.57 – 0.59	RRT 0.58	813.51
2	0.70 – 0.73	RRT 0.71	1007.58
3	0.74 – 0.76	RRT 0.75	1007.58

The identities of degradants associated with peaks at RRT 0.58, RRT 0.71, and RRT 0.75 were elucidated from examination of their mass fragmentation patterns and the aforementioned UV spectra. The MS data was collected by performing secondary mass fragmentation on the primary ion of the compounds identified from their RRT by HPLC. Confirmation of the proposed identities using an orthogonal technique, such as

Chapter 4

NMR, has not been carried out to date. However the degradants exhibit some characteristic fragment ions in the Q-TOF-MS, providing valuable structural information. Additionally the mass accuracy measurement capability of the Q-TOF-MS is such that prediction of the molecular weight of the analytes of interest can be used to confirm their empirical formulae.

4.4.2.1 Elucidation of the structure of the product at RRT 0.58

LC/MS and LC/MS/MS were used to analyse the product appearing at RRT 0.58 in the degraded everolimus samples. Positive ion ESI spectra were recorded (Figure 116), and these showed a major peak at m/z 813.51, corresponding to the adduct ion of $[M+Na]^+$, where $M = 790.52$. Further LC/MS/MS fragmentation performed in positive mode yielded the MS spectrum shown in Figure 117, with the major fragments and their relative abundance are listed in

Table 15. The proposed fragmentation pattern is shown in Figure 118.

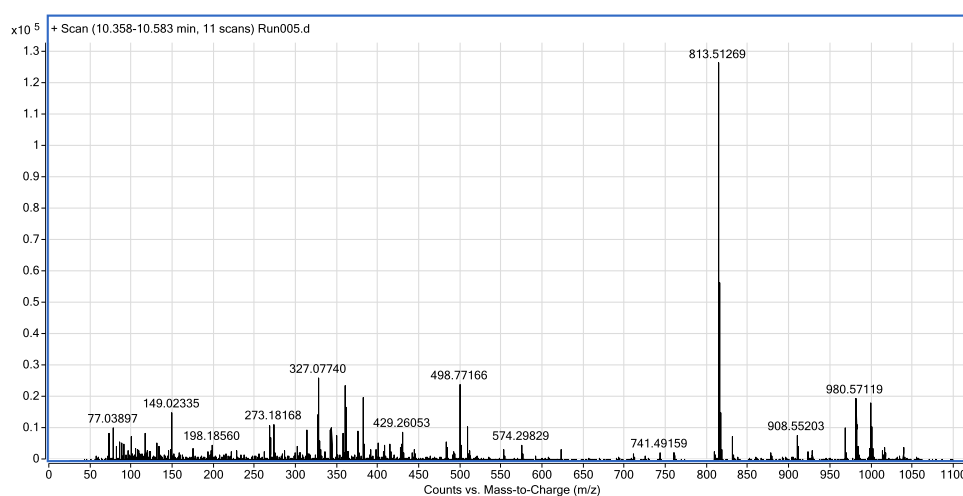


Figure 116 LC/MS analysis of RRT 0.58 in a degraded everolimus sample. Positive ion ESI spectra showed a major peak at m/z 813.51, corresponding to the adduct ion of $[M+Na]^+$, where $M = 790.52$

Chapter 4

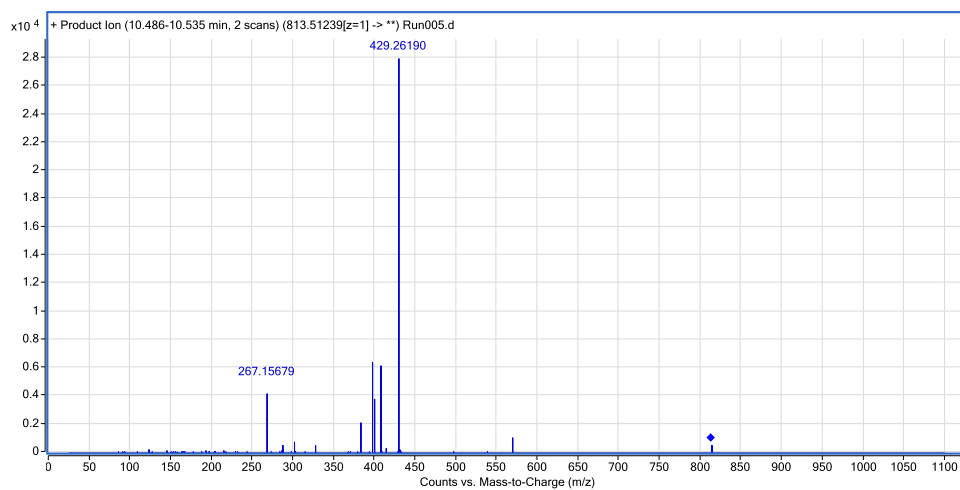


Figure 117 MS spectrum from LC/MS/MS fragmentation performed for RRT 0.58 in positive mode.

Table 15 Major fragments of peak at RTT 0.58

<i>m/z</i> (Abundance)
429.2619 (27,931)
407.24202 (6,263)
399.24962 (3,824)
397.23391 (6,398)
383.21956 (2,108)
267.15679 (4,189)

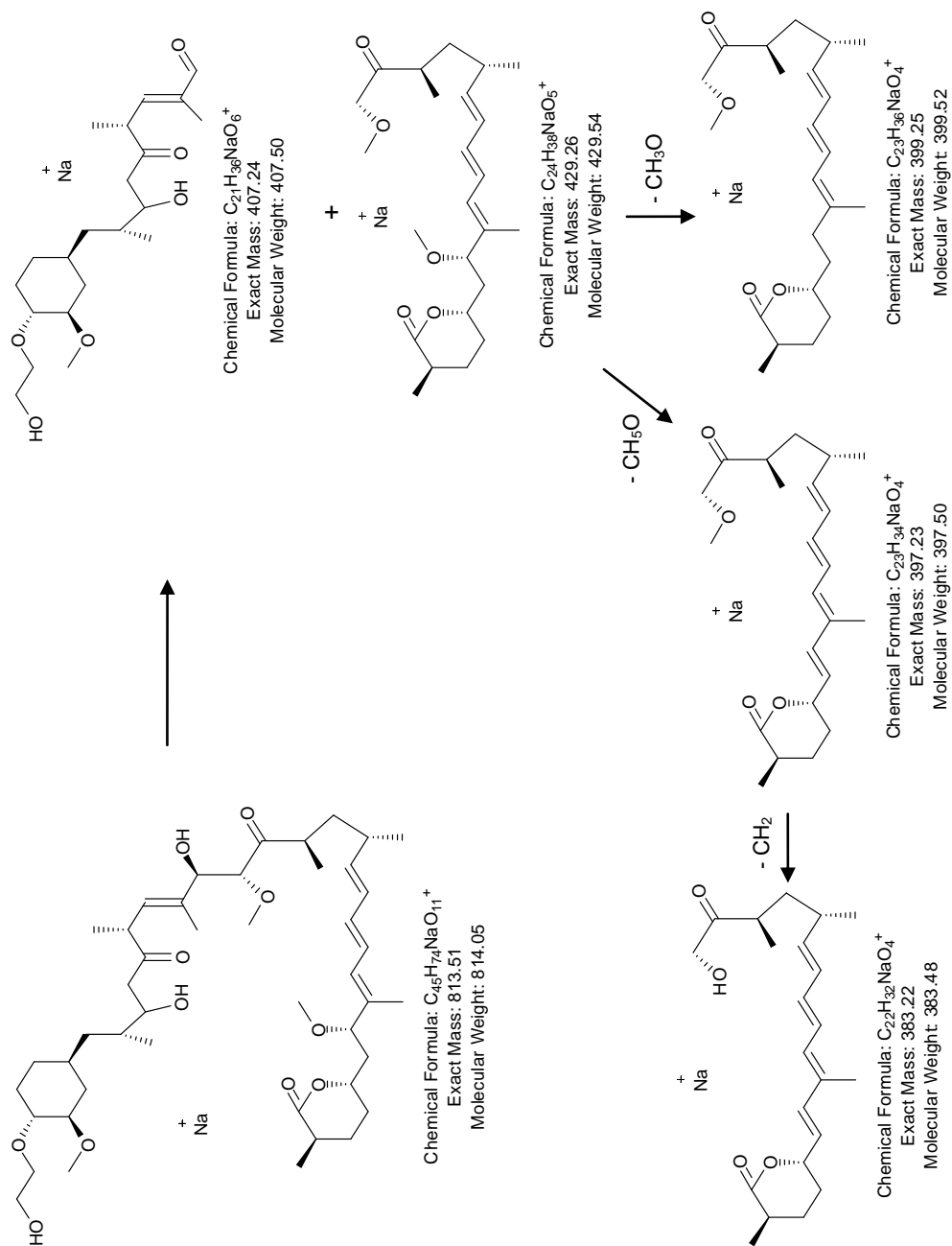


Figure 118 Proposed fragmentation pattern of peak at RRT 0.58

Chapter 4

4.4.2.2 Elucidation of the structures of products at RRT 0.71 and RRT 0.75

LC/MS and LC/MS/MS were used to analyse the products at RRT 0.71 and RRT 0.75 in the degraded everolimus samples. Positive ion ESI spectra were recorded (Figure 120 and Figure 123 respectively), these showed a major peak at m/z 1007.58 for both degradants, corresponding to the adduct ion of $[M+Na]^+$, where $M = 984.59$. Further LC/MS/MS fragmentation performed for the peak at RRT 0.71 in positive mode yielded the MS spectrum shown in Figure 121, with the major fragments and their relative abundance are listed in

Table 16. Further LC/MS/MS fragmentation performed for the peak at RRT 0.75 in positive mode yielded the MS spectrum shown in Figure 124, with the major fragments and their relative abundance are listed in

Chapter 4

Table 17. The two degradants have a molecular weight corresponding to [everolimus + 27], suggesting that they correspond to the addition of the same moiety corresponding to 27 a.m.u. at different locations of the parent everolimus compound. The LC/MS/MS fragmentation patterns for the peaks at RRT 0.71 and RRT 0.75 are distinctly different from one another.

Thorough analysis of these fragments and utilization of the accurate mass capabilities of the Q-TOF MS, chemical structures for these two degradants have been proposed. The proposed empirical formula for both compounds is $C_{54}H_{84}N_2O_{14}$ with mass error of 1.99 ppm. This suggests the addition of a single carbon and nitrogen in the form of a cyanide group to the everolimus molecule. A process of elimination used to evaluate the cyanide group added to different locations on the parent molecule, everolimus, suggested the two structures shown in Figure 119 for the products at RRT 0.71 and RRT 0.75. The proposed fragmentation pattern for the products at RRT 0.71 and RRT 0.75 are shown in Figure 122 and Figure 125, respectively.

Chapter 4

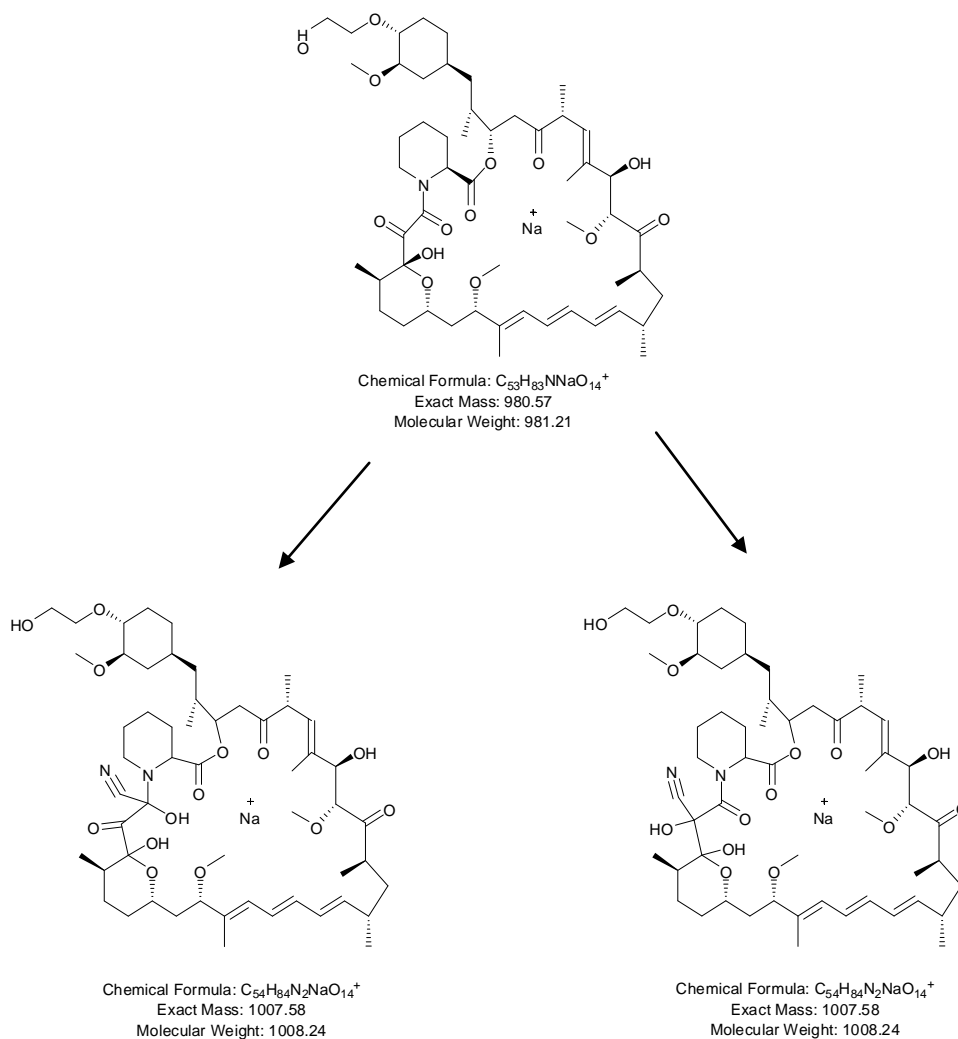


Figure 119 The proposed structures for the peaks at RRT 0.71 (left hand side) and RRT 0.75 (right hand side), originating from the parent molecule, everolimus.

Table 16 Major fragments of for the peak at RRT 0.71

<i>m/z</i> (Abundance)
1007.58128 (57,887)
795.50175 (51,502)
601.30857 (119,613)
574.29871 (16,750)
429.26231 (169,629)
397.23455 (14,634)
389.2284 (115,412)

Chapter 4

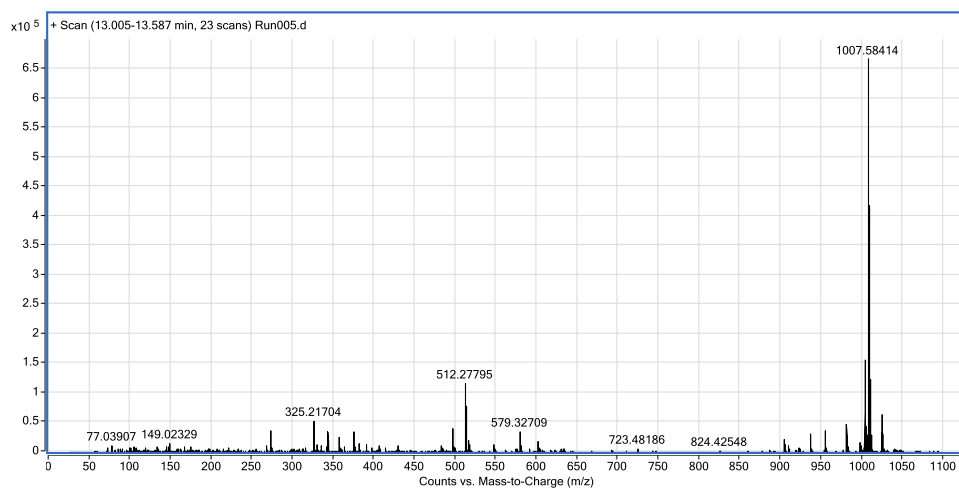


Figure 120 LC/MS used to analyse the peak at RRT 0.71 in the degraded everolimus samples. The positive ion ESI spectra showed a major peak at m/z 1007.58, corresponding to the adduct ion of $[M+Na]^+$, where $M = 984.59$

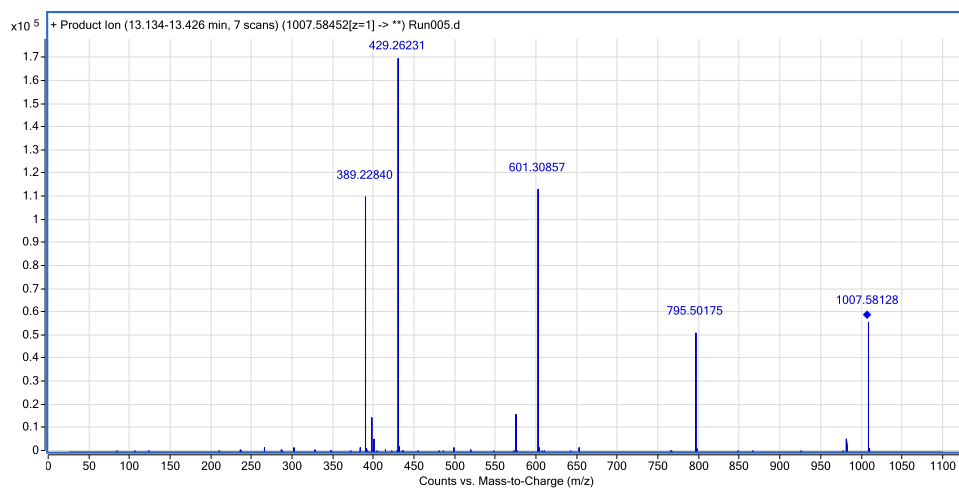


Figure 121 MS spectrum from LC/MS/MS fragmentation performed for the peak at RRT 0.71 in positive mode.

Chapter 4

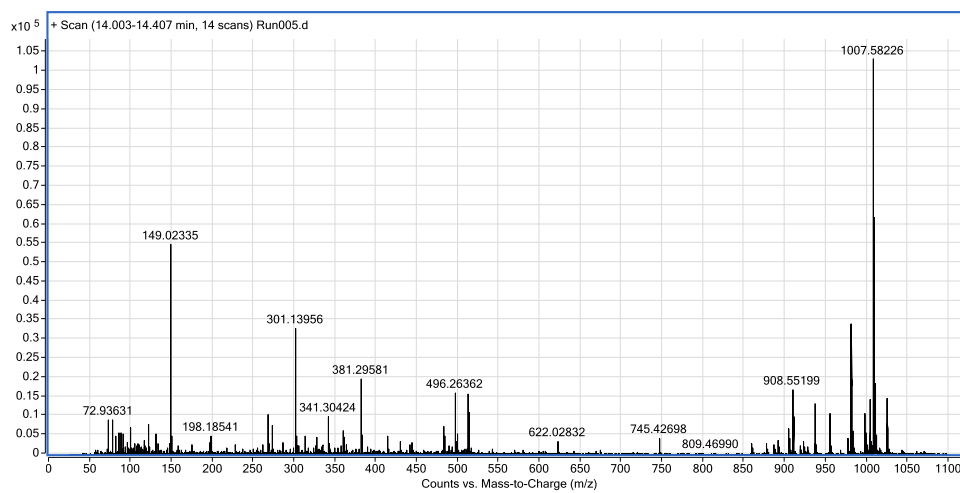


Figure 123 LC/MS used to analyse the peak at RRT 0.75 in the degraded everolimus samples. The positive ion ESI spectra showed a major peak at m/z 1,007.58, corresponding to the adduct ion of $[M+Na]^+$, where M = 984.59

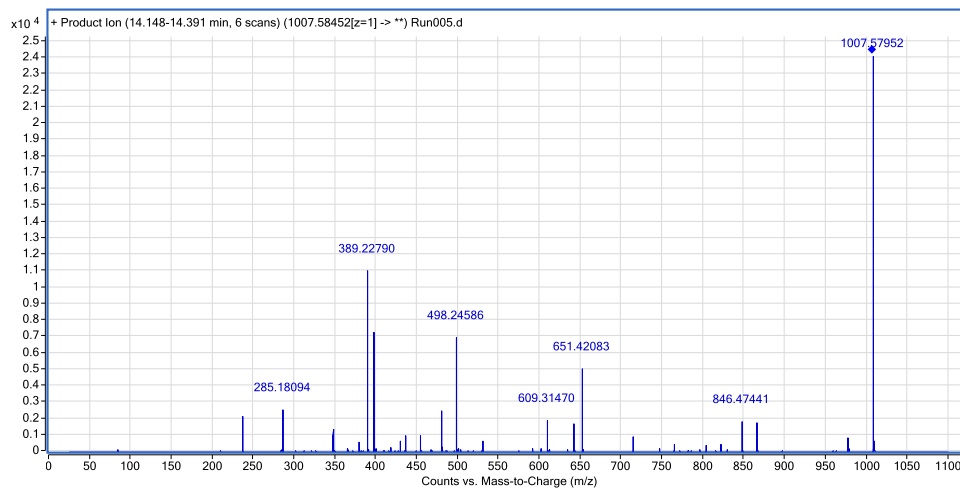


Figure 124 MS spectrum from LC/MS/MS fragmentation performed for peak at RRT 0.75 in positive mode.

Chapter 4

Table 17 Major fragments of for the product at RRT 0.75

<i>m/z</i> (Abundance)
1007.57952 (24,639)
864.48728 (1,894)
846.47441 (1,865)
651.42083 (5,156)
641.34095 (1,731)
609.3147 (1,921)
498.24586 (7,176)
480.23254 (2,496)
397.23376 (7,264)
389.2279 (11,503)
347.12247 (1,433)
285.18094 (2,607)
236.05407 (2,177)

4.5 Chapter conclusion

In this chapter it has been shown that everolimus, which readily undergoes base degradation, can form base induced degradation products when prepared in acetonitrile. These degradation products, at the initial observation appeared sporadic in occurrence, but they have now been successfully recreated in acetonitrile solutions. The conditions necessary for the degradation to occur have been identified by using DoE. Alkaline impurities from untreated soda-lime glassware used to package acetonitrile are the main source of this contamination. Propionitrile, an impurity related to the manufacture of acetonitrile, will augment the degradation of everolimus in the presence of the base contamination. Discovery of this important interaction would have been difficult to establish without the DoE approach taken. Furthermore, water has been shown to impact the relative concentration of the degradation products, unsurprising considering the pH dependence of the degradation route.

Distillation of acetonitrile is effective at removing or reducing the ability of acetonitrile to cause everolimus degradation. The effectiveness of distillation at eliminating degradation is down to the removal of non-volatile or high boiling point alkaline impurities from the solvent. The source of the base contamination is through leaching of alkaline impurities from soda-lime glass. Use of borosilicate glass, fluorinated soda-lime glass and stainless steel for the packaging of acetonitrile will prevent this build-up of alkaline impurities in acetonitrile. Furthermore, the addition of acid to acetonitrile will prevent the formation of these specific degradation products of everolimus by increasing the pH. A word of caution however: if excess acid is added then acid related degradation products will be formed.

The structured experimental approach taken in this investigation has shown the power of well-constructed experimental designs. The use of statistical methods proved successful in helping to establish drug degradation routes and to identify the main factors involved. For laboratories dealing with the widely used family of rapamycin drugs, some degradation prevention measures have been evaluated and shown to be effective. It is hoped that this will be of benefit to these laboratories by extending the workable shelf-life of samples and in the prevention of laboratory investigations associated with the appearance of unknown degradation products in finished product testing.

Chapter 4

LC-MS/MS has led to the identification of the site on the everolimus molecule that is open to modification under the degradation mechanisms and structures of the degradation products have been proposed. However, follow up work with NMR and crystallography, if possible, is recommended to confirm exact structures.

Chapter 5

The use of near infrared spectroscopy as an alternative to traditional wet chemistry techniques in drug eluting stent process control.

5 Chapter introduction

DES coating solutions are solvent based formulations that are applied to stents to form a thin film. These solvent-cast films are made up of a drug and polymer mixture which remains behind after solvent removal. In this chapter partial least squares (PLS) regression analysis was applied to the near infrared (NIR) spectral data gathered from DES coating solutions. These NIR methods are being proposed as an alternative to existing liquid chromatography and gravimetry methods for the measurement of the concentration of constituents in the coating solutions, achieved through the construction of NIR calibrations. The approach taken provides for a process analytical technology (PAT) solution for the control of the critical pharmaceutical formulation step in the production of these medical products.

The DES products to which this analysis was applied are Boston Scientific's PROMUS everolimus-eluting stent and to one of the company's non-commercialized paclitaxel-eluting stents. The drug and polymer constituents for these DES are, 1) everolimus and poly-vinylidene fluoride hexafluoropolymer (PVDF-HFP; 15% HFP), and 2) paclitaxel and D,L-Polylactic acid (PLA), respectively. In both cases PLS regression was used to construct calibration models for the measurement of the drug and polymer components from their NIR spectra.

Application of NIR to the analysis of the coating solutions used in the PROMUS everolimus eluting stent has been reported by ABB Analytical[70] based on samples provided by our laboratory to evaluate their equipment. The work reported here permits extension of that reported proof of concept evaluation into practice in a real world DES manufacturing environment. Amongst the challenges encountered were applying the

Chapter 5

NIR methodology to a rather low concentration of everolimus (mean = 0.41% w/w, and range = 0.1 to 0.7% w/w), compared to that reported previously (range = 0 to 2.3% w/w)[70], and overcoming the DES manufacturing process related variables. The foremost process related challenge for the PLS calibrations was accounting for the ubiquitous water content. PLS calibration models were successfully created to provide quality control assessment of the coating solutions, and also to improve the calibrations for the other, functional components. Spectra pre-treatments, detailed in Table 3 (Chapter 1), were used prior to PLS, with first derivative combined with scattering correction proving most effective as described in section 5.1.3.

Reference inputs to the PLS calibration models were the weight percentage content (% w/w) of the components in solution, although other reference inputs were also evaluated. A detailed analysis of the manufacturing process was carried out to identify process variables that impacted the robustness of the calibration models. Principal component analysis (PCA) of the calibration spectra provided valuable guidance towards the selection of appropriate spectra for the PLS calibration models. Through PCA, inclusions of calibration data in the models to account for acceptable process variation were implemented to improve the robustness of the models.

5.1 Results and Discussion

5.1.1 Experimental design

A close examination of process variables was carried out prior to development of experimental designs from which were taken the sample sets for the calibration and test set samples. Construction of stable PLSR calibrations require that allowed process variation is included. Such variation involved spanning the coating solution weight specifications for polymer and drug, different batches of polymer and drug, and different batches of solvent. Calibration sets were made up in the laboratory and were supplemented with actual process samples to account for any variation between them. For example, laboratory samples were not filtered whereas process samples are filtered to remove any particulate matter that may block the coating apparatus. All analysis was carried out in a laboratory with controlled temperature (19-22°C) and humidity (45-55% RH), these conditions mimic the environmental control in the production facility.

Chapter 5

Coating solutions with varying amounts of drug, polymer and solvent were first formulated according to the experimental designs with all component amounts measured by weight. These solutions were analysed using a NIR spectrometer and HPLC as described in Chapter 2. Table 9, Table 10, Table 11, and Table 12 in Chapter 2 show the experimental design and actual quantities for each laboratory scale sample. The HPLC results were used to confirm that the recorded gravimetric weights were correct for each solution.

5.1.2 Spectral analysis

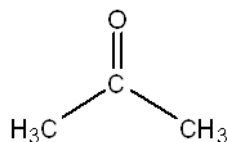
NIR spectra of the stent coating solutions are typical of transmission spectra gathered in this region of the electromagnetic spectrum, consisting of numerous relatively broad bands. These bands have their origin in overtones and combinations of fundamental vibrations that are usually visible in the mid infra-red region ($400 - 4000 \text{ cm}^{-1}$). Unlike bands in the mid infra-red region, it can be difficult to assign NIR bands. It is not necessary to assign the bands for quantitative purposes when using the principal component approach; however where possible it makes practical sense to understand the source of the bands in the regions of the spectrum that are utilized in multivariate calibrations. Interrogation of the calibration models through evaluation of the spectral regions used to construct them can help target more stable models overall. Therefore separate spectra of each of the components used in the formulation solutions were gathered to help with this band assignment.

5.1.2.1 Everolimus coating solutions

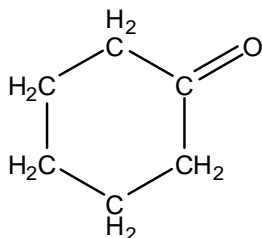
The spectrum of the everolimus coating solution, Figure 126, is dominated by the contributions from acetone and cyclohexanone, Figure 127, as these two components make up 68.3 and 29.3 mass percentage of the coating solution, respectively. The spectra show bands with total absorbance in the region $4,500 - 4,000 \text{ cm}^{-1}$, bands corresponding to C-C bonds around $4,600 \text{ cm}^{-1}$, C=O 2nd overtone stretch bands around $5,100 \text{ cm}^{-1}$, bands for the 1st overtone C-H stretch in the region $6,000 - 5,500 \text{ cm}^{-1}$, bands for the 1st overtone of C-H combinations in the region $7,500 - 6,800 \text{ cm}^{-1}$, and bands for the 2nd overtone C-H stretch in the region $9,000 - 8,100 \text{ cm}^{-1}$ [82].

Chapter 5

Acetone:



Cyclohexanone:



The methyl C-H bands of acetone have higher wavenumbers compared to the ethyl C-H bands of cyclohexanone. The methyl bands are clearly seen shifted to the left in Figure 128 which shows overlaid spectra of acetone in cyclohexanone going from 0 to 100% w/w concentration.

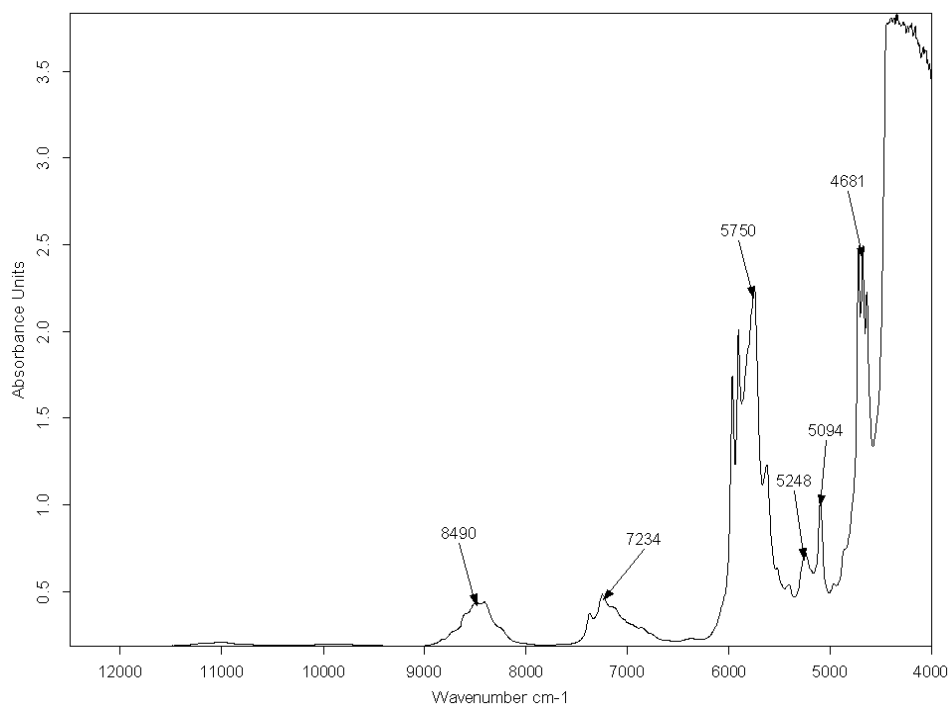


Figure 126 Spectrum of everolimus coating collected using transmission mode in a 7mm cuvette.

Chapter 5

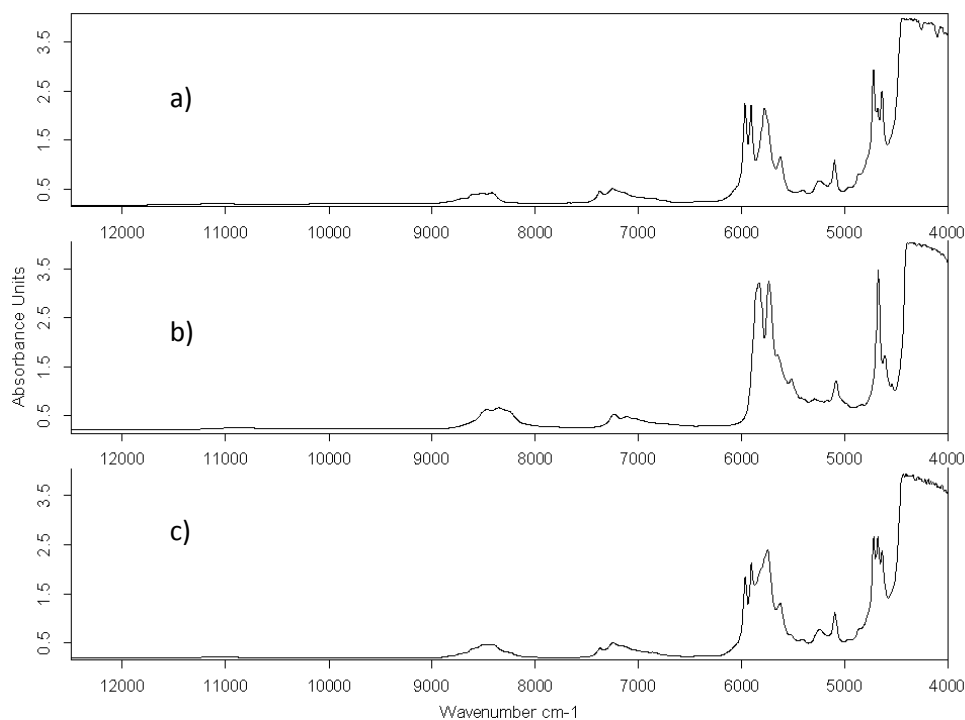


Figure 127 Transmission spectra of (a) acetone, (b) cyclohexanone and (c) the everolimus coating solution.

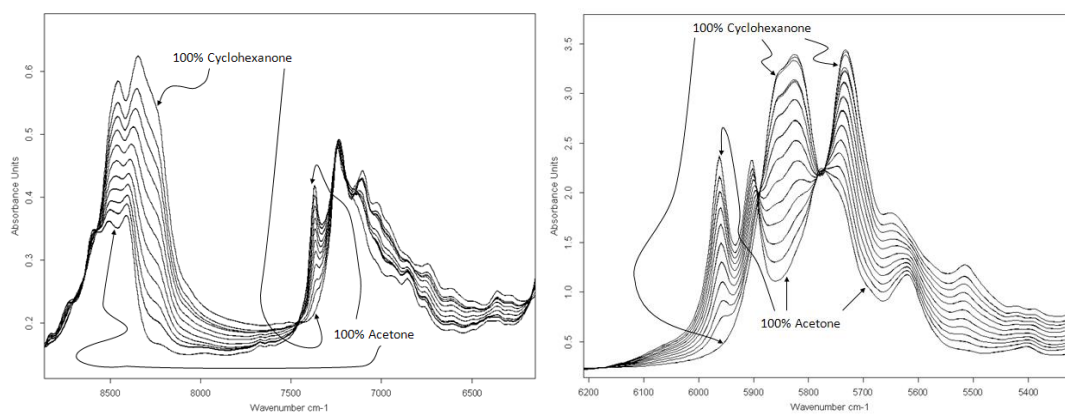


Figure 128 Overlaid transmission spectra of acetone and cyclohexanone solutions incrementally going from 100% acetone to 100% cyclohexanone in 10% steps.

Another feature of the spectra is the presence of absorbance bands associated with water, which show up around $5,250\text{ cm}^{-1}$ and in the region $7,150 - 6,900\text{ cm}^{-1}$ [82]. The water band at $5,239\text{ cm}^{-1}$ is evident in Figure 129, presenting the overlaid spectra from coating solutions with added water content ranging from 0.17 to 0.50 % w/w.

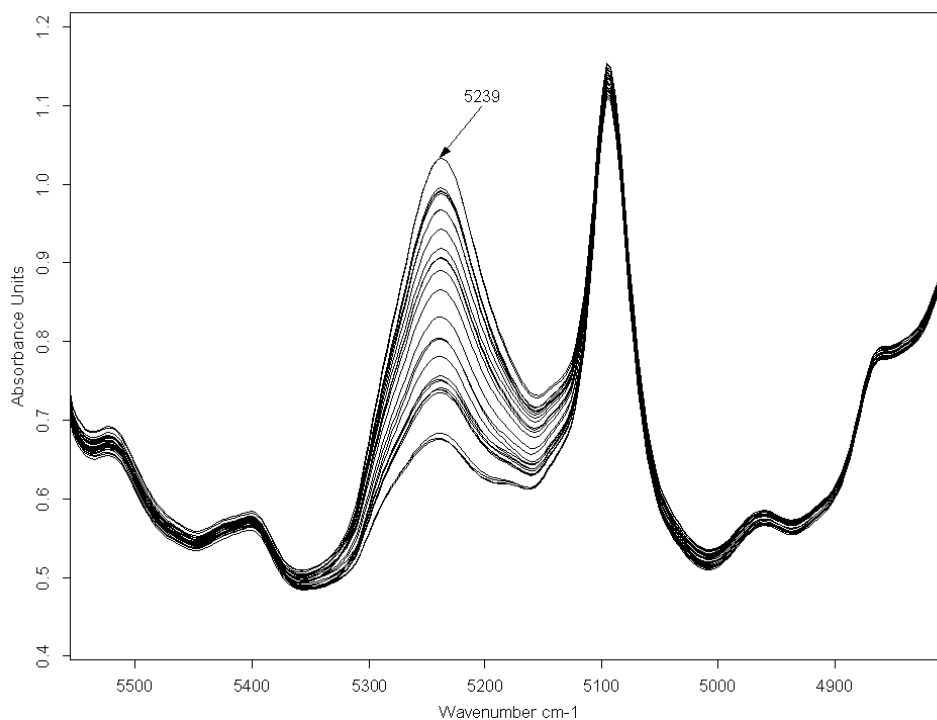


Figure 129 Variation in water absorbance combination band at 5239 cm^{-1} with change in water content absorbance band in everolimus coating solution.

In addition to the acquisition of spectra with varying solvent concentrations, spectra were gathered from solutions of PVDF-HFP, and everolimus individually dissolved in acetone with a background subtracted spectrum of acetone. The concentration of everolimus and PVDF-HFP were reduced by making serial dilutions, and the spectra were overlaid to look for shifting spectral bands related to the concentration variation of the solutions. Each set of overlaid spectra is shown in Figure 130 and Figure 131 for everolimus and PVDF-HFP, respectively. For everolimus, which has 3 hydroxyl groups, R-OH bands appear at $4,831$ and $6,800\text{ cm}^{-1}$ corresponding to combination and 1st overtone vibrations[82], respectively. Additionally the 2nd overtone for C-H-O appears at $5,236\text{ cm}^{-1}$ [82], which incidentally coincides with one of the water absorption bands. The C-H bands at $5,858$ and $6,998\text{ cm}^{-1}$ [82] are in equal proportion to the O-H bands. Meanwhile the spectrum of PVDF-HFP is dominated by C-H absorption bands only, this can be noted by the reduction in the size of the methyl bands of acetone at $5,753$ and $5,944\text{ cm}^{-1}$ and the increase of the ethyl band at $5,845\text{ cm}^{-1}$.

Chapter 5

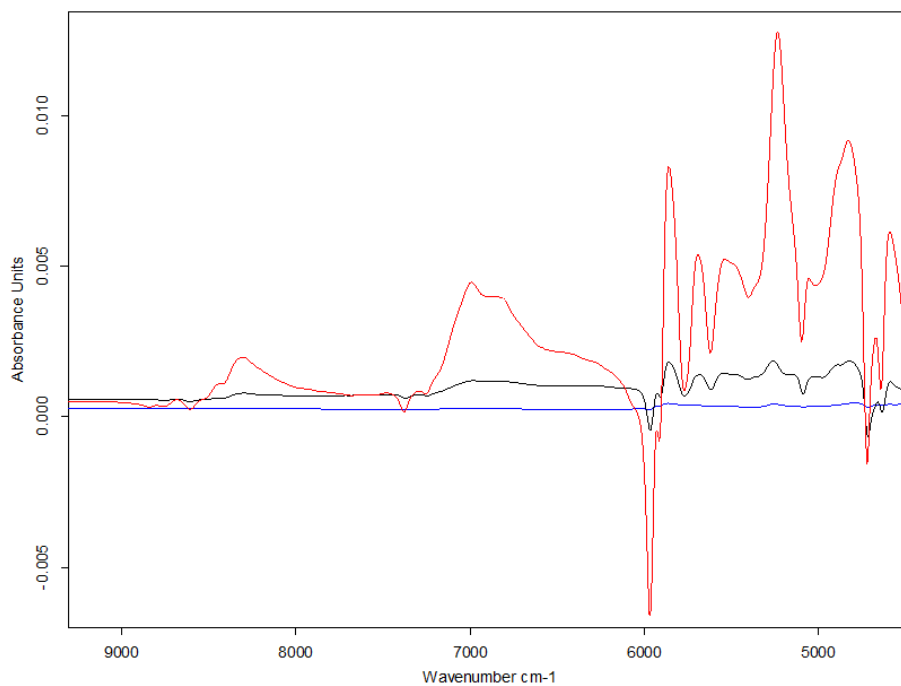


Figure 130 Overlaid spectra of 3 different concentrations of everolimus solutions of 70 mg/mL (red), 7 mg/mL (black), and 0.7 mg/mL (blue) (Note: acetone background subtracted)

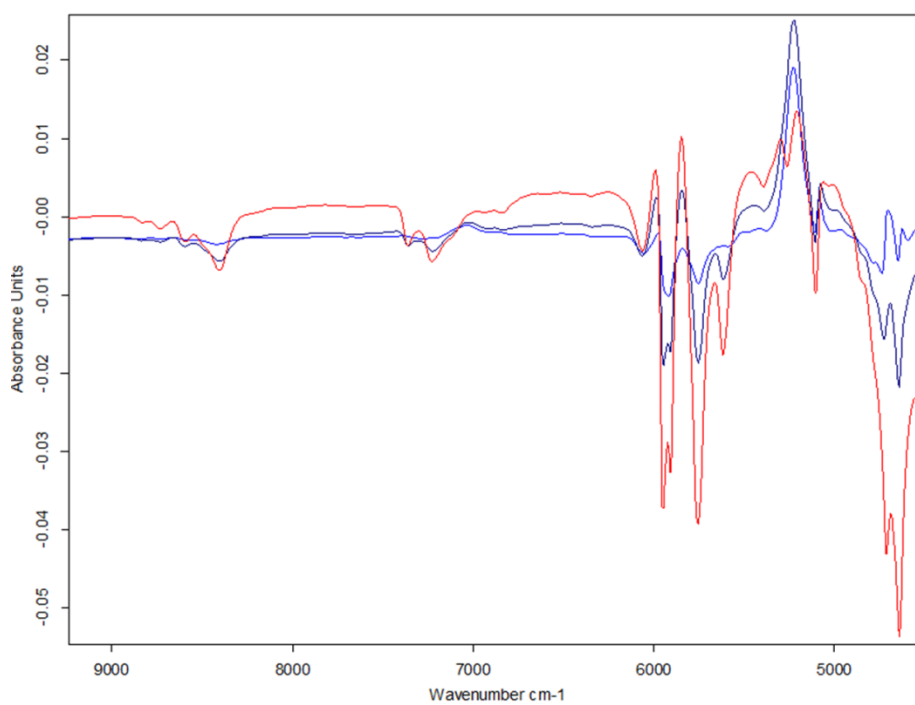
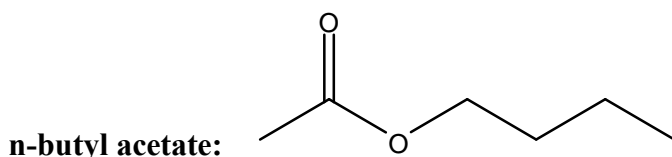


Figure 131 Overlaid spectra of 3 different concentrations of PVDF-HFP solutions, of 70 mg/mL (red), 7 mg/mL (black), and 0.7 mg/mL (blue) (Note: acetone background subtracted).

5.1.2.2 Paclitaxel coating solutions

The spectrum of the paclitaxel coating solution is dominated by the contributions from n-butyl acetate, Figure 132, as the solvent makes up 96% w/w of the coating solution, and there are no visibly discernible differences between the spectra for the coating solution and that of the solvent alone. The path length used for this analysis was 18mm, a relatively long path length, and consequently total absorbance occurs in some spectral regions. The long 18 mm path length was selected because the vessels used on the stent coating equipment are of that diameter, thus it facilitated the option of in-line measurement of the coating solutions. These clear borosilicate glass coating solution vessels were used for collection of all spectra in the laboratory thereby providing an easier route to transfer the method to the production environment. From Figure 132, combination bands showing total absorbance in the region 4,500 - 4,000 cm^{-1} , and total absorbance for bands of the 1st overtone C-H stretch in the region 6,000 - 5,500 cm^{-1} [82]; and a total absorbance band corresponding to C-C bonds around 4,600 cm^{-1} [82] are evident. Bands in the spectrum unaffected by total absorbance, and therefore available for spectral interpretation are; RCO_2R 2nd overtone stretch bands around 5,170 cm^{-1} [82], bands for the 1st overtone of C-H combinations in the region 7,500 - 6,800 cm^{-1} [82], and bands for the 2nd overtone C-H stretch in the region 9,000 - 8,100 cm^{-1} [82].



Chapter 5

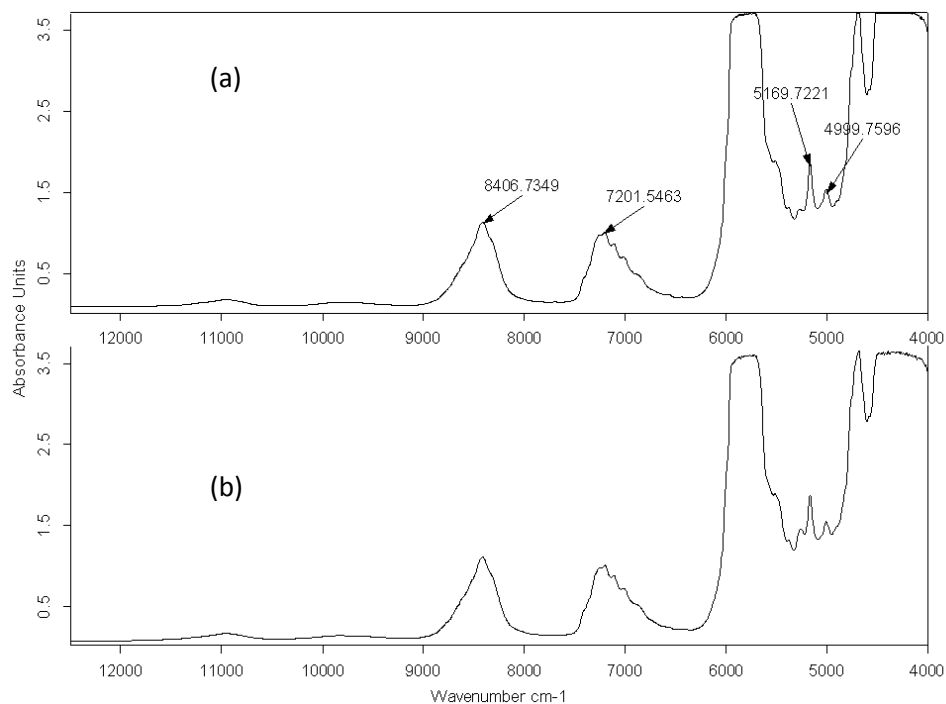


Figure 132 Spectra of (a) n-butyl acetate, and (b) the paclitaxel coating solution.

As with the everolimus coating solutions a feature of the spectra are the absorbance bands associated with water, which show up around $5,250\text{ cm}^{-1}$ and in the region $7,150 - 6,900\text{ cm}^{-1}$ [82]. The water band at $5,267\text{ cm}^{-1}$ is highlighted in Figure 133, showing spectra from coating solutions with added water content ranging from 0.04 to 0.52% w/w, and plots of the 2nd derivative spectral treatment of this region.

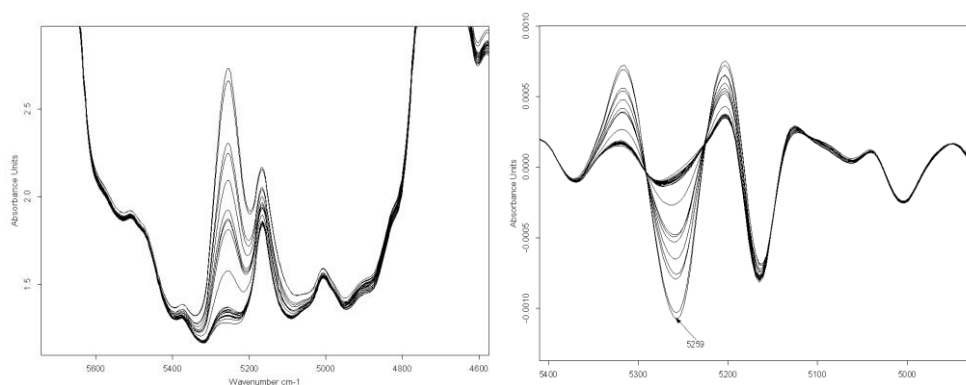


Figure 133 Variation in water absorbance band at $5,267\text{ cm}^{-1}$ in paclitaxel coating solution from 0.04 %w/w to 0.52 %w/w, and Water absorbance band with 2nd derivative spectral treatment on the right.

A spectrum was gathered from a solution of paclitaxel dissolved in nBA at a relatively high concentration (5% w/w), and compared to the spectrum of nBA alone and to paclitaxel coating solutions in the calibration model range of 1.2 to 2.5% w/w. The spectra were overlaid to look for shifting spectral bands related to the concentration variation of paclitaxel in Figure 134 showing spectral discrimination in the region of

Chapter 5

4,800 cm^{-1} and 6,900 cm^{-1} , corresponding to R-OH absorption bands. Paclitaxel has 3 hydroxyl groups.

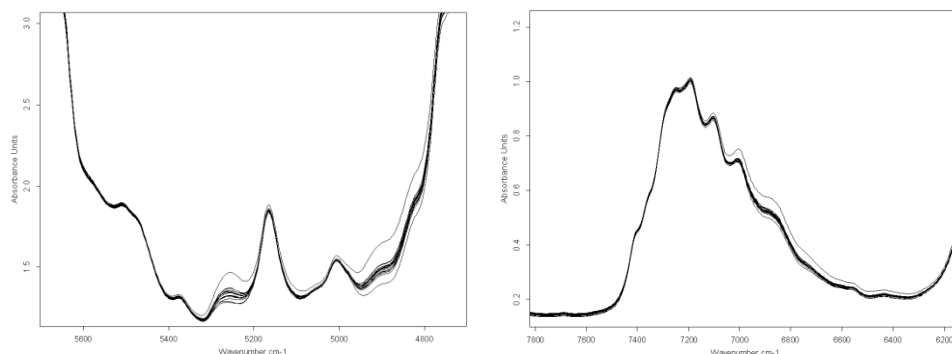


Figure 134 High concentration (5%) paclitaxel solution, overlaid with 100% nBA and 15 calibration solutions in the range 1.2 to 2.5%.

The regions of spectral activity associated with paclitaxel are even more apparent when the spectrum of nBA is subtracted from that of the paclitaxel solution, Figure 135. In contrast the subtraction of nBA spectrum from the spectrum of a 5% w/w PLA solution does not show much in the way of significant changes. This just signifies that there are no O-H bonds in PLA and C-H absorption bands dominate for PLA and nBA. As such, the subtraction of nBA results in a relatively flat looking spectrum for PLA. The region of the spectrum that appears to show the clearest spectral activity is associated with the 1st overtone of C-H combinations around 7,460 – 6,900 cm^{-1} , Figure 135.

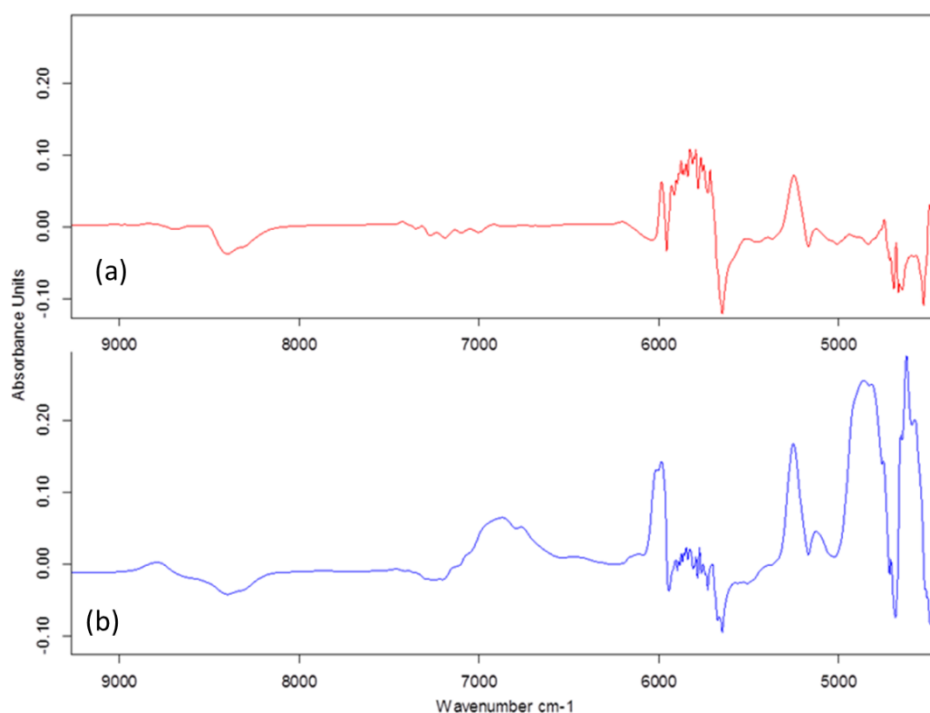


Figure 135 Spectra of (a) PLA and (b) paclitaxel, generated by creating 5% w/w solutions of each in nBA and then subtracting a pure nBA background.

5.1.3 Everolimus coating solutions

Calibrations were built using the gravimetric data collected when the individual components were weighed out during formulation (%w/w). These input data were verified using HPLC for the everolimus content (coefficient of variation = 0.8%), and gravimetric analysis post evaporation of the solvents for the overall solid components (referred to as: % solids method). The weight of PVDF was indirectly calculated by subtracting the measured quantity of everolimus from the total solids (% solids – HPLC). Plots comparing the gravimetric inputs to the reference methods are shown in Figure 136 and Figure 137 for everolimus and PVDF-HFP respectively. For both method comparisons there is good agreement between the reference method and the gravimetric formulation inputs, and as expected the HPLC method is a better predictor for everolimus content than the % solids method is for PVDF-HFP, this a consequence of the indirect and non-specific measurement approach taken for PVDF-HFP. It was decided to use the gravimetric measurements as reference data for the NIR calibrations as these measurements have equivalent or better accuracy and precision than the HPLC and % solids – HPLC methods respectively.

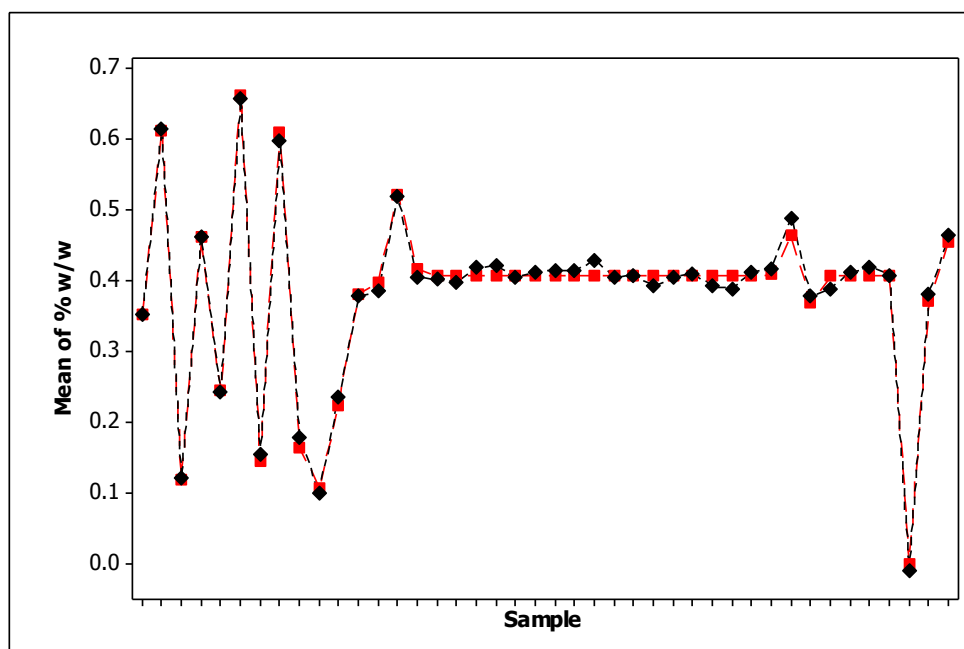


Figure 136. Comparison of the HPLC measurement of everolimus (in black) to the weight of everolimus added to the formulation solution (in red).

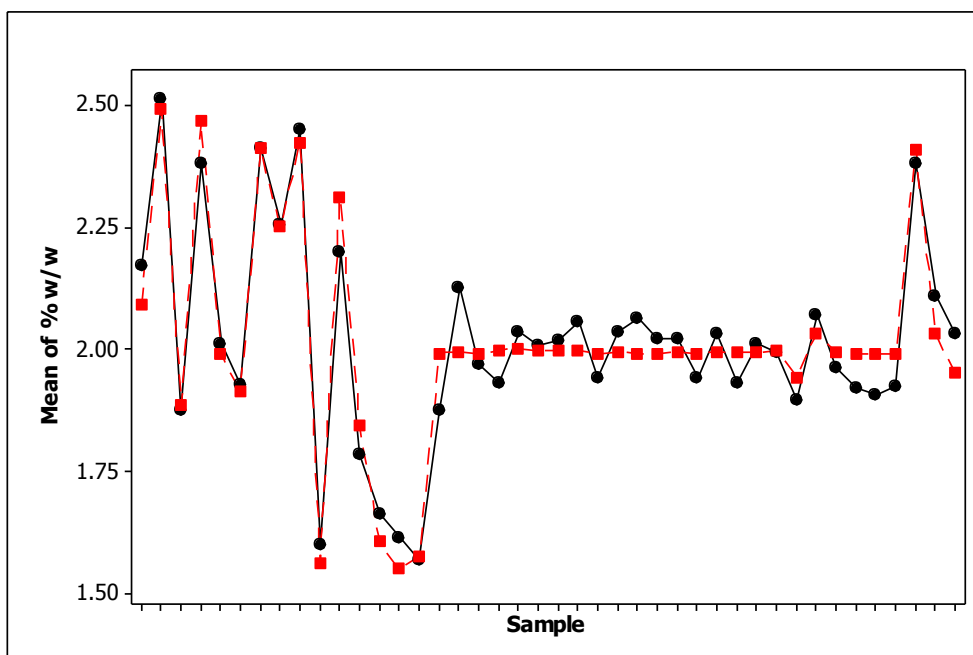


Figure 137. Comparison of measured PVDF-HFP (in black) to the weight of PVDF-HFP added to the formulation solution (in red) - % solid content minus the everolimus HPLC measurement was used to derive the measured PVDF-HFP quantity

In order to create a robust calibration model for the everolimus coating solution an iterative approach was taken. Firstly a feasibility study was carried out using laboratory solutions only (lab-only calibration), this was followed by an extension of the laboratory solutions data set incorporating deliberate water variation and the addition of solutions from the process. Cross-validation and test set validation were used to assess the calibration models. The following sections describe the calibration model development process in detail.

5.1.3.1 Feasibility assessment using laboratory calibration set

Initially, to demonstrate proof-of-concept that viable calibration models could be created for the everolimus coating solutions, a set of 15 coating solutions were formulated in the laboratory according to a mixture DoE (Table 9, Chapter 2). The NIR frequency range explored was between $9,172$ and $4,582$ cm^{-1} , as Figure 138 shows that this range eliminates the region of total absorbance below $4,582$ cm^{-1} and the region with very little spectral information greater than $9,172$ cm^{-1} . Principal component analysis (PCA) of the unprocessed spectra was used to check the calibration spectra for outliers. The scores plot in Figure 139 of principal component 1 (PC1) and PC2 shows a homogeneous spread of the coordinate points, indicating that no outliers dominate.

Chapter 5

The next thesis section provides detailed PCA of the final calibration set, thus in-depth PCA is not described for this feasibility study.

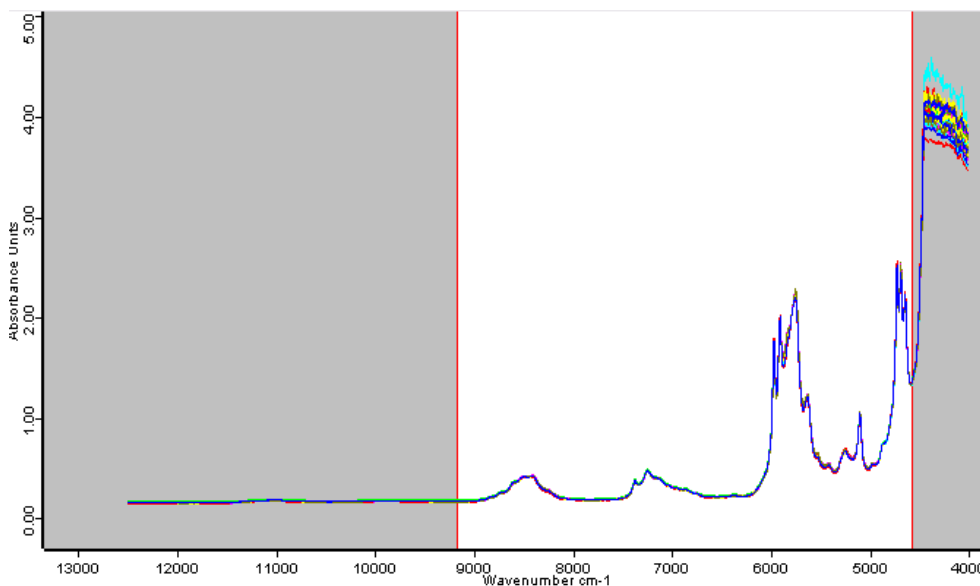


Figure 138 The NIR spectra of the calibration set with frequency range between 9,172 and 4,582 cm^{-1} highlighted. Spectra are from a range of everolimus coating solutions with everolimus concentration of 0.11 to 0.68 %w/w.

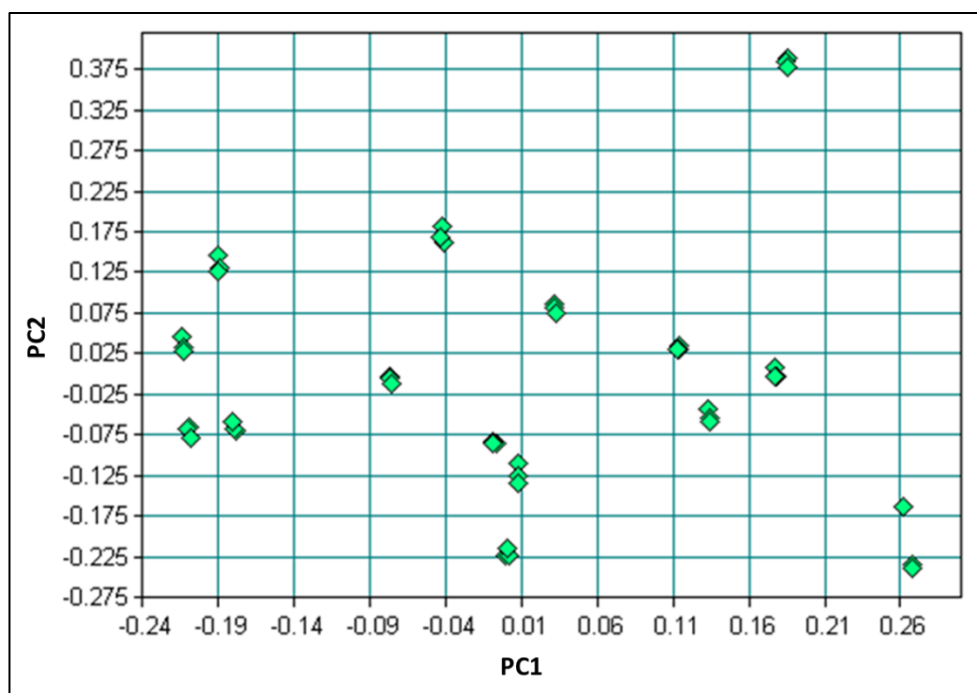


Figure 139 The scores plot principal component 1 (PC1) and PC2 showing the spread of the coordinate points.

Using the 15 unique solutions a leave-one-out cross-validation was performed to assess different NIR methods, each NIR method having a different combination of pre-

Chapter 5

treatment and frequencies selected. First derivative spectral pre-treatments gave the best results for NIR optimisation, particularly in combination with scatter correction techniques such as straight line subtraction (SLS), multiplicative scatter correction (MSC) and vector normalization (VN). The preliminary work done to the regions of the NIR spectrum that contain band shifts associated with changes in component concentration helped with reducing the frequency range to eliminate regions that were not useful.

Test set validation was carried out, on the most promising NIR methods selected through cross-validation, by using spectra from 10 unique solutions to construct the calibration and using spectra from 5 independent unique solutions as the test set. Selection of the optimum number of PLS factors was decided, primarily upon choosing the model with the lowest RMSE values before the decrease in RMSE was negligible. Figure 140 shows plots of RMSE versus the number of PLS factors for each of the 4 coating solution components. The RMSE values were also assessed based on achieving $\leq 2\%$ precision for each component as outlined in Table 18. For example the target concentration for the everolimus in the coating solution is 0.408%w/w with a target precision of 0.008%w/w. Because there are just 15 unique solutions, and 5 of these were selected as a test set to calculate RMSEP, then the RMSECV was given more weight than RMSEP when choosing the optimum number of PLS latent variables. Test-set validation for quantitative methods usually require many more samples, e.g. minimum of 50, to allow enough samples for the calibration and test set.

Table 18 Target concentration of the everolimus coating solution components, and 2% of the target concentration for each component.

Component	Target conc. (%w/w)	2% of Target (%w/w)
Everolimus	0.408	0.008
PVDF-HFP	2.00	0.04
Acetone	68.3	1.4
Cyclohexanone	29.3	0.6

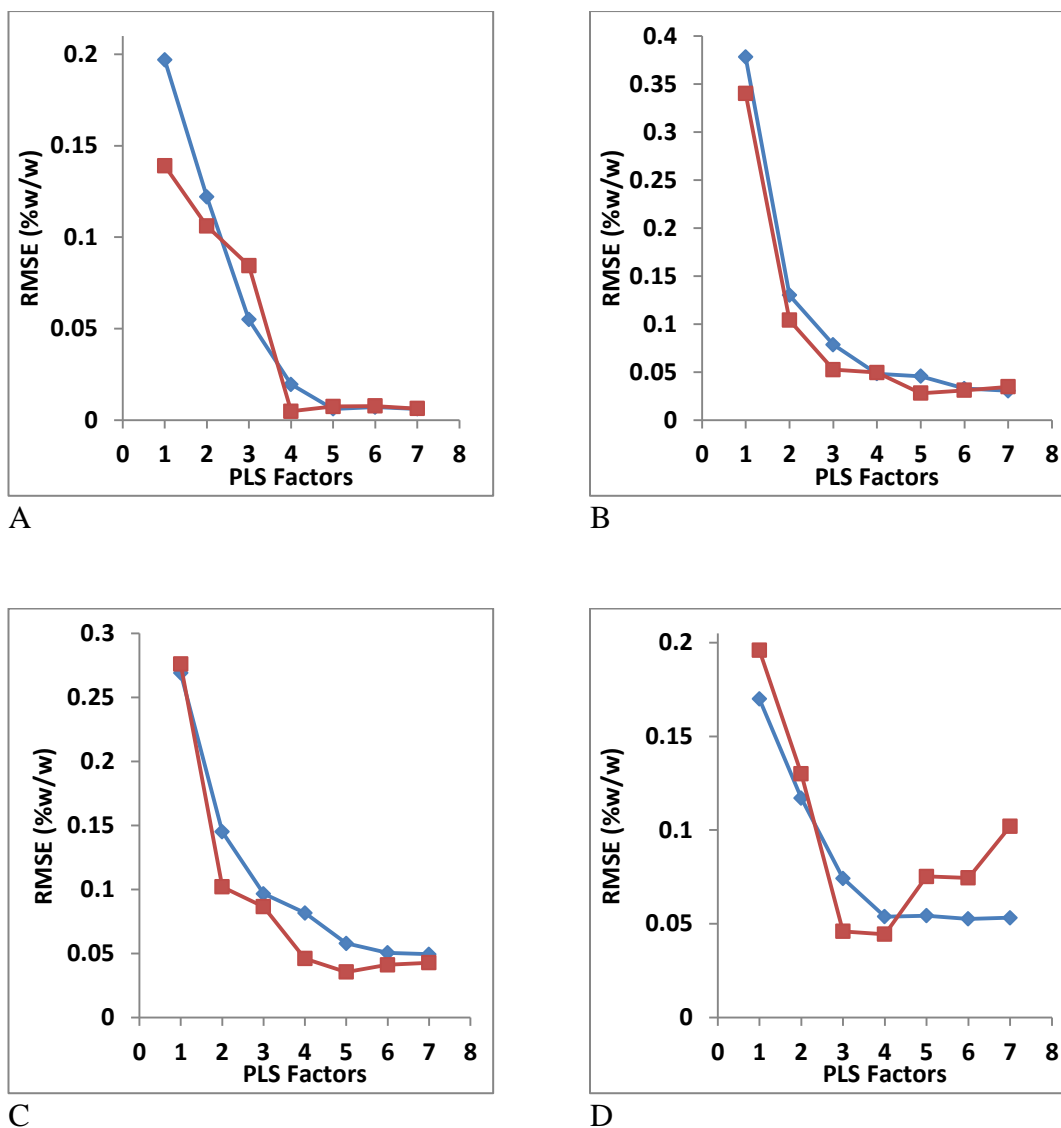


Figure 140 PLS factors (latent variables) versus RMSECV (blue) and RMSEP (red) for the calibration model of A - everolimus, B- PVDF-HFP, C – Acetone, and D - Cyclohexanone

It was concluded that no more than 5 PLS factors should be used for everolimus and PVDF-HFP concentration, no more than 4 PLS factors for cyclohexanone concentration, and no more than 3 for acetone concentration. The results of the cross-validation for some of the pre-treatments and frequency region selections are shown in Table 19 for everolimus, Table 20 for PVDF-HFP, Table 21 for acetone, and Table 22 for cyclohexanone.

Chapter 5

Table 19. Results of cross-validation for everolimus concentration using 15 lab solutions only. The optimum model is shown in bold font.

Data pre treatment	Frequency ranges (cm ⁻¹) ¹⁾	PLS factors	RMSECV %w/w	RMSEP %w/w	R ²
SLS	7502 - 6098 & 4602 - 4582	4	0.0180	0.0122	99..02
1 st deriv. + MSC	9172 – 6098	4	0.0190	0.0122	98.9
1 st deriv.	7502 - 6098	5	0.0224	0.0114	98.49
1 st deriv. + SLS	7502 - 6098 & 4602 - 4582	5	0.0142	0.0125	99.39
1 st deriv. + SLS	7502 - 6098 & 4602 - 4590	5	0.0144	0.0125	99.37
1 st deriv. + VN	9172 – 5446 & 4602 - 4582	5	0.0112	0.0056	99.62
1 st deriv. + SLS	9172 – 6098	5	0.0172	0.0160	99.11
1 st deriv. + MSC	9172 – 6098	5	0.0086	0.0084	99.78
1st deriv. + MSC	7502 - 6098 & 4602 - 4582	5	0.0061	0.0048	99.89
1 st deriv. + SLS	7502 – 6098	5	0.0144	0.0123	99.38

Table 20. Results of cross-validation for PVDF-HFP concentration using 15 lab solutions only. The optimum model is shown in bold font.

Data pre treatment	Frequency ranges (cm ⁻¹) ¹⁾	PLS factors	RMSECV %w/w	RMSEP %w/w	R ²
1st deriv. + MSC	9172 – 8335	5	0.0486	0.0714	99.2
1st deriv. + MSC	9172 - 8335	4	0.0483	0.0494	97.8
1st deriv. + MSC	9172 – 7498 & 4602 - 4582	5	0.0535	0.0304	97.52
1st deriv.	9172 - 7498	5	0.0677	0.109	96.03
1st deriv. + VN	9172 – 7498 & 4602 - 4582	5	0.0532	0.0579	97.55

Chapter 5

Table 21. Results of cross-validation for acetone concentration using 15 lab solutions only. The optimum model is shown in bold font.

Data pre treatment	Frequency ranges (cm ⁻¹)	PLS factors	RMSECV %w/w	RMSEP %w/w	R ²
MSC	9172 – 7498 & 4602 - 4582	3	0.106	0.786	99.84
VN	8335 – 7498 & 6102 - 5446	3	0.105	0.0877	99.84
VN	9172 – 7498 & 6102 - 5446	3	0.0966	0.0865	99.87
1st deriv. + VN	9172 – 7498	3	0.139	0.101	99.73
1 st deriv. + MSC	9172 – 7498 & 4602 - 4582	3	0.102	0.101	99.85

Table 22. Results of cross-validation for cyclohexanone concentration using 15 lab solutions only. The optimum model is shown in bold font.

Data pre treatment	Frequency ranges (cm ⁻¹)	PLS factors	RMSECV %w/w	RMSEP %w/w	R ²
1 st deriv.	9172 – 7498 & 6102 - 5446	4	0.0548	0.0451	99.95
Constant offset elimination	6102 – 5446 & 4602 - 4582	4	0.0558	0.0506	99.95
1st deriv. + VN	9172 – 7498, 6102 – 5446, & 4602 - 4582	4	0.0557	0.0475	99.95
MSC	9172 – 7498 & 6102 - 5446	3	0.0563	0.0303	99.95
1st deriv. + SLS	9172 – 8335 & 6102 - 5446	4	0.0538	0.0444	99.95

Chapter 5

The optimum PLS model selected for each component is further described as follows:

Everolimus - concentration range 0.1061 - 0.661% w/w. The combination of first derivative and MSC was chosen for pre-treatment in the frequency regions 7,502.1 to 6,098.1 cm^{-1} and 4601.6 to 4,582.3 cm^{-1} , resulting in 371 combined data points. The smaller region, 4,601.6 to 4,582.3 cm^{-1} , is not included in the spectra displayed in Figure 141 (A) as it does not provide for useful visual interpretation. Figure 141 (B) shows the calibration curve for the model which exhibits close correlation between predicted and theoretical everolimus concentration.

The PLS regression vector in Figure 141 (C) is a graphical display of the calibration function that shows the wavenumbers at which relevant information for everolimus absorbance can be found. Dominant features in the PLS regression vector can be attributed to everolimus content in the coating solution by comparing it to Figure 130. Because the spectra are treated by first derivative, dominant features are indicated by zero-crossings of the regression vector. Spectral features in the 5 PLS loading vectors shown in Figure 141 (D) were used to provide evidence that the model is specific for everolimus concentration. The PLS loading vectors can be used to determine if too much noise is being fitted. The higher the number of the PLS loading vector the more noise is visible. In this case all of the loading vectors look smooth, and not sharp. Sharp loading vectors may indicate that too much noise is being fitted. This visual observation of the regression vectors is a simple but effective means of avoiding over-fitting by selection of too many PLS factors, as described by O’Gorman et al[118].

Similarly the PLS models for PVDF-HFP (1.553 – 2.493% w/w), acetone (64.00 – 72.64% w/w), and cyclohexanone (25.35 – 33.16% w/w) are described in Figure 142, Figure 143, and Figure 144, respectively. All of the models provide close correlation between predicted and theoretical component concentration. Therefore, the laboratory solution based-model provided confidence that successful application of a NIR procedure was at least feasible.

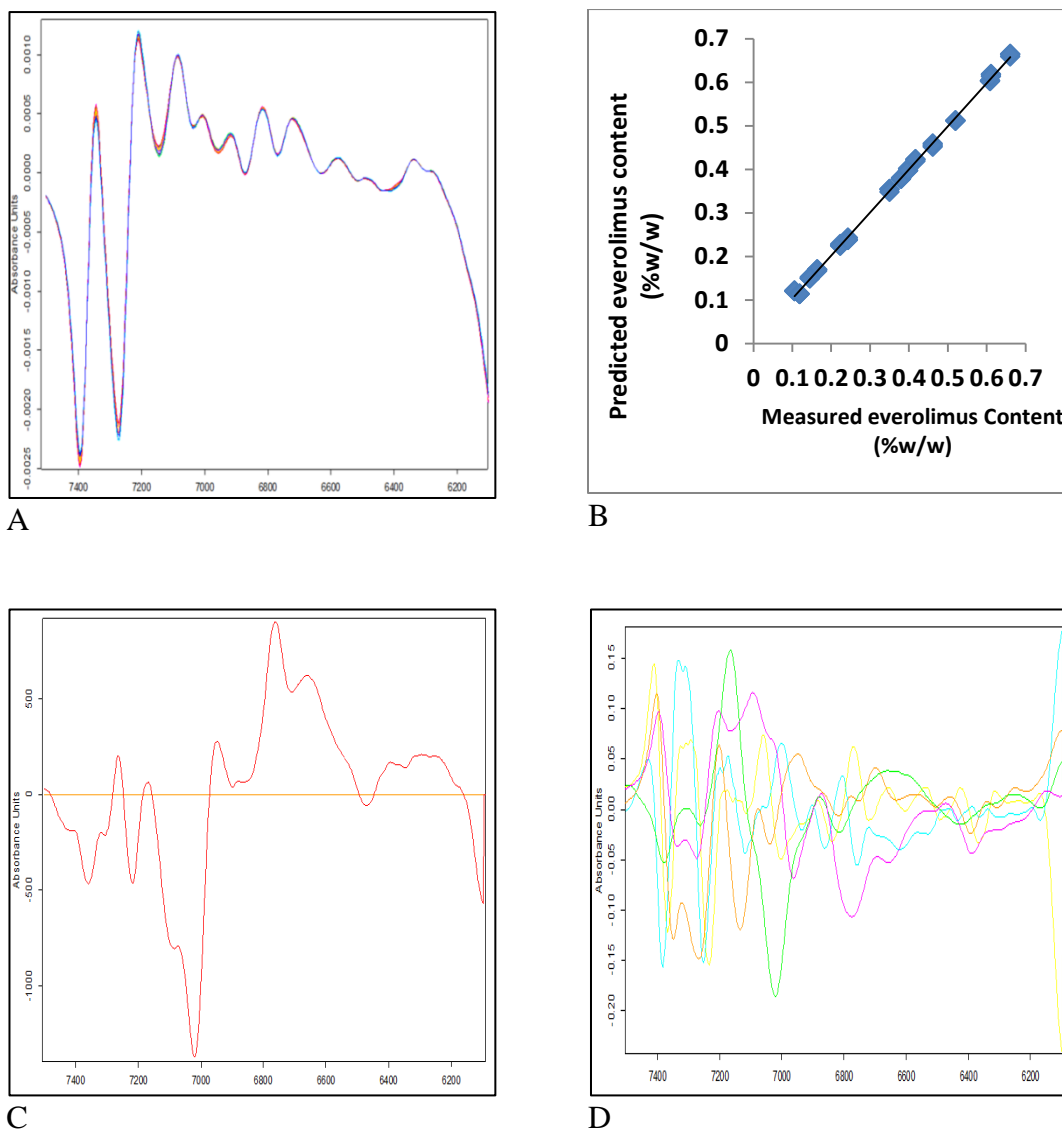


Figure 141. (A) Calibration spectra showing the 7,502 to 6,098 cm^{-1} region used in the calibration model for everolimus following first derivative + MSC pre-treatment. (B) Calibration plot of actual versus predicted everolimus concentration from the laboratory only based calibration data set. (C) Everolimus concentration calibration regression coefficient vector. (D) PLS factor loadings for everolimus concentration (orange = factor 1, pink = factor 2, green = factor 3, blue = factor 4, and yellow = factor 5)

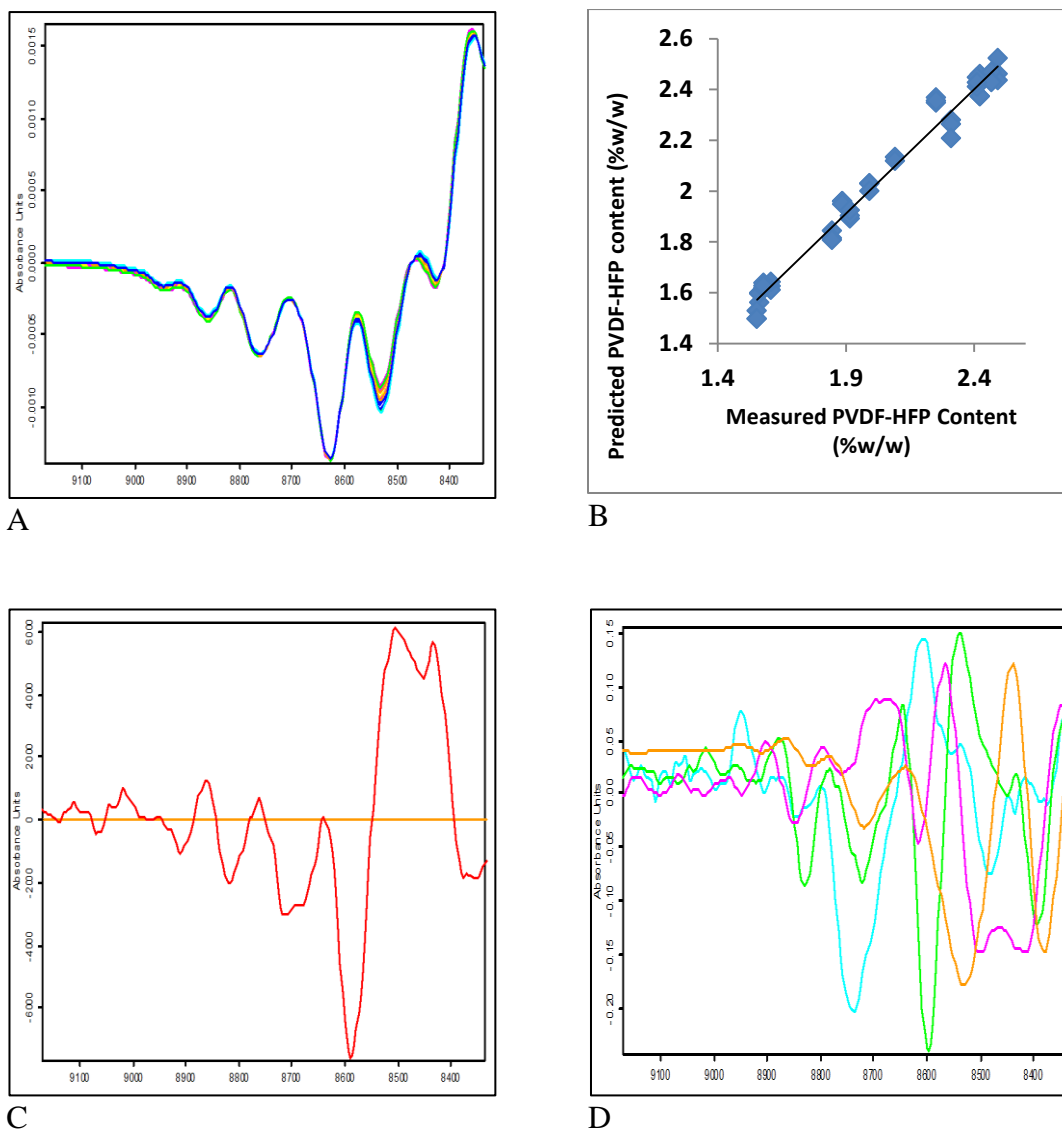


Figure 142. (A) Calibration spectra showing the 7,172 to 8,335 cm^{-1} region used in the calibration model for PVDF-HFP following first derivative + MSC pre-treatment. (B) Calibration plot of actual versus predicted PVDF-HFP concentration from the laboratory only based calibration data set. (C) PVDF-HFP concentration calibration regression coefficient vector. (D) PLS factor loadings for PVDF-HFP concentration (orange = factor 1, pink = factor 2, green = factor 3, and blue = factor 4)

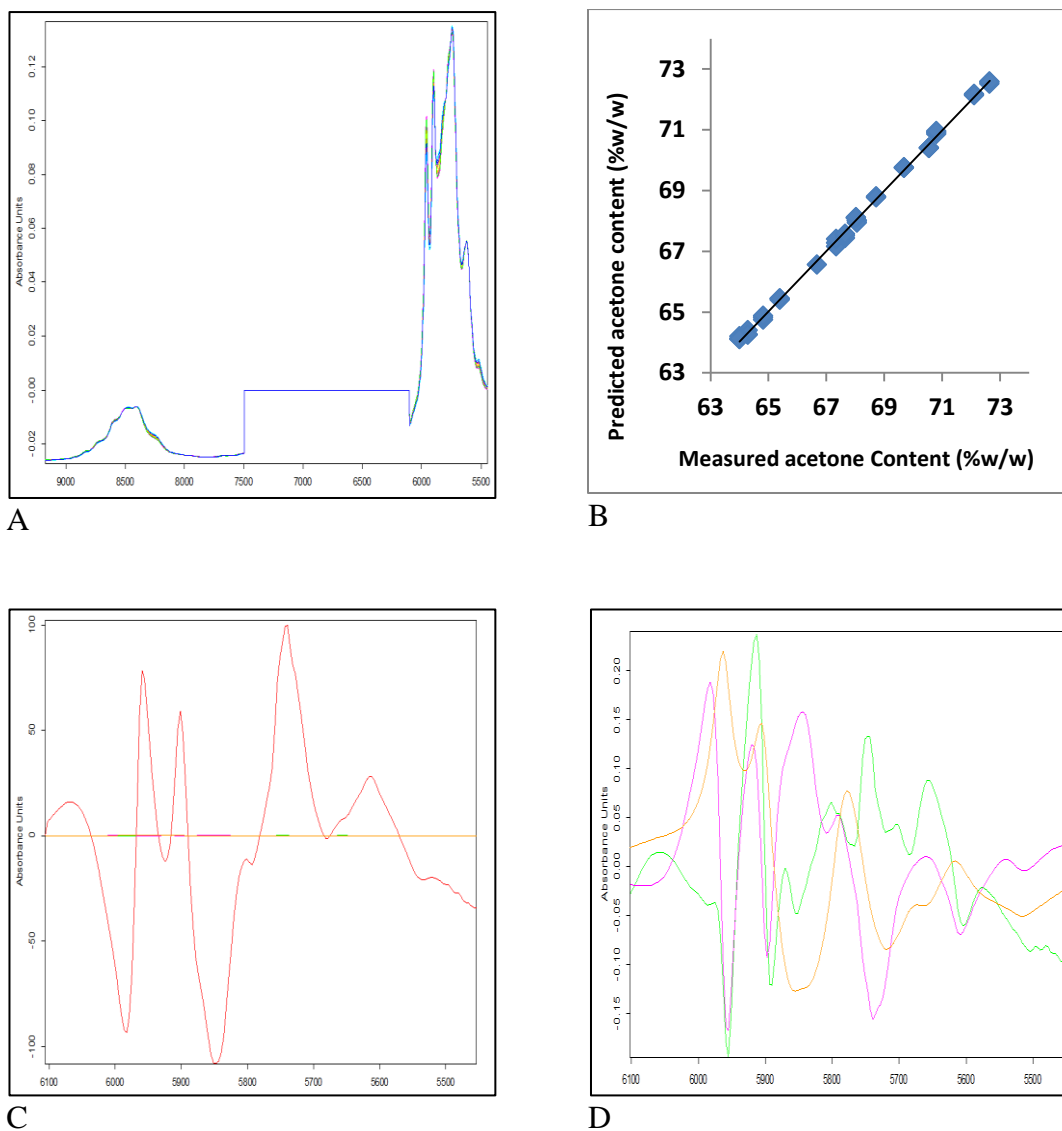


Figure 143. (A) Calibration spectra showing the 9,172 – 7,498 & 6,102 – 5,446 cm^{-1} regions used in the calibration model for acetone following vector normalisation pre-treatment. (B) Calibration plot of actual versus predicted acetone concentration from the laboratory only based calibration data set. (C) Acetone concentration calibration regression coefficient vector just for the 6,102 – 5,446 cm^{-1} region. (D) PLS factor loadings for acetone concentration just for the 6,102 – 5,446 cm^{-1} region (orange = factor 1, pink = factor 2, and green = factor 3)

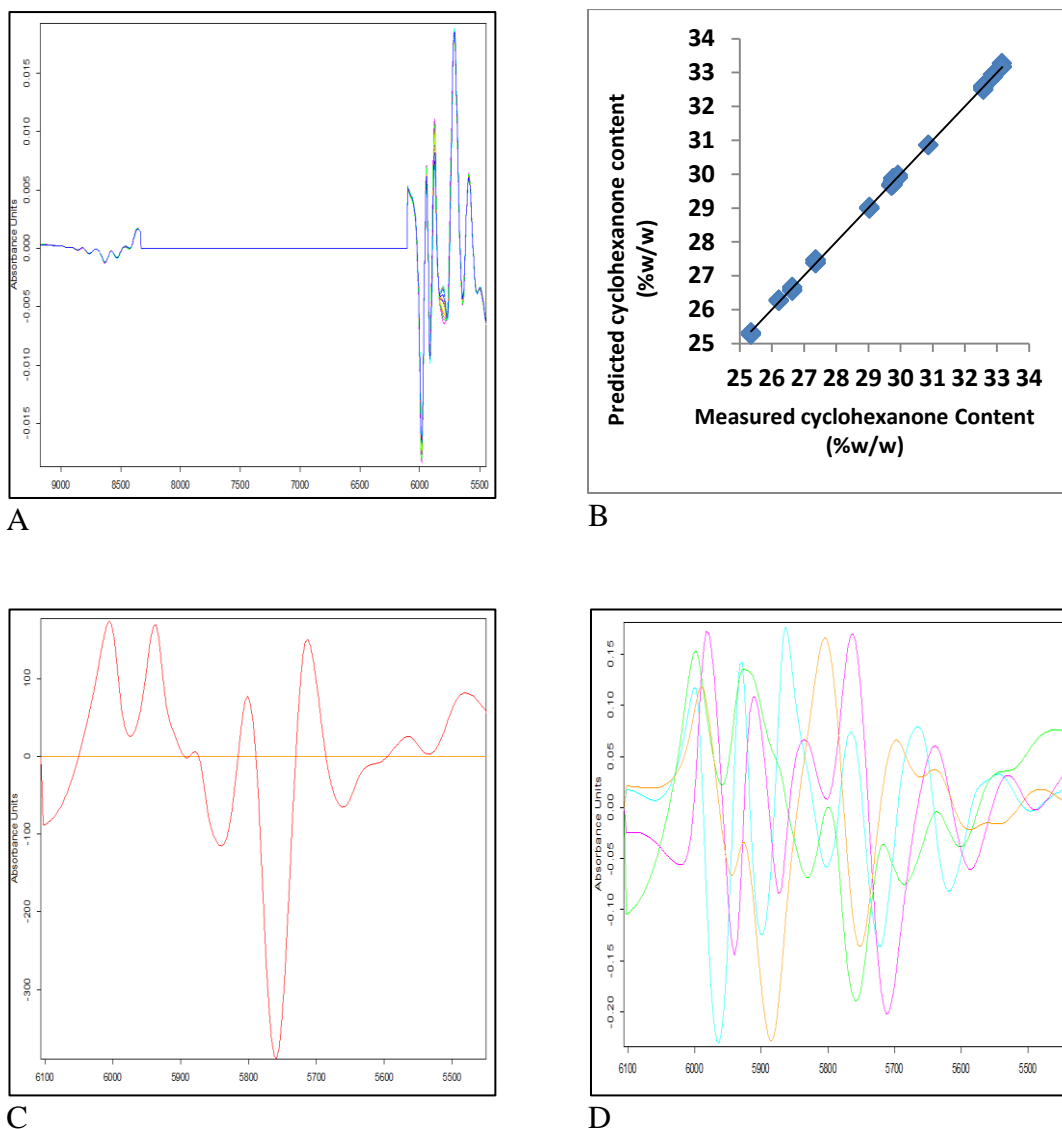


Figure 144. (A) Calibration spectra showing the 9,172 – 8,335 & 6,102 – 5,446 cm^{-1} regions used in the calibration model for cyclohexanone following first derivative and straight line subtraction pre-treatment. (B) Calibration plot of actual versus predicted cyclohexanone concentration from the laboratory only based calibration data set. (C) Cyclohexanone concentration calibration regression coefficient vector just for the 6,102 – 5,446 cm^{-1} region. (D) PLS factor loadings for cyclohexanone concentration just for the 6,102 – 5,446 cm^{-1} region (orange = factor 1, pink = factor 2, green = factor 3, and blue = factor 4)

5.1.3.2 Water variation

It should be noted that solvents, whilst purified, may have trace levels of other materials that can have a significant impact on spectral variation. This is true for water in particular because it is easily introduced to solvents and solutions from the environment, and because it has high absorbance in the NIR region of the electromagnetic spectrum. That high variability in the levels of residual water in solvents occurs for the solutions under investigation was discovered when acetone sourced from a new supplier was introduced to the everolimus coating solution preparation process. Upon inspection of the water absorption bands at around 5,000 and 7,000 cm^{-1} it became apparent that the absorption band is larger in one supplier's acetone as opposed to another, as illustrated from the spectra in Figure 145.

Acetone is a hygroscopic solvent so it is possible for it to take up water readily from the atmosphere under uncontrolled environmental conditions. The equipment used for coating the everolimus eluting stents is not in a humidity controlled environment, and neither is the formulation preparation area. The level of water in the coating solutions would thus be expected to increase over time and exposure level. The rate of water uptake is dependent upon the relative humidity, which can vary greatly. Everolimus has 3 R-OH groups that have associated absorption bands that are in the vicinity of the overtone and combinations bands of water, Figure 130. Additionally the concentration of everolimus in the coating solutions, approximately 0.408% w/w, is near the lower limit of sensitivity for NIR predictions of pharmaceutical components in solution. In general the detection limit for NIR is approximately 0.1% [84], although for some specific cases lower values may be attained especially in the case of trace water analysis [119]. Therefore variations in the spectral noise have potential to affect the quality of the calibrations for everolimus significantly.

Chapter 5

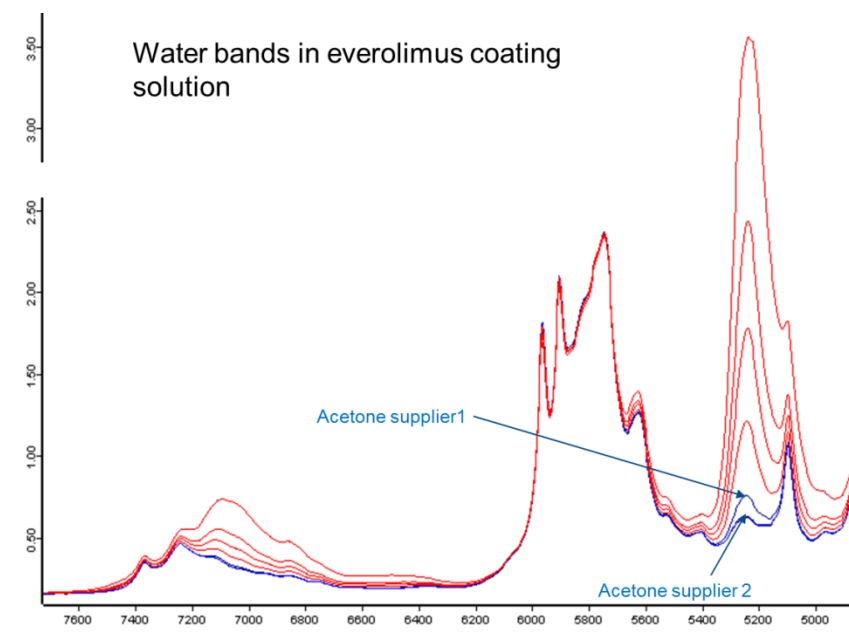


Figure 145 Everolimus coating solutions made with two different acetone suppliers, with additional laboratory samples included to emphasise the water bands (shown in red).

To counteract this unavoidable interference from water, calibration solutions were formulated with quantities of water which spanned the range expected in coating solutions (0.2 to 0.5% w/w), Table 10, Chapter 2. These solutions were then spiked with known quantities of water to reach the required levels. The level of water in each solution was verified using Karl Fischer titrimetry^{‡‡}. These 20 calibration solutions were combined with an initial 15 solutions created in the laboratory and further 48 solutions that were sourced from the actual process. The total of 83 unique calibration solutions is a large enough data set to make test set validation possible.

^{‡‡} The coefficient of variation for the Karl Fischer titration used is $\leq 5\%$, with an accuracy of $\pm 0.01\%$ w/w.

5.1.3.3 Principal component analysis of the calibration spectra

The first step was to assess if the samples were equivalent and suitable for chemometric analysis, this was done by PCA analysis. Initially, principal components (PCs) were calculated without any spectral pre-processing in the range 9,103 – 4,548 cm^{-1} . Three groups of spectra^{§§} were used, calibration set #1 (Table 9), calibration set #2 (Table 10), and 69 process solutions (Table 11). The scores plot showing PC1 versus PC2 clearly shows 2 clusters which are circled in Figure 146, each of the spectra groups are highlighted in different colours; process solutions shown in pink, calibration solutions #1 shown in light blue, and calibration solutions #2 shown in dark blue. PC1 shows that both calibration solution groups are clearly different from one another, with some process solutions associated with both of these groups. Review of the collection time of the spectra from both clusters identified that a different vial type was used in one cluster versus the other, thereby explaining the different spectral variation picked out by PC1. The vials used for preparing calibration set #1 and the process solutions that appear in the same cluster in Figure 146 were acquired from the same vendor, Bruker Optics. However when the vials were compared it was found that they were slightly different, the outer diameter of the vials were equivalent, however due to a slight vial-wall thickness difference the actual sample pathlength was slightly different.

^{§§} The spectra were mean centred to ensure that the data varies around zero, this is achieved by computing the overall mean of all spectra, and then subtracting this value from each individual spectrum.

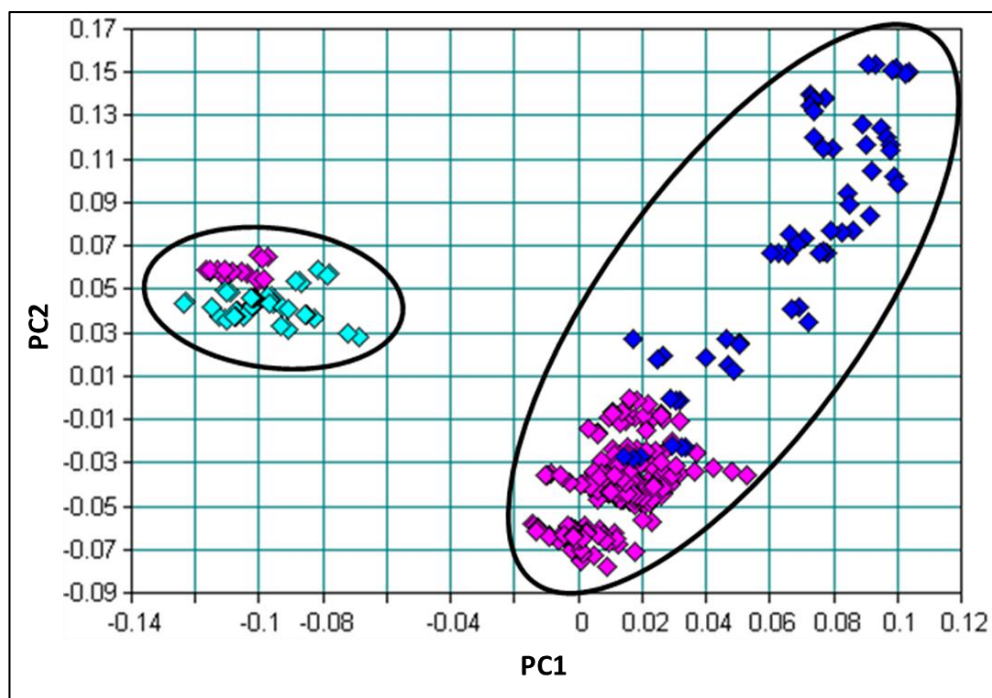


Figure 146 Score plot for the NIR data set showing PC2 (y-axis) plotted against PC1 (x-axis). Two data clusters are circled. The pink data points correspond to process solutions, the light blue data points correspond to calibration set #1, and the dark blue data points correspond to calibration set #2.

Spectral features corresponding to each PC may be visualized by plotting the loading vector for each PC versus the wavenumber. The loading plot for the first PC is shown Figure 147; for the most part the loading plot matches the spectrum of a typical coating solution. A similar spectrum can be created by subtracting a coating solution from calibration set #1 from a coating solution in calibration set #2, shown in Figure 148. This suggests that this first PC explains the variation in the spectrum associated with a slight difference in path length of the sample vial, thus explaining the two clusters in Figure 146. Additionally a large band at the frequency associated with water absorption in the loading plot at about $5,200\text{ cm}^{-1}$ picks out the difference in water concentration between the two laboratory calibration sets. Calibration set #2 has a higher concentration of water to enable the creation of a calibration model for water content.

Chapter 5

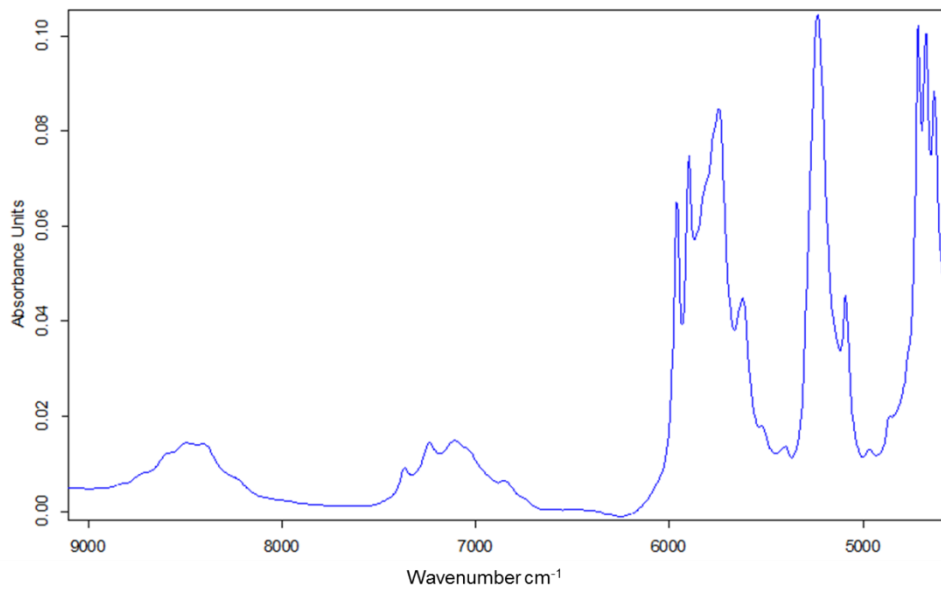


Figure 147 Loading plot for PC1.

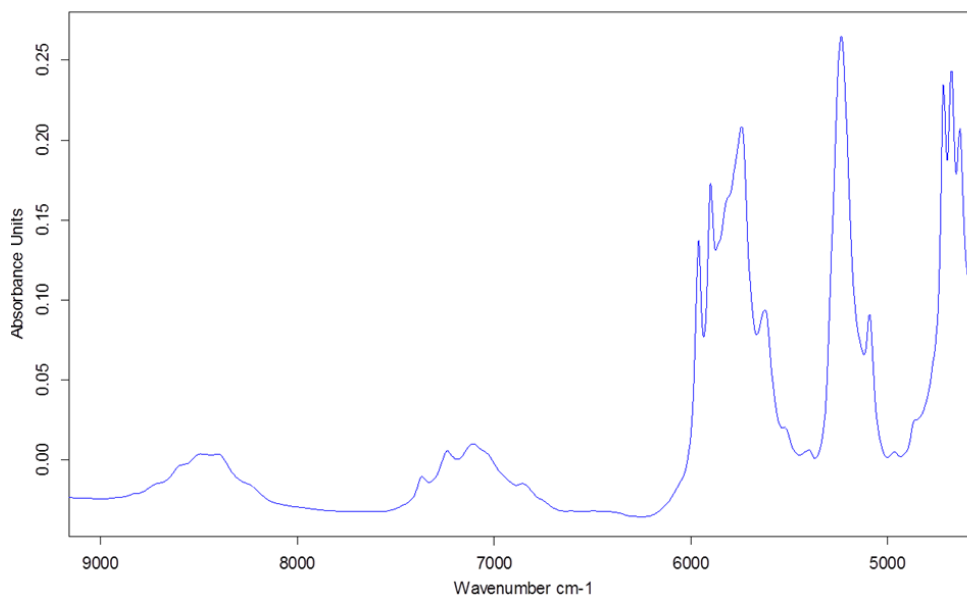


Figure 148 Spectrum of a coating solution from vial type 1 subtracted from the spectrum from vial type 2.

Chapter 5

Interpretation of the scores plots is made easier because of the experimental design approach used to create the 2 calibration sets. For example, it is apparent that PC2 and PC3 correspond to the spectral features that explain the concentration of water and acetone when their score plot, Figure 149, is compared to a scatterplot of the concentration of acetone versus water in Figure 150. The loadings for PC2 and PC3 are shown in Figure 151. These loadings match the spectrum of water subtracted from an average spectrum of the everolimus coating solution (PC2), and the spectrum from the subtraction of cyclohexanone from acetone (PC3) shown in Figure 152. Therefore the trend seen in the score plots explains the spectral variation due to the water content in PC2, and PC3 explains the acetone concentration. However PC's 4 to 9 do not appear to relate to the concentration of everolimus and PVDF-HFP. This indicates that, even though the calibration design has a deliberate range of everolimus, and PVDF-HFP concentrations included, other spectral variations contribute more to the overall variation in the PCA.

PC10 and PC 11 show a matching pattern for everolimus and PVDF-HFP respectively. Evidence that PC10 is linked to everolimus concentration is shown by comparing the PC3 vs. PC10 scores plot to the scatterplot of acetone and everolimus concentrations used in the samples, Figure 153 and Figure 154 respectively. The experimental design pattern for calibration set #1, shown in the scatterplot using broken lines, is visible in the scores plot. The pattern for PVDF-HFP is not as clear, Figure 155 and Figure 156. In fact, even though PC 10 and 11 do correspond to the concentration of everolimus and PVDF-HFP, it is doubtful that they could be used to build a stable calibration model. There is a danger for these higher PCs, that any model created with them would be over-fitted and of little use for predicting unknowns. The next step was to try some spectral pre-treatments to remove some of the variation that may exist in the spectral data and to look at reducing the size of spectral frequencies used.

Chapter 5

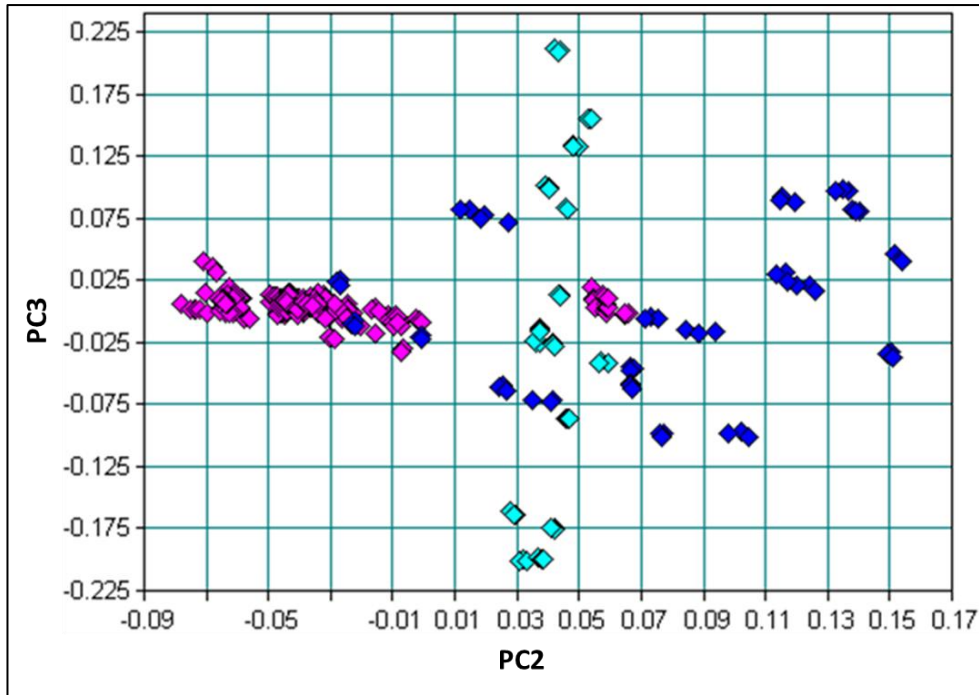


Figure 149 Score plot of PC2 vs. PC3. The component concentrations in the process solutions is narrow compared to the laboratory-formulated coating solutions, thus the spectral variation associated with concentration of each component in the laboratory coating solutions (dark and light blue) is wider than for the process solutions (pink). The water concentration in the first set of laboratory coating solutions (light blue) was not deliberately varied, consequently the water concentration is not wide.

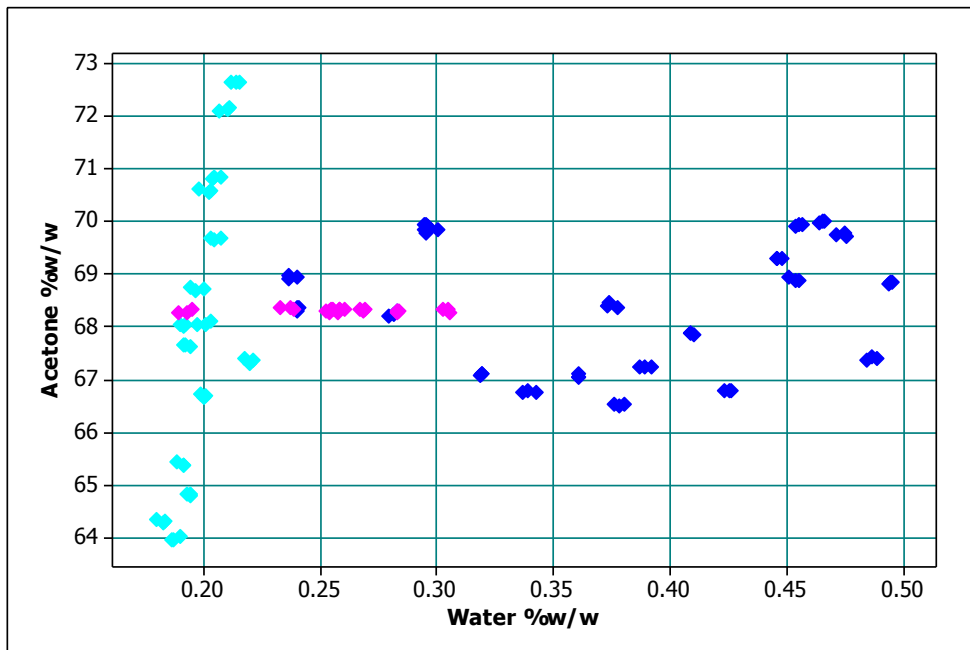


Figure 150 Scatterplot for the concentration of water versus acetone in the everolimus coating solutions.

Chapter 5

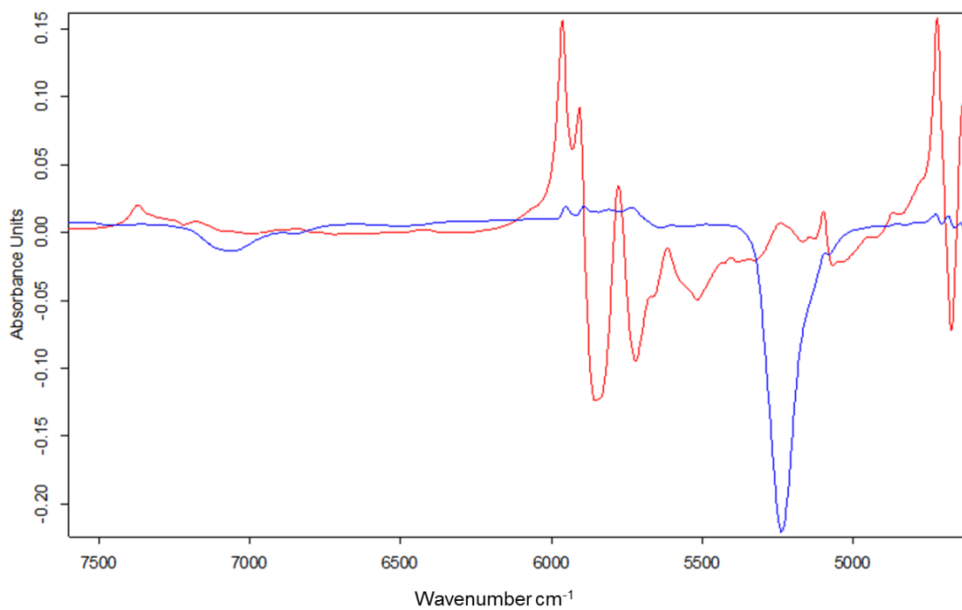


Figure 151 Loadings for PC2 (blue) and PC3(red)

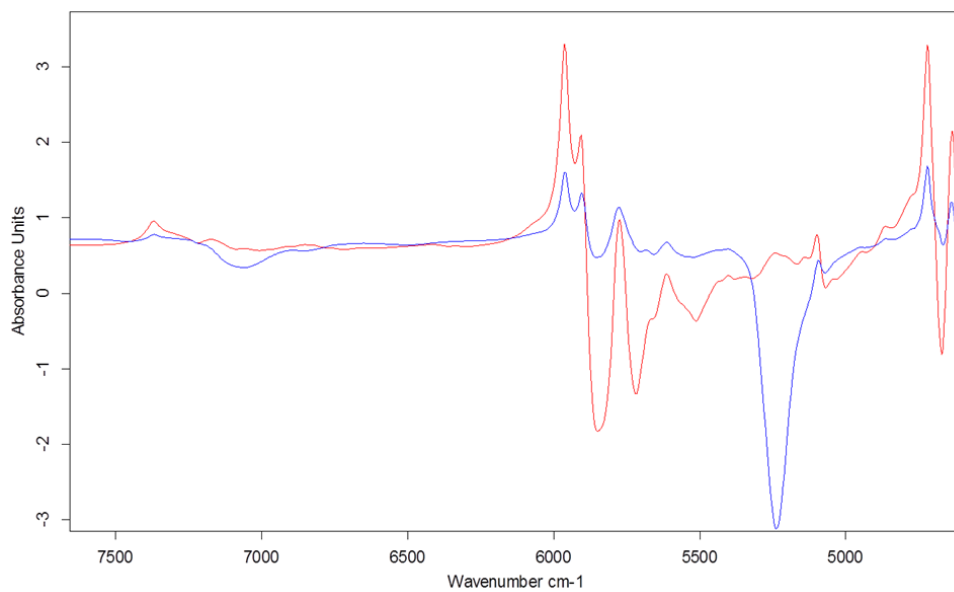


Figure 152 Spectra of Cyclohexanone subtracted from acetone (red), and the spectrum of a low water content coating solution subtracted from the spectrum of a high water content coating solution (blue)

Chapter 5

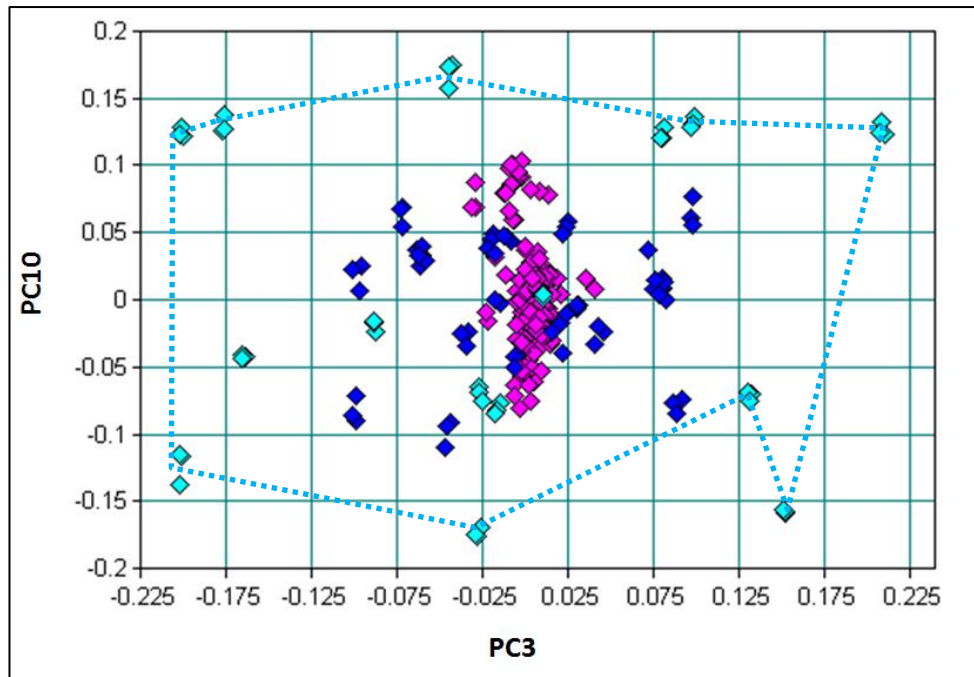


Figure 153 PC3 vs. PC10 scores plot

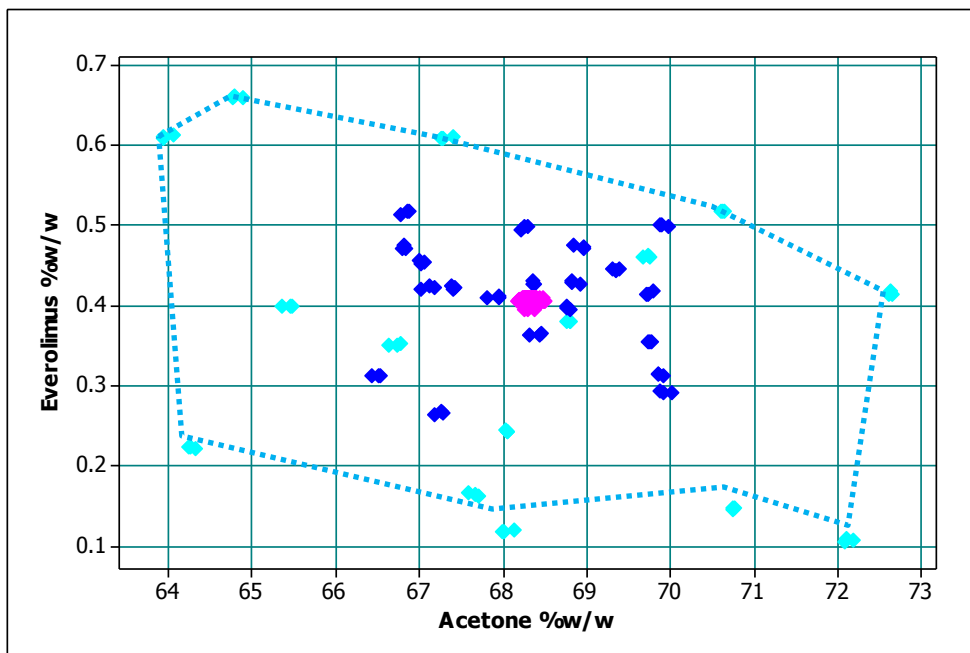


Figure 154 Scatterplot of acetone and everolimus concentrations used in the calibration samples.

Chapter 5

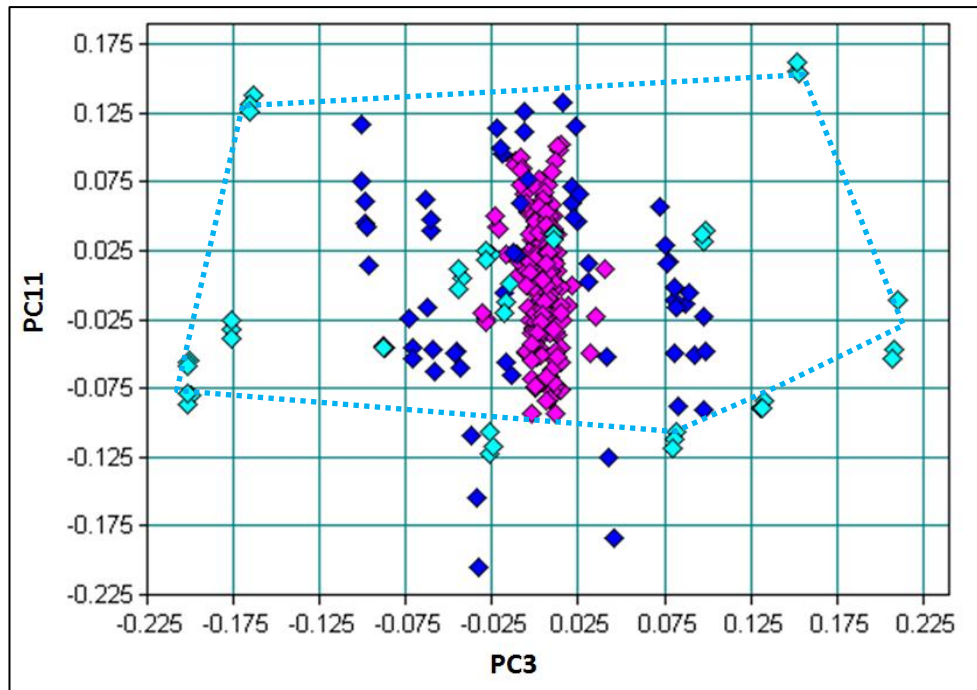


Figure 155 PC3 vs. PC11 scores plot

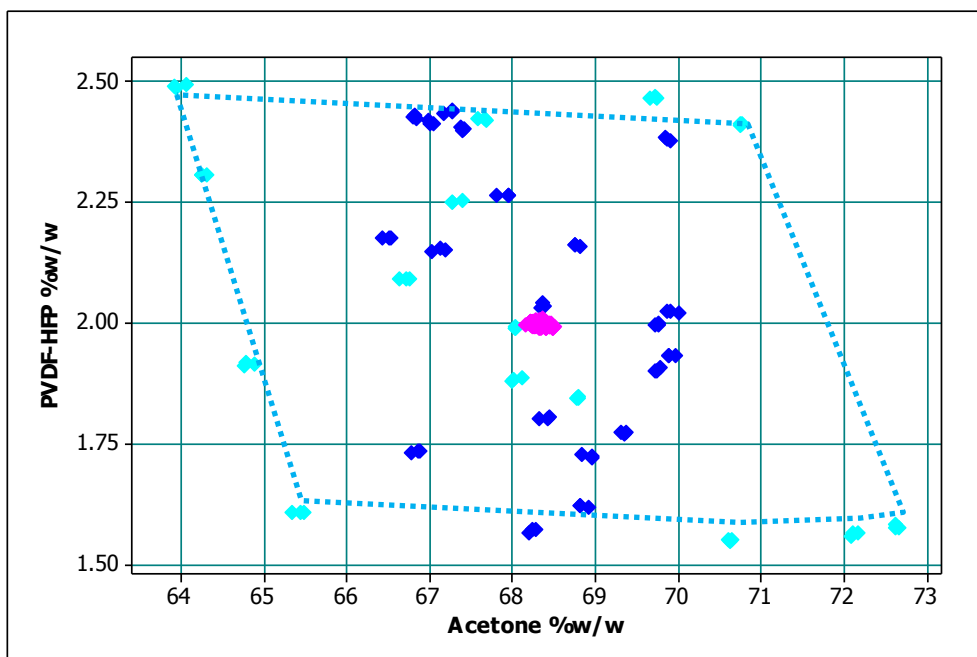


Figure 156 Scatterplot of acetone and PVDF-HFP concentrations used in the calibration samples.

A trial and error approach was used to assess various spectral pre-treatment options. This meant selecting the full spectral range, or smaller wavelength ranges and applying several of the pre-treatments available. Each pre-treatment was applied equally to the entire calibration data set, i.e. individual spectra or subsets of spectra were not treated differently and then combined with the remainder of the calibration set for development

Chapter 5

of the calibration models. The treated spectra were then used to develop a calibration model using PLS, the calibration model was assessed, noted and then another pre-treatment was tried. The criteria for assessment of the PLS calibration models is covered in section 5.1.3.4. This iterative approach is necessary to arrive at the optimum calibration model. Following assessment of several pre-treatment options, first derivative plus multiplicative scattering correction (1st Der + MSC) came out as the most effective. MSC is a common pre-treatment that can correct for differences in wavelength between spectra caused by light scattering, this is achieved by shifting and scaling each spectrum to fit a given target spectrum[94], [120]. The target spectrum is usually the mean spectrum of the spectra in the calibration set[95].

PCA carried out after mean centring and 1st Der + MSC spectral pre-treatment in the range 9,103 – 4,548 cm⁻¹ resulted in the reduction in the number of PCs required to find a correlation to the experimental design. The scores plot, shown in Figure 157, of the first and second PC corresponds to water and cyclohexanone concentration. This is confirmed through comparison to the scatterplot of the water concentration and cyclohexanone concentration shown in Figure 158. Thus demonstrating, the spectral pre-treatment has removed the vial-type associated variation seen as PC1 without spectral pre-processing.

Since PC2 was identified as corresponding to the concentration of cyclohexanone, the scores for this PC were plotted against the higher ranking PCs. The resulting scores plots were compared to the experimental design by comparison to the scatterplots of PVDF-HFP and everolimus plotted against cyclohexanone shown in Figure 159 and Figure 162, respectively. Figure 160 shows that PC5 has some correlation to the concentration of PVDF-HFP, however a significant amount of the expected-variation for PVDF-HFP remains unexplained by PC5 as evidenced by the poor correlation of many of the coordinate points lying outside the experimental design space traced in the score plot. Examination of higher ranking PCs show that PC10 also correlates to PVDF-HFP, this is shown in Figure 161. Figure 163 demonstrates that PC8 corresponds to everolimus concentration.

Chapter 5

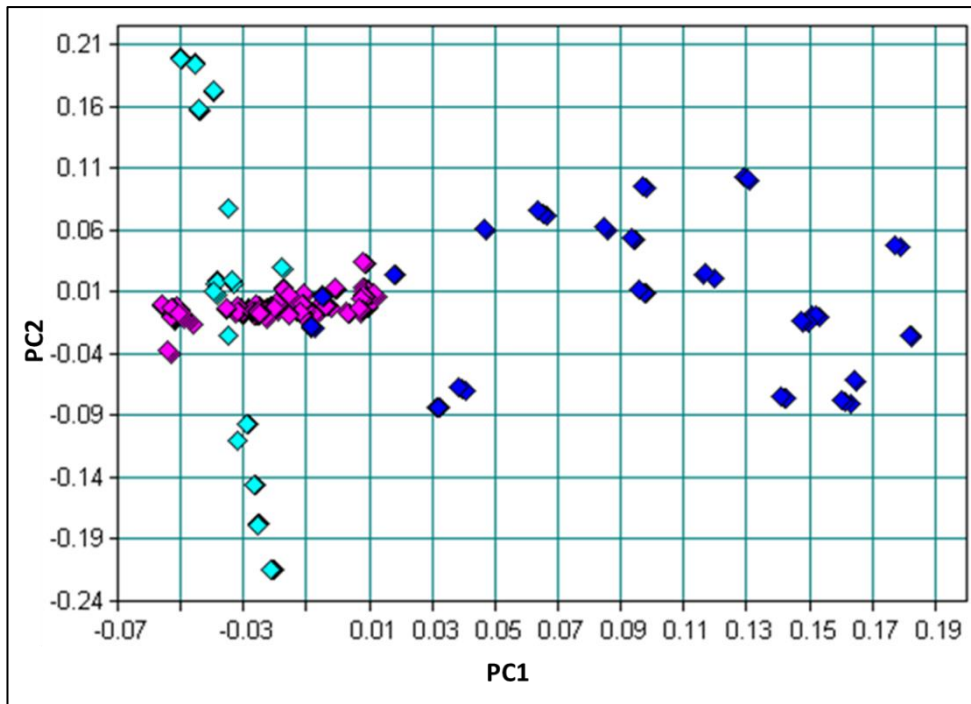


Figure 157 The first and second PC scores plot after first derivative plus multiplicative scattering correction.

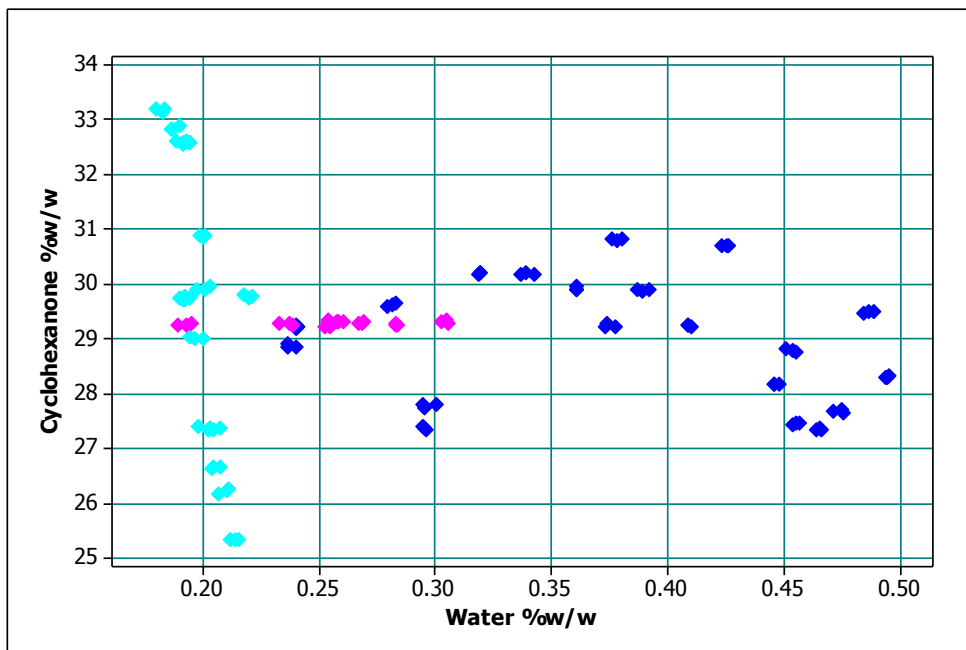


Figure 158 Scatterplot for the concentration of water versus acetone in the everolimus coating solutions.

Chapter 5

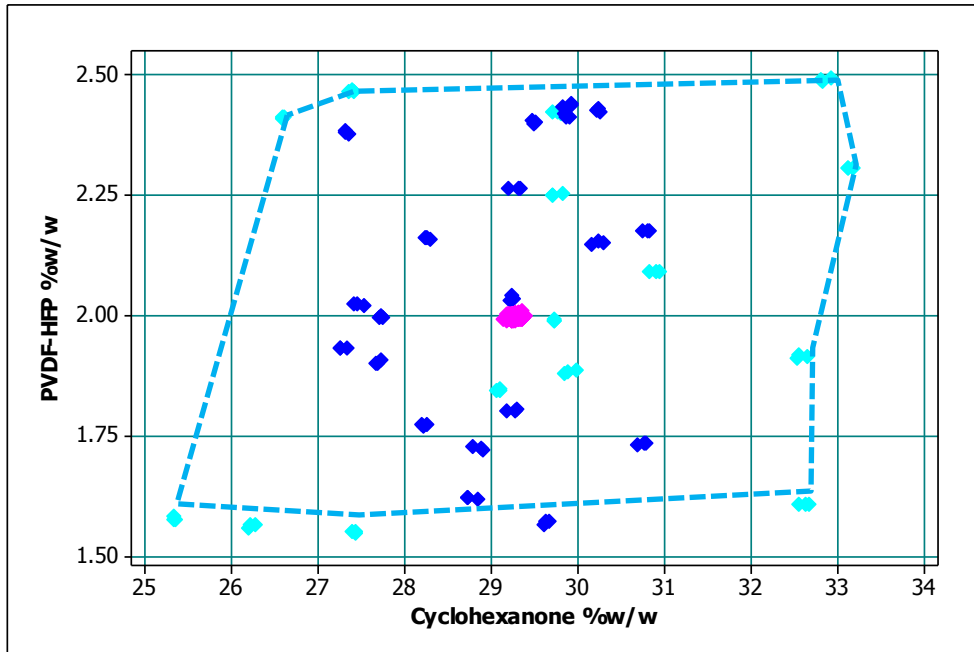


Figure 159 Scatterplot for the concentration of PVDF-HFP versus cyclohexanone in the everolimus coating solutions.

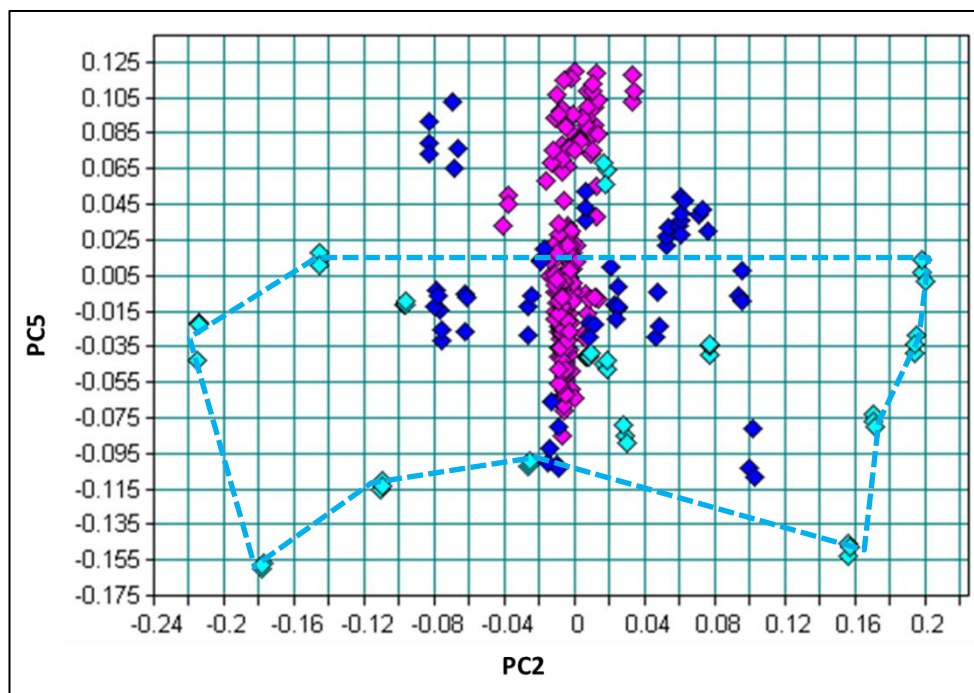


Figure 160 Scoresplot of PC2 versus PC5 after first derivative plus multiplicative scattering correction.

Chapter 5

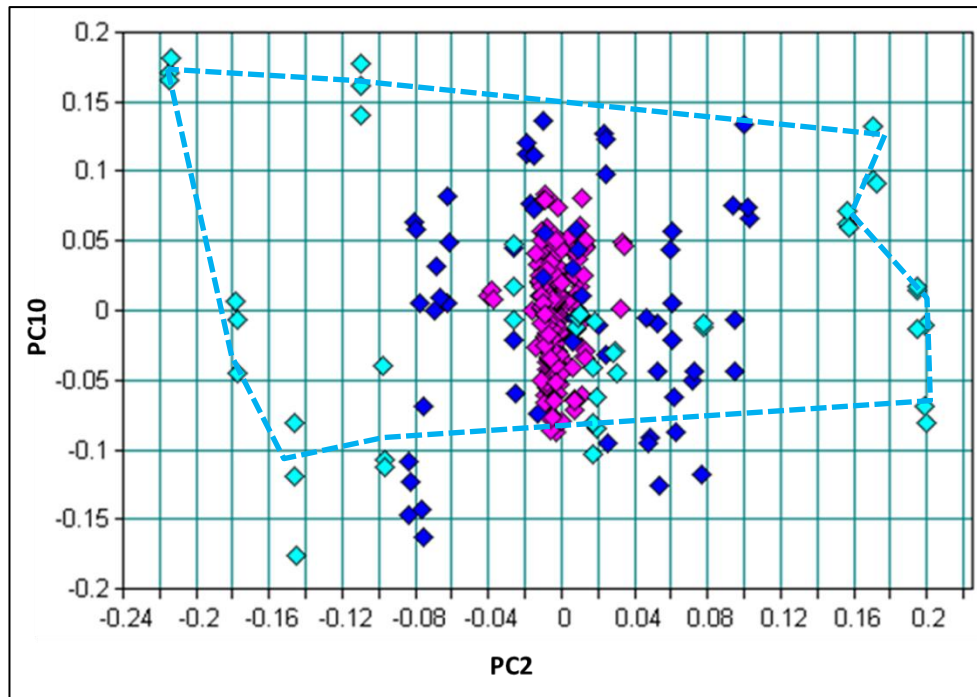


Figure 161 Scoresplot of PC2 versus PC10 after first derivative plus multiplicative scattering correction.

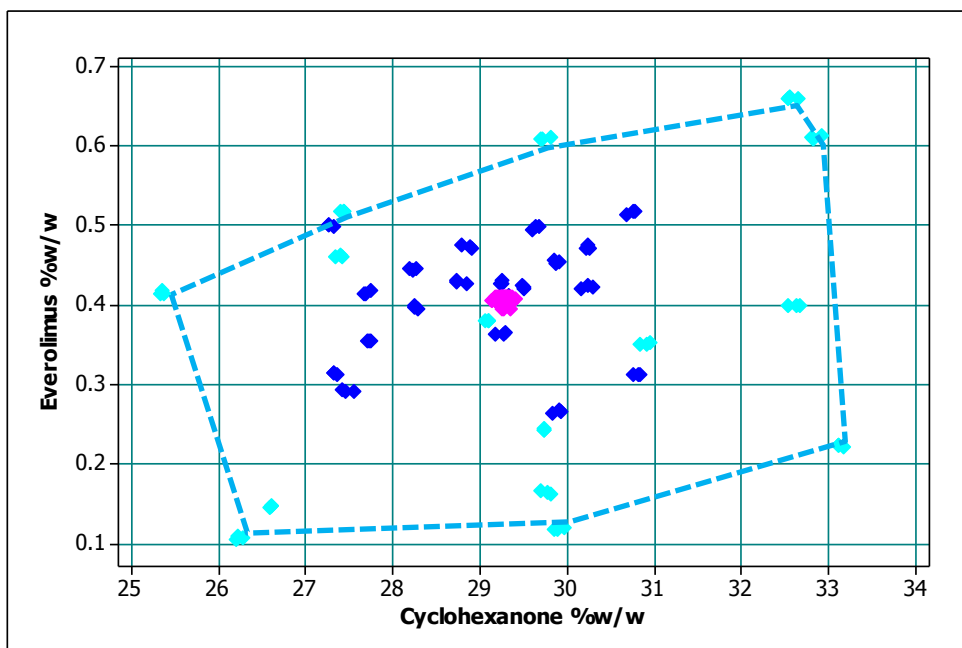


Figure 162 Scatterplot for the concentration of everolimus versus cyclohexanone in the everolimus coating solutions.

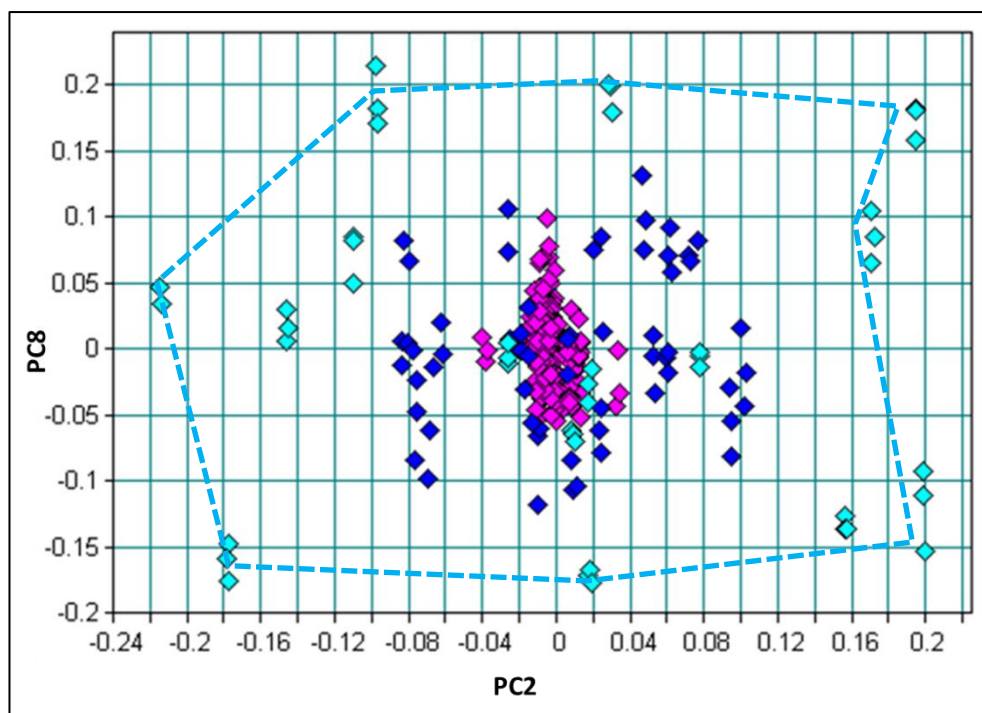


Figure 163 Scoresplot of PC2 versus PC8 after first derivative plus multiplicative scattering correction.

The coating solutions formulated in the laboratory intentionally have a wider concentration range than that of the production coating solutions, thereby facilitating the development of a calibration that incorporates the allowable concentration tolerance of the manufacturing process. This approach also enables the measurement of samples with component concentrations outside of the tolerance so that a reliable measurement of the deviation from the target concentration can be achieved in batches that fail to meet the concentration specification. PCA analysis demonstrates that the laboratory solutions are of a similar, overlapping population as the production samples, therefore it is appropriate to include both in the calibration models.

PCA assessment of the spectra indicates that contribution to spectral variation from each component of the solutions can be determined using multivariate analysis. Spectral pre-treatment methods can be used to reduce the number of PCs required and correct for differences in sample vials. However the high ranking PCs for everolimus and PVDF-HFP indicate that additional optimisation may be required to avoid over-fitting, such as selection of smaller frequency ranges. The reason for the everolimus and PVDF-HFP variation not being explained until the 5th, 8th and 10th PC are not apparent from PCA. Given that the first 2 PC's are taken up with water and solvent concentration, the remaining PC's account for other sources of spectral variation. Further optimisation

was carried out whilst using PLS to construct the calibration models, as shown in the next section of the thesis.

5.1.3.4 Final everolimus coating solution NIR methods.

Using 104 unique solutions (69 process solutions, and 35 laboratory solutions) a leave-one-out cross-validation was performed to assess different NIR methods, each NIR method having a different combination of pre-treatment and frequencies selected. First derivative spectral pre-treatments gave the best results for NIR optimisation, particularly in combination with scatter correction techniques such as straight line subtraction (SLS), multiplicative scatter correction (MSC) and vector normalization (VN). The pre-treatment method selection process was done through an iterative approach of applying the pre-treatment to the spectra, then carrying out PLS model development, followed by evaluation of the model.

Selection of the optimum number of PLS factors was decided, primarily upon choosing the model with the lowest RMSE values before the decrease in RMSE was negligible. PCA of the calibration spectra indicated that more PLS factors may be required than was the case for the lab-only feasibility study, it is thought that this is on account of incorporation of a larger set of spectra with variation from two manufacturing facilities, variation in sampling and measurement (e.g. the sample vial type), and the use of several different batches of solution components. Figure 164 shows plots of RMSE versus the number of PLS factors for each of the 4 coating solution components. The RMSE values were also assessed based on achieving $\leq 2\%$ error for each component as outlined in Table 18. Because a sufficiently large number of unique solutions were selected as a test set to calculate RMSEP ($n = 34$), then the RMSECV and RMSEP were given equal weight when choosing the optimum number of PLS latent variables. Test set validation was carried out by using spectra from 66% of the unique solutions randomly selected to construct the calibration, and using the remaining 34% of spectra as the test set.

Chapter 5

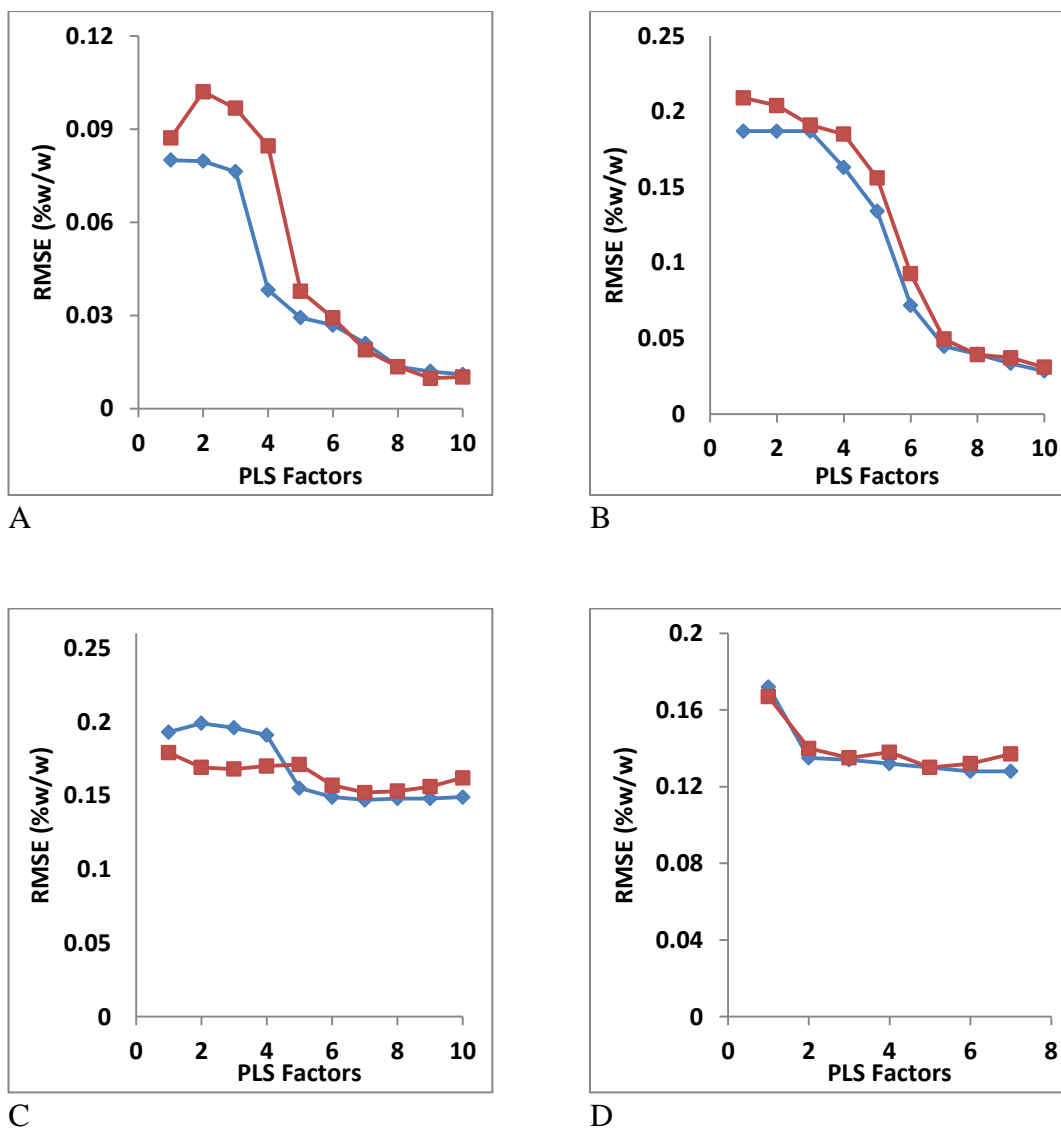


Figure 164 PLS factors (latent variables) versus RMSECV (blue) and RMSEP (red) for the calibration model of A - everolimus, B- PVDF-HFP, C – acetone, and D - cyclohexanone

It was concluded that no more than 8 PLS factors should be used for everolimus, no more than 7 PLS factors for PVDF-HFP concentration, no more than 3 PLS factors for cyclohexanone concentration, and no more than 2 for acetone concentration. The results of the cross-validation for some of the pre-treatments and frequency region selections are shown in Table 23 for everolimus, Table 24 for PVDF-HFP, Table 25 for acetone, and Table 26 for cyclohexanone.

Chapter 5

Table 23. Results of cross-validation for everolimus concentration using 104 unique solutions. The optimum model is shown in bold font.

Pre treatment	Frequency ranges (cm ⁻¹) ¹⁾	PLS factors	RMSECV %w/w	RMSEP %w/w	R ²
1 st deriv.	7502 – 6098 & 5450 - 4598	8	0.0165	0.0285	95.63
1 st deriv. + SLS	9115 - 6098	8	0.0142	0.0166	96.77
1st deriv. + VN	7502 - 6098	8	0.0135	0.0135	97.07
1 st deriv. + MSC	7502 - 6098	8	0.0160	0.0185	95.87

Table 24. Results of cross-validation for PVDF-HFP concentration using 104 unique solutions. The optimum model is shown in bold font.

Pre treatment	Frequency ranges (cm ⁻¹) ¹⁾	PLS factors	RMSECV %w/w	RMSEP %w/w	R ²
1st deriv. + MSC	6102 - 4599	7	0.0455	0.0501	93.7
1st deriv. + MSC	9115 – 8304 & 6102 - 4599	7	0.0448	0.0495	93.89
1st deriv. + VN	9115 – 7498	7	0.0538	0.0718	91.17

Table 25. Results of cross-validation for acetone concentration using 104 unique solutions. The optimum model is shown in bold font.

Pre treatment	Frequency ranges (cm ⁻¹)	PLS factors	RMSECV %w/w	RMSEP %w/w	R ²
1st deriv.	7502 – 5446	2	0.206	0.232	96.79
1st deriv. + MSC	9115- 4599	2	0.197	0.230	97.06
1st deriv. + MSC	7502 – 5446	1	0.193	0.211	97.19

Table 26. Results of cross-validation for cyclohexanone concentration using 104 unique solutions. The optimum model is shown in bold font.

Pre treatment	Frequency ranges (cm ⁻¹)	PLS factors	RMSECV %w/w	RMSEP %w/w	R ²
1st deriv. + VN	7502– 6800	2	0.137	0.143	98.39
1 st deriv. + MSC	6102 - 5446	3	0.133	0.14	98.50
1st deriv. + MSC	6102 - 5446	2	0.135	0.135	98.43

Chapter 5

The optimum PLS model for each component is further described as follows:

Everolimus - concentration range 0.1061 - 0.661% w/w. The combination of first derivative and MSC was chosen for pre-treatment in the frequency region 7,502.1 to 6,098.1 cm^{-1} displayed in Figure 165 (A). Figure 165 (B) shows the calibration curve for the model which exhibits close correlation between predicted and theoretical everolimus concentration.

The PLS regression vector in Figure 165 (C) shows the wavenumbers at which relevant information for everolimus absorbance can be found. Dominant features in the PLS regression vector can be attributed to everolimus content in the coating solution by comparing it to Figure 130. Spectral features in the 8 PLS loading vectors shown in Figure 165 (D) were used to provide evidence that the model is specific for everolimus concentration. The PLS loading vectors can be used to determine if too much noise is being fitted. The loading vectors 6, 7, and 8 of the loading vectors look slightly jagged which may indicate that some noise is being fitted.

Similarly the PLS models for PVDF-HFP (1.553 – 2.493% w/w), acetone (64.00 – 72.64% w/w), and cyclohexanone (25.35 – 33.16% w/w) are described in Figure 166, Figure 167, and Figure 168, respectively. All of the models provide close correlation between predicted and theoretical component concentration.

For PVDF-HFP calibration models, it was observed that they suffered less from the interference of water absorption bands and are more stable in general. The stability of the models is likely a consequence of higher concentration, 2% w/w for PVDF-HFP compared to 0.41% w/w for everolimus, as well as the lack of functional groups that share absorption bands with water.

Chapter 5

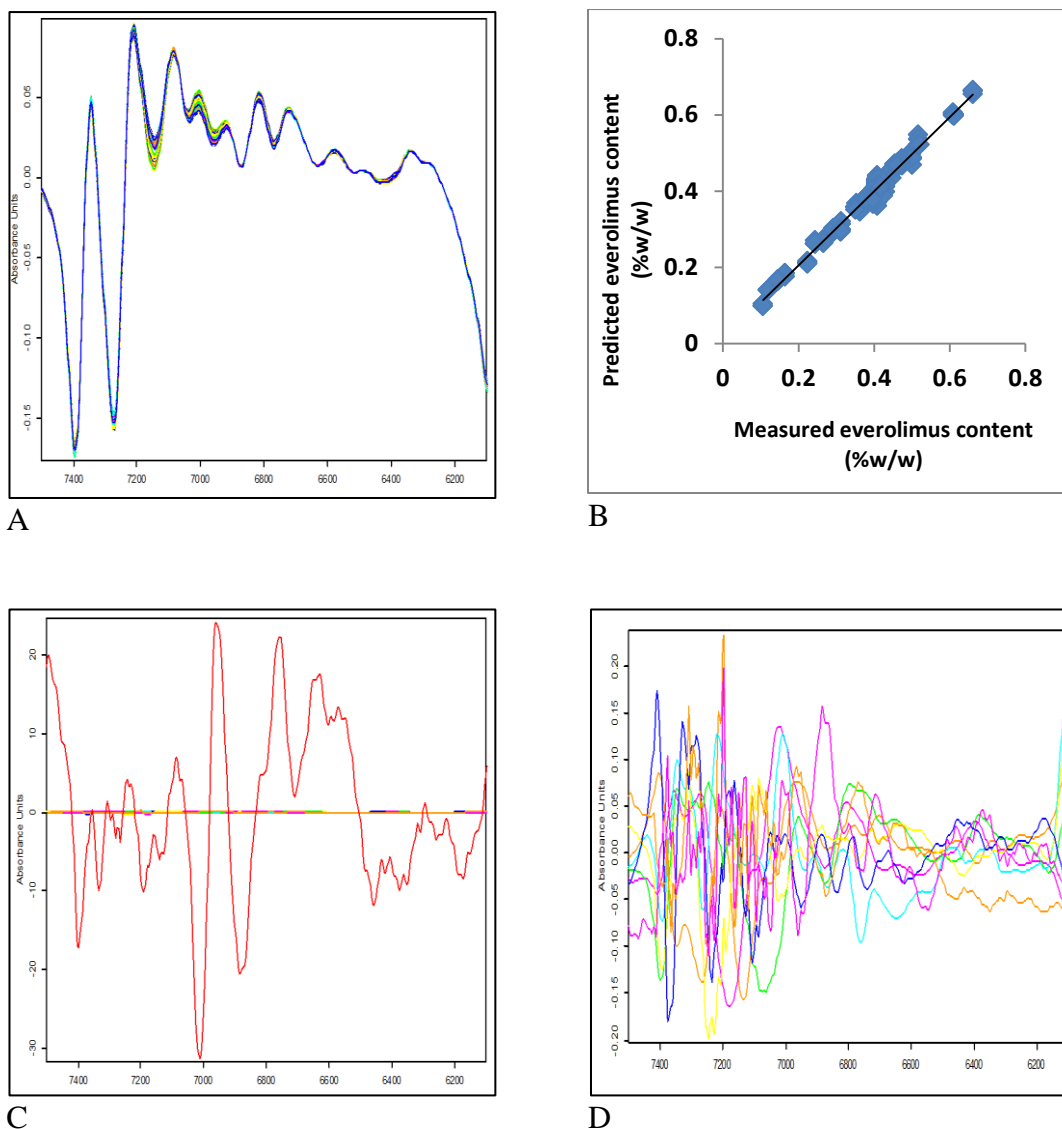


Figure 165. (A) Calibration spectra showing the 7,502 to 6,098 cm^{-1} region used in the calibration model for everolimus following first derivative + VN pre-treatment. (B) Calibration plot of actual versus predicted everolimus concentration from the laboratory only based calibration data set. (C) Everolimus concentration calibration regression coefficient vector, the first PLS loading weight vector. (D) PLS factor loadings for everolimus concentration (pink#1 = factor 1, orange#1 = factor 2, dark blue = factor 3, yellow = factor 4, light blue = factor 5, green = factor 6, pink#2 = factor 7, and orange #2 = factor 8).

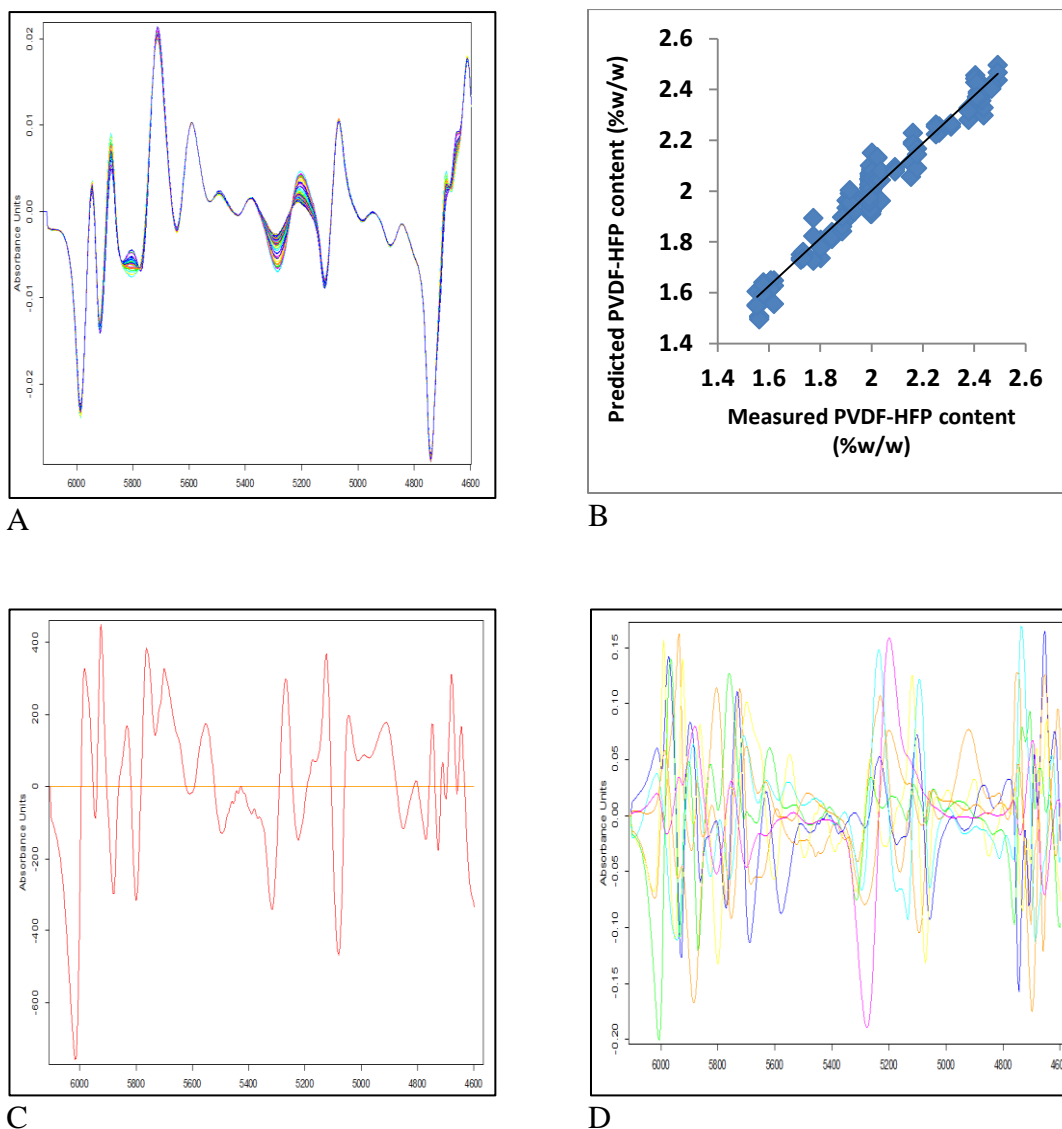


Figure 166. (A) Calibration spectra showing the 6,102 to 4,598 cm^{-1} region used in the calibration model for PVDF-HFP following first derivative + MSC pre-treatment (the other region used, 9,115 to 8,305 cm^{-1} is not shown). (B) Calibration plot of actual versus predicted PVDF-HFP concentration from the laboratory only based calibration data set. (C) PVDF-HFP concentration calibration regression coefficient vector, the first PLS loading weight vector. (D) PLS factor loadings for PVDF-HFP concentration (orange#1 = factor 1, pink = factor 2, green = factor 3, light blue = factor 4, yellow = factor 5, dark blue = factor 6, and orange #2 = factor 7).

Chapter 5

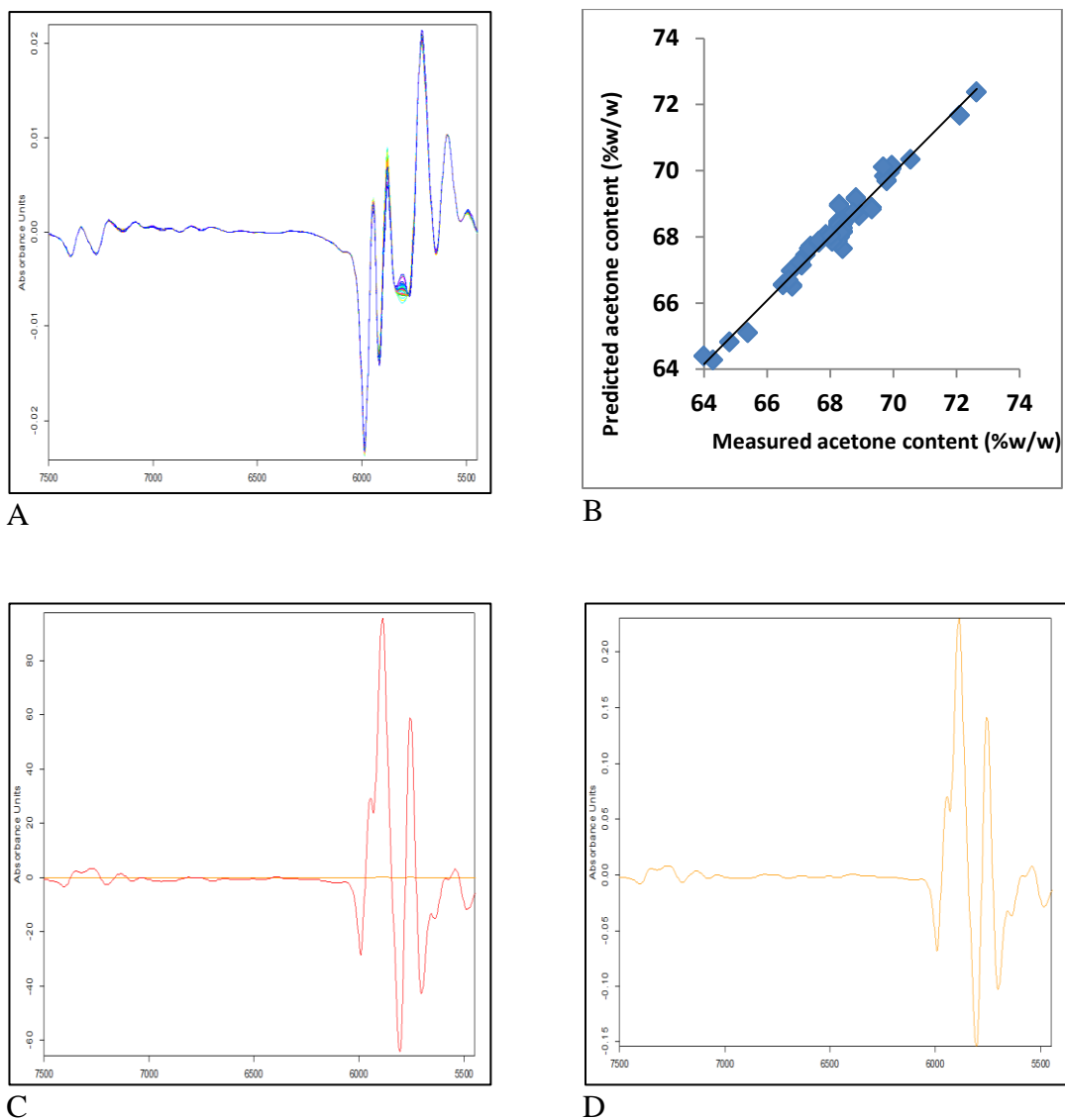


Figure 167. (A) Calibration spectra showing the 7,502- 5,446 cm^{-1} region used in the calibration model for acetone following first derivative + MSC pre-treatment. (B) Calibration plot of actual versus predicted acetone concentration from the laboratory only based calibration data set. (C) Acetone concentration calibration regression coefficient vector, the first PLS loading weight vector. (D) PLS factor loading for acetone concentration.

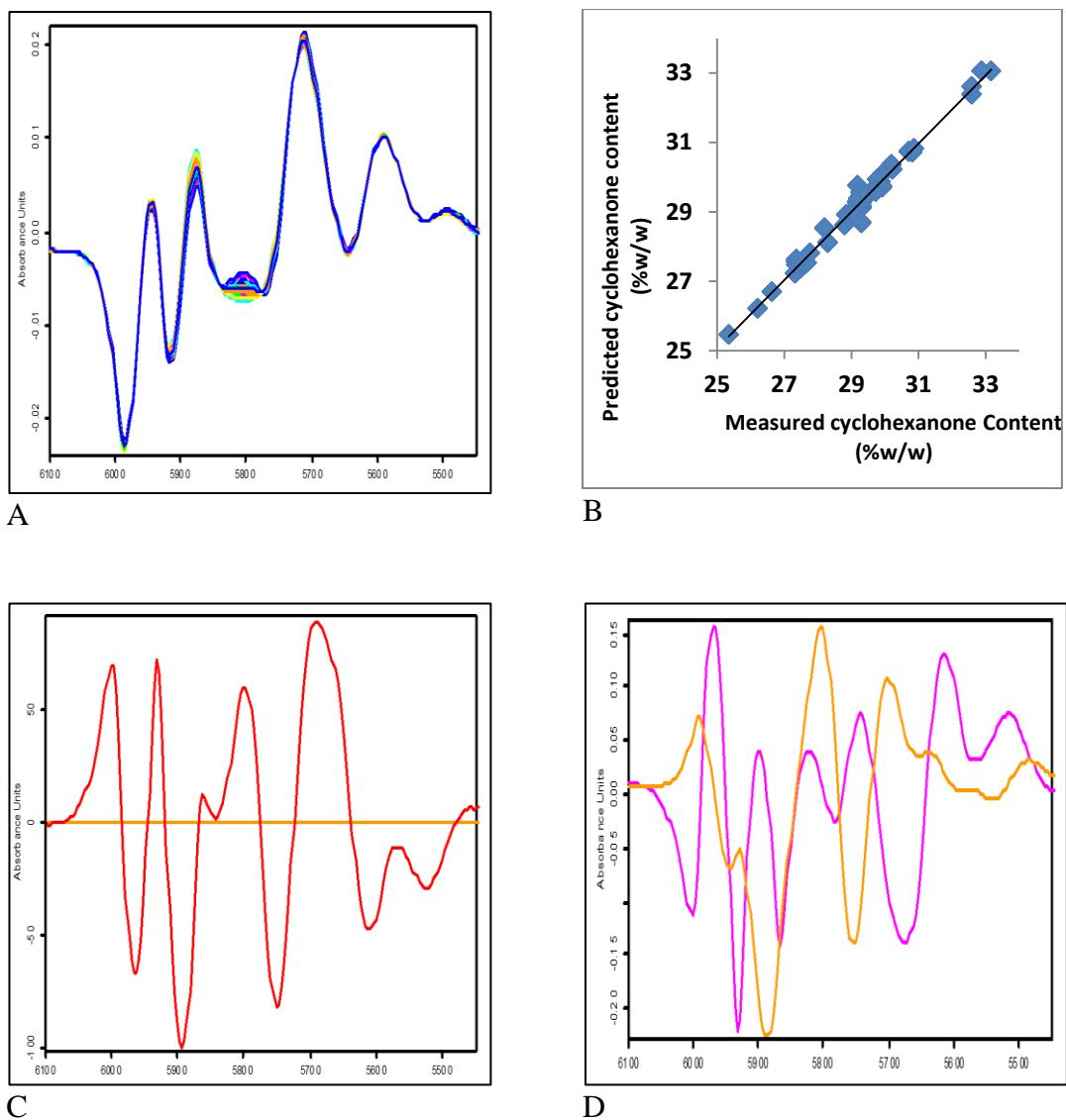


Figure 168. (A) Calibration spectra showing the 6,102 – 5,446 cm^{-1} region used in the calibration model for cyclohexanone following first derivative and MSC pre-treatment. (B) Calibration plot of actual versus predicted cyclohexanone concentration from the laboratory only based calibration data set. (C) Cyclohexanone concentration calibration regression coefficient vector, the first PLS loading weight vector. (D) PLS factor loadings for cyclohexanone concentration (orange = factor 1, and pink = factor 2)

5.1.3.5 Water content analysis

The presence of water, in addition to contributing to interference to the calibration model, can be viewed as potential process interference. Water acts as an anti-solvent for the drugs and polymers used in both coating solutions, and in particular paclitaxel is almost completely water insoluble and readily forms paclitaxel dihydrate crystals in the presence of water [121]. It was observed in formulation studies that paclitaxel crystals form in coating solutions when water levels are in excess of 3,000 ppm [Internal study at Boston Scientific]. As a result, water at excess levels can lead to clogging of applicators by precipitated solid components of the coating solutions, or result in below target levels of drug being applied to the stents. In order to make trending of the level of water in the coating solutions possible, a NIR calibration was created for the everolimus coating solutions using the 5 component data set listed in Table 10, Chapter 2, plus additional process solutions. The 5 components are everolimus, PVDF-HFP, acetone, cyclohexanone and water. The reference method used in this case was KF titration. The optimum calibration model developed for water is described in Figure 169, the model was validated using cross-validation after the spectra went through a 2nd derivative pre-treatment. The calibration set consisted of a mix of laboratory and process solutions with a range of water content from 0.18 to 0.40% w/v. Pre-treated spectra are shown in Figure 169, and the calibration plot is given in Figure 170.

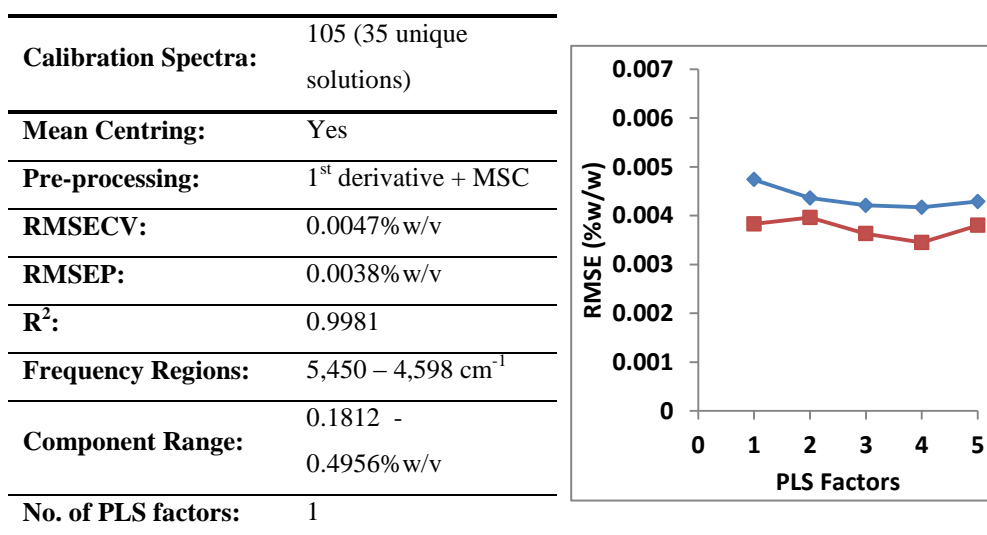


Figure 169. Summary of the calibration model for water.

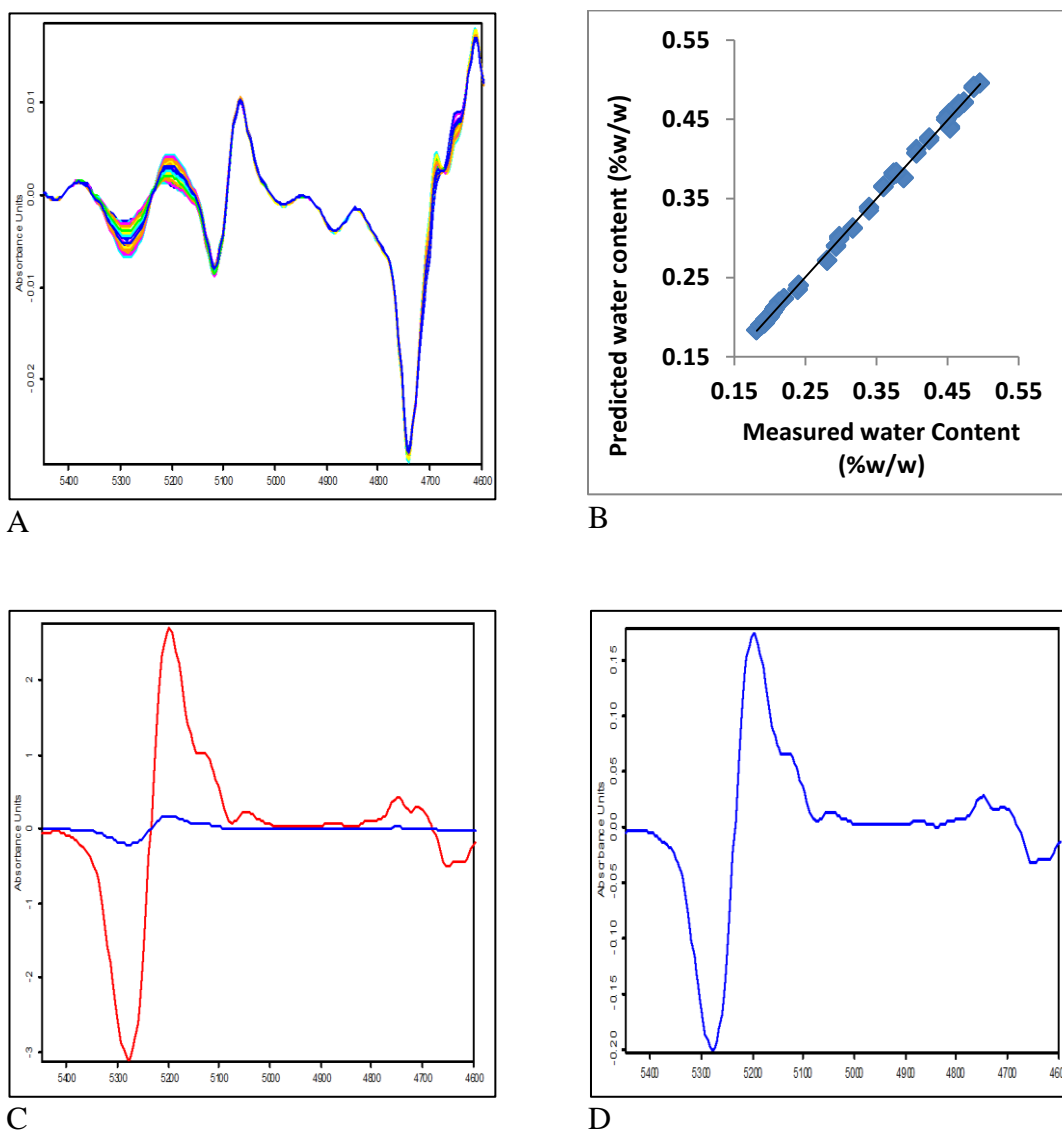


Figure 170. (A) Calibration spectra showing the 5,450 – 4,598 cm⁻¹ region used in the calibration model for water following first derivative and MSC pre-treatment. (B) Calibration plot of actual versus predicted water concentration from the laboratory only based calibration data set. (C) Water concentration calibration regression coefficient vector, the first PLS loading weight vector. (D) PLS factor loading factor 1 for water concentration.

Chapter 5

5.1.3.6 The application of methods developed to the commercial everolimus eluting stent manufacturing process.

Following the development of the NIR methods described, these methods were applied to the measurement of coating solutions from the commercial process for a period of 18 months, with random batches selected for analysis. These data were compared to the alternative off-line methods of HPLC and gravimetry for everolimus and PVDF-HFP, respectively. The accuracy of the NIR method compared favourably to HPLC for 167 unique batches of coating solutions tested over this period. The mean everolimus and PVDF-HFP concentration were 0.404% w/w and 2.02% w/w by NIR compared to 0.413% w/w and 2.00 % w/w by HPLC and gravimetry, respectively. The corresponding gravimetric inputs to the coating solution formulations had a mean of 0.407% w/w and 2.00% w/w for everolimus and PVDF-HFP, respectively. However the precision of the NIR method for everolimus did not match that of HPLC, with standard error of the mean (SE) of 0.0021% w/w compared to 0.0004% w/w, respectively. The opposite is the case for PVDF-HFP with the NIR method having better precision, SE of the NIR method was 0.002% w/w compared with 0.004% w/w for the gravimetry method. This is unsurprising as the final NIR method selected for everolimus has a RMSE = 0.0135%, considering that the target concentration of everolimus is 0.407% w/w the NIR method would struggle to match the precision of HPLC methods at that concentration level.

The mean concentration and SE of acetone and cyclohexanone by NIR were 68.3% w/w (SE = 0.01% w/w) and 29.25 w/w (SE = 0.015 w/w), these match the gravimetric inputs very closely thus confirming that NIR is suitable for continuous monitoring of these two solution components.

Final assessment of the NIR methods developed for the everolimus coating solutions have shown that NIR is capable of performing quantitative analysis of the four different components in the coating solutions, plus water. NIR provides a non-destructive, fast alternative to existing wet chemistry methods in DES formulation control. The relatively low concentration of everolimus means that the precision of the NIR method for everolimus does not equal that of the alternative HPLC method. As such, consideration must be given to the purpose of the in-process test. In this case a highly precise in-process method may not be necessary because the finished product has a final

Chapter 5

quality control check after a batch of stents is coated. The quality control analysis provides a HPLC assay of a number of stents from the finished product batch, and this ensures that the correct amount of drug has been applied and that the variation is within a specified range. Thus, the DES production process does not rely on a very precise measurement of everolimus in the formulation, however for long term process trending and confirmation of the use of the correct compounds in the everolimus DES formulations, the NIR methods described offer much to production staff. The fast feedback of results means that mistakes can be recognised quickly before they progress to more costly component scrap or reduction in finished product yield in the manufacturing process. Further, the additional information that can be provided through water content measurements, and other raw material or production environment factors that result in spectral variation, provides extra tools to recognise unplanned formulation changes that can impact product quality.

5.1.4 Paclitaxel coating solutions

As with the everolimus coating solution calibrations, the calibration models for paclitaxel coating solutions were built using the gravimetric data. The gravimetric data was collected when the individual components were weighed out during formulation (% w/w). These input data were verified using gel permeation chromatography (GPC). The coefficient of variation of the GPC method is 0.8% and 2.4% for paclitaxel and PLA respectively. Plots comparing the gravimetric inputs to the reference method are shown in Figure 171 and Figure 172 for paclitaxel and PLA, respectively. For paclitaxel comparisons there is good agreement between the reference method and the gravimetric formulation inputs. However the accuracy of the GPC method is impacted by the molecular weight of the PLA, as Figure 172 clearly shows an underestimation of the quantity of PLA measured when 2 batches of lower molecular weight polymer are used in the formulation. Incidentally, these two batches of polymer were acceptable for use on the DES as their use did not impact upon the desired performance criteria for the coated stents. Similar to the everolimus case described previously, it was decided to use

Chapter 5

the gravimetric measurements as reference data for the NIR calibrations as these measurements have equivalent or better accuracy and precision than the GPC method***.

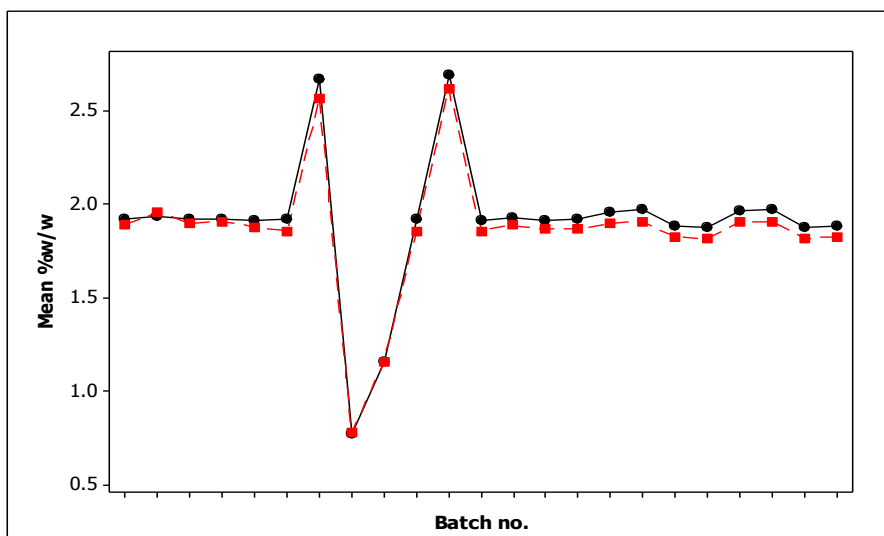


Figure 171 Plot comparing the gravimetric inputs(in black) to the reference GPC method (in red) for paclitaxel.

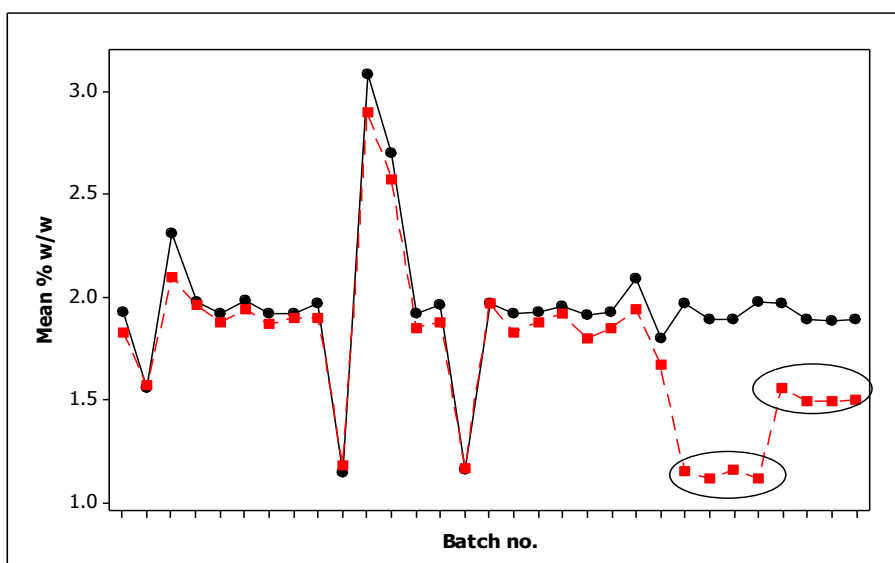


Figure 172 Plot comparing the gravimetric inputs (in black) to the reference GPC method (in red) for PLA. Batches of coating solution formulated with lower molecular weight PLA are circled.

*** The coefficient of variation for the GPC method for paclitaxel is $\leq 2.0\%$ and for PLGA it is $\leq 5.0\%$. The precision of the method is $\leq 1.0\%$ for both analytes. The accuracy of the method is $100 \pm 2\%$ for paclitaxel and $100 \pm 5\%$ for PLGA in the range $1.76\% \text{ w/v} \pm 20\%$ for both compounds.

Chapter 5

5.1.4.1 Paclitaxel coating solution NIR method development

Calibration models for the components of the paclitaxel coating solutions were developed after the everolimus coating solution NIR methods, thus inclusion of water content as a factor from the outset was implemented to avoid the same issues with model instability. The everolimus coating solutions were analysed using 7mm borosilicate glass vials in the transmission cell of the NIR spectrophotometer. Aliquots of the coating solution are removed from 2 - 4 L reservoirs of solution and placed in the measurement vials. However, for the paclitaxel coating process solution reservoirs are much smaller, consisting of about 100mL of coating solution which are subdivided into 15mL quantities which are used in the coating applicators. The 15mL quantity is placed in a clear borosilicate-glass bottle, 18 mm in diameter, with a crimped cap. The cap has a septum which is perforated to insert a tube through which the coating solution is removed to the applicator. The NIRS method described in section 5.1.4 was developed by using the same 18mm glass vials in a custom made holder for the transmission cell of an NIR spectrophotometer. As a result, the coating solution can be analysed at-line without removing it from the coating vial. This at-line analysis ensures that the same solution used to coat the stent is measured using NIR instead of an approach based on aliquot sampling typical for most laboratory tests.

The frequency regions between $9,200 - 6,250 \text{ cm}^{-1}$ and $5,600 - 4,800 \text{ cm}^{-1}$ were assessed for the calibration model development. The overlaid calibration spectra in Figure 173 show that selection of these spectral regions removes areas of total absorbance. Principal component analysis (PCA) was performed to get an overview of the acquired spectra to look for outliers and to identify suitable spectra for the calibration set. PCs were calculated without any spectral pre-processing apart from mean centering in the range $9,200 - 6,250 \text{ cm}^{-1}$ and $5,600 - 4,800 \text{ cm}^{-1}$. A mixture of laboratory solutions ($n = 25$) and process solutions ($n = 5$) were used, details of which are provided in Table 12, Chapter 2.

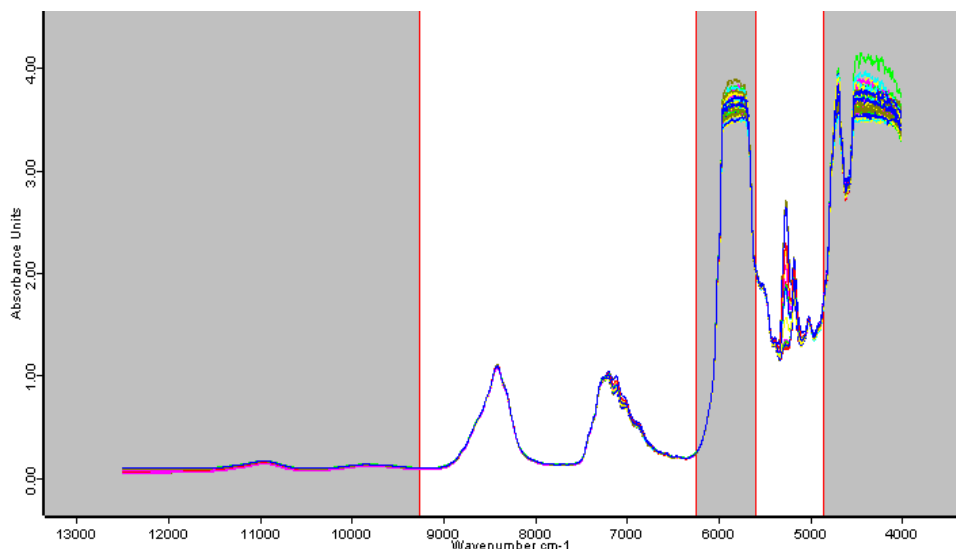


Figure 173 Overlaid calibration spectra for paclitaxel coating solutions. The frequency regions between 9200 – 6250 and 5600 – 4800 cm^{-1} were assessed for the calibration model development.

It is apparent that PC1 and PC2 correspond to the spectral features that explain the concentration of water and paclitaxel when their score plot, Figure 174 is compared to a scatterplot of the concentration of paclitaxel versus water in Figure 175. The scores plots showing PC2 versus PC3, and PC3 versus PC4 are shown in Figure 176 and Figure 177, respectively. Spectral pre-treatment methods were not used for the PCA, as any investigated did not change the scores plots significantly. Spectral pre-treatments and frequency range reduction were carried out whilst using PLS to construct the calibration models. The coating solutions formulated in the laboratory have a wider concentration range than that of the production coating solutions; this is visible from the wider spread in the coordinate points from the lab solutions in the scores plots. PCA analysis demonstrates that the laboratory solutions are of the same population as the production samples, therefore it is appropriate to include both in the calibration models.

The construction of the calibration models for paclitaxel coating solutions followed a similar approach to that of the everolimus coating solutions. Specific details of the final models selected and pre-processed spectra are shown in Table 27. The calibration models developed transpired to require fewer PLS factors than those for the everolimus coating solutions. The need for fewer PLS factors is likely a consequence of higher drug concentration, 1.92% w/w for paclitaxel compared to 0.41% w/w for everolimus, and fewer solution components e.g. one solvent instead of two.

Chapter 5

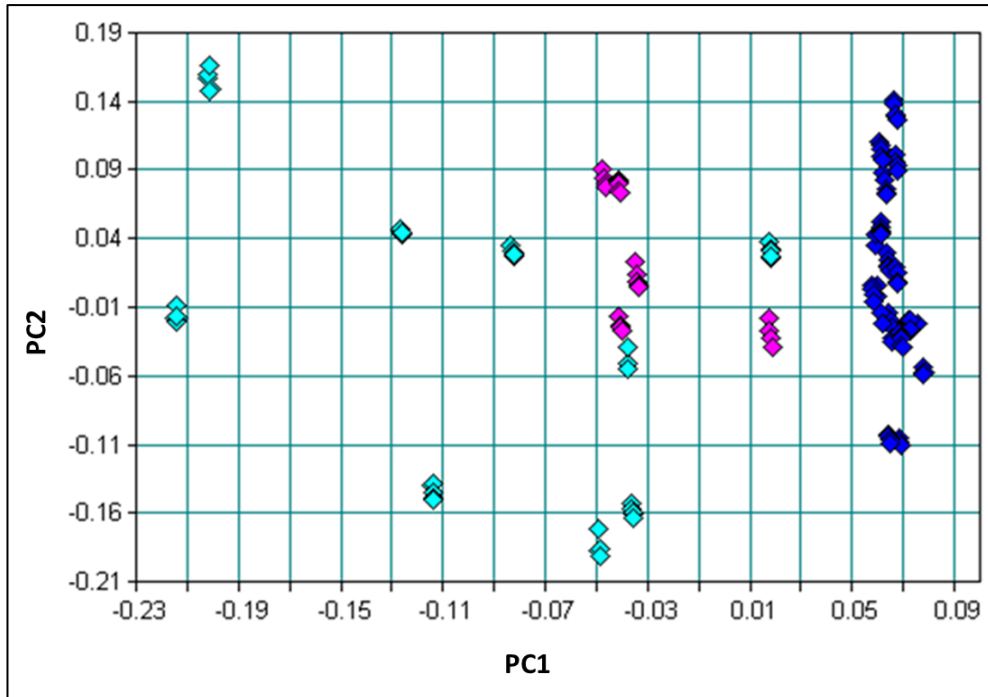


Figure 174 Scores plot for PC1 versus PC2.

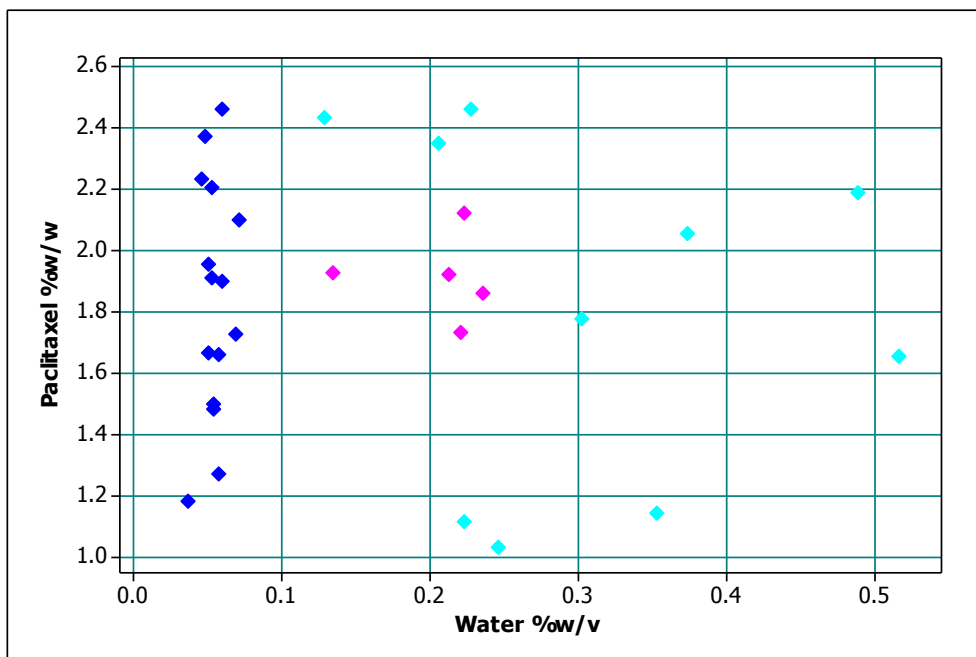


Figure 175 Scatterplot showing the concentration of water versus paclitaxel in the calibration set.

Chapter 5

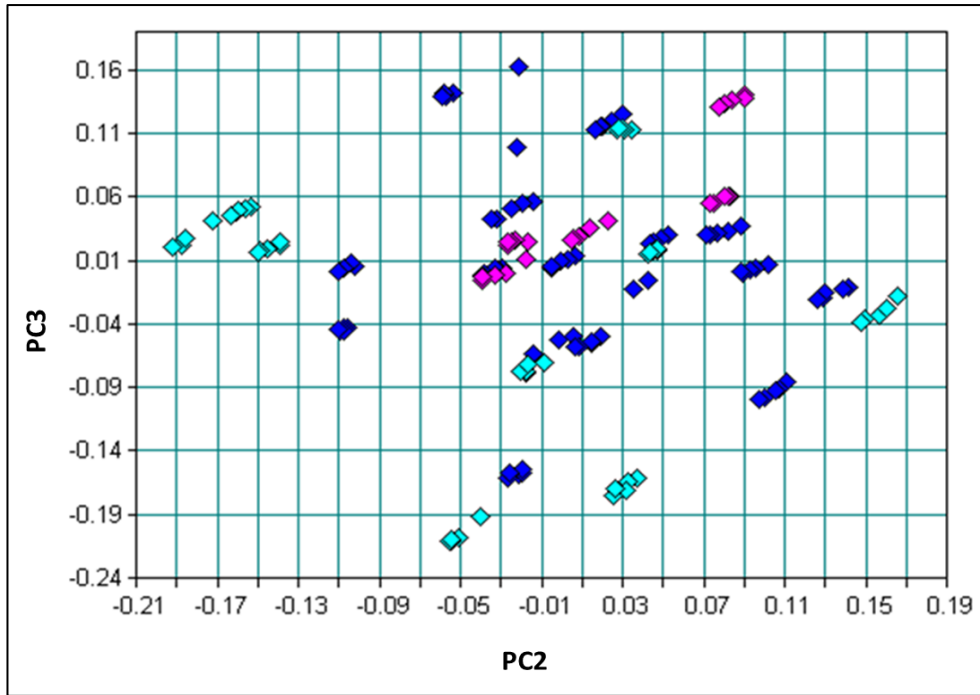


Figure 176 Scoresplot showing PC2 versus PC3.

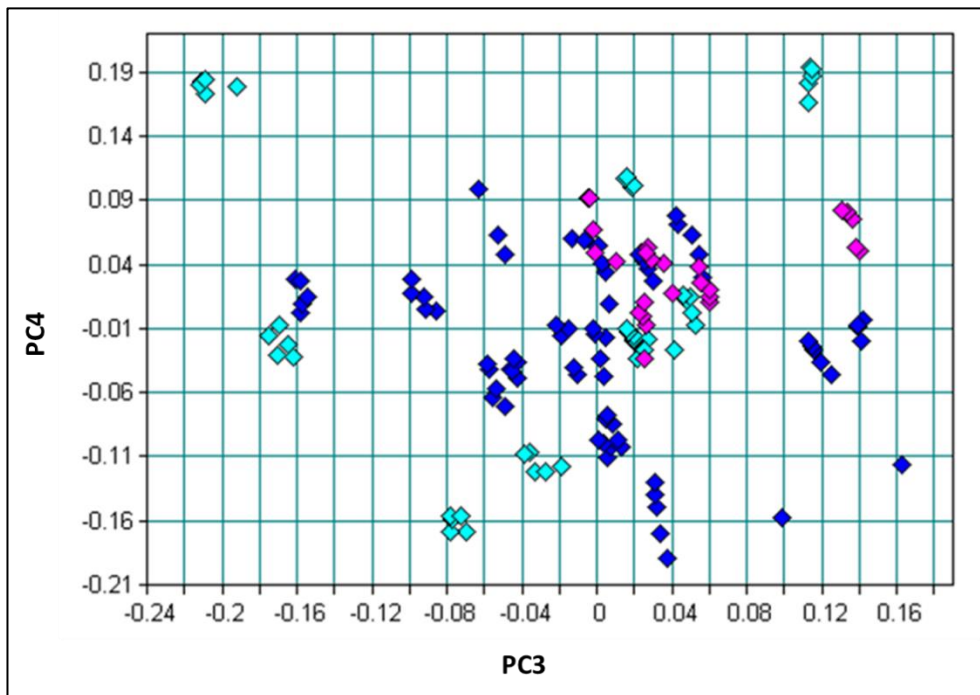


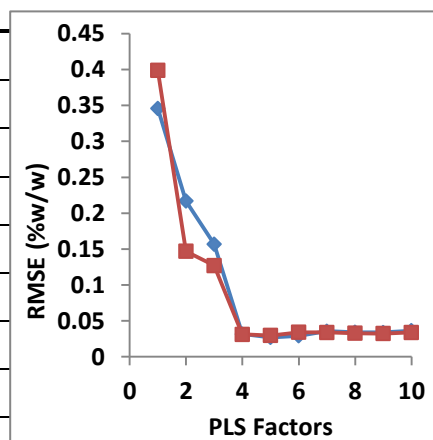
Figure 177 Scores plot showing PC3 versus PC4.

Chapter 5

Table 27. Calibration models developed for paclitaxel coating solutions

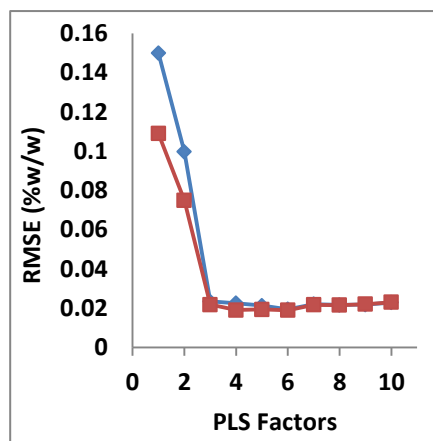
(a) Paclitaxel:

Calibration Spectra:	145 (29 solutions)
No. of PLS factors	4
Mean Centring:	Yes
Pre-processing:	Vector normalisation
RMSECV:	0.0318 %w/w
RMSEP:	0.0313 %w/w
R ² :	0.9940
Frequency Regions:	9,261 – 7,749 cm ⁻¹
Component Range:	1.033 - 2.464% w/w



(b) PLA:

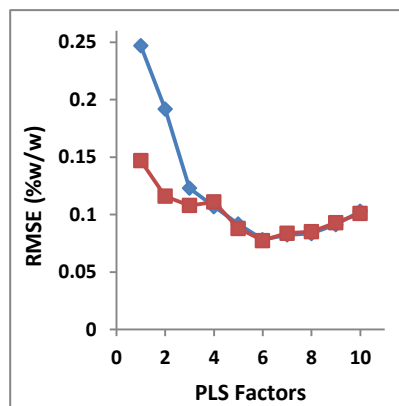
Calibration Spectra:	145 (29 solutions)
No. of PLS factors	3
Mean Centring:	Yes
Pre-processing:	1 st derive. + VN
RMSECV:	0.0234 %w/w
RMSEP:	0.0190%w/w
R ² :	0.9975
Frequency Regions:	9,261 – 7,749 cm ⁻¹
Component Range:	1.028 - 2.410% w/w



Chapter 5

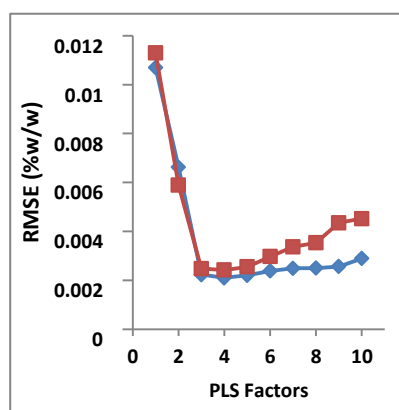
(a) N-butyl acetate:

Calibration Spectra:	145 (29 solutions)
No. of PLS factors	3
Mean Centring:	Yes
Pre-processing:	1 st derive. + MSC
RMSECV:	0.123 % w/w
RMSEP:	0.116 % w/w
R ² :	0.9755
Frequency Regions:	9,261 – 7,749 cm ⁻¹
Component Range:	94.84 - 97.78%w/w



(b) Water:

Calibration Spectra:	145 (29 solutions)
No. of PLS factors	3
Mean Centring:	Yes
Pre-processing:	Vector normalisation
RMSECV:	0.0022 % w/w
RMSEP:	0.0025 % w/w
R ² :	0.9940
Frequency Regions:	9,261 – 7,624 & 5,593 – 4,849 cm ⁻¹
Component Range:	0.0363 - 0.5161% w/w



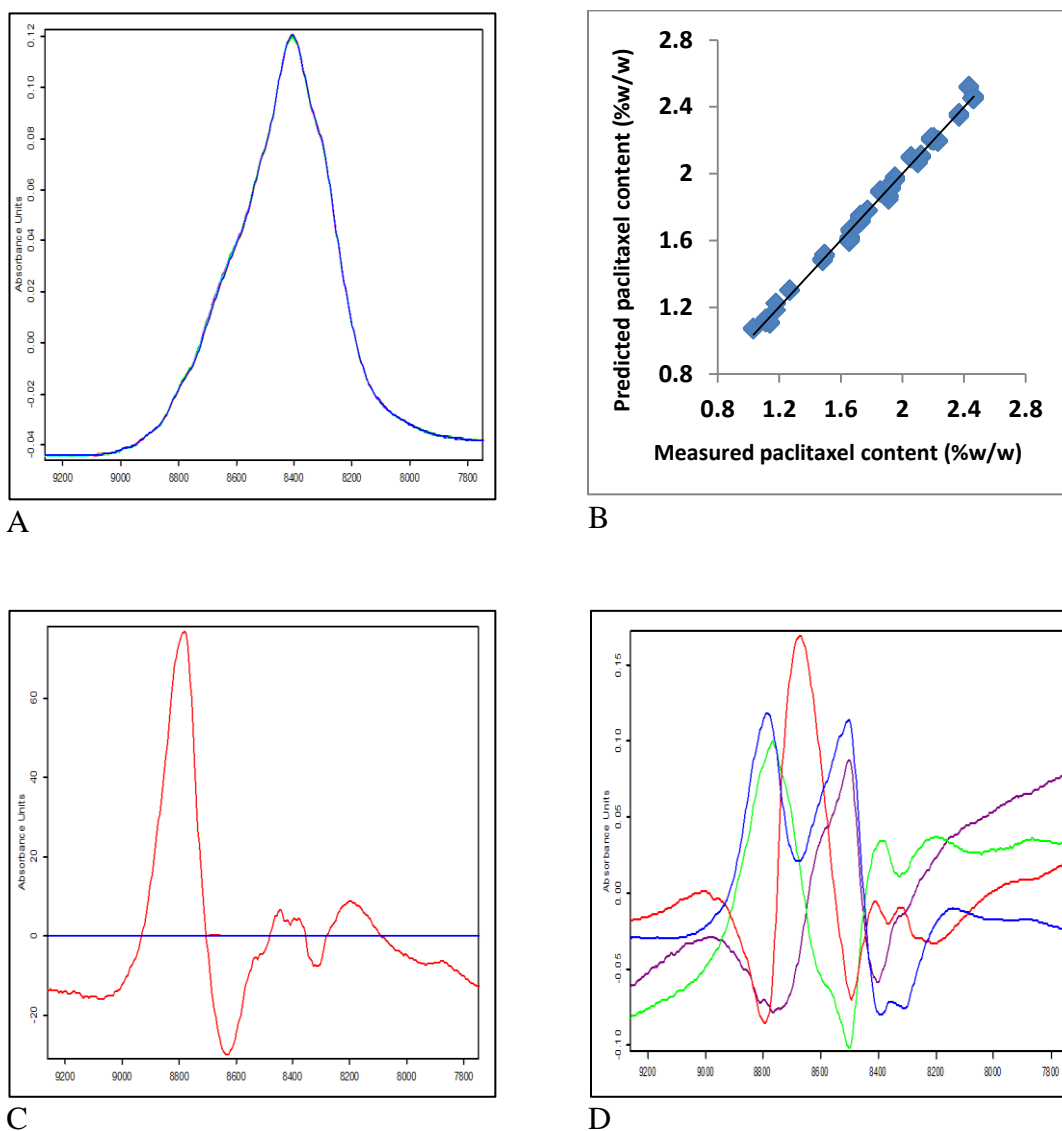


Figure 178. (A) Calibration spectra showing the 9,261 – 7,749 cm^{-1} region used in the calibration model for paclitaxel following first derivative and MSC pre-treatment. (B) Calibration plot of actual versus predicted paclitaxel concentration from the laboratory only based calibration data set. (C) Paclitaxel concentration calibration regression coefficient vector, the first PLS loading weight vector. (D) PLS factor loadings for paclitaxel concentration (Blue = Factor 1, Red = factor 2, green = factor 3, and purple = factor 4).

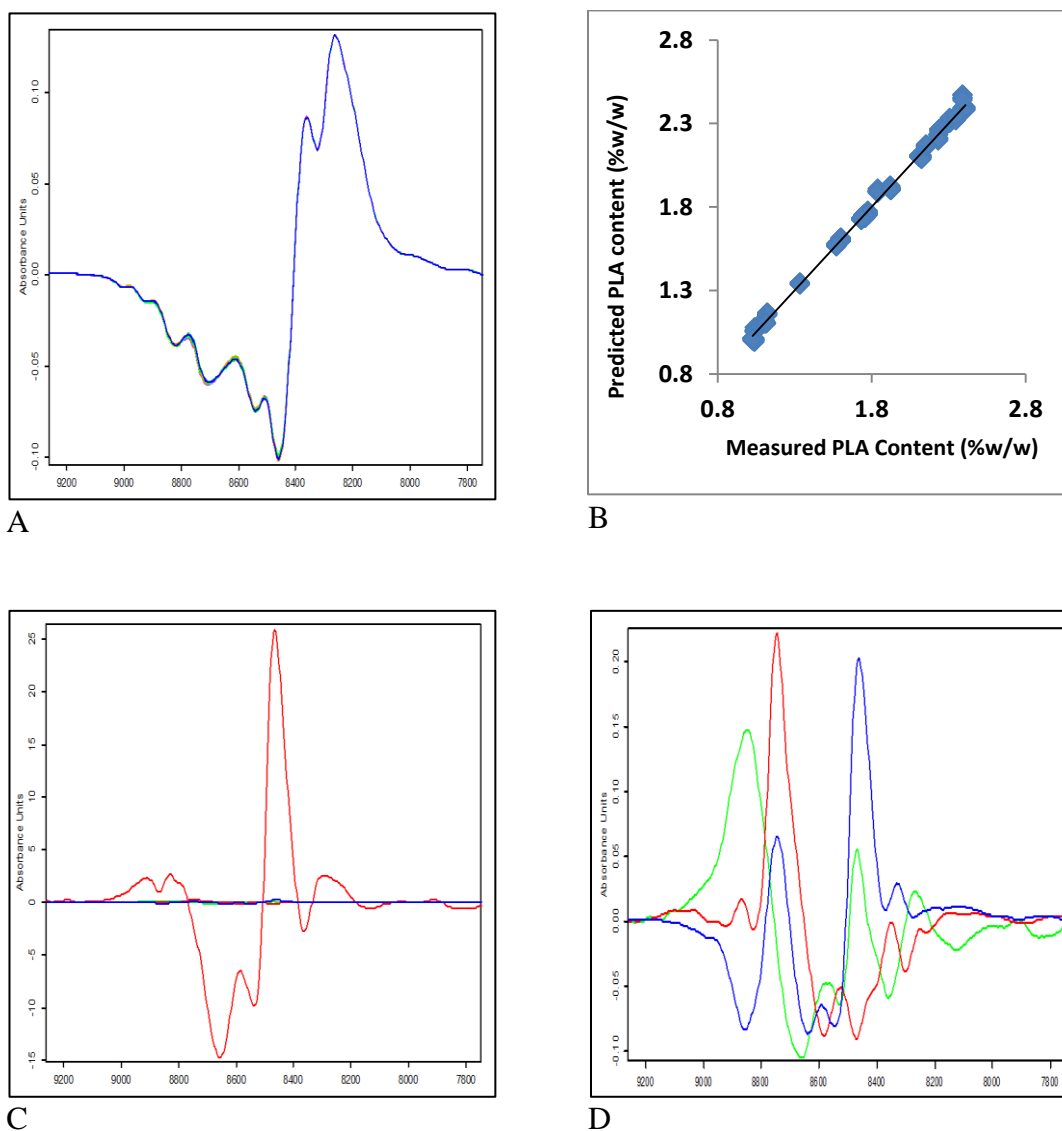


Figure 179. (A) Calibration spectra showing the 9,261 – 7,749 cm^{-1} region used in the calibration model for PLA following first derivative and MSC pre-treatment. (B) Calibration plot of actual versus predicted PLA concentration from the laboratory only based calibration data set. (C) PLA concentration calibration regression coefficient vector, the first PLS loading weight vector. (D) PLS factor loading factors for PLA concentration (blue = factor 1, red = factor 2, and green = factor 3).

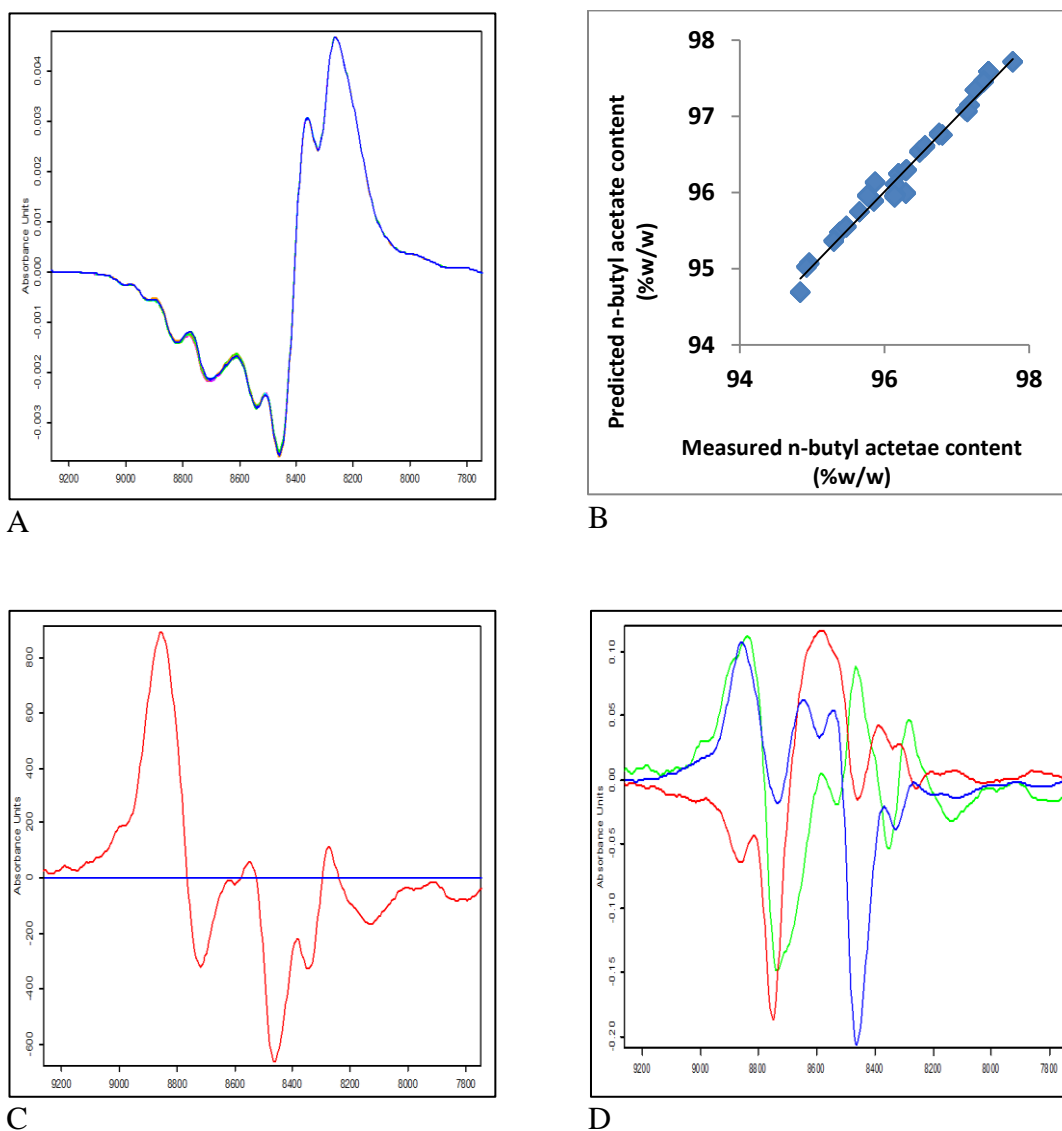


Figure 180. (A) Calibration spectra showing the 9,261 – 7,749 cm^{-1} region used in the calibration model for n-butyl acetate following first derivative and MSC pre-treatment. (B) Calibration plot of actual versus predicted n-butyl acetate concentration from the laboratory only based calibration data set. (C) N-butyl acetate concentration calibration regression coefficient vector, the first PLS loading weight vector. (D) PLS factor loading factors for n-butyl acetate concentration (blue = factor 1, red = factor 2, and green = factor 3).

Chapter 5

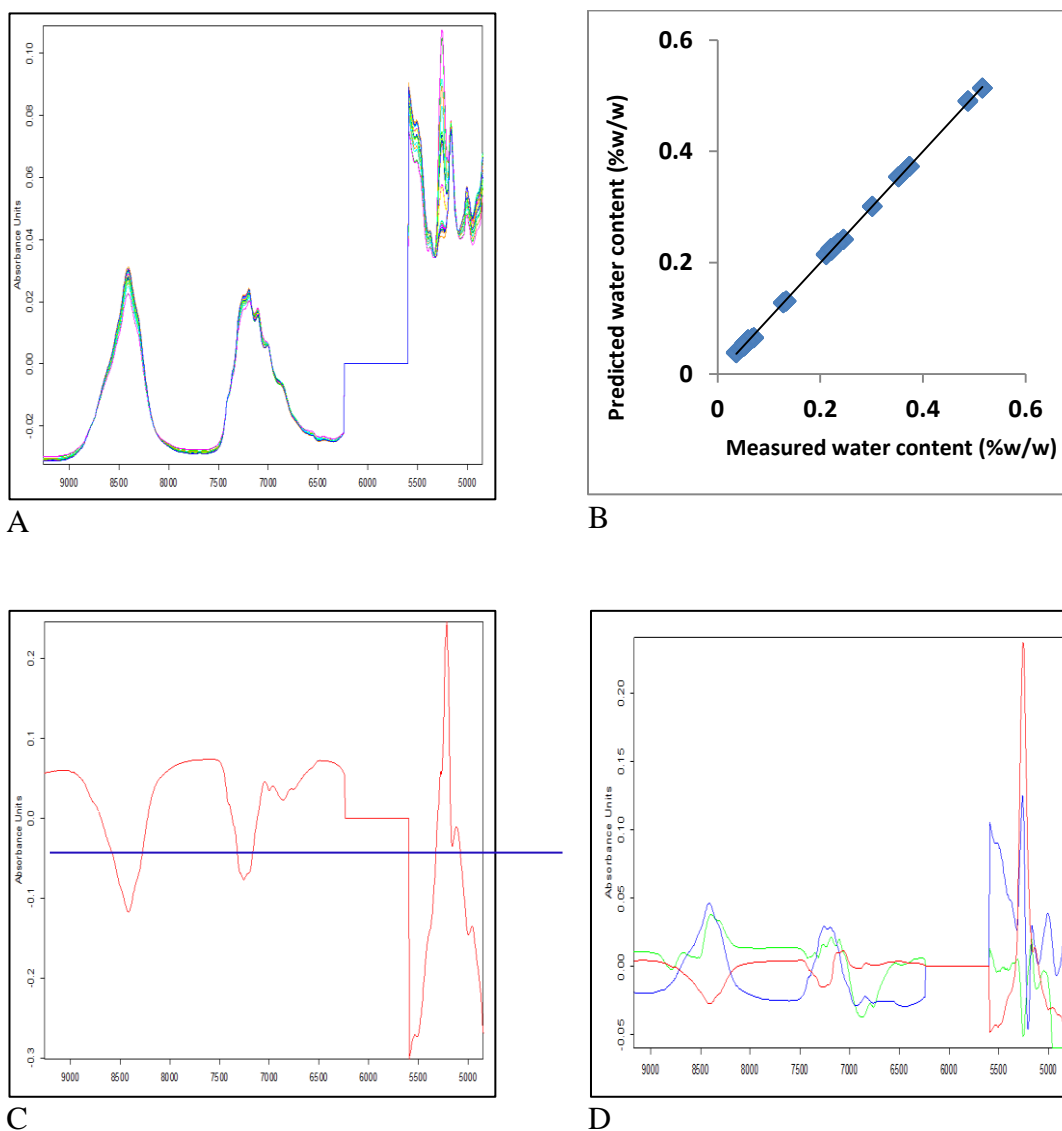


Figure 181. (A) Calibration spectra showing the 5,450 – 4,598 cm^{-1} region used in the calibration model for water following first derivative and MSC pre-treatment. (B) Calibration plot of actual versus predicted water concentration from the laboratory only based calibration data set. (C) Water concentration calibration regression coefficient vector, the first PLS loading weight vector. (D) PLS factor loading factor 1 for water concentration (red = factor 1, blue = factor 2, and green = factor 3).

Chapter 5

In contrast to the NIR method developed for measuring everolimus concentration in the everolimus coating solutions, the methods developed for paclitaxel coating solutions show that a more accurate measurement of components can be achieved at concentrations $> 0.5\%$ w/w. By way of demonstrating this, 12 unique batches of coating solution were collected from the manufacturing process and tested using NIR and GPC for paclitaxel and PLA concentration. The resultant mean \pm one standard error for the HPLC method was $1.879 \pm 0.003\%$ w/w and $1.858 \pm 0.005\%$ w/w for paclitaxel and PLA, respectively. The corresponding NIR measurements were $1.905 \pm 0.004\%$ w/w and $1.914 \pm 0.005\%$ w/w for paclitaxel and PLA, respectively. These results compare quite favourably, thus the added benefits that the NIR methods offer can be obtained whilst also achieving equivalent performance to the GPC method. The n-butyl acetate was measured at $96.12 \pm 0.01\%$ w/w, in close agreement with the gravimetric measurements. Furthermore, the water concentration was compared to the Karl Fischer titration method, with the methods in close agreement at $0.145 \pm 0.007\%$ w/w and $0.156 \pm 0.009\%$ w/w for KF and NIR, respectively.

5.2 Chapter conclusion

The aim of a PAT approach is to implement robust processes that are flexible enough to accommodate a defined level of variability in process materials through adjustment of the process conditions. A knowledge base created through the collection, analysis and evaluation of research, development and manufacturing data facilitates the design and implementation of a PAT system. The knowledge base also provides the justification for a science and risk based approach to analytical method and process monitoring and control. NIR is one tool that has the potential to be applied at the process to provide the real-time feedback to build this knowledge base.

In this chapter NIR transmission spectroscopy was used to determine the drug and polymer content in different DES coating solutions. The results show that NIR is an excellent analytical technique for rapid and convenient analysis of these types of samples. Key to this assessment is the statistical error of the calibration models developed and whether it is within acceptable levels for pharmaceutical assays. NIR is not generally used as a trace level technique to provide accurate quantitative analysis <

Chapter 5

0.5% w/w^{†††}, and indeed the NIR method developed for everolimus coating solution demonstrated that the measurement of everolimus at 0.41% w/w does not reach the same level of accuracy as the conventional HPLC assays typically used for this type of analysis in the pharmaceutical industry. There may be room for improving the accuracy of the everolimus measurement at these low levels which is outside the scope of the work carried out for this thesis. For example one thing to try would be increasing the pathlength of the sample cuvette to maximize the transmitted signal. For the polymer, solvent and water components of the coating solutions the performance of the NIR method equals the performance of the alternative wet chemistry methods. The assay of the paclitaxel coating solution demonstrated that the NIR method of measurement for the drug component at 2% w/w matches the accuracy of the established HPLC assay.

It has been demonstrated that calibration approaches that use samples prepared in the laboratory alone do not result in calibrations that provide accurate determinations. Samples from the manufacturing process are required for effective NIR calibration models. However, the role of laboratory samples in the early stages to prove the concept, and their role to extend and fill out the calibration range has demonstrated that a calibration approach including laboratory samples and manufacturing samples is both efficient and effective.

The critical importance of the vials used for collecting spectra was discovered, and sufficient controls are required to ensure that the same vial type is used for building the calibration and for subsequent sample analysis. Even though the two batches of sample-vials used for the everolimus coating solution method were sourced from the same supplier and had the same part number, it was an important lesson to learn that this does not guarantee that the vials are equivalent. Two options should be considered to account for variation in the sample vials. The first option is to ensure that vials from the same batch are used exclusively for the calibration set and all subsequent process samples, however this may be difficult to achieve in practice. Vial batch size may not be adequate to provide sufficient quantities for all of the samples over the life cycle of the product, which may span 10 to 15 years. A more practical alternative would be to include the variation in vial type in the calibration set by sourcing vials from multiple

^{†††} Except in the case of water concentration when the method is accurate at trace levels.

Chapter 5

batches for inclusion. Variation in vial type can then be countered by selection of an appropriate spectral pre-treatment (as shown in the case of the everolimus coating solution) or through the multivariate analysis method, thereby ensuring that the calibration is robust to vial variation.

Successful use of NIR in these off-line studies is encouraging for future studies utilizing the technique for at-line and in-line quantification of drugs and polymers present in DES coating solutions. It is also of interest to note that the NIR method is capable of monitoring the water content of the coating solutions, providing additional process knowledge to the DES manufacturer.

6 References

- [1] World Health Organization, “Global status report on noncommunicable diseases.,” Geneva, 2010.
- [2] World Health Organization, “Global atlas on cardiovascular disease prevention and control.,” Geneva, 2011.
- [3] R. Ross, “Atherosclerosis—an inflammatory disease,” *New England Journal of Medicine*, vol. 340, no. 2, pp. 115–126, 1999.
- [4] C. Treasure and J. Klein, “Beneficial effects of cholesterol-lowering therapy on the coronary endothelium in patients with coronary artery disease,” *The New England Journal of Medicine*, vol. 332, no. 8, pp. 481–487, 1995.
- [5] R. G. Favaloro, “Critical analysis of coronary artery bypass graft surgery: a 30-year journey.,” *Journal of the American College of Cardiology*, vol. 31, no. 4 Suppl B, p. 1B–63B, Mar. 1998.
- [6] I. M. Singh and D. R. Holmes, “Myocardial revascularization by percutaneous coronary intervention: past, present, and the future.,” *Current Problems in Cardiology*, vol. 36, no. 10, pp. 375–401, Oct. 2011.
- [7] S. Koga, S. Ikeda, K. Futagawa, K. Sonoda, T. Yoshitake, Y. Miyahara, and S. Kohno, “The use of a hydrophilic-coated catheter during transradial cardiac catheterization is associated with a low incidence of radial artery spasm.,” *International Journal of Cardiology*, vol. 96, no. 2, pp. 255–8, Aug. 2004.
- [8] J. Simon, “Technical White Paper - Hydrophilic Coatings : Considerations for product development and choice,” www.biocoat.com. [Online]. Available: <http://info.biocoat.com/hydrophilic-coating-white-paper>. [Accessed: 22-Jan-2013].
- [9] P. J. Buscemi and P. C. Slaikou, “US Patent US005693034A Lubricous polymer network,” U.S. Patent US005693034A1997.
- [10] FDA, “Guidance for Industry and FDA Staff Non-Clinical Engineering Tests and Recommended Labeling for Intravascular Stents and Associated Delivery Systems,” *Guidance for industry and FDA staff*, 2010.
- [11] A. Israelsson and J. Utas, “Medical device with hydrophilic coating,” U.S. Patent 6,629,61 B12003.
- [12] I. Nazarova, J. Lindquist, and D. J. Horn, “Hydrophilic coating that reduces particle development on ester-linked poly(ester-block-amide),” U.S. Patent 0217186 A12010.
- [13] R. De Moura, P. R. G. Fernandes, F. A. Aouada, A. F. Rubira, and E. C. Muniz, “Optical and morphological characterization of polyacrylamide hydrogel and liquid crystal systems,” *European Polymer Journal*, vol. 41, pp. 2134–2141, 2005.
- [14] B. Suthar, H. X. Xiao, D. Klempner, and K. C. Frisch, “A Review of Kinetic Studies on the Formation of Interpenetrating Polymer Networks,” *Polymers for Advanced Technologies*, vol. 7, no. November, pp. 221–233, 1995.
- [15] A. D. McNaught and A. Wilkinson, “IUPAC Compendium of Chemical Terminology 2nd Edition (1997),” in *IUPAC. Compendium of Chemical Terminology, (the “Gold Book”)*, 2nd ed., Blackwell Scientific Publications, Oxford, 1997, p. 2305.
- [16] L. H. Sperling, “Interpenetrating Polymer Networks : An Overview,” in *Interpenetrating Polymer Networks*, D. Klempner, L. H. Sperling, and L. A. Utracki, Eds. American Chemical Society, 1994, pp. 3–38.
- [17] P. Serruys, M. Kutryk, and A. T. L. Ong, “Coronary-artery stents,” *New England Journal of Medicine*, vol. 354, pp. 483–495, 2006.

References

- [18] P. W. Serruys, M.-C. Morice, A. P. Kappetein, A. Colombo, D. R. Holmes, M. J. Mack, E. Ståhle, T. E. Feldman, M. van den Brand, E. J. Bass, N. Van Dyck, K. Leadley, K. D. Dawkins, and F. W. Mohr, "Percutaneous Coronary Intervention versus Coronary-Artery Bypass Grafting for Severe Coronary Artery Disease," *New England Journal of Medicine*, vol. 360, no. 10, pp. 961–972, 2010.
- [19] D. J. Maron, W. J. Kostuk, M. Knudtson, M. Dada, P. Casperson, D. Ph, C. L. Harris, D. Pharm, B. R. Chaitman, L. Shaw, G. Gosselin, S. Nawaz, L. M. Title, G. Gau, A. S. Blaustein, D. C. Booth, E. R. Bates, J. A. Spertus, D. S. Berman, and G. B. J. Mancini, "Optimal Medical Therapy with or without PCI for Stable Coronary Disease," *New England Journal of Medicine*, vol. 356, no. 15, pp. 1503–1516, 2012.
- [20] K. R. Kamath, J. J. Barry, and K. M. Miller, "The Taxus drug-eluting stent: a new paradigm in controlled drug delivery.," *Advanced drug delivery reviews*, vol. 58, no. 3, pp. 412–36, Jun. 2006.
- [21] M. A. M. Beijk and J. J. Piek, "XIENCE V everolimus-eluting coronary stent system: a novel second generation drug-eluting stent.," *Expert Review of Medical Devices*, vol. 4, no. 1, pp. 11–21, Jan. 2007.
- [22] M. A. Costa and D. I. Simon, "Molecular basis of restenosis and drug-eluting stents.," *Circulation*, vol. 111, no. 17, pp. 2257–73, May 2005.
- [23] W. Khan, S. Farah, and A. J. Domb, "Drug eluting stents: Developments and current status.," *Journal of Controlled Release : Official Journal of the Controlled Release Society*, vol. 161, no. 2, pp. 703–712, Feb. 2012.
- [24] R. C. Braun-Dullaes, M. J. Mann, and V. J. Dzau, "Cell Cycle Progression : New Therapeutic Target for Vascular Proliferative Disease," *Circulation*, vol. 98, no. 1, pp. 82–89, Jul. 1998.
- [25] S. O. Marx and a. R. Marks, "Bench to Bedside: The Development of Rapamycin and Its Application to Stent Restenosis," *Circulation*, vol. 104, no. 8, pp. 852–855, Aug. 2001.
- [26] B. Kahan, R. Wong, C. Carter, S. Katz, J. Von Fellenberg, C. Van Buren, and S. Appel-Dingemanse, "A phase I study of a 4-week course of SDZ-RAD (RAD) in quiescent cyclosporine-prednisone-treated renal transplant recipients.," *Transplantation*, vol. 68, no. 8, pp. 1100–1106, 1999.
- [27] P. Schiff and S. Horwitz, "Taxol stabilizes microtubules in mouse fibroblast cells," *Proceedings of the National Academy of Sciences of the United States of America*, vol. 77, no. 3, pp. 1561–1565, 1980.
- [28] K. D. Dawkins, E. Grube, G. Guagliumi, A. P. Banning, K. Zmudka, A. Colombo, L. Thuesen, K. Hauptman, J. Marco, W. Wijns, J. J. Popma, J. Koglin, and M. E. Russell, "Clinical efficacy of polymer-based paclitaxel-eluting stents in the treatment of complex, long coronary artery lesions from a multicenter, randomized trial: support for the use of drug-eluting stents in contemporary clinical practice.," *Circulation*, vol. 112, no. 21, pp. 3306–13, Nov. 2005.
- [29] S. Windecker and P. Jüni, "The drug-eluting stent saga.," *Circulation*, vol. 119, no. 5, pp. 653–6, Feb. 2009.
- [30] G. Acharya and K. Park, "Mechanisms of controlled drug release from drug-eluting stents.," *Advanced Drug Delivery Reviews*, vol. 58, no. 3, pp. 387–401, Jun. 2006.
- [31] N. Bege, S. O. Steinmüller, M. Kalinowski, R. Reul, S. Klaus, H. Petersen, C. Curdy, J. Janek, and T. Kissel, "Drug eluting stents based on Poly(ethylene carbonate): optimization of the stent coating process.," *European Journal of Pharmaceutics and Biopharmaceutics : Official Journal of Arbeitsgemeinschaft für Pharmazeutische Verfahrenstechnik e.V.*, vol. 80, no. 3, pp. 562–70, Apr. 2012.

References

- [32] M. I. Papafaklis, Y. S. Chatzizisis, K. K. Naka, G. D. Giannoglou, and L. K. Michalis, "Drug-eluting stent restenosis: effect of drug type, release kinetics, hemodynamics and coating strategy.," *Pharmacology & Therapeutics*, vol. 134, no. 1, pp. 43–53, May 2012.
- [33] "USP <788> Particulate matter in injections," *United States Pharmacopeia*, vol. 34, pp. 326–328, 2011.
- [34] USP, "USP <1788> Methods for the determination of particulate matter in injections and ophthalmic solutions," *United States Pharmacopeia*, vol. 34, pp. 843–854, 2011.
- [35] U.S. FDA, "DES guidance document workshop guidance for coronary DES: Engineering Evaluation," in *FDA Workshop*, 2008, pp. 1–137.
- [36] T. Barber, *Control of particulate matter contamination in healthcare manufacturing*. CRC Press, 2000.
- [37] US FDA, "Coronary Drug-Eluting Stents - Nonclinical and Clinical Studies," *Guidance for Industry*, 2008.
- [38] A. Dorantes and U.S. FDA, "Performance Tests for Drug-eluting Stents: Regulatory Perspectives," in *American Association of Pharmaceutical Sciences (AAPS) Workshop on Special Dosage Forms - What's New with In-Vitro Drug Release?*, 2009.
- [39] Q. Chen, D. Zielinski, J. Chen, S. Nowak, and C. Chun, "Structural identification and characterization of potential degradants of zotarolimus on zotarolimus-coated drug-eluting stents," *Journal of Pharmaceutical and Biomedical Analysis*, vol. 50, pp. 778–786, 2009.
- [40] J. Tailor, A. Raval, C. Engineer, H. Kotadia, and D. Kothwala, "Development and Validation of a Reversed-Phase HPLC Method for In- Vitro Loading and Release Analysis of Paclitaxel Coated Stent," *Trends Biomater. Artif. Organs*, vol. 22, no. 2, pp. 75–82, 2008.
- [41] M. Kamberi, S. Nayak, K. Myo-Min, T. P. Carter, L. Hancock, and D. Feder, "A novel accelerated in vitro release method for biodegradable coating of drug eluting stents: Insight to the drug release mechanisms.," *European journal of pharmaceutical sciences : official journal of the European Federation for Pharmaceutical Sciences*, vol. 37, no. 3–4, pp. 217–22, Jun. 2009.
- [42] L. L. Lao and S. S. Venkatraman, "Paclitaxel release from single and double-layered poly(DL-lactide-co-glycolide)/poly(L-lactide) film for biodegradable coronary stent application.," *Journal of Biomedical Materials Research. Part A*, vol. 87, no. 1, pp. 1–7, Oct. 2008.
- [43] US FDA, "Drug Substance Chemistry , Manufacturing , and Controls Information," *Guidance for Industry*, 2010.
- [44] M. Kamberi, S. Nayak, K. Myo-Min, T. P. Carter, L. Hancock, and D. Feder, "A novel accelerated in vitro release method for biodegradable coating of drug eluting stents: Insight to the drug release mechanisms.," *European Journal of Pharmaceutical Sciences : official journal of the European Federation for Pharmaceutical Sciences*, vol. 37, no. 3–4, pp. 217–22, Jun. 2009.
- [45] A. C. P. Jacobs, W. Dewé, A. Flament, M. Gibella, "A new validation approach applied to the GC determination of impurities in organic solvents," *Journal of Pharmaceutical and Biomedical Analysis*, vol. 40, no. 2, pp. 294–304, 2006.
- [46] M. Holčápek, R. Jirásko, and M. Lísa, "Recent developments in liquid chromatography-mass spectrometry and related techniques.," *Journal of Chromatography. A*, vol. 1259, pp. 3–15, Oct. 2012.

References

- [47] O. J. Pozo, P. Van Eenoo, K. Deventer, and F. T. Delbeke, "Detection and characterization of anabolic steroids in doping analysis by LC-MS," *TrAC Trends in Analytical Chemistry*, vol. 27, no. 8, pp. 657–671, Sep. 2008.
- [48] I. V Chernushevich, a V Loboda, and B. a Thomson, "An introduction to quadrupole-time-of-flight mass spectrometry.," *Journal of Mass Spectrometry*, vol. 36, no. 8, pp. 849–65, Aug. 2001.
- [49] G. L. Glish and R. W. Vachet, "The basics of mass spectrometry in the twenty-first century.," *Nature Reviews. Drug discovery*, vol. 2, no. 2, pp. 140–50, Feb. 2003.
- [50] S. Baldelli, S. Murgia, S. Merlini, S. Zenoni, N. Perico, G. Remuzzi, and D. Cattaneo, "High-performance liquid chromatography with ultraviolet detection for therapeutic drug monitoring of everolimus.," *Journal of Chromatography. B, Analytical Technologies in the Biomedical and Life Sciences*, vol. 816, no. 1–2, pp. 99–105, Feb. 2005.
- [51] Y. Chen, G. M. Brill, N. J. Benz, M. R. Leanna, M. K. Dhaon, M. Rasmussen, C. C. Zhou, J. a Bruzek, and J. R. Bellettini, "Normal phase and reverse phase HPLC-UV-MS analysis of process impurities for rapamycin analog ABT-578: application to active pharmaceutical ingredient process development.," *Journal of Chromatography. B, Analytical Technologies in the Biomedical and Life Sciences*, vol. 858, no. 1–2, pp. 106–17, Oct. 2007.
- [52] A. R. Oyler, B. E. Segmuller, Y. Sun, A. Polshyna, R. Dunphy, B. L. Armstrong, P. Achord, C. a Maryanoff, L. Alquier, and Y. V Il'ichev, "Forced degradation studies of rapamycin: identification of autoxidation products.," *Journal of Pharmaceutical and Biomedical Analysis*, vol. 59, pp. 194–200, Feb. 2012.
- [53] K. Hallensleben, M. Raida, and G. Habermehl, "Identification of a new metabolite of macrolide immunosuppressant, like rapamycin and SDZ RAD, using high performance liquid chromatography and electrospray tandem mass spectrometry.," *Journal of the American Society for Mass Spectrometry*, vol. 11, no. 6, pp. 516–25, Jun. 2000.
- [54] R. Steffan, "Base catalyzed degradations of rapamycin," *Tetrahedron Letters*, vol. 34, no. 23, pp. 3699–3702, Jun. 1993.
- [55] J. a Findlay and L. Radics, "On the chemistry and high field nuclear magnetic resonance spectroscopy of rapamycin," *Canadian Journal of Chemistry*, vol. 58, no. 6, pp. 579–590, Mar. 1980.
- [56] M. Ricciutelli, P. Di Martino, L. Barboni, and S. Martelli, "Evaluation of rapamycin chemical stability in volatile-organic solvents by HPLC.," *Journal of Pharmaceutical and Biomedical Analysis*, vol. 41, no. 3, pp. 1070–4, Jun. 2006.
- [57] Y. V Il'ichev, L. Alquier, and C. A. Maryanoff, "Degradation of rapamycin and its ring-opened isomer : role of base catalysis," *ARKIVOC*, vol. xii, pp. 110–131, 2007.
- [58] C. Vidal, G. I. Kirchner, and K. Sewing, "Structural Elucidation by Electrospray Mass Spectrometry : An Approach to the In Vitro Metabolism of the Macrolide Immunosuppressant SDZ RAD," *Journal of the American Society for Mass Spectrometry*, vol. 9, pp. 1267–1274, 1998.
- [59] W. Yang, C. a Digits, M. Hatada, S. Narula, L. W. Rozamus, C. M. Huestis, J. Wong, D. Dalgarno, and D. a Holt, "Selective epimerization of rapamycin via a retroaldol/aldol mechanism mediated by titanium tetrakisopropoxide.," *Organic letters*, vol. 1, no. 12, pp. 2033–5, Dec. 1999.
- [60] K. El-Haik and K. Yang, "Fundamentals of Experimental Design," in *Design for Six Sigma, A Roadmap for Product Development*, 2nd ed., McGraw-Hill, 2003, pp. 413–468.
- [61] A. Jiju, *Design of experiments for engineers and scientists*. Burlington, MA: Oxford, 2003.

References

- [62] D. Montgomery, "Introduction to Factorial Designs," in *Design and analysis of experiments*, 7th ed., John Wiley & Sons, 2010, pp. 162–184.
- [63] V. K. Aggarwal, A. C. Staubitz, and M. Owen, "Optimization of the Mizoroki–Heck Reaction Using Design of Experiment (DoE)," *Organic Process Research & Development*, vol. 10, no. 1, pp. 64–69, Jan. 2006.
- [64] J. J. Chen, T. C. Nugent, C. V. Lu, S. Kondapally, P. Giannousis, Y. Wang, and J. T. Wilmot, "Rapid Improvement of a Reductive Sulfonylation Using Design of Experiment Methods," *Organic Process Research & Development*, vol. 7, no. 3, pp. 313–317, May 2003.
- [65] P. F. Gavin and B. a Olsen, "A quality by design approach to impurity method development for atomoxetine hydrochloride (LY139603).," *Journal of Pharmaceutical and Biomedical Analysis*, vol. 46, no. 3, pp. 431–41, Feb. 2008.
- [66] D. Montgomery, "Introduction," in *Design and analysis of experiments*, 7th ed., John Wiley 7 Sons, 2008, pp. 1–24.
- [67] R. P. Cogdill, C. a Anderson, M. Delgado-Lopez, D. Molseed, R. Chisholm, R. Bolton, T. Herkert, A. M. Afnán, and J. K. Drennen, "Process analytical technology case study part I: feasibility studies for quantitative near-infrared method development.," *AAPS PharmSciTech*, vol. 6, no. 2, pp. E262–72, Jan. 2005.
- [68] R. P. Cogdill, C. a Anderson, M. Delgado, R. Chisholm, R. Bolton, T. Herkert, A. M. Afnan, and J. K. Drennen, "Process analytical technology case study: part II. Development and validation of quantitative near-infrared calibrations in support of a process analytical technology application for real-time release.," *AAPS PharmSciTech*, vol. 6, no. 2, pp. E273–83, Jan. 2005.
- [69] R. P. Cogdill, C. a Anderson, and J. K. Drennen, "Process analytical technology case study, part III: calibration monitoring and transfer.," *AAPS PharmSciTech*, vol. 6, no. 2, pp. E284–97, Jan. 2005.
- [70] S. Bonenfant, F. Despagne, and ABB Analytical, "Analysis of Drug Eluting Stent Coating Solutions Using FT-NIR Spectroscopy," *spectroscopyonline.com Application Notebook*, vol. September, 2009.
- [71] US Food and Drug Administration, *Guidance for Industry Guidance for Industry PAT — A Framework for Innovative Pharmaceutical Development, Manufacturing and Quality Assurance*, no. September. 2004.
- [72] L. X. Yu, "Pharmaceutical quality by design: product and process development, understanding, and control.," *Pharmaceutical Research*, vol. 25, no. 4, pp. 781–91, Apr. 2008.
- [73] X. Xu, M. a Khan, and D. J. Burgess, "A quality by design (QbD) case study on liposomes containing hydrophilic API: I. Formulation, processing design and risk assessment.," *International Journal of Pharmaceutics*, vol. 419, no. 1–2, pp. 52–9, Oct. 2011.
- [74] I. Benson, "Food Compositional Analysis using Near Infra-red Absorption Technology," in *Instrumentation and Sensors for the Food Industry*, 2000.
- [75] D. Cozzolino, S. Roumeliotis, and J. Eglinton, "Monitoring water uptake in whole barley (*Hordeum vulgare* L.) grain during steeping using near infrared reflectance spectroscopy," *Journal of Food Engineering*, vol. 114, no. 4, pp. 545–549, Feb. 2013.
- [76] D. Wu, P. Nie, J. Cuello, Y. He, Z. Wang, and H. Wu, "Application of visible and near infrared spectroscopy for rapid and non-invasive quantification of common adulterants in *Spirulina* powder," *Journal of Food Engineering*, vol. 102, no. 3, pp. 278–286, Feb. 2011.

References

- [77] G. Reich, "Near-infrared spectroscopy and imaging : Basic principles and pharmaceutical applications," *Advanced Drug Delivery Reviews*, vol. 57, pp. 1109–1143, 2005.
- [78] J. Rantanen, H. Wikström, R. Turner, and L. S. Taylor, "Use of in-line near-infrared spectroscopy in combination with chemometrics for improved understanding of pharmaceutical processes.," *Analytical chemistry*, vol. 77, no. 2, pp. 556–63, Jan. 2005.
- [79] Y. Roggo, P. Chalus, L. Maurer, C. Lema-martinez, and N. Jent, "A review of near infrared spectroscopy and chemometrics in pharmaceutical technologies," *Journal of Pharmaceutical and Biomedical Analysis*, vol. 44, pp. 683–700, 2007.
- [80] M. Jamrógiewicz, "Journal of Pharmaceutical and Biomedical Analysis Application of the near-infrared spectroscopy in the pharmaceutical technology," *Journal of Pharmaceutical and Biomedical Analysis*, vol. 66, pp. 1–10, 2012.
- [81] P. Stchur, D. Cleveland, J. Zhou, and R. G. Michel, "A review of recent applications of near infrared spectroscopy, and of the characteristics of a novel PbS CCD array-based near-infrared spectrometer," *Applied Spectroscopy Reviews*, vol. 37, no. 4, pp. 383–428, Nov. 2002.
- [82] H. W. Siesler, Y. Ozaki, S. Kawata, and H. M. Heise, *Near Infrared Spectroscopy*. WILEY-VCH, 2002.
- [83] L. Bokobza, "Near infrared spectroscopy," *Journal of near infrared spectroscopy*, vol. 6, pp. 3–17, Sep. 1998.
- [84] C. Pasquini, "Near Infrared Spectroscopy: fundamentals, practical aspects and analytical applications," *Journal of the Brazilian Chemical Society*, vol. 14, no. 2, pp. 198–219, Apr. 2003.
- [85] M. Jamrógiewicz, "Journal of Pharmaceutical and Biomedical Analysis Application of the near-infrared spectroscopy in the pharmaceutical technology," *Journal of Pharmaceutical and Biomedical Analysis*, vol. 66, pp. 1–10, 2012.
- [86] M. S. Kemper, E. J. Magnuson, S. R. Lowry, W. J. McCarthy, N. Aksornkoae, D. C. Watts, J. R. Johnson, and a J. Shukla, "Use of FT-NIR transmission spectroscopy for the quantitative analysis of an active ingredient in a translucent pharmaceutical topical gel formulation.," *AAPS pharmSci*, vol. 3, no. 3, p. E23, Jan. 2001.
- [87] Office of Science and Technology, "Near-infrared spectroscopy. Innovative technology summary report," Washington DC, 1999.
- [88] M. Blanco, J. Coello, H. Iturriaga, S. Maspoch, and C. De Pezuela, "Critical Review Near-infrared spectroscopy in the pharmaceutical industry," *Analyst*, vol. 123, no. August, pp. 135–150, 1998.
- [89] S. C. Rutan, O. E. de Noord, and R. R. Andréa, "Characterization of the sources of variation affecting near-infrared spectroscopy using chemometric methods.," *Analytical chemistry*, vol. 70, no. 15, pp. 3198–201, Aug. 1998.
- [90] E. Alm, R. Bro, S. B. Engelsen, B. Karlberg, and R. J. O. Torgrip, "Vibrational overtone combination spectroscopy (VOCSY)-a new way of using IR and NIR data.," *Analytical and Bioanalytical Chemistry*, vol. 388, no. 1, pp. 179–88, May 2007.
- [91] R. P. Cogdill, C. A. Anderson, and J. K. Drennen, "Using NIR Spectroscopy as an Integrated P A T Tool," *Spectroscopy*, vol. 19, no. 12, pp. 104 – 109, 2004.
- [92] M. Stading, A. Rindlav-Westling, and P. Gatenholm, "Humidity-induced structural transitions in amylose and amylopectin ® lms," *Carbohydrate Polymers*, vol. 45, pp. 209–217, 2001.
- [93] J. S. Boateng, H. N. E. Stevens, G. M. Eccleston, A. D. Auffret, M. J. Humphrey, and K. H. Matthews, "Development and mechanical characterization of solvent-cast polymeric

References

- films as potential drug delivery systems to mucosal surfaces.,” *Drug Development and Industrial Pharmacy*, vol. 35, no. 8, pp. 986–96, Aug. 2009.
- [94] L. Stordrange, F. O. Libnau, D. Malthe-Sorensen, and O. M. Kvalheim, “Feasibility study of NIR for surveillance of a pharmaceutical process, including a study of different preprocessing techniques,” *Journal of Chemometrics*, vol. 16, no. 8–10, pp. 529–541, Aug. 2002.
- [95] T. Naes, T. Isaksson, T. Fearn, and T. Davies, *Multivariate Calibration and Classification*. NIR Publications, 2002.
- [96] H. Mark and J. Workman, “Chemometrics in Spectroscopy - What Can NIR Predict?,” *Spectroscopy*, vol. 22, no. June, pp. 20–26, 2007.
- [97] A. C. Olivieri, N. M. Faber, J. Ferré, R. Boqué, J. H. Kalivas, and H. Mark, “Uncertainty estimation and figures of merit for multivariate calibration (IUPAC Technical Report),” *Pure and Applied Chemistry*, vol. 78, no. 3, pp. 633–661, 2006.
- [98] D. M. Haaland and E. V. Thomas, “Partial least-squares methods for spectral analyses. 1. Relation to other quantitative calibration methods and the extraction of qualitative information,” *Analytical Chemistry*, vol. 60, no. 11, pp. 1193–1202, Jun. 1988.
- [99] K. Danzer, M. Otto, and L. A. Currie, “Guidelines for calibration in analytical chemistry Part 2. Multispecies calibration (IUPAC Technical Report),” *Pure and Applied Chemistry*, vol. 76, no. 6, pp. 1215–1225, 2004.
- [100] K. R. Beebe and B. R. Kowalski, “An introduction to multivariate calibration and analysis,” *Analytical Chemistry*, vol. 59, no. 17, p. 1007A–1017A, Sep. 1987.
- [101] S. Wold, J. Trygg, A. Berglund, and H. Antti, “Some recent developments in PLS modeling,” *Chemometrics and Intelligent Laboratory Systems*, vol. 58, no. 2, pp. 131–150, Oct. 2001.
- [102] D. M. Haaland and E. V. Thomas, “Partial least-squares methods for spectral analyses. 2. Application to simulated and glass spectral data,” *Analytical Chemistry*, vol. 60, no. 11, pp. 1202–1208, Jun. 1988.
- [103] J.-P. Conzen, *Multivariate Calibration*, 2nd ed. Bruker Optik GmbH, 2006.
- [104] D. Burns and E. W. Ciurczak, *Handbook of Near-Infrared Analysis*, 2nd ed. New York - Basel: Marcel Dekker, Inc., 2001.
- [105] M. M. Ian, G. Downey, P. Robert, and D. Bertrand, “Developments in near infrared spectroscopy,” *Analytical Proceedings*, vol. 29, pp. 7–9, 1992.
- [106] I. Vessey and C. E. Kendall, “Determination of particulate matter in intravenous fluids.,” *The Analyst*, vol. 91, no. 81, pp. 273–9, Apr. 1966.
- [107] S. D. Kochevar, “Basic Guide to Particle Counters and Particle Counting,” Particle Measuring Systems, Inc., Boulder, Colorado, USA, 2006.
- [108] S. Fakirov, *Handbook of Condensation Thermoplastic Elastomer*. Wiley-VCH, 2005.
- [109] T. Trotta, “Polyetheramide tubing for medical devices,” U.S. Patent EP 0 566 755 B11996.
- [110] B. S. Chernev and G. C. Eder, “Spectroscopic characterization of the oligomeric surface structures on polyamide materials formed during accelerated aging.,” *Applied Spectroscopy*, vol. 65, no. 10, pp. 1133–44, Oct. 2011.
- [111] B. De Gans, R. Kita, B. Müller, and S. Wiegand, “Negative thermodiffusion of polymers and colloids in solvent mixtures Negative thermodiffusion of polymers and colloids in solvent mixtures,” vol. 8073, 2003.
- [112] G. B. Levy, I. Caldas, D. Fergus, and S. Laboratories, “Evaluation of Polyvinylpyrrolidone Preparations,” *Analytical Chemistry*, vol. 24, no. 11, pp. 1799–1803, 1952.

References

- [113] K. Weissermel and H.-J. Arpe, *Acrylonitrile*, 2nd ed. New York: , 1993.
- [114] D. D. Perrin, W. L. F. Armarego, and D. R. Perrin, *Purification of laboratory chemicals*, 2nd ed. New York: Pergammon Press, 1980, pp. 79–81.
- [115] American Chemical Society, *Reagent Chemicals: Specifications and Procedures*, 10th ed. Oxford Universirt Press, 2006.
- [116] J. Poole, H. C. Snyder, and R. J. Ryder, “Corrosion retarding fluorine treatment of glass surfaces,” U.S. Patent 3,314,7721967.
- [117] Metrohm, “Application Bulletin No. 80/3 e : Determination of acid and base number in petroleum products.”
- [118] A. O’Gorman, G. Downey, A. a Gowen, C. Barry-Ryan, and J. M. Frias, “Use of Fourier transform infrared spectroscopy and chemometric data analysis to evaluate damage and age in mushrooms (*Agaricus bisporus*) grown in Ireland.,” *Journal of Agricultural and Food Chemistry*, vol. 58, no. 13, pp. 7770–6, Jul. 2010.
- [119] M. S. Baptista, C. D. Tran, and G. H. Gao, “Near-infrared detection of flow injection analysis by acoustooptic tunable filter-based spectrophotometry.,” *Analytical Chemistry*, vol. 68, no. 6, pp. 971–6, Mar. 1996.
- [120] J. M. Hernández-Hierro, J. Valverde, S. Villacreces, K. Reilly, M. Gaffney, M. L. González-Miret, F. J. Heredia, and G. Downey, “Feasibility Study on the Use of Visible-Near-Infrared Spectroscopy for the Screening of Individual and Total Glucosinolate Contents in Broccoli.,” *Journal of agricultural and food chemistry*, vol. 60, pp. 7352 – 7358, Jul. 2012.
- [121] R. T. Liggins, W. L. Hunter, and H. M. Burt, “Solid-state characterization of paclitaxel.,” *Journal of Pharmaceutical Sciences*, vol. 86, no. 12, pp. 1458–63, Dec. 1997.
- [122] Nigmatulin, R. Iskanderovich, and J. C. Friedly, *Dynamics of Multiphase Media*. Washington DC: Hemisphere, 1991.
- [123] F. R. Young, *Cavitation*. New York: McGraw-Hill, 1989.
- [124] J. Grosrey, “Cavity cleaning apparatus,” U.S. Patent 9,212,6851992.

Appendix 1

The Closed Loop Particulate apparatus from prototype to final design

7 Introduction

Alternative particulate counting equipment to the beaker methods described in sections 2.1.2.1 and 0 were developed to provide a better way to collect particulate data from PTCA devices. Modification of the sampling mechanism was of prime consideration to improve accuracy and precision of the methods and to speed up the analysis time. Various prototypes were explored before selecting the adopted closed loop particulate (CLP) and dual loop particulate (DLP) apparatuses. The test device is tracked through an arterial model which is integrated with the sampling mechanism of the LO detector, and any particles removed are transported to a particle counter where the particles are counted and sized. The equipment can be used in either a flow-through or a closed-loop configuration.

The following basic steps were followed to test SDS devices on the initial prototypes:

- 1) LPW of known volume is added to the mixing chamber and circulated through the apparatus using a pump. A blank measurement is taken using a sampling tube which is located in the mixing chamber and connected to the particle counter. This measurement establishes the suitability of the apparatus and water for particle testing.
- 2) An SDS is tracked through the glass arterial model and exits into a deployment chamber where the stent is deployed; following this the balloon is deflated and withdrawn leaving the stent behind.
- 3) Particulate measurements may be taken post-tracking, pre-deployment and post-deployment or other combinations if required.
- 4) The apparatus is drained and the stent removed.
- 5) The entire apparatus is then flushed out with LPW and the system setup and primed once more.

Appendix 1

The two options explored to achieve these steps were a closed loop and a flow through configuration. The two options are fundamentally different in terms of sampling.

The **flow through design** operates under the principle that water, after passing through the arterial model and the LO detector, is discarded. The **closed-loop design** operates under the principle that a fixed volume of water is continually recirculated through the detector and the arterial model. Thus, the flow through approach is more akin to the typical USP <788> method. In both designs the arterial model is accessed by the device through a mixing chamber. Exiting the mixing chamber is a glass capillary which acts as a guide catheter through which the test device is advanced. At the end of this capillary, the device must negotiate its way through a tortuous shaped pathway which is used to simulate a coronary artery. Finally, the stent can be deployed in a detachable chamber at the end of the artery. Initially 4 different arrangements were considered. Each arrangement has a central mixing chamber from which the arterial model extends; schematics of the 4 arrangements are provided in Figure 182 to Figure 185.

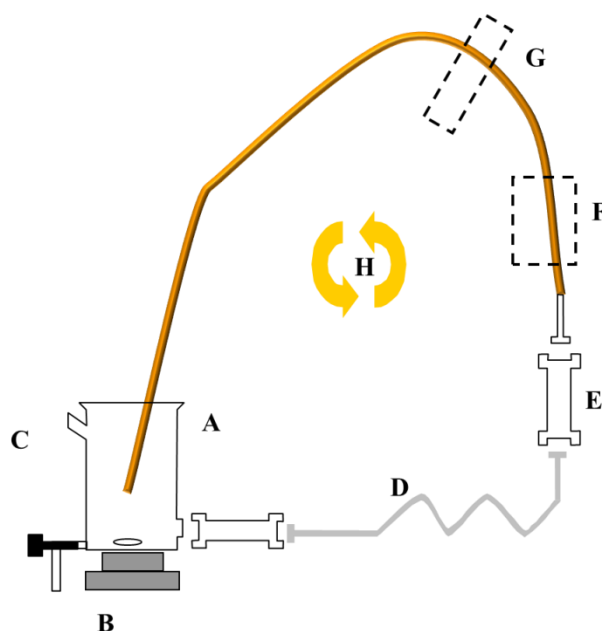


Figure 182 Single closed loop apparatus with in-line particle counter. Comprised of (A) a graduated mixing chamber with (B) a magnetic stirrer for agitation and (C) an inlet through which the test device is inserted. (D) An exchangeable artery model connects to (E) a stent deployment chamber. (F) A peristaltic pump pulls water through the artery model from the mixing chamber and (G) pushes it through an in-line light obscuration detector, after which it returns to the mixing chamber to complete (H) the circulation loop.

Appendix 1

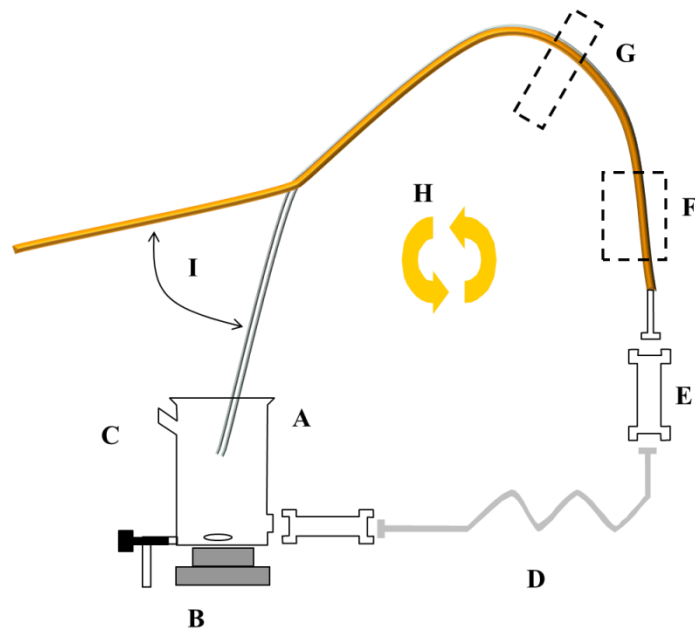


Figure 183 Single loop, flow-through apparatus with in line particle counter. Comprised of (A) a graduated mixing chamber with (B) a magnetic stirrer for agitation and (C) an inlet through which the test device is inserted. (D) An exchangeable artery model connects to (E) a stent deployment chamber. (F) A peristaltic pump pulls water through the artery model from the mixing chamber and (G) pushes it through an in-line light obscuration detector, after which it returns to the mixing chamber to complete (H) the circulation loop. (I) The flow can be diverted to waste after exiting the particle counter by removing the return flow tube from the mixing chamber.

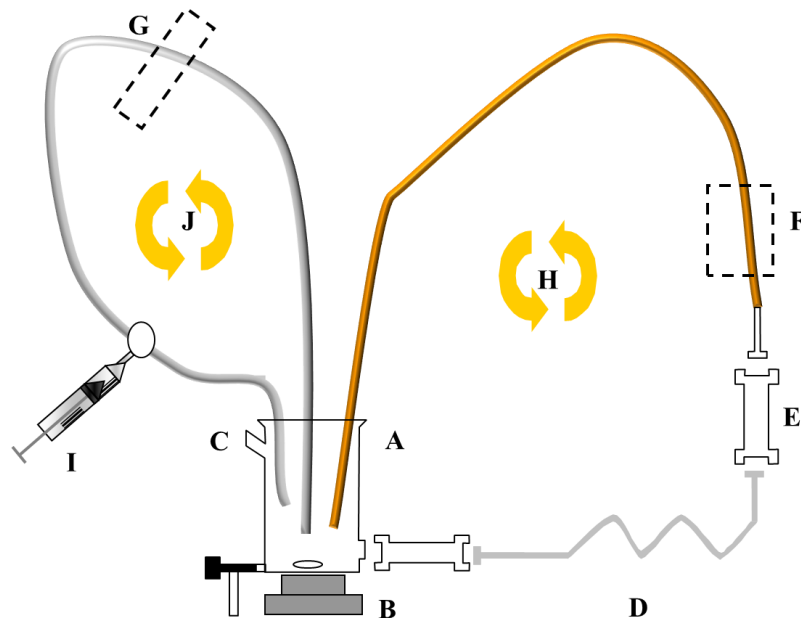


Figure 184 Dual closed loop apparatus comprised of (A) a graduated mixing chamber with (B) a magnetic stirrer for agitation and (C) an inlet through which the test device is inserted. (D) An exchangeable artery model connects to (E) a stent deployment chamber. (F) A peristaltic pump pulls water through the artery model from the mixing chamber and returns it to the mixing chamber to complete (H) the circulation loop. A second loop with (G) an in-line particle counter driven by (I) a syringe pump, creates (J) the sampling loop.

Appendix 1

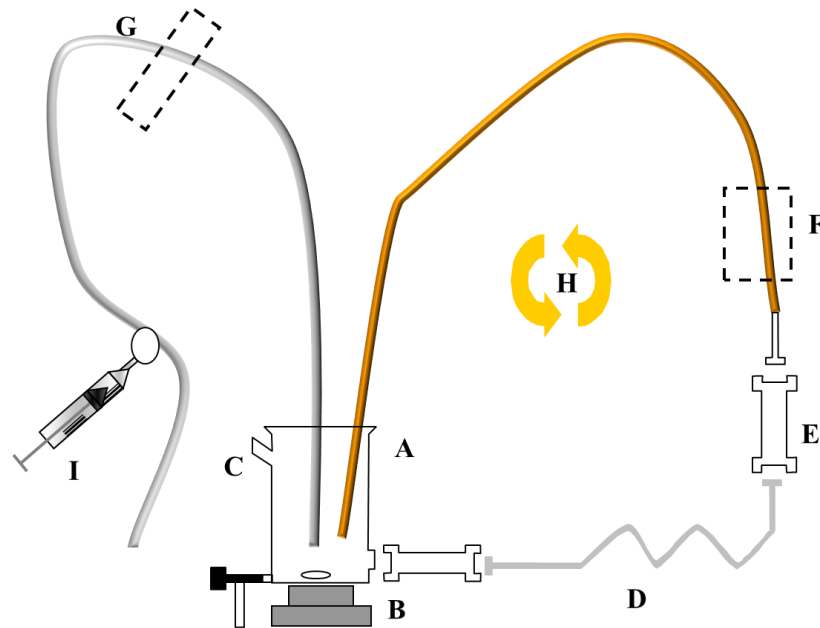


Figure 185 Dual loop, flow through apparatus comprised of (A) a graduated mixing chamber with (B) a magnetic stirrer for agitation and (C) an inlet through which the test device is inserted. (D) An exchangeable artery model connects to (E) a stent deployment chamber. (F) A peristaltic pump pulls water through the artery model from the mixing chamber and returns it to the mixing chamber to complete (H) the circulation loop. (G) An in-line particle counter driven by (I) a syringe pump samples from the closed circulation loop and discards the sample to waste.

Appendix 1

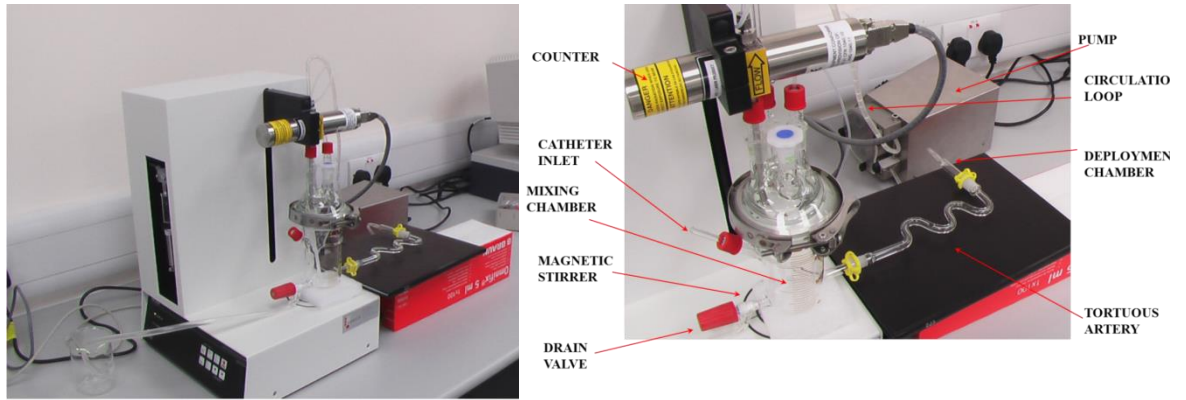
7.1 Early prototypes

One of the first prototype particle counting apparatuses was constructed of glass and was attached to a HIAC 9703 LO particle counter. This set-up could be used as a dual closed loop apparatus (Figure 184) or as a dual loop flow through apparatus (Figure 185). The equipment can be alternated between both by simply directing the return tube from the LO counter back to the mixing chamber (closed loop) or to waste (flow through). Images of the early apparatuses are shown in Figure 186. The HIAC particle counter, with syringe auto sampler and magnetic stirrer, was used as normal for beaker sampling. However, a customised glass mixing chamber and simulated artery were positioned where the beaker would normally sit.

Another early prototype used a PMS APSS 200 Liquilaz particle counter. This set-up, shown in Figure 187, could also be used as a dual closed loop apparatus or as a dual loop flow through apparatus. The equipment was alternated between both by changing the direction of the return flow from the counter using a three-way valve in the customised glass fixture. A peristaltic pump was used to circulate the water through the glassware in both of these early prototypes.

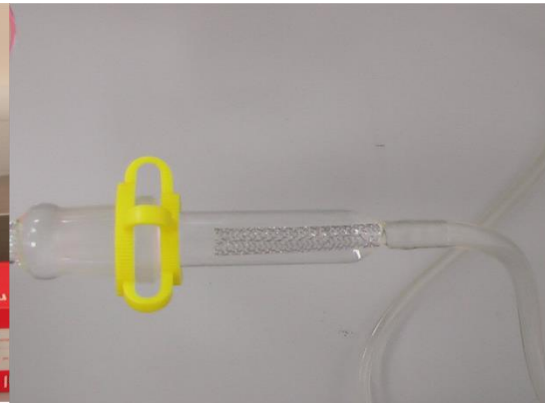
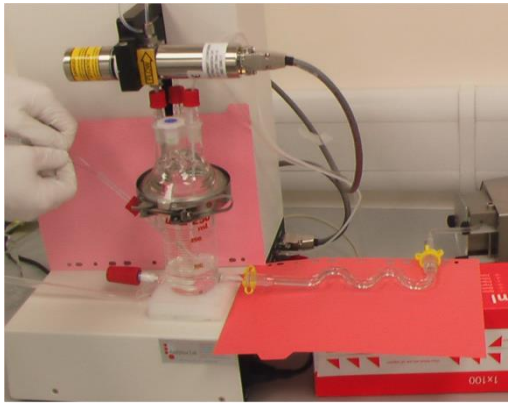
Figure 188 shows a schematic of a single closed loop apparatus which could be operated in flow-through or closed loop configurations. The glassware used was similar to that shown in Figure 187, but the particle counter has been removed from the syringe auto-sampler and is incorporated in the circulation loop. A PMS APSS 200 Liquilaz particle counter was used for the single closed loop apparatus in favour of the HIAC counter because the software and tubing connections were more adaptable.

Appendix 1



A

B

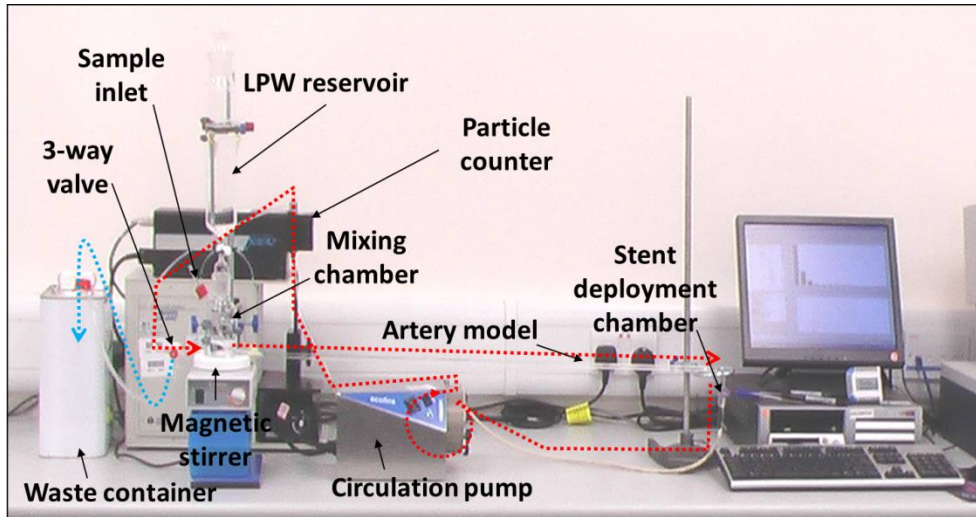


C

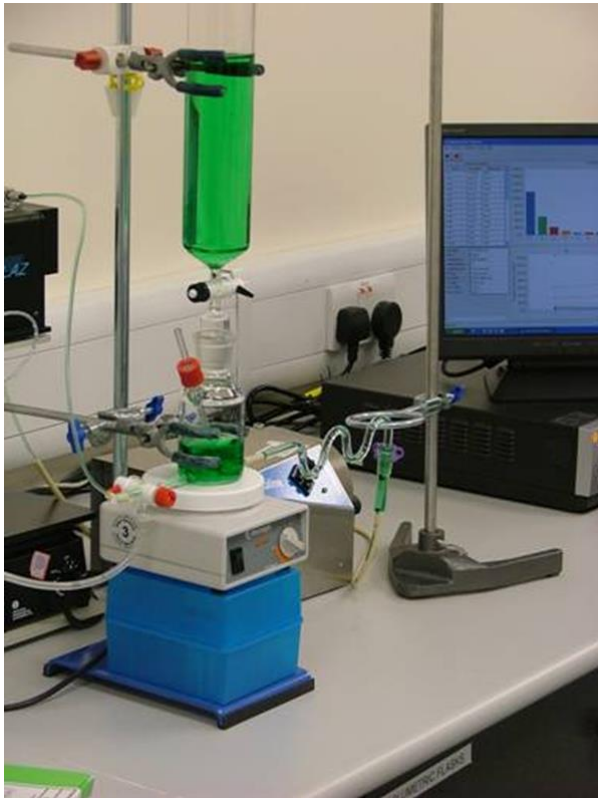
D

Figure 186 Images of an early prototype of the particle counting apparatus with a HIAC 9703 particle counter. The equipment can be alternated between flow-through and closed-loop by simply directing the return tube from the counter back in to the mixing chamber (Closed loop) or to waste (flow through). (A) The HIAC 9703 particle counter with syringe auto-sampler and magnetic stirrer with the test apparatus mounted. (B) A labelled image of the apparatus. (C) An image of the test apparatus in operation, a test sample is being tracked in to the equipment. (D) Image of the stent deployment chamber with a deployed stent in situ.

Appendix 1



A



B

Figure 187 Images of an early prototype of the particle counting apparatus with an EMS APSS Liquilaz particle counter. The equipment can be alternated between flow-through and closed-loop by changing the direction of the return flow from the counter using a three-way valve. (A) Labelled image of the apparatus attached to the EMS APSS Liquilaz particle counter with syringe auto-sampler and magnetic stirrer. (B) The same apparatus, this time with a shorter artery model attached. The water is dyed green to highlight its location in the apparatus.

Appendix 1

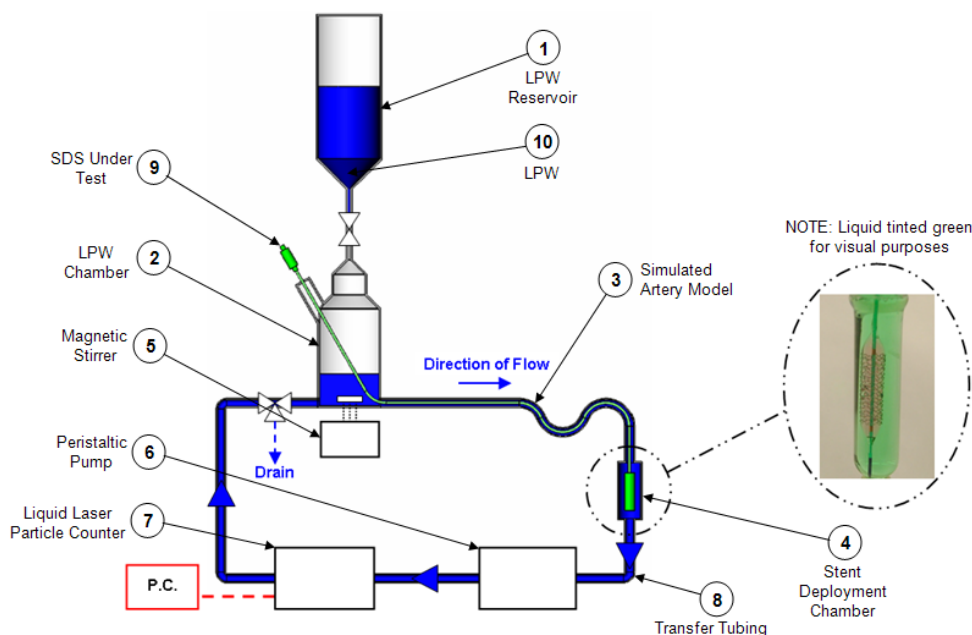


Figure 188 Schematic of a single closed loop apparatus. This apparatus may be operated in flow-through mode by switching a 3 way valve, positioned after the particle counter, to drain the water to waste instead of recirculating through the mixing (LPW) chamber.

7.2 Single closed loop particulate apparatus

The single closed loop particulate apparatus (CLP) finally adopted, Figure 189, is based on the single closed loop apparatus shown in Figure 188 with modifications to optimize particle counting. The magnetic stirrer was removed and the agitation required to suspend particles is supplied entirely by the circulating water from the peristaltic pump. The mixing chamber was redesigned so that the lowest point in a conical chamber is the exit point for the water circulation loop, ensuring the particles are forced to exit the chamber. The returning flow to the chamber is directed upwards thus generating turbulence to distribute particles homogeneously. The flow rate of the system was increased from 20 mL/min to 70 mL/min to compensate for the removal of the agitation previously provided by the magnetic stirrer. The overall volume of the apparatus was reduced to approximately 35 mL. The position of the 3-way valve was changed to a location between the peristaltic pump and the particle counter. The change in location allows for isolation of the particle counter when aggressive cleaning agent or solvents are used to clean the apparatus and to protect the particle counter flow cell from high pressures that may be created by the pump.

Appendix 1

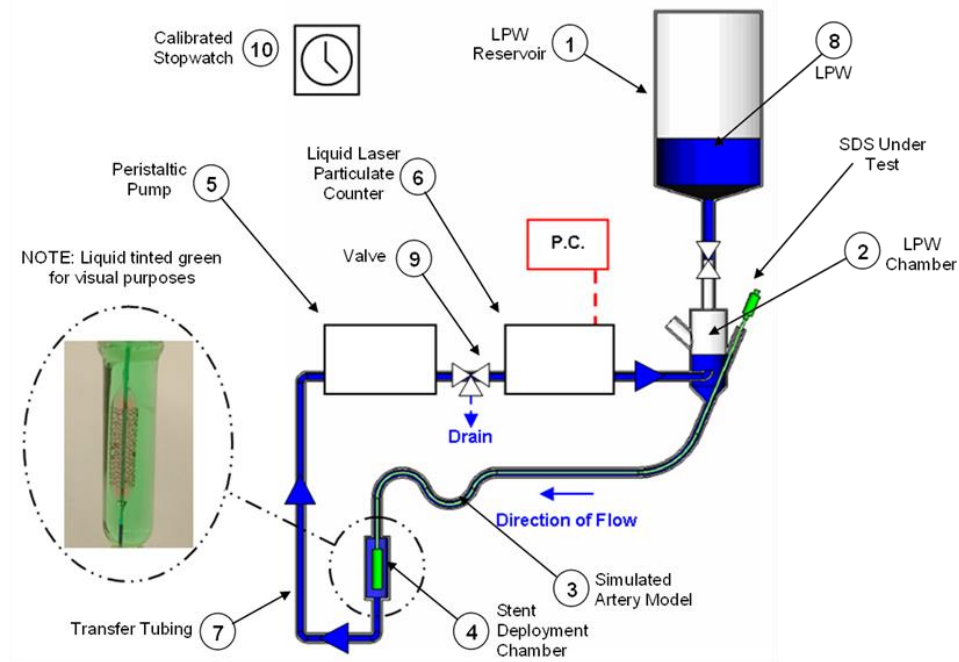


Figure 189 Schematic of the single closed loop particulate apparatus

The apparatus was positioned in a laminar air flow (LAF) hood; to reduce environmental particulate contamination. A subsequent iteration of this design is shown in Figure 190, in which the serpentine-type tortuous pathway has been replaced by a more challenging shaped artery model based on the ASTM standard requested by the FDA[10], [37]. This new iteration also replaces the unconstrained deployment of stents within a stent deployment chamber with constrained deployment in a silicone tube, and also incorporates a guide wire that facilitates tracking of the devices through the tortuous track model.

Appendix 1

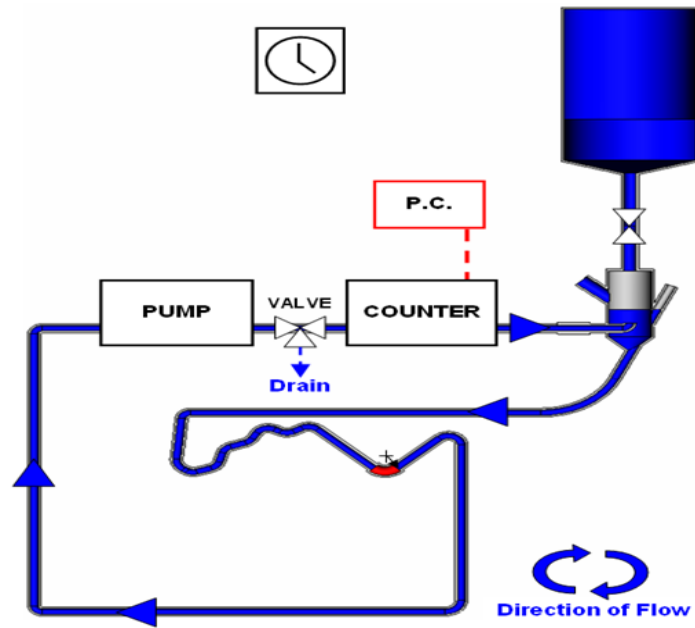


Figure 190 Schematic of the single closed loop apparatus with ASTM coronary artery model and simulated artery tubing (in red).

7.3 CLP prototype selection

Two particle counting instruments were evaluated in the laboratory; these were the APSS from Particle Measuring Systems (PMS) and the Ryoco 9703 from HIAC. Figure 186 and Figure 187 show the HIAC and PMS equipment, respectively, integrated with prototype track models. Initially the counters were evaluated using their own integrated syringe pumps to measure the same samples from beakers. Comparison between both particle counters is shown in Figure 191. The number of particles $\geq 10 \mu\text{m}$ determined using both instruments shows very good agreement, but some deviation is observed between instrument readings for the $\geq 25 \mu\text{m}$ particle counts. The variation may be in part due to the method of sampling from a beaker rather than a difference in equipment; this is a topic that will be discussed in detail later.

Appendix 1

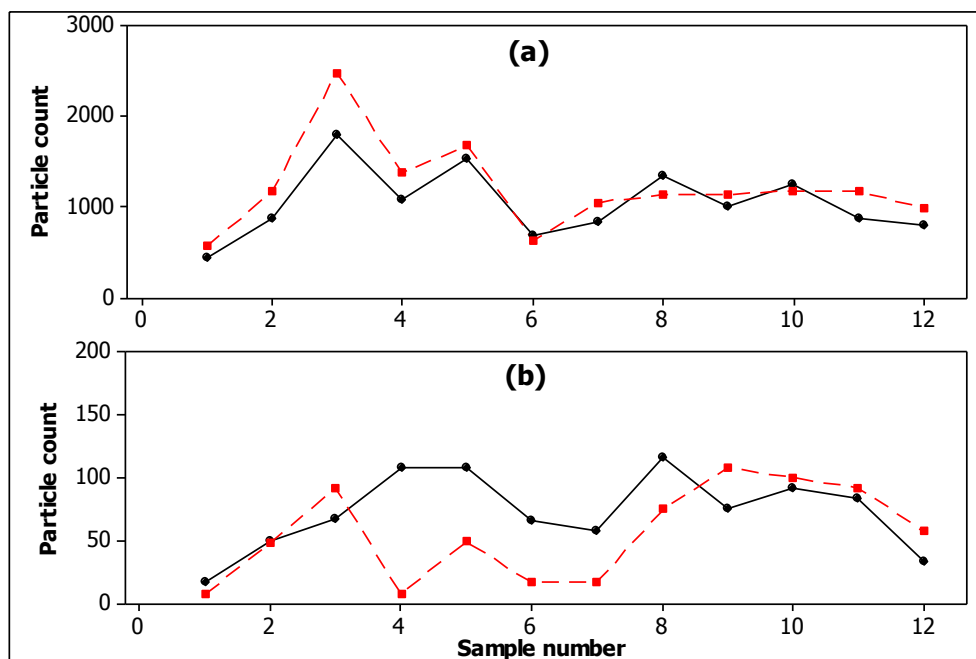


Figure 191 Comparison of (a) $\geq 10 \mu\text{m}$ and (b) $\geq 25 \mu\text{m}$ particle counts for the light obscuration particle counters from the HIAC Ryoco 9703 (in black) and the PMS APPS (in black).

Next both particle counters were coupled with custom built track models in a dual loop configuration as shown in Figure 184 and Figure 185. Once analysed, the water was either returned to the circulation loop (dual closed loop apparatus) or discarded to waste (flow through dual loop apparatus). Both counters performed comparably in a dual loop configuration, however when it came to single closed loop configurations the ease of adaptability of the Liquilaz E20 sensor for in-line use and also the suitability of the PMS software, Samplersight, which can be used for continuous sampling without the requirement for software upgrades, resulted in selection of the PMS instrument for future studies.

Next, an assessment to compare the closed loop and the flow through apparatus using the prototype equipment in Figure 188 was carried out. To create the flow through apparatus, the tubing was disconnected between the detector and the mixing chamber so the water exiting the detector was sent to a waste receptacle. With the equipment thus setup, a device was tracked, deployed and retracted successfully, while particle counts were collected as shown in Figure 192^{†††}.

^{†††} The software was configured to take measurements for every 50mL passing through the detector. The apparatus was prevented from running dry by continually replenishing LPW as the waste water was being drained away. After each step, LPW

Appendix 1

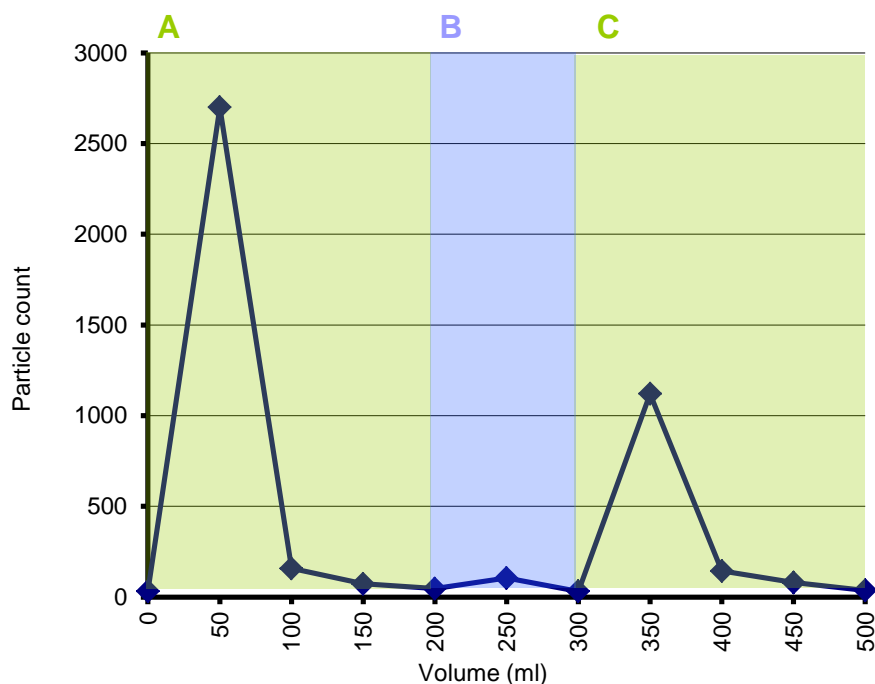


Figure 192 The $\geq 10\mu\text{m}$ particle count from a stent delivery system using the flow through apparatus. The graph is divided for the three procedural steps of (A) SDS tracking and stent deployment, (B) blanking with the device in situ, and (C) catheter withdrawal.

The flow through apparatus thus proved to be a feasible approach; however a number disadvantages presented during the assessment. The main issue is that the volume of water used to carry out the test is relatively large, 500 mL, and it proved complex to simultaneously add water and to carry out the other steps such as tracking and deploying the device.

The closed loop approach was next tried as shown in Figure 188, it was immediately apparent that this was a more user friendly option, hence a large data set was gathered for the initial trial in comparison to the flow-through evaluation. Four different batches of SDSs were tested, with a sample size of 5 per batch. The software was configured to take measurements for every 50 mL passing through the detector. To create a closed loop apparatus, the tubing was connected between the detector and the mixing chamber so the water exiting the detector was sent back into the mixing chamber. With the equipment thus setup, a device was tracked, then the system was drained and a blank

was flushed through the apparatus to remove particles and particle counts were monitored to ensure the water once again met blank acceptance criteria (Not more than 10 particles per 10 mL $\geq 10\mu\text{m}$, and not more than 2 particles per 10 mL $\geq 25\mu\text{m}$). Following stent deployment 100 ml of LPW was washed through the system. After device retraction 200 mL of LPW was passed through the apparatus.

Appendix 1

taken, then the stent was deployed, meanwhile particle counts were collected as shown in Figure 193. An evaluation with 10 µm particle size standards was also carried out at a concentration of 3000 and 60 particles (n = 5 for each), these particle counts are in the region of the SDS and stent particle counts seen on the SDS devices tested, respectively.

The flow through approach has potential as a means for measuring the particle counts from SDSs however the closed loop option has a few distinct advantages over it. The main advantages are the ability to re-analyse the water sample, the confidence of using the same water used to establish the blank to test the sample, and the lower volume of water used to rinse the sample reduces data variability. The four prototypes were thus reduced to the single closed loop design given in Figure 188.

The initial goal of the simulated use assessment was to obtain a particle count from steps associated with tracking a stent delivery system (SDS) followed by a separate measurement for deployment of the stent, in this case a DES. The options explored for doing this were to:

1. Track the device in to the blank apparatus, take a measurement, then re-blank the system by flushing with LPW with the SDS in situ, and then deploy the stent and take a separate measurement.
2. Track the device in to a pre-blanked apparatus, take a measurement, and then deploy the stent and take a second measurement.

Appendix 1

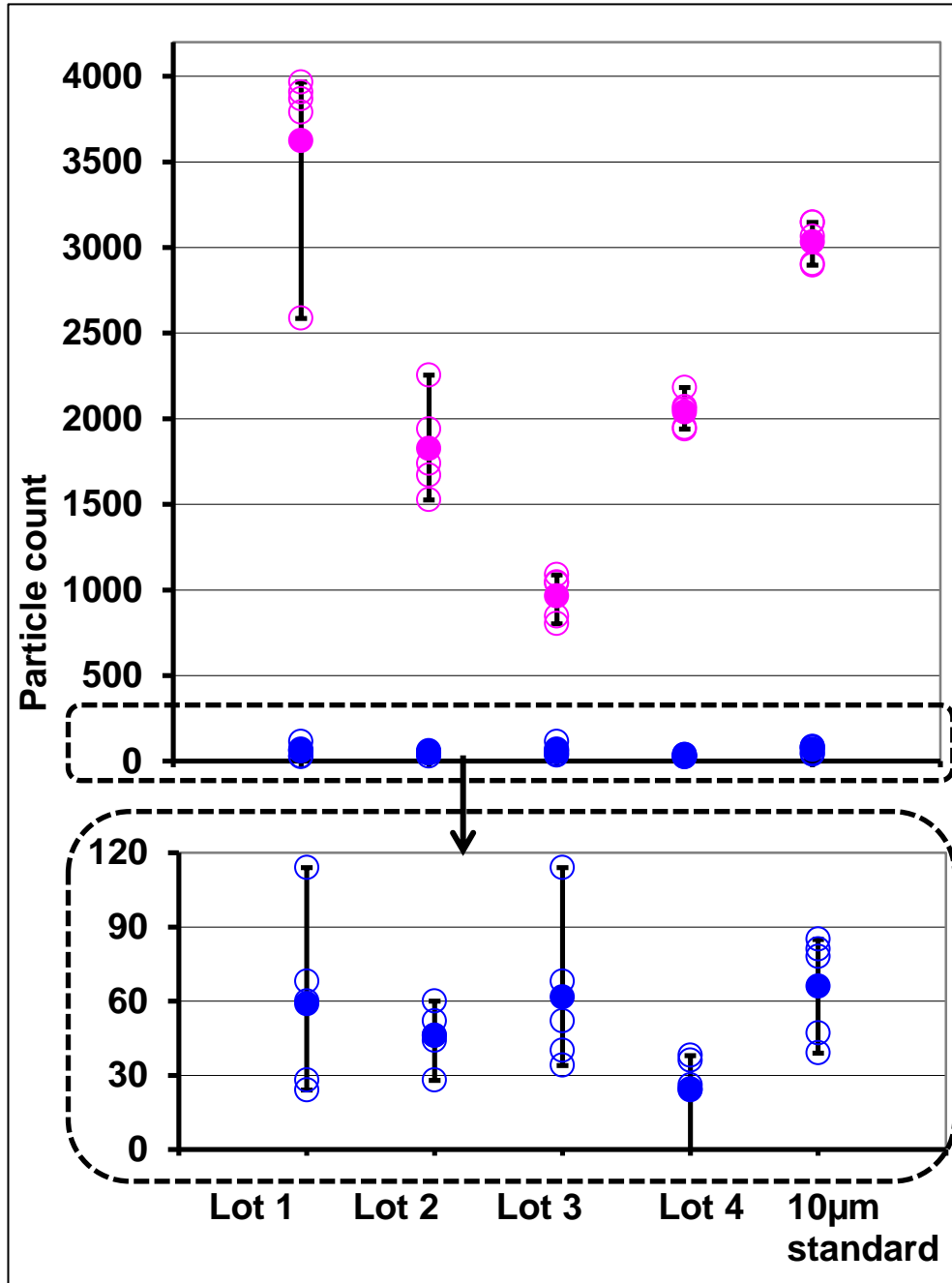


Figure 193 Graph showing $\geq 10 \mu\text{m}$ particle count in the assessment of the closed loop approach used to test four different batches of SDSs, with a sample size of 5 per batch. The software was configured to take measurements for every 50mL passing through the detector. Each device was tracked and then a measurement was taken (pink data points in upper plot), then the system was drained and a blank taken, then the stent was deployed and a second measurement was taken (blue data points in upper and lower plot). An evaluation with $10\mu\text{m}$ particle size standards was also carried out at a concentration of 3000 and 60 particles ($n = 5$ for each), these particle counts are in the region of the SDS and stent particle counts seen on the SDS devices tested, respectively

Appendix 1

In the former the particles created from stent deployment would be kept separate from those particles created when tracking the device, in the latter the first measurement would need to be subtracted from the second to calculate the particle contribution from the stent deployment. The latter option appears the simplest as it does not require extra flushing of the equipment or the taking of a second blank measurement. However on closer consideration it is a less favourable option, mainly because the particles released from tracking the SDS may change over time, making it difficult to truly measure the particle contribution of the stent in a closed loop apparatus. As the particle count from the SDS is larger than that from stent deployment, perhaps by as much as 2 orders of magnitude, any variation in this measurement may mask the contribution from the stent in a closed loop apparatus. This is not a problem using the flow through apparatus as the particles are not re-introduced to the equipment. A more detailed discussion on the effect of taking multiple measurements using the CLP method is provided in section 7.8.

The closed loop method relies on the principle of taking measurements of a homogeneous sample and this enables the volume sampled to be several times the volume of the water in the apparatus. There is a limitation to the minimum volume required to ensure that no air bubbles are introduced to the particle counter, the major disadvantage with this is that the entire volume cannot be measured in a flow through type measurement. This effect may be reduced by increasing the entire volume of liquid used in the test, therefore reducing the percentage of water remaining unsampled, however this is not without drawbacks too. Increasing the volume of the rinse solution increases the length of time taken to gather measurements as a larger volume of water must be sampled, and it also increases the levels of noise in the form of residual particles present in the blank water. The impact of residual particles present in the blank is demonstrated in Figure 194, where it's shown that the level of residual particles present in the 50mL CLP system is an order of magnitude lower than the 350mL beaker used in the simulated beaker test, as would be expected.

Appendix 1

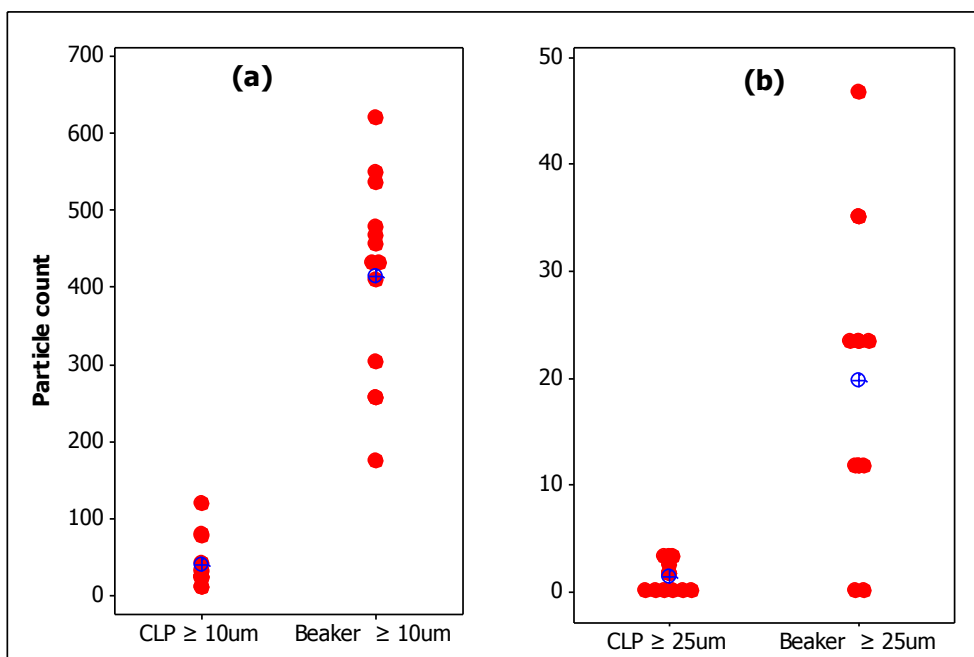


Figure 194 (a) $\geq 10 \mu\text{m}$ and (b) $\geq 25 \mu\text{m}$ particle counts in low particulate water in a 50mL volume CLP apparatus versus a 350 mL beaker.

7.4 Comparison between the beaker and CLP methods.

The apparatus shown in Figure 188 was used to evaluate the CLP design versus the more traditional beaker style method. The CLP method was compared to the simulated beaker method described in section 0 using 150 to 9,000 standard particles of 10 and 25 μm in size. Figure 195 shows the line plots for the CLP method (top) and two plots for the beaker method, the centre plot is the pre track measurement outlined in Figure 36, step 7, and the lower plot is from the post track measurement from the same method, step 11. Both methods are linear over the range selected, with R^2 values from the linear regression near unity. The CLP method has the best linear fit with $R^2 = 0.999$, the beaker pre-track measurement is next best with $R^2 = 0.996$ and the poorest fit is the beaker post track measurement with $R^2 = 0.971$, the variation in the methods can be gauged from the residual standard deviation of 49, 239, and 696 particles, respectively. As such the CLP method has better precision than both beaker method steps, with the precision for the post-track measurement being poorest.

Appendix 1

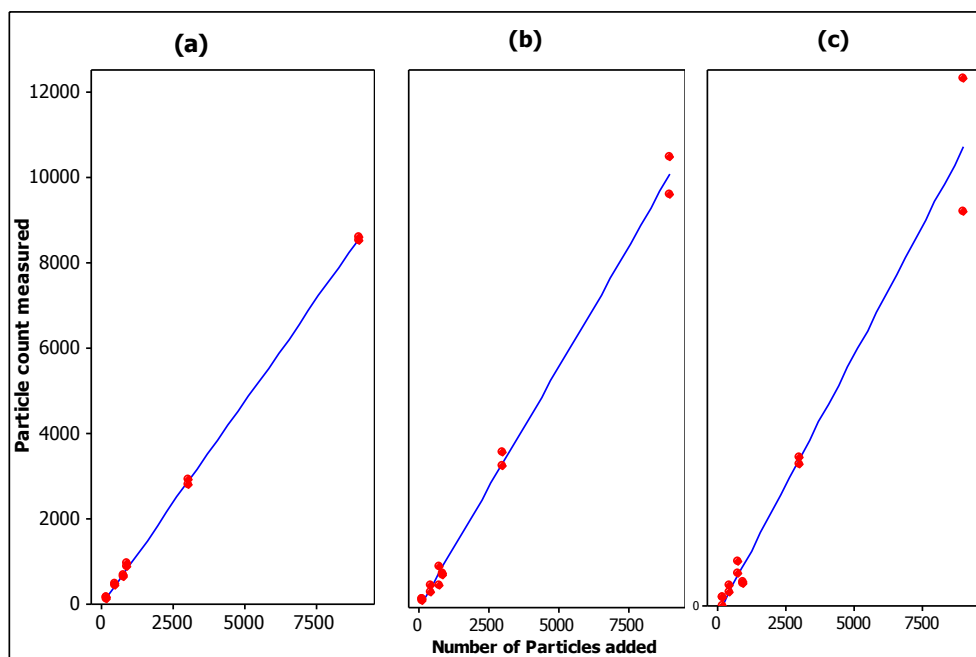


Figure 195 Line plots for the 10 μm particle count measured by LO (y axis) versus the number of particles added (x axis) on (a) the CLP method and (b and c) the beaker simulated use method. Results from the beaker method are from (a) step 7 (pre track) and (b) step 11 (post track) outlined in Figure 36.

Figure 196 shows the particle counts for 10 and 25 μm particles plotted as a percentage of the number of particles added to the CLP and Beaker methods. The variation on the CLP method is lower than the beaker method, and the 25 μm particle counts are more variable than the 10 μm counts for the beaker method. It is apparent that the 10 μm particle count increases between the pre and post track measurements for the beaker method, probably due to the ingress of environmental particles from the track model and flushing syringe used as part of the procedure. The 25 μm particle count is decreased compared to that for the 10 μm particle count, and becomes much more variable between the two beaker measurements. This may be due to particles falling out of suspension (stratifying) or becoming entrapped in the track model.

Appendix 1

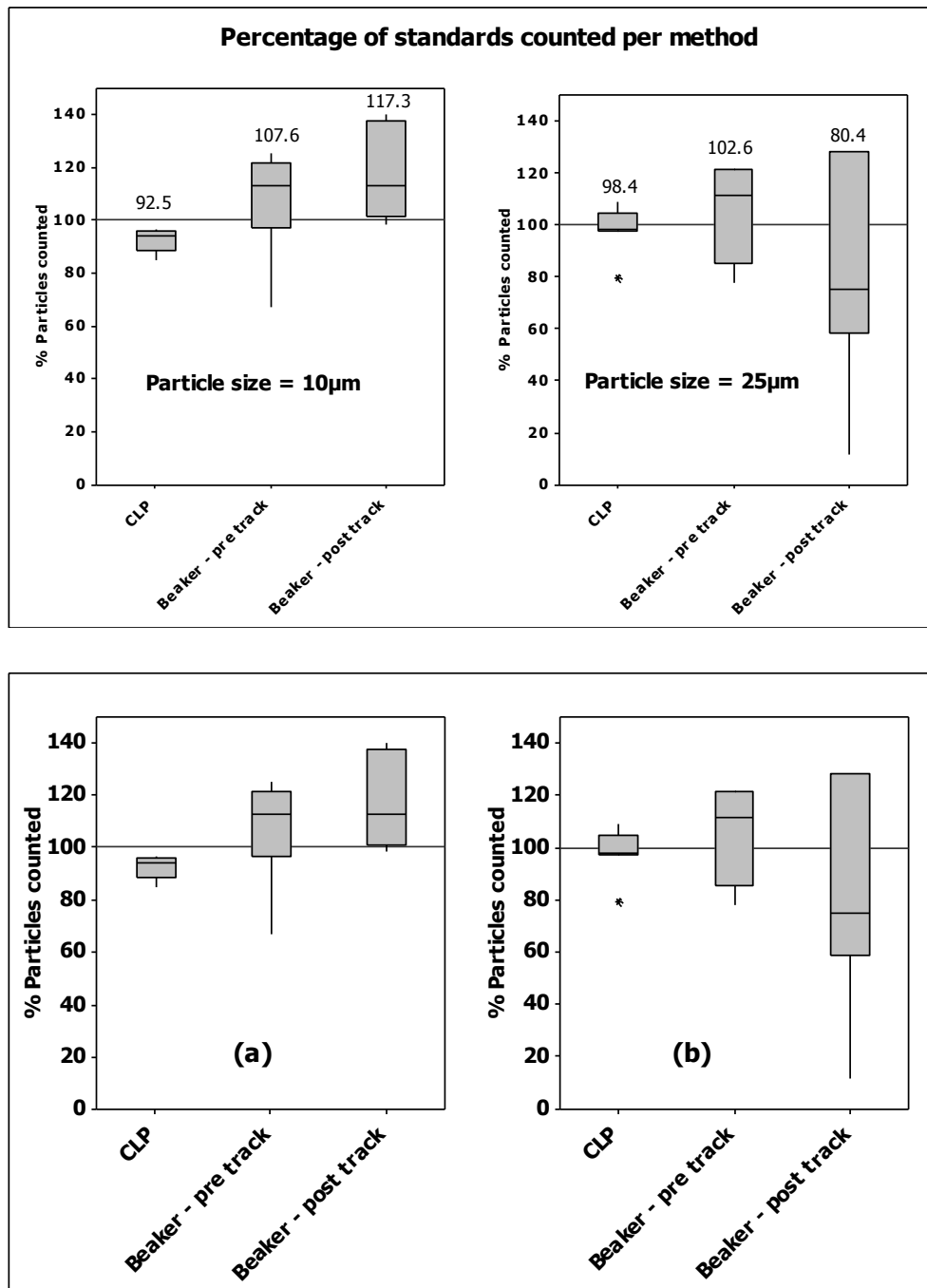


Figure 196 Plots of the percentage of (a) 10 µm particles and (b) 25 µm particles counted for the CLP method and beaker simulated use method. Results from the beaker method are from step 7 (pre track) and step 11 (post track) outlined in Figure 36.

Following on from this, a comparison between methods using stent delivery systems (SDSs) was performed. The SDSs used for this comparison are TAXUS Liberté products manufactured by Boston Scientific. Three operators trained and experienced in both methods were each given 10 devices from the same batch of product and asked to test them, 5 on each method. The test is destructive so that a sample once analysed cannot be reanalysed, from experience, replicate measurements of at least 5 samples are

Appendix 1

required for meaningful comparisons between groups. The output from the test method comparison for the $\geq 10 \mu\text{m}$ and $25 \mu\text{m}$ particle counts is given in Figure 197 and Figure 198 respectively. It is apparent from the data that the CLP method is much more repeatable than the beaker method.

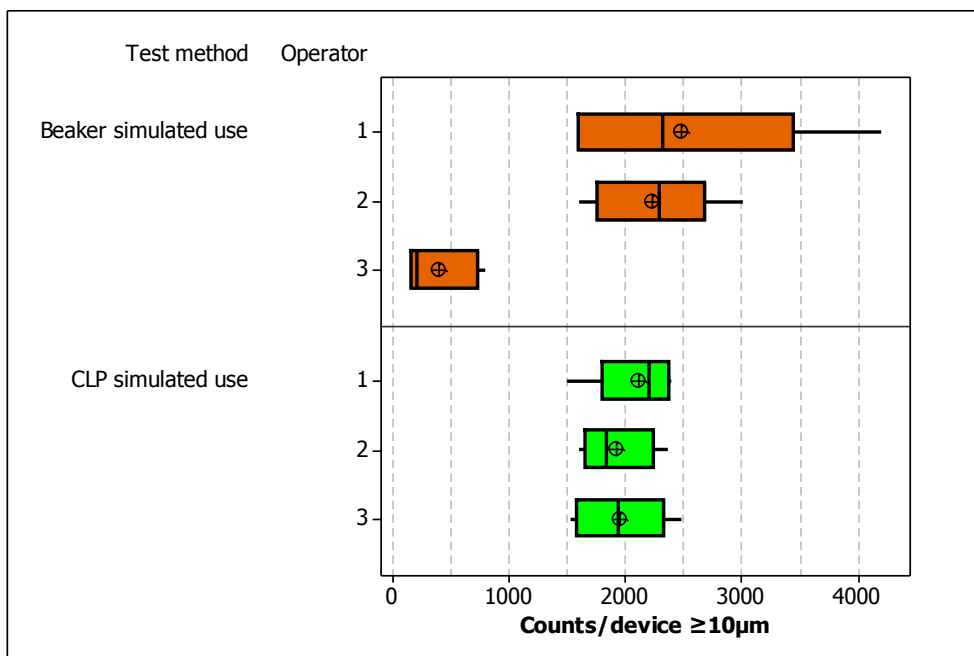


Figure 197 Plot showing the $\geq 10 \mu\text{m}$ particle count results achieved by 3 operators on the beaker method (in orange) and CLP simulated use test method (in green).

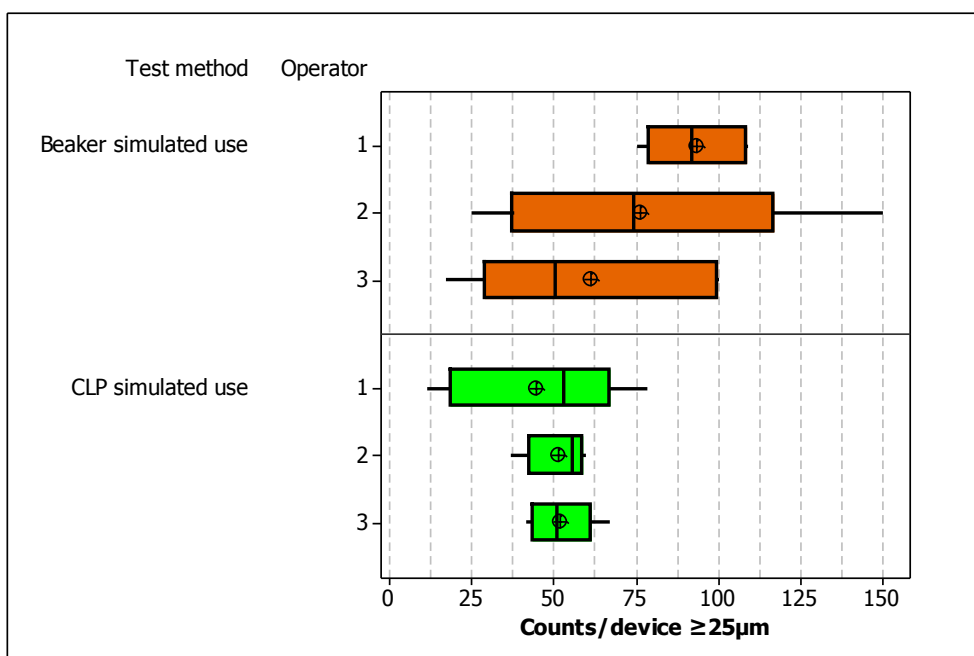


Figure 198 Plot showing the $\geq 25 \mu\text{m}$ particle count results achieved by 3 operators on the beaker method (in orange) and CLP simulated use test method (in green).

Appendix 1

While it was encouraging to see that the CLP apparatus was capable of generating repeatable results with standards and devices, the cause of the variation in the beaker method results was investigated. The results from the simpler beaker method, the product cleanliness method described in section 2.1.2.1, were compared to the CLP method. The product cleanliness method is not a simulated use method, the stent is deployed in one beaker of LPW water and the catheter is coiled up and placed in another beaker of LPW water, refer to Figure 199 for an image of the coiled catheter. An aliquot of the water from both beakers is tested for particulate matter and the sum is used to give a total particulate matter count for the device.

The results from testing 241 devices in the product cleanliness method and for testing 159 devices in the CLP method are plotted in Figure 200. It should be noted that the manifold of the device is not included in the rinse for the CLP method; this is because the manifold is external to the patient's artery during the clinical procedure. However, notwithstanding the fact that less of the device is tested in the CLP method than the product cleanliness method the results are dramatically different. Given that the CLP method should represent a greater challenge to the product because it is tracked through a tortuous pathway it is surprising to see that the average product cleanliness particle counts is much higher and the data is much more variable.

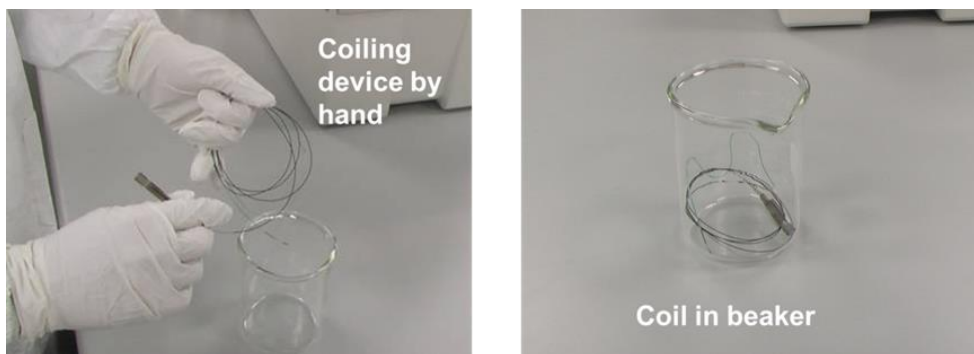


Figure 199 Technique for coiling a catheter for evaluation by the product cleanliness method.

Appendix 1

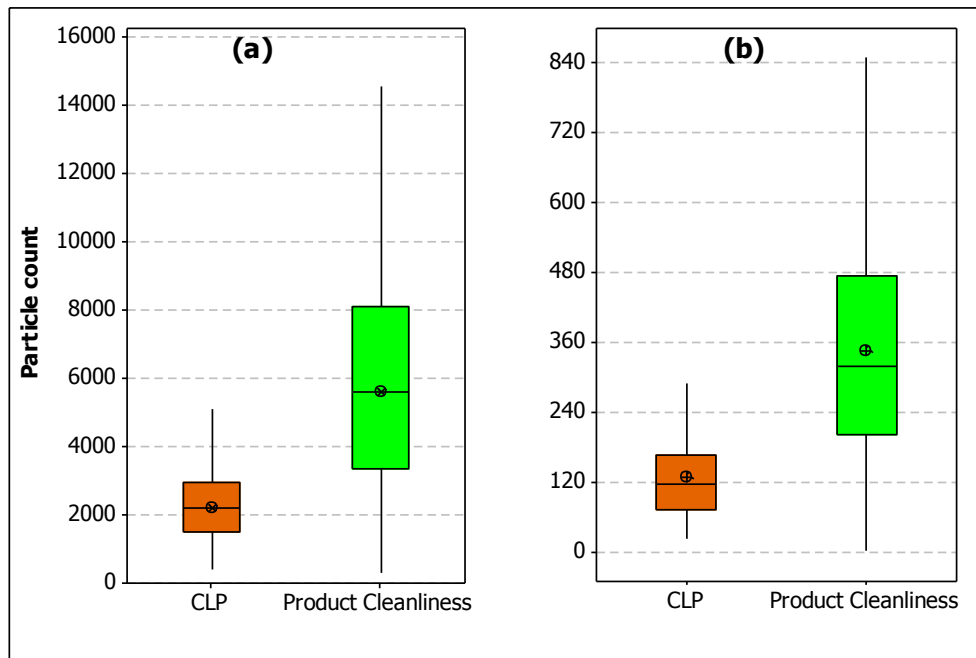


Figure 200 (a) $\geq 10 \mu\text{m}$ and (b) $\geq 25 \mu\text{m}$ particle counts generated by testing 159 devices using the CLP method (in orange) and 241 devices in product cleanliness beaker method (in green).

A reason for the offset between the two methods was believed to be the technique used to coil the catheter, which is operator dependant. Conical flasks, it was discovered allow for easier coiling of devices than beakers, the sloping sides shape the catheters into a repeatable, neat coil at the base (refer to Figure 201). The narrow neck also facilitates clamping of the proximal end and manifold in order to fix the device in place during the test.

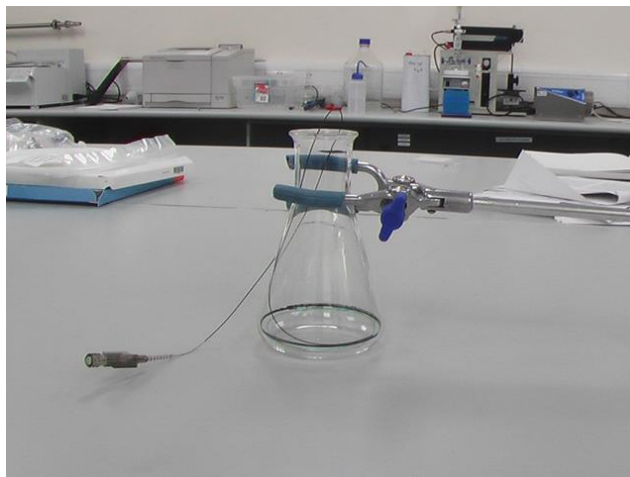


Figure 201 Image of an SDS coiled and clamped in a conical flask.

Twenty (20) devices from the same batch were analysed using the CLP method, using a straight capillary track in place of the tortuous track model, and 10 devices were tested using a version of the product cleanliness method but with 200 ml conical flasks in

Appendix 1

place of beakers. A blank reading was first obtained from the water in the conical flask, then 1,025 mm of the device was coiled into the water and the stent deployed in the same flask. The flask was then swirled for 30secs, the device was removed and the solution immediately analysed for particulate matter. Five (5) devices were also tested on each method to measure the particle contribution from the manifold and the proximal end of the catheter which is not normally tested in the simulated use methods, because this portion of the catheter is not designed for use in the body.

Figure 202 and Figure 203 show the results from the distal section of the catheter (approximately 1 metre) and deployment, and the proximal section of the catheter including the manifold respectively. This test returned values that were approximately 150% of devices tested using the CLP method. However the variation in data decreased greatly from that collected using the product cleanliness beaker method, previously shown in Figure 200. The particle counts measured from the manifold confirm that the additional particles observed in Figure 200 on the product cleanliness method were not entirely from the manifold.

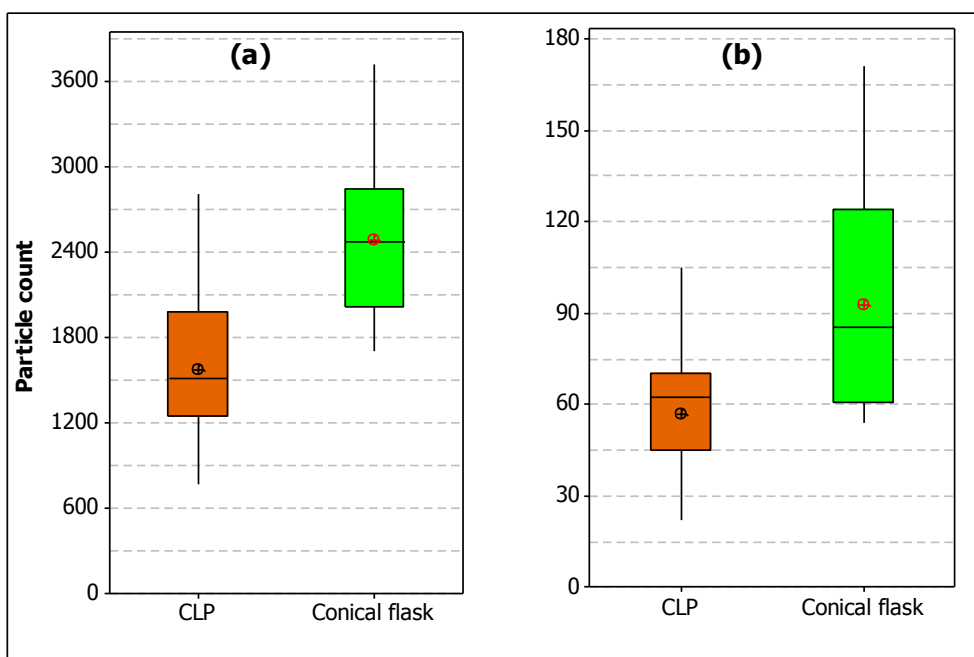


Figure 202 Plot (a) $\geq 10 \mu\text{m}$ and plot (b) $\geq 25 \mu\text{m}$ showing particle counts from 20 devices tested with the CLP method (in orange) versus 10 devices tested with the conical flask method (in green). The distal 1,025 mm section of the catheter and deployment were tested.

Appendix 1

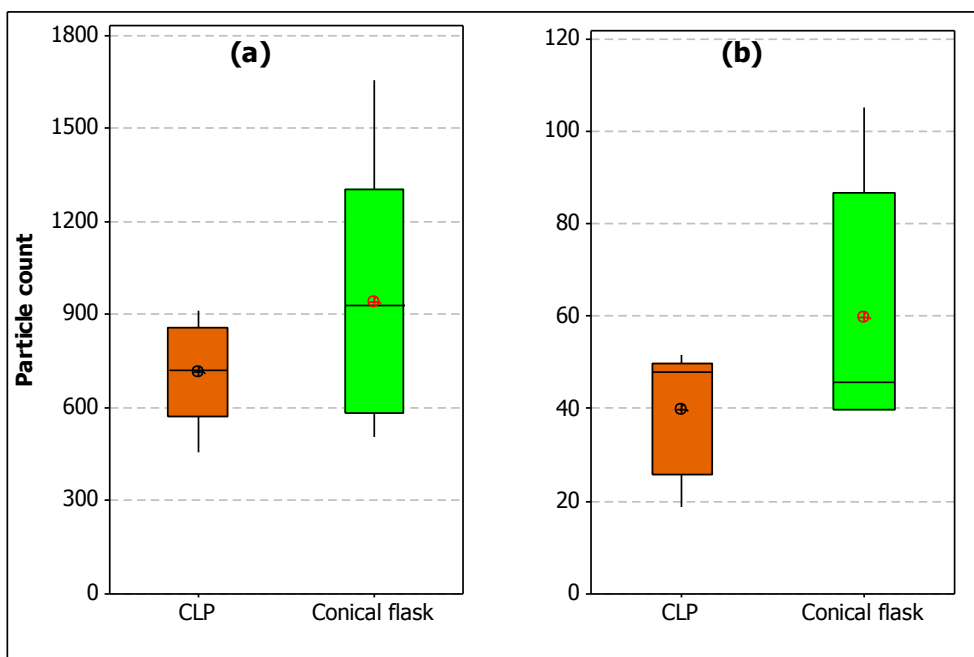


Figure 203 Plot (a) $\geq 10 \mu\text{m}$ and plot (b) $\geq 25 \mu\text{m}$ showing particle counts from 20 devices tested with the CLP method (in orange) versus 10 devices tested with the conical flask method (in green). The proximal section of the catheter, including the manifold were tested.

Next, the effect on particle count of conical flask diameter or number of coils that the catheter is wound was carried out. Three (3) different diameter conical flasks with 65, 85 and 110 mm diameter were selected. Five (5) catheters from the same batch were tested in the 3 different size conical flasks and compared against particle counts from the CLP apparatus on a track model without any curves. It is apparent from the results shown Figure 204 that a greater number of particles shed using smaller diameter flasks. The 110 mm diameter conical flask gave similar results to the CLP equipment with a non-tortuous artery track model. The data may explain the variation seen in the product cleanliness particulate data shown in Figure 200, as for this method the catheter is coiled by hand and there is no control over the diameter of the coil. In conclusion to this section, even though the simulated use and product cleanliness beaker methods appear to be straight forward and simple they are susceptible to a great deal of variation, limiting their use as comparative tests. Controlling the diameter of the coil using a standard conical flask greatly reduces variation in the data.

Appendix 1

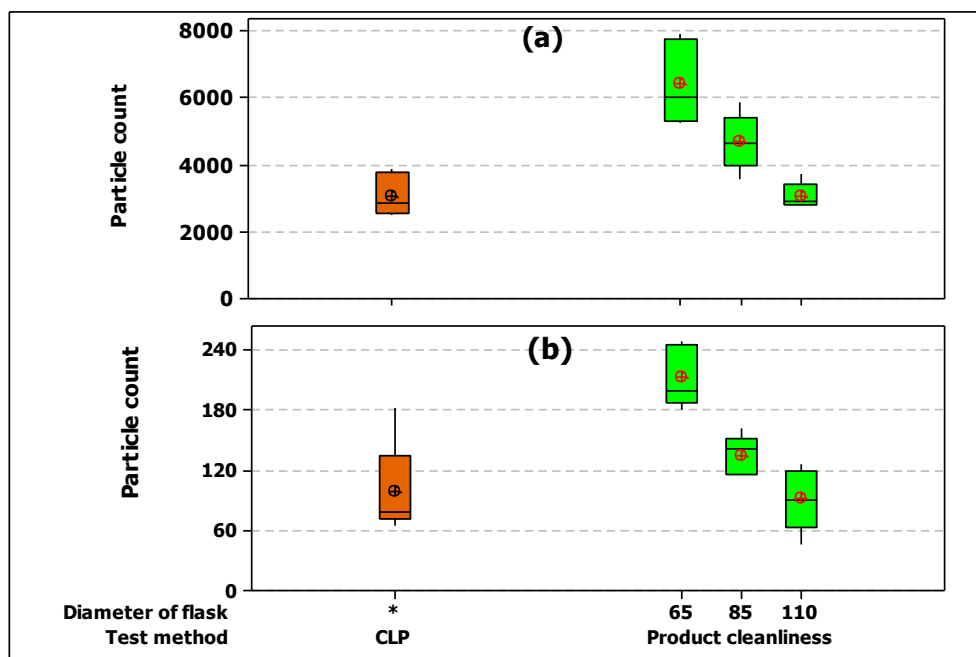


Figure 204 Plot (a) $\geq 10 \mu\text{m}$ and plot (b) $\geq 25 \mu\text{m}$ showing the particle count from 5 SDS devices in 3 different diameter conical flasks with 65, 85 and 110 mm diameter (in green) compared against particle counts from the CLP apparatus on a track model without any curves (in orange).

7.5 Tortuosity of artery track fixture

Given that the level of particles removed from catheters may be dependent upon the interaction between the test fixture and the test sample. The tortuosity of the simulated artery fixture was evaluated to understand this relationship more fully. The number of curves, internal diameter, and shape of artery fixtures were thus assessed by fabricating 8 different simulated artery models, Figure 205. Five (5) devices from the same batch were tracked through each artery fixture and a particle count gathered - Figure 205. The 8 arterial track models clearly result in different $\geq 10\mu\text{m}$ particle counts, with those models having the fewest curves (track models *d* and *e*) producing the fewest particles.

To further understand the impact of tracking through a fixed arterial model the devices were then retracted and reinserted 5 more times after taking the initial measurement and a second particle count measured, the results of this 5X track experiment are shown in Figure 206. The impact of further tracking of the devices through the arterial models acts to further highlight the effect of the shape of the tortuous path. Interestingly the diameter of the track model has no significant effect as can be seen by comparing track models *a* and *b*. The coiled track models *f* and *g* are the spiral equivalents of the serpentine track models *b* and *c*, respectively. The spiral shape results in more

Appendix 1

interaction between the catheter and the wall of the capillary, and this is the most probable explanation for the higher particle counts observed in the spiral model versus their serpentine counter parts. The link between the level of interaction between the catheter and the walls of the rack model is further highlighted by comparing the particle counts from track model *h* and *a*. Track model *h* has a larger radius of curvature than track model *a*, this will result in more friction between the catheter and the inside lumen of the capillary as it rounds the curves of larger radius.

These experiments emphasise the difficulty with acquiring particle counts from medical devices under simulated use conditions. The number of particles removed from the device and counted will be relative to the test apparatus selected and the test procedure. Such as the tortuosity of the arterial track model, the number of times the device is manoeuvred through the track model and many other parameters that can influence the device to test apparatus interaction. However, accepting that the number of particles counted will be inextricably linked to the test method conditions, the variability in the results can be minimised by the development of a controlled test procedure. Repeatability of the conditioning steps used to assess the sample for particulate matter is of paramount importance. This repeatability can only be achieved by understanding the many variables that may impact upon particle counts. These variables include the properties of the materials that the device is made from, the properties of the particles, the test equipment, and the intended use of the device.

Appendix 1

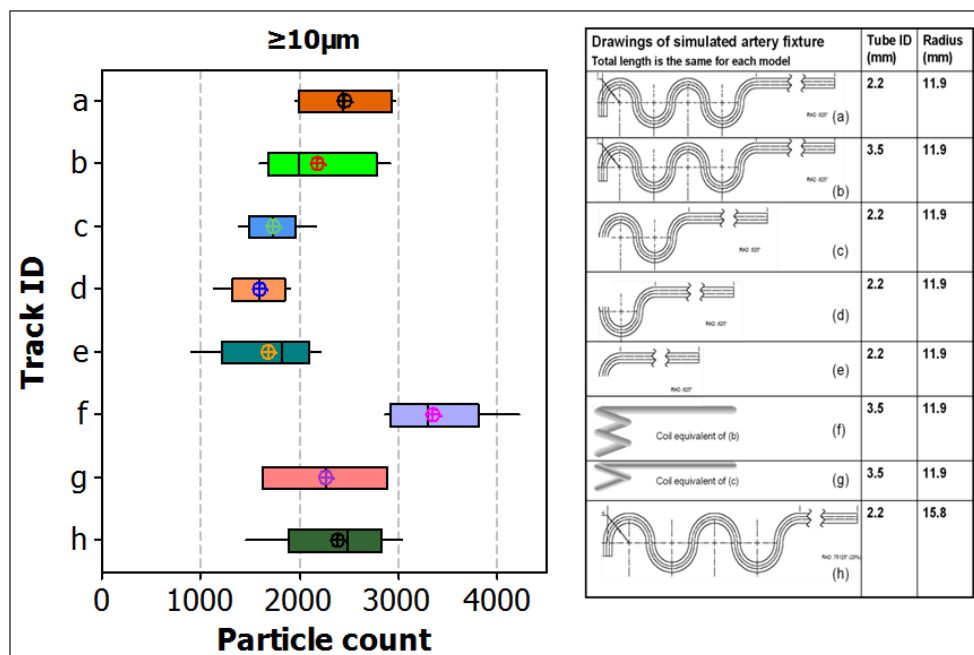


Figure 205 Comparison of the effect of different arterial track models after 1 track through the model on the $\geq 10 \mu\text{m}$ particle count from an SDS device.

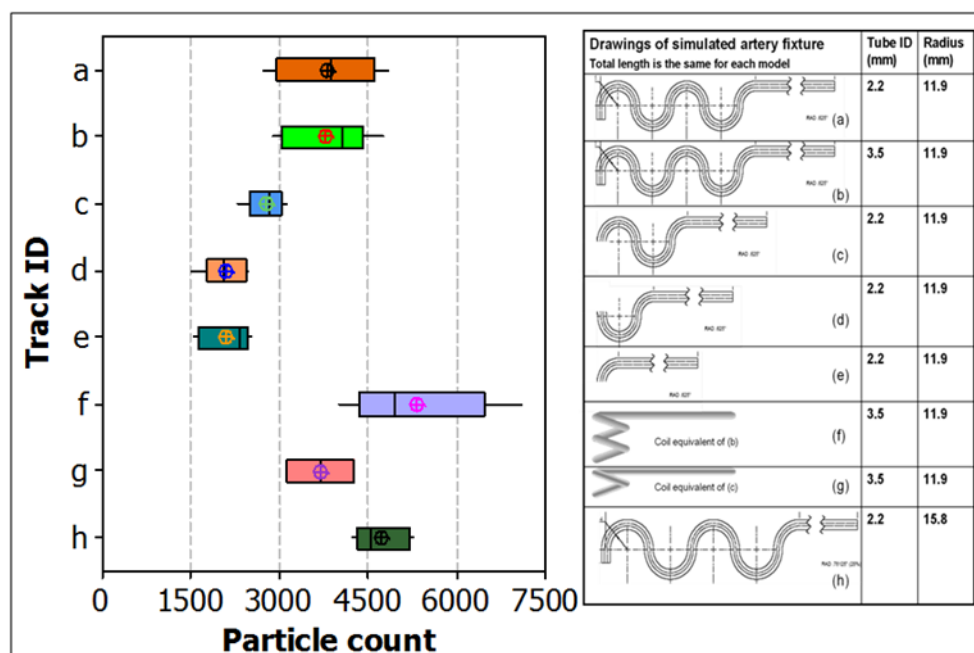


Figure 206 Comparison of the effect of different arterial track models after 5 tracks through the model on the $\geq 10 \mu\text{m}$ particle count from an SDS device.

7.6 Dual closed loop particulate apparatus

The dual closed loop particulate apparatus (DLP) finally adopted differs from the early DLP prototypes in that the sampling loop is driven by a peristaltic pump and not the

Appendix 1

proprietary syringe pump supplied with the particle counter. The DLP design differs from the CLP in several ways. The new design includes a completely redesigned mixing chamber with a second pump for the extra loop, and an additional third pump to drain the equipment. The DLP apparatus is designed specifically to achieve much higher agitation through increased flow rate, and thus the internal diameter of the pump tubing in the circulation loop was increased from 2.4 to 8mm to achieve these flow rates. A schematic drawing of the dual closed loop apparatus is shown in Figure 207. Optimisation of equipment blanking is also facilitated by way of real-time measurement of the particle counts during rinsing. The increased flow rate necessitates the use of more LPW, and to accommodate this, a larger 10L LPW reservoir was designed and filtration of the water is carried out in-line rather than separately into bottles.

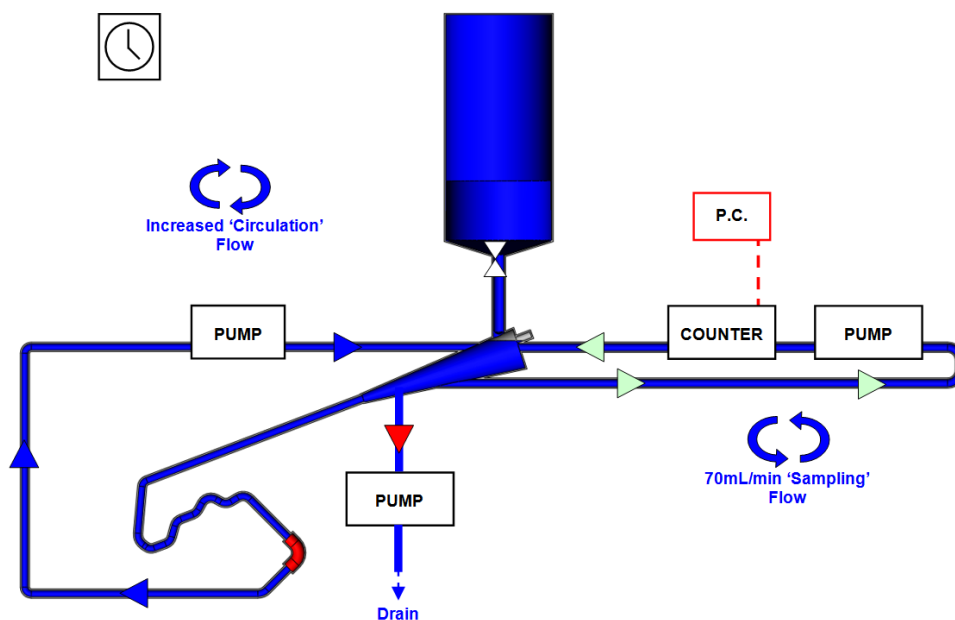


Figure 207 Schematic drawing of the dual closed loop apparatus.

7.7 Dual loop particulate equipment design

The major design changes that occurred between the single closed loop apparatus (CLP) and the dual closed loop apparatus (DLP) were introduced to enable suspension of larger particles. This was achieved by increasing the flow rate of the system. A modification of the existing CLP system in the laboratory was carried out to prove the concept before starting work on a final design. However, in the CLP system configuration, increasing the flow-rate in the single closed loop increases the flow-rate through the laser counter. The laser counter is calibrated to work with a sample rate of

Appendix 1

70 mL/min which is deemed by the supplier as the maximum sample rate it can operate at without reducing accuracy and reliability, so increasing the flow-rate in the CLP configuration would cause significant inaccuracies in the laser counter. Increasing the flow-rate through the laser counter also introduces the risk of breaking the flow cell due to the increase in pressure; therefore the decision was made to split the system into a dual loop configuration. The first, circulation loop can be adjusted to operate at flow rates higher than 70mL/min in order to transport and suspend particles without any risk on the performance or integrity of the laser counter. A second, detector loop was introduced to feed from the sample loop at 70mL/min and present the particles to the laser counter.

As a result of introducing a second loop at a higher flow rate some modifications to the glassware were made. Many of these changes were incorporated to prevent the formation of bubbles, which can mistakenly be counted as particles by the detector, this phenomenon is further discussed in section 7.13.1.

The closed loop particulate test equipment consists of 3 main functional parts, these 3 parts are:

- 1) The detector.
- 2) The water handling/circulation system.
- 3) The sample test fixture.

The sample test fixture is designed to be swapped out depending upon the nature of test required, such as the simulated use test which requires the ASTM tortuous track fixture, or the baseline test which requires unconstrained deployment without tracking. The equipment forms a closed system of fixed volume when all three parts are integrated together. A rigid frame assembly is used to house and support the various components of the equipment. Finally, the entire system is placed in a laminar airflow (LAF) hood that uses HEPA filtered air to reduce environmental contamination of the system and to provide a clean bench for the handling of test samples. Figure 208 shows a basic schematic of the particulate equipment

Appendix 1

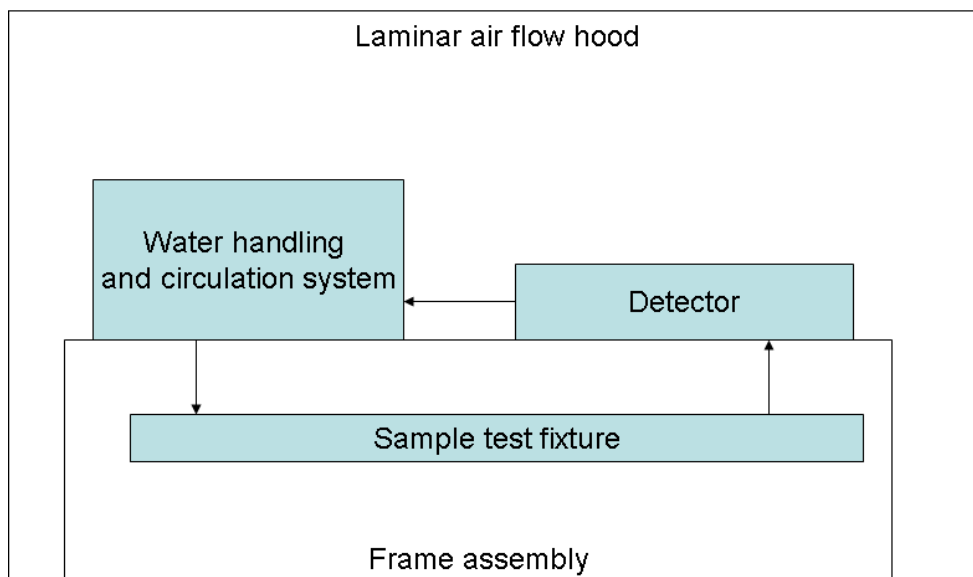


Figure 208 Schematic of modular particulate test apparatus

7.7.1 Water handling and circulation system

The water handling and circulation system describes the mechanisms used to introduce water to the particulate test equipment, circulate it through the equipment and finally drain it away. A schematic of the water handling and circulation system used in the DLP apparatus is shown in Figure 209. Water is introduced to a 10 litre reservoir through a 0.2 μm filter; this reservoir is used to hold low particulate water for use in cleaning the test equipment and for taking measurements. A hand operated valve is used to dispense the water in to the sample test fixture. Water is drained from the test equipment using a peristaltic pump attached to a siphon tube located in the sample test fixture. When switched on the pump sucks the water from the test equipment and dispenses it to waste.

Appendix 1

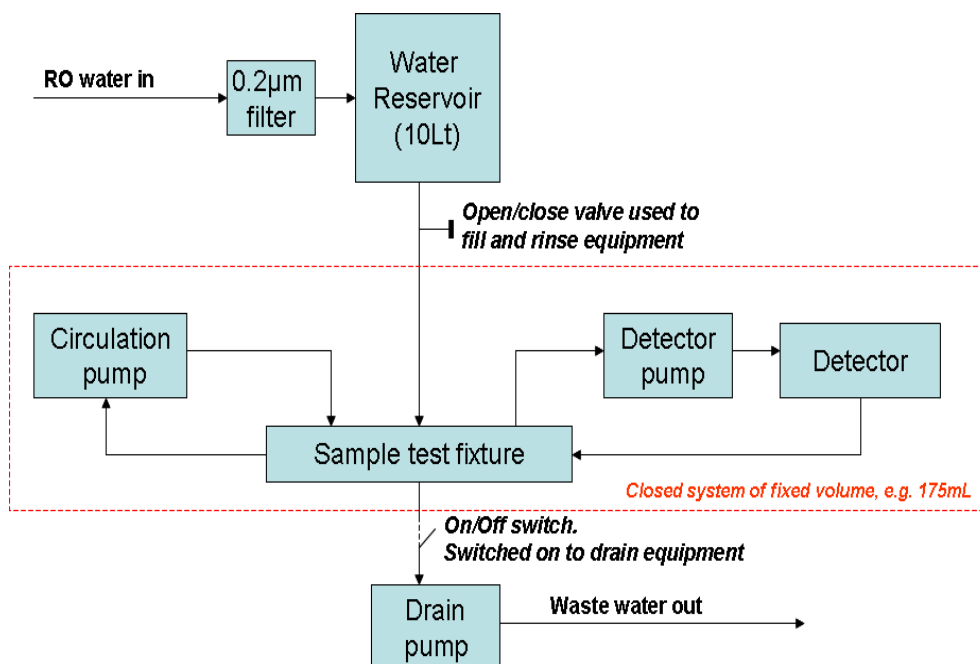


Figure 209 Schematic of water handling and circulation system. The broken red line encloses the components that make up the closed system where a fixed volume of water is circulated during measurements.

Water is circulated through the sample test fixture using a peristaltic pump; this circulation pump^{§§§} has two functions:

- 1) To distribute particles homogeneously throughout the test equipment by maintaining continuous circulation and mixing during measurements.
- 2) To agitate the water to prevent particles from settling out of suspension, thereby ensuring that larger particles are counted and sized by the detector.

When preparing the system prior to taking a measurement the circulation pump is switched to reverse to purge the equipment of air, once the system is free of air the circulation pump is returned to the forward direction. The circulation pump is sometimes switched off to allow for specific actions to be carried out; the reasons for these pump stoppages are as follows:

^{§§§} The circulation pump remains switched on and pumping in the forward direction for every measurement.

Appendix 1

- 1) When balloon catheters are inflated in the sample test fixture they prevent flow of water through the circuit, with the pump switched on this would cause generation of air bubbles which would be counted as particles in the detector.
- 2) The flow of water over deployed stents in an unconstrained vessel can cause them to move which in turn makes it impossible for the placement of a secondary balloon catheter in the stent to be used for overexpansion.
- 3) When introducing multiple aliquots of particle standards to the equipment the pump is switched off to allow time for the operator to dispense all of the standard solution in to the test equipment.

After completion of these actions and before taking a measurement, the pump is always switched on again and allowed to circulate for a predetermined time, which has been validated using particle count standards to ensure adequate mixing before taking a measurement.

The detector pump is used to circulate water from the sample test fixture and flow it through the LO detector. The detector pump is fitted with 2.4 mm internal diameter tubing and is calibrated to run at a flow rate of 70 ± 2 mL/min. The LO detector is calibrated to count and size particles at 70 mL/min by the manufacturer and this flow rate must be maintained to ensure accurate measurements. The liquid is pumped in a circuit from the test sample fixture through the detector and back into the test sample fixture again, this circuit is relatively short and has a narrow internal diameter to ensure that particles cannot drop out of suspension. The detector pump is operated continually throughout measurements and is only stopped when the test equipment is idle. The detector pump is briefly operated in reverse prior to taking blank measurements to purge the detector and tubing of air bubbles, the pump is returned to the forward direction before beginning each measurement.

7.7.2 Sample test fixture

The function of the sample test fixture is to provide a fixture to introduce and contain the test sample whilst allowing for the capture of any particulate matter in an aqueous suspension. The fixture has ports to provide integration to the water handling and circulation system. The sample test fixture has variable design features required for specific tests.

Appendix 1

Common to all of the sample test fixtures is the mixing chamber. This chamber has several functions, these are:

- 1) Agitation and mixing of water in the system using the circulation loop which has its exit and entry ports in the mixing chamber.
- 2) Sampling point for the detector loop; and return point for the detector loop.
- 3) Entry point for test samples (devices) and for reference standards.
- 4) Entry point for low particulate water from reservoir.
- 5) The water fill level is indicated on the side of the mixing chamber, this ensures that the system is always filled with the same volume of water for measurements.
- 6) The siphon for draining the system is located in the mixing chamber.

Figure 210 shows a schematic of how the mixing chamber integrates with the rest of the equipment.

The DLP test equipment forms two loops, a *circulation loop* that runs at a high flow rate and is powered by the circulation pump, and the *detector loop* that runs at 70mL/min and is powered by the detector pump. The mixing chamber is common to both loops, thus the detector is continually sampling from the entire volume of liquid used during a test. The length of time for each measurement determines the total volume measured, i.e. $2 \text{ min} \times 70 \text{ mL/min} = 140 \text{ mL}$. The volume of liquid sampled was determined during test method development and is based on achieving acceptable count accuracy on the recovery of a known quantity of reference particles added to the test equipment.

Throughout measurements the water in the DLP system is under continuous circulation through both loops and is mixed in the mixing chamber, thereby ensuring that the particles are homogeneously distributed throughout the entire volume of water in the closed system. This feature is very useful because no water and particles are removed during a measurement, this allows for the sampling of the volume of the entire system multiple times over, or for continuous measurement if required. This provides the capability of obtaining a very accurate measure of the particles in the system which is especially important when very few particles are present, and in which case a large volume of water must be sampled to provide statistically sufficient data.

Appendix 1

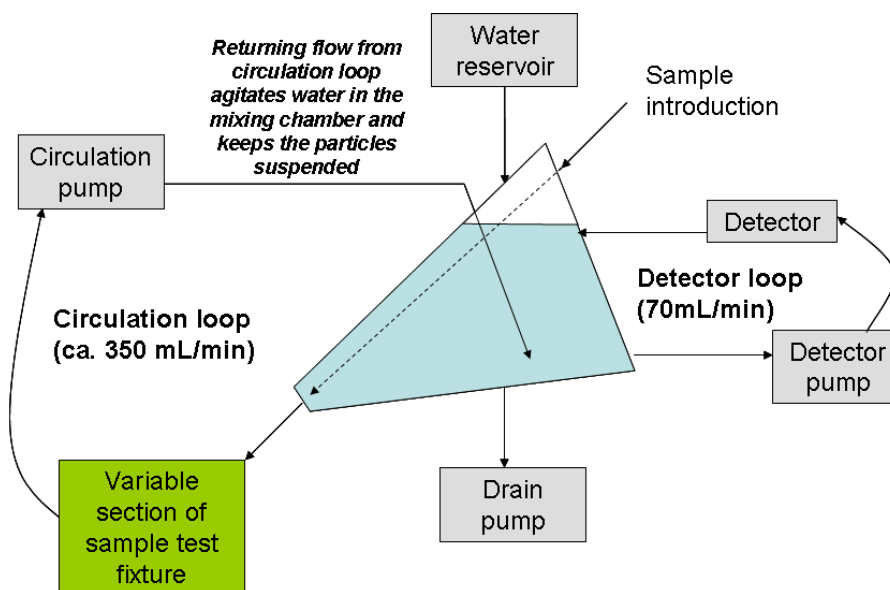


Figure 210 Schematic of the mixing chamber showing how it integrates with the other components of the test equipment.

The test devices are introduced via a glass capillary in the mixing chamber, the exit point from this capillary is under the level of water, and as such any particles on the devices exiting the capillary will be removed into the surrounding water. Devices are advanced through the capillary and exit the mixing chamber to a section of the sample test fixture that differs in design depending on the test method required. This variable section is also an integral part of the circulation loop; therefore any particles removed from the device are re-circulated into the mixing chamber where they can be sampled by the detector.

Particle reference standards are introduced to the mixing chamber through a port above the level of the water in the system. The particles are supplied as a suspension and are injected either by syringe or pipette under the level of the water in the mixing chamber. The reference particles are mixed and dispersed throughout the entire system by the circulation loop, and are sampled by the detector loop. A wait time is required to achieve a homogeneous dispersion of the particles; this was established during development of the methods and was validated in method validation. The wait time is observed before every blank, standard and device measurement to ensure adequate dispersion of particles.

7.8 Separation of measurement steps

The challenges of separating the particle count contribution of one simulated step from another, mentioned earlier in section 7.3, will be addressed in more detail here. The difficulty with the particulate matter tests required for medical devices are that the test sample is comprised of solid components that need to be washed to remove particles prior to analysis. In accordance with the regulatory guidelines the test samples may have to be preconditioned in very particular ways to obtain this suspension of particles in solution such as after tracking of the device through a specific tortuous pathway, deployment of a stent, inclusion of compatible accessory devices, etc[10], [37]. Particles obtained in this manner are not the same as those sampled from parenteral products. Particles in a parenteral liquid have reached equilibrium with their environment, however particles just wetted on a medical device may take a period of time to reach this equilibrium. They may swell, dissolve, break apart, etc. All of this makes it more difficult to develop a reproducible test method to evaluate particles from medical devices.

The change in particle count was explored by taking the water used to wash devices and analysing it over time. Firstly, SDSs were tracked through the CLP apparatus 20 times in order to create a substantial particle count. Measurements were taken of the solutions at several time-points and compared to a control consisting of 10 μm size standards. The experiment was also conducted in parallel in conical flasks, using the product cleanliness method described in section 7.4; this was introduced as a further control.

The results of the experiment are shown in Figure 211. It can be seen that the SDS particle count decreases over time, especially in the $\geq 10 \mu\text{m}$ particle size channel. This decrease is not as a result of stratification as evidenced by the measured number of particle standards, which remains at the same level over time. The numbers of particles decrease in both the CLP and conical flasks. The rate of particle count reduction is non-linear, the CLP method shows a logarithm dependant rate of reduction with time. Therefore the decrease in particle count observed in the CLP method is not a consequence of particles sticking to the surfaces on the CLP apparatus (a potential root cause that had been speculated), for which a linear effect would be expected.

Appendix 1

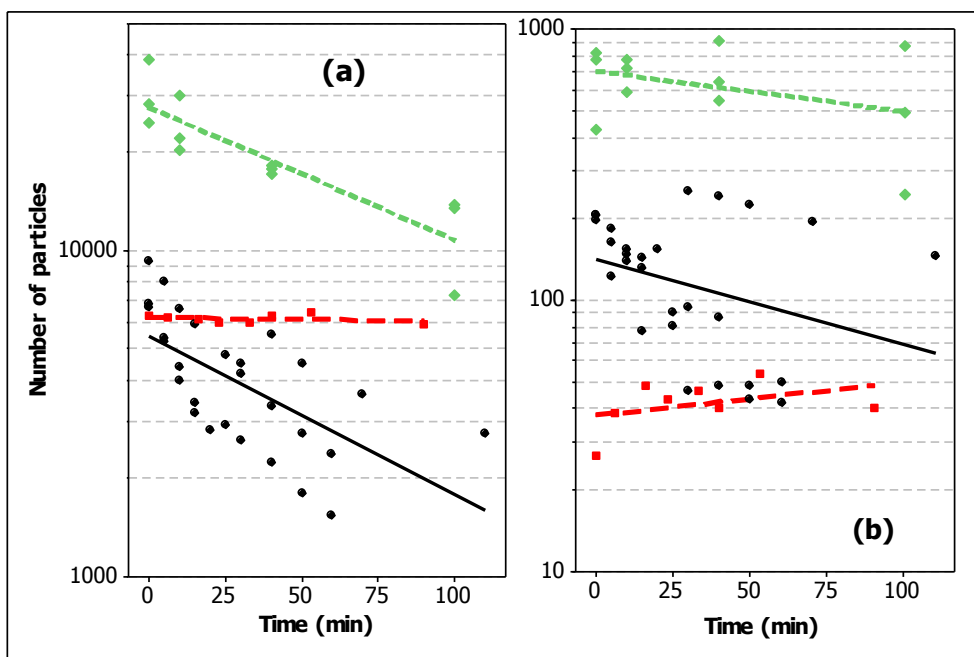


Figure 211 Plot (a) $\geq 10 \mu\text{m}$ and plot (b) $\geq 25 \mu\text{m}$ showing the behaviour of SDS particle counts over time using the CLP method (in black) and using a conical flask (in green). The particle count for $10 \mu\text{m}$ and $25 \mu\text{m}$ polystyrene reference standards added to the CLP method are also shown (in red). Note the x-axis has a log scale.

The data suggests that a mechanism other than stratification or adherence of particles to the equipment is occurring. The key to understanding what mechanism is involved was to identify the type of particles present. The mechanism was explored and is addressed in section 3.3.2, where it was shown that the particles observed in the experiment are Nylon-12 derived leachates which form particles that are water soluble. However at the time of the development of the test method this mechanism was not known, nonetheless the impact that this phenomenon has on the test method was a primary concern. The implication of the particles dissolving or breaking apart over time is that the particle count will be different depending upon the length of time taken to prepare the sample. In addition, the approach of taking cumulative measurements from sequential steps, such as tracking, deployment, retraction of an SDS in the same volume of liquid would prove to be troublesome, this is illustrated in Figure 212.

Appendix 1

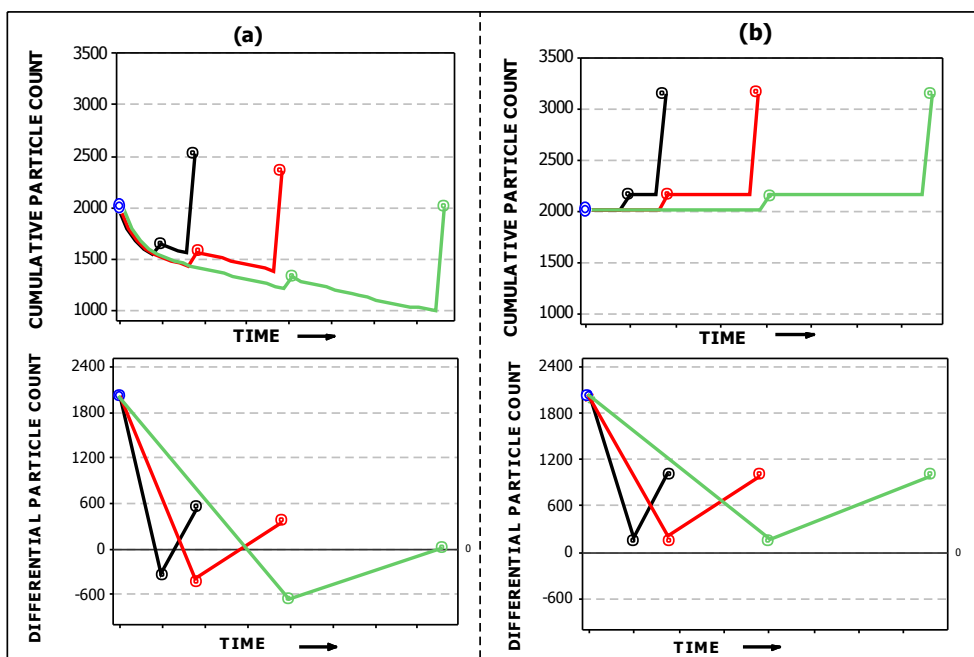


Figure 212 Hypothetical plots showing the effect of time on a system in which the quantity of particles reduces over time and in which more than one measurement must be acquired from a device. (a) The cumulative particle count (at the top) and differential particle count (at the bottom) from an SDS that is tracked, deployed and retracted in a CLP system in the same water, with separate particle counts acquired for each of the 3 steps. Three different scenarios are illustrated in which the length of time to carry out the test are varied, quick = black, normal = red, and slow = green. (b) 2 similar plots are shown, however in this case the CLP system is drained and blanked after each measurement; i.e. filled again with low particle water before proceeding with the next step.

The hypothetical plots shown in Figure 212 demonstrates how “one-pot” sequential measurements can lead to erroneous particle counts in a system where the quantity of particles reduces over time, and where more than one measurement must be acquired. The length of time between measurements is dependent on several factors, such as operator technique, inputting sample and measurement details in the software, and the completion of any preparation steps for the device. Depending on the type of test, it may be difficult to control this lag-time precisely, which can lead to biased and variable data. The plots are illustrative of the impact that the disappearance of particles created in earlier steps have on subsequent measurements. The overall result is an undercount of the true number of particles. In the case where the rate of disappearance of particles is in excess of the particle contribution from a subsequent step, the difference may be a negative particle count, which is a meaningless result.

Figure 212 (b) shows the effect of draining and blanking the CLP system after each measurement. The influence of diminishing particles over time is removed by re-establishing the baseline between each measurement. Unfortunately this leads to longer test times in general as a blank must be acquired between each measurement, however

Appendix 1

the integrity of the data requires such additional steps. Consequently, the approach of taking a blank between each measurement was adopted as the standard methodology for the particulate matter methods described in this thesis in which more than one measurement is required. Although, consideration was given to alternative approaches, detailed herein:

- 1) Change the test medium so that particles are prevented from disappearing, such as using an alternative liquid to water in which the particles are preserved. .
- 2) Use a correction factor based on dissolution rate of particles to adjust the particle count.

It was decided not to pursue approach (1) above, because the particles present may have varied physiochemical properties, a medium which would suit one particular particle type may not be compatible with others. In addition water is inexpensive, safe to handle and dispose of, and is relatively easy to filter to remove particles. Other non-aqueous media would not be so straightforward, and additives to water such as salts would present other issues with regard to precipitation and contamination of the equipment. Approach (2) above was not taken because it would require substantial effort with respect to understanding the type of particles present and their behaviour. It had already been established that the rate of disappearance of the particles is non-linear. The exact times for each test would need to be recorded and used in any calculation. This approach would require significant data manipulation and would be complex for multiple steps in which not all the particles generated may be of the same type.

Even with the implementation of inter-measurement blanking the test methods still need to be time-bound. The length of time given to track, deploy, retract, etc., devices is stipulated in the test procedures and these time intervals are observed even though the steps do not take the full time to carry out. This ensures that all samples are measured at the same time; therefore keeping the results relative. In this way it is possible to make meaningful comparisons between test groups and as a means to carry out trending and quality control of the devices.

A consequence of the approach taken to blank the system between measurements is that the device is sometimes left in the equipment while the equipment is being flushed out and filled again. This led to concerns about the impact of flushing water over the

Appendix 1

devices during this blanking process, the question posed was whether additional particles were removed during this process and were as such unaccounted for? The next section addresses this concern.

7.9 Blanking with devices in-situ

The device remains within the test fixture when re-blanking between some measurements. There may be concern about the possibility that some particles are removed during the blanking sequence resulting in non-measurement of device related particles. To prevent against this potential loss of particles no physical manipulation of the test articles occurs during blanking. However, blanking of the test equipment does involve circulation of water over the device. Therefore studies were carried out to determine if the circulating water removes particles from devices when rinsing the equipment between measurement steps.

The time taken to measure particles for the DLP method is 2 minutes. During this time water is continuously circulating through the test equipment. The particle count is gathered by sampling 4 x 35 mL aliquots of the water from the test equipment, with each 35 mL aliquot taking 30 seconds to measure. Therefore, the particle count can be expressed as a function of time over this 2 minute period, if the continuous flow over devices acted to wash off more particles, then the particle count would increase over this time period. Plots showing no increase in particle count over the 2 minutes are provided in Figure 213 collected from 21 separate measurements with an SDS device present. In addition, equipment blank measurements would be expected to increase over the 2 minute measurement time if particles are washed from devices, Figure 214 demonstrates that the number of particles remain constant during the blanking steps.

Appendix 1

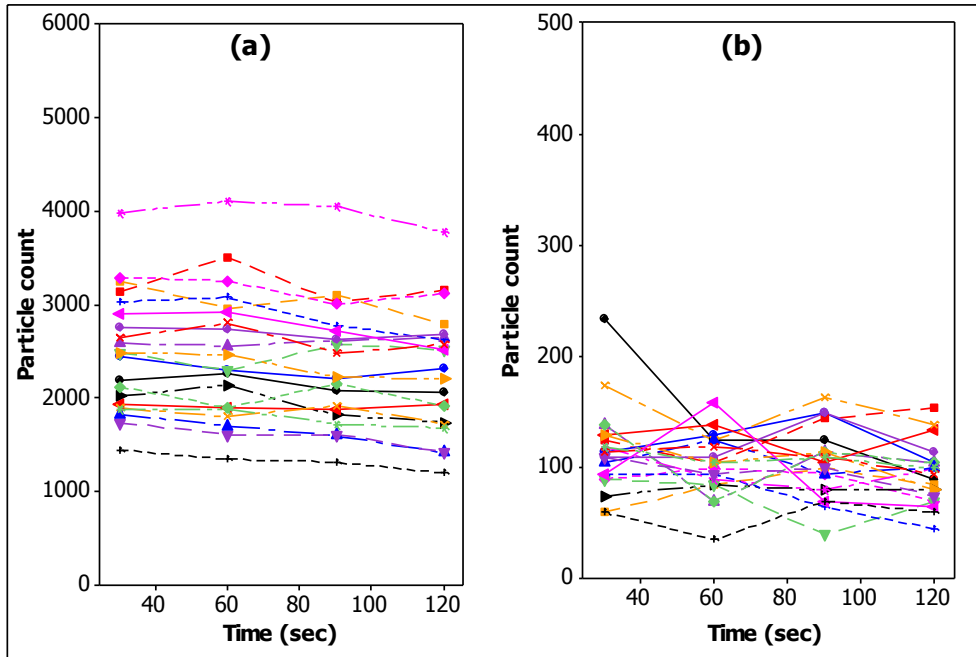


Figure 213 (a) $\geq 10 \mu\text{m}$ and (b) $\geq 25 \mu\text{m}$ particle counts from 21 separate measurements over 2 minutes when SDS devices are present in the DLP equipment.

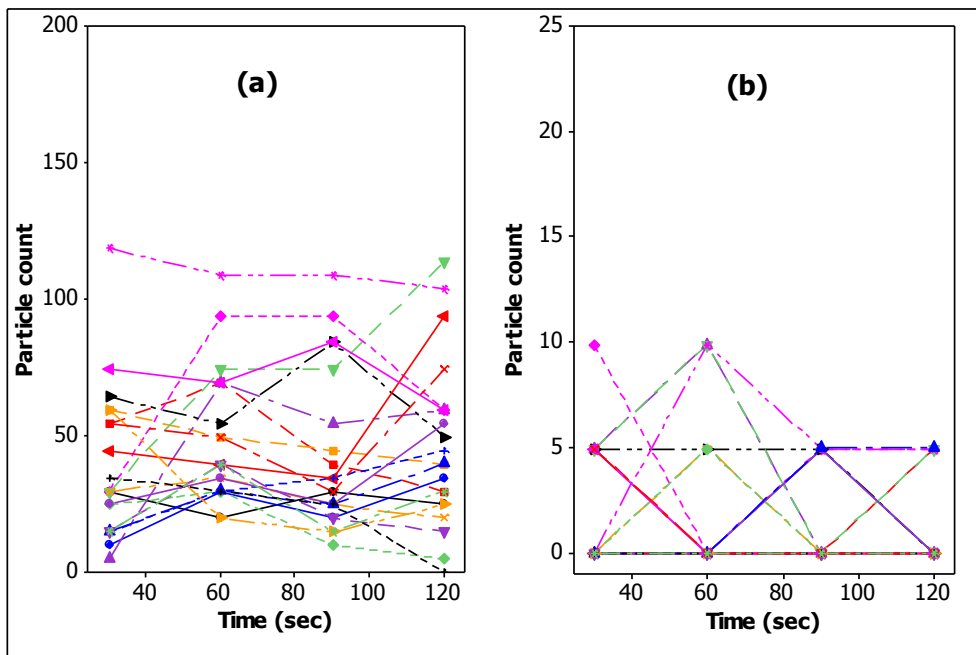


Figure 214 (a) $\geq 10 \mu\text{m}$ and (b) $\geq 25 \mu\text{m}$ particle counts from 21 separate blank measurements over 2 minutes as water is continuously circulating through the particulate test equipment with an SDS device present.

In order to demonstrate that no further particles are removed during blanking, some additional studies were carried out. The test equipment was set up as normal, and a blank measurement was taken. A stent delivery system (SDS) was tracked into test equipment and particle counting was commenced, instead of taking the normal 2 minute measurement the particle count was monitored over 5 minutes. Afterwards the water in

Appendix 1

the test equipment was drained away, and then it was filled with low particulate water. The SDS remained in-situ for the duration. A particle count was taken over a 20 minute period as the water in the test equipment was circulated over the device; this is representative of the typical blanking procedure where LPW is rinsed through the test equipment until all residual particulate from the previous measurement are removed. Figure 215 shows the results from this study, where the particle count after the device is placed in the test equipment does not increase over the initial 5 minute period. Figure 215 also shows that the particle count does not increase over a typical 20 minute blanking process****.

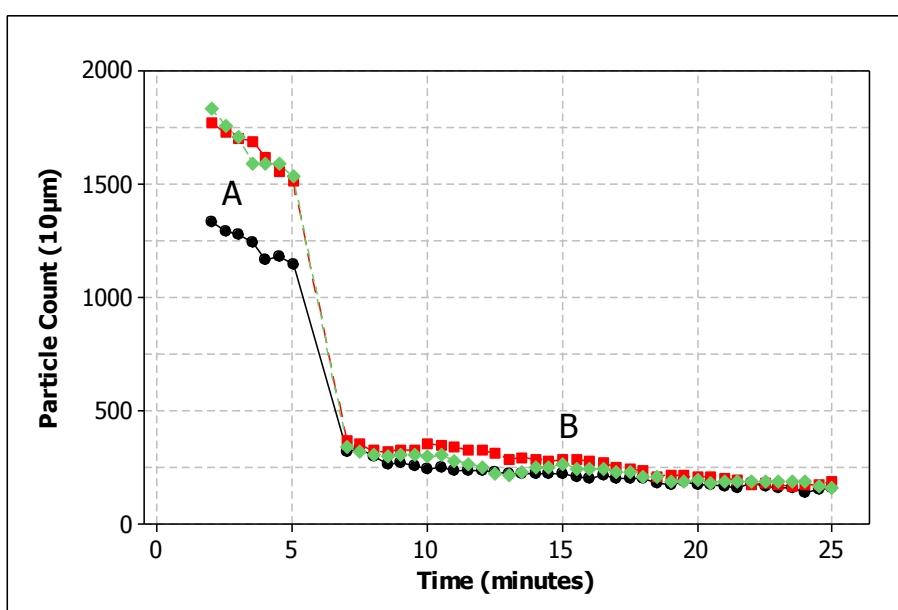


Figure 215 Plot showing (A) particle counts over 5 minutes with 3 separate devices in the particulate test equipment, and (B) after the device has been removed and the water has been replaced.

By way of demonstrating that residual particles remain in the test equipment after emptying the system once and then replenishing with low particulate water, 3,000 x 10 µm particles were added to a blanked system. Measurements were taken in the same way as described above for the SDS assessment. The results are shown in Figure 216.

**** Note that the residual particles remaining in the system for this study are above the blank acceptance criteria, which is ≤ 175 particles ≥ 10 µm. In a typical blanking process the number of residual particles is reduced by continuous draining of the water in the system while replenishing it with more low particulate water.

Appendix 1

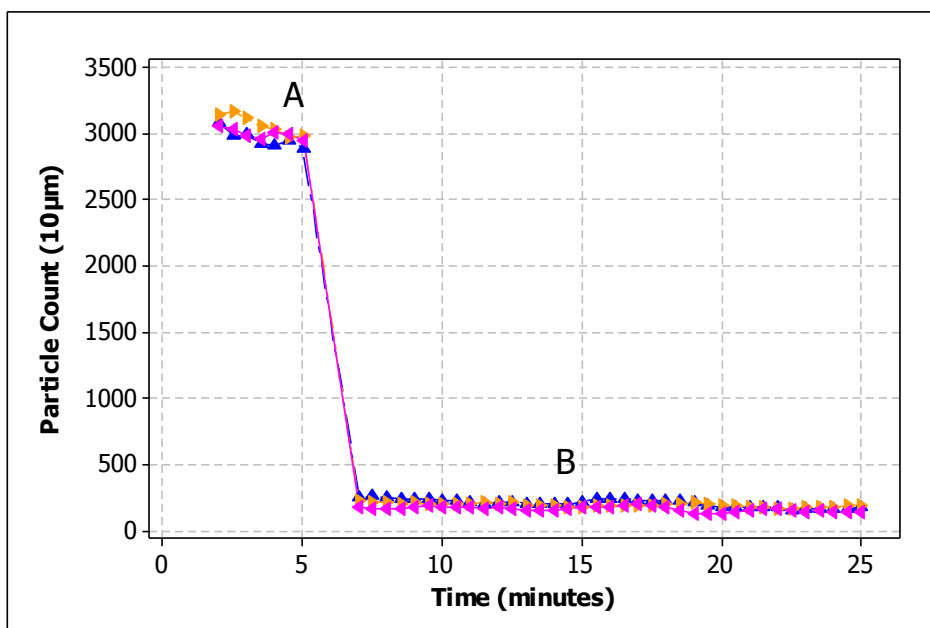


Figure 216 Plot showing (A) $\geq 10\mu\text{m}$ particle counts over 5 minutes with 3 separate aliquots of $10\mu\text{m}$ polystyrene reference particles in the particulate test equipment, and (B) after the standards were drained from the equipment and replaced with LPW.

Figure 215 shows that the particle count from the devices drops off gradually over time. The mechanisms underlying this gradual decrease in particle count may be any one of the following processes:

- 1) Swelling.
- 2) Particle break-up, e.g. from agglomerates to smaller particles
- 3) Particle dissolution.
- 4) Change of refractive index as they absorb water.
- 5) Change in particle shape.
- 6) Settling out of heavy particles and as particles interact with the surfaces of the equipment.
- 7) Floatation of light particles the top of the water.

The equipment is designed to minimize particle settling by maintaining continuous agitation, however this will not prevent the other processes occurring. Therefore the test methods are controlled within specific time intervals to ensure that all test articles are tested at the same time; this is required to make meaningful comparisons between test groups and as a means to carry out trending and quality control of the devices.

Appendix 1

To further investigate that the draining, cleaning and blanking between measurements does not remove unaccounted for particles an additional experiment was conducted. Testing was conducted on 20 SDS devices from the same finished goods lot. Two arms to the experiment were carried out, with 10 devices tested per arm as follows:

- 1) The devices were tested with inter-step measurements followed by cleaning and blanking for tracking (measurement 1), deployment (measurement 2) and retraction (measurement 3).
- 2) The devices were tested without cleaning and blanking between the tracking, deployment and retraction. Just one measurement was taken after retraction.

The sum from measurement 1, 2 and 3 from arm 1 were compared to the results for the single measurement of arm 2. The results of the experiment, (Figure 217 to Figure 219), show equivalent particle counts in both study arms. Thus, no additional particles are removed from the devices in situ during the draining, cleaning and blanking steps.

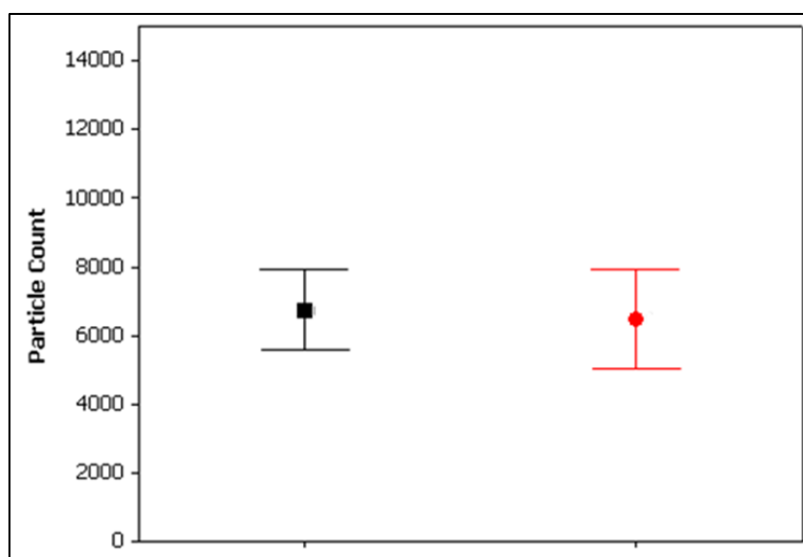


Figure 217 Plot showing particulate counts $\geq 10\mu\text{m}$ from arm 1 (in black) and arm 2 (in red). Arm 1 results were collected when the devices were tested with inter-step measurements (arm 1, in black) followed by cleaning and blanking for tracking (measurement 1), deployment (measurement 2) and retraction (measurement 3). Arm 2 results were collected when the devices were tested without cleaning and blanking between the tracking, deployment and retraction. Just one measurement was taken after retraction.

Appendix 1

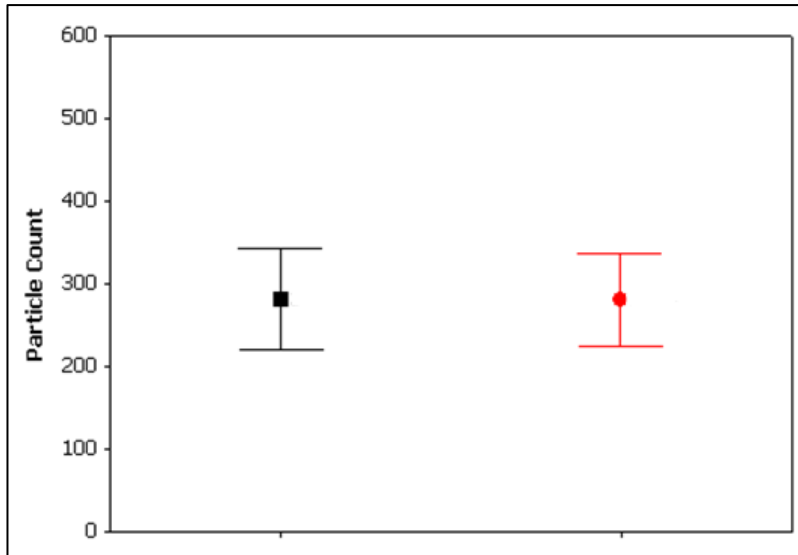


Figure 218 Plot showing particulate counts $\geq 25\mu\text{m}$ from arm 1 (in black) and arm 2 (in red). Arm 1 results were collected when the devices were tested with inter-step measurements (arm 1, in black) followed by cleaning and blanking for tracking (measurement 1), deployment (measurement 2) and retraction (measurement 3). Arm 2 results were collected when the devices were tested without cleaning and blanking between the tracking, deployment and retraction. Just one measurement was taken after retraction.

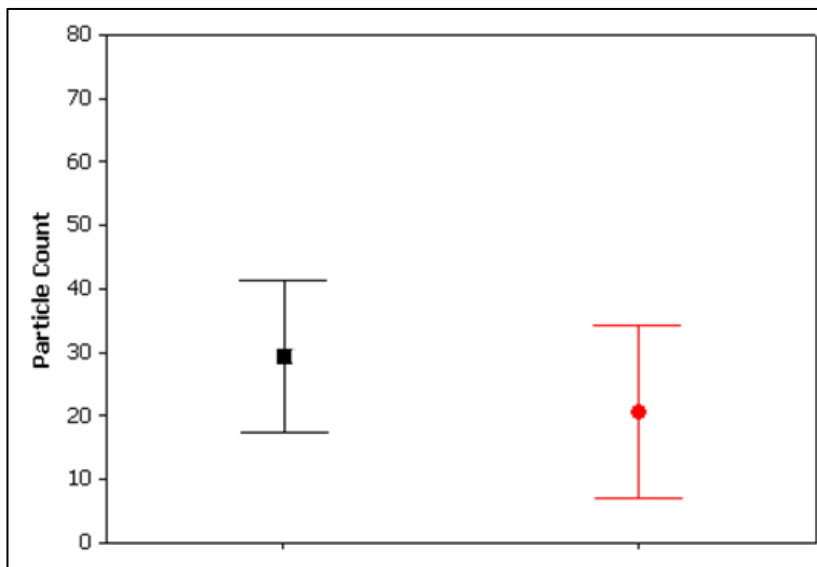


Figure 219 Plot showing particulate counts $\geq 50\mu\text{m}$ from arm 1 (in black) and arm 2 (in red). Arm 1 results were collected when the devices were tested with inter-step measurements (arm 1, in black) followed by cleaning and blanking for tracking (measurement 1), deployment (measurement 2) and retraction (measurement 3). Arm 2 results were collected when the devices were tested without cleaning and blanking between the tracking, deployment and retraction. Just one measurement was taken after retraction.

7.10 Impact of flowing water over the device

The CLP test method differs from the beaker methods because the water is continually circulating over the device, or ‘washing’ it. Circulating water continuously is a necessary feature for the CLP test as it transports the sample to the detector, suspends particles, and homogenises the test solution. However the question has to be asked; does flow impact on observed particulate load? To resolve this question 5 devices each from 2 batches were tracked with a flow rate of 140 mL/min and compared in Figure 220 to 5 devices from the same batches that were tracked without flow. The particle counts are equivalent with flow and without; this indicates that flow has negligible effect on the final particle count. This is consistent with the data discussed in section 7.9, where it was shown to no further particles are removed from devices during blanking with the device in situ.

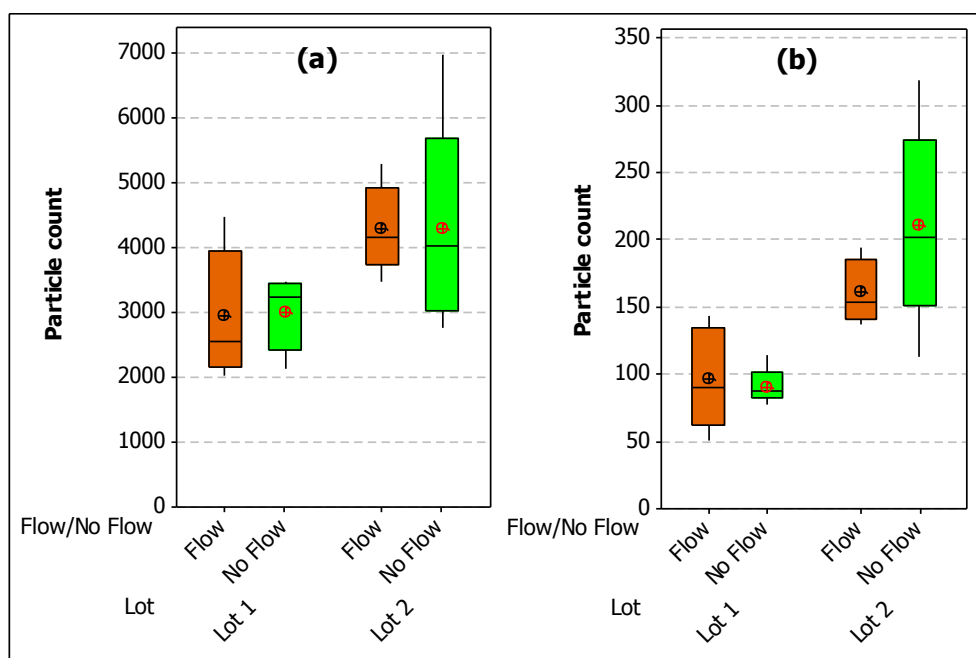


Figure 220 (a) $\geq 10 \mu\text{m}$ and (b) $\geq 25 \mu\text{m}$ particle counts from 2 batches of devices tracked with a flow rate of 140 mL/min compared to 5 devices from the same batches that were tracked without flow.

7.11 Length of SDS tested and challenged

A study was devised to determine if the number of particles removed from SDSs has a linear relationship to the length of the device tested. Three (3) devices from 2 batches were incrementally introduced to the CLP apparatus fitted with a straight glass

Appendix 1

capillary, (track (e) Figure 205). Particle counts were obtained at 6 points during stent delivery based upon the length of the device that was inserted; beginning with the addition of the balloon and stent, and then 260, 525, 715, 935 and 1,025 mm increments of the remainder of the catheter. Figure 221 provides an image of these 6 sections on the catheter. The data, shown in Figure 222, shows a linear increase in particle count with incremental introduction to the straight capillary between 260 and 1,025 mm. Interestingly the rate of increase is equivalent for the two lots of product tested with slopes of 0.35 and 0.37, for batches 1 and 2 respectively. However the regression lines do not pass through the origin, with the y-intercept equal to 375 and 117 particles for lot 1 and 2 respectively, this indicates that the distal 260mm of the device contributes more particles than an equivalent length proximal to this.



Figure 221 Image of a SDS indicating the different portions of the catheter that were incrementally tested for particulate matter.

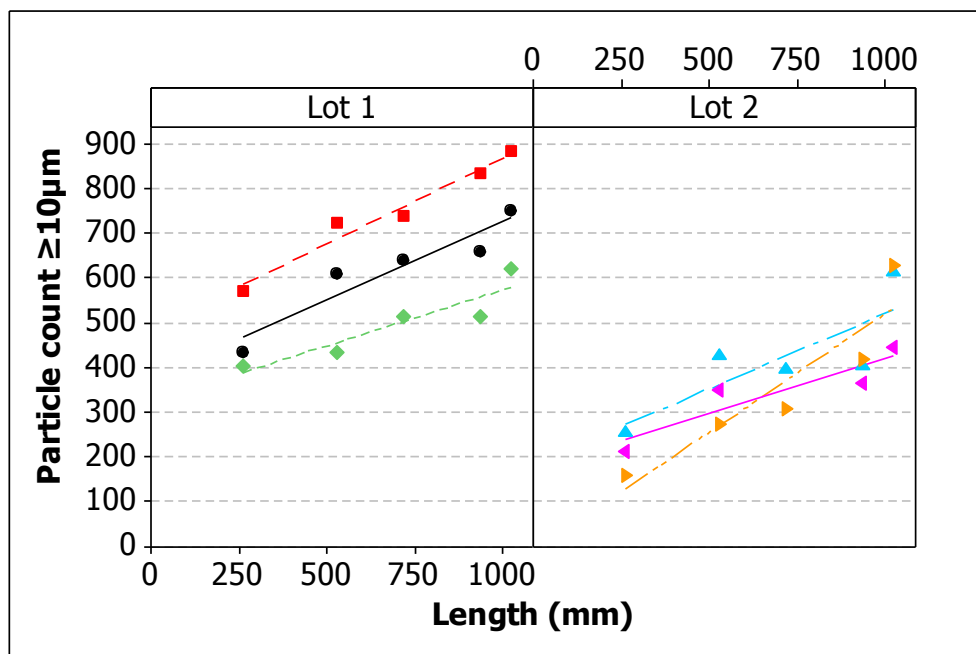


Figure 222. Plots of the $\geq 10 \mu\text{m}$ particle count from two batches of SDS devices showing a linear increase in particle count with incremental introduction to the straight capillary between 260 and 1,025mm.

The particle counts from tracking devices through a straight capillary were in turn compared to devices from the same batches that were tracked through a more

Appendix 1

challenging serpentine track model, (track (a) in Figure 205). Particle counts were taken prior to tracking the devices through the curved section of the track model at 715 mm and then after the devices had been advanced through the serpentine curves at 1,025 mm; (Figure 223). The difference due to tracking is made apparent when compared to devices tracked through a curved section. More particles are produced as a result of the challenging curves (4 - 6 times).

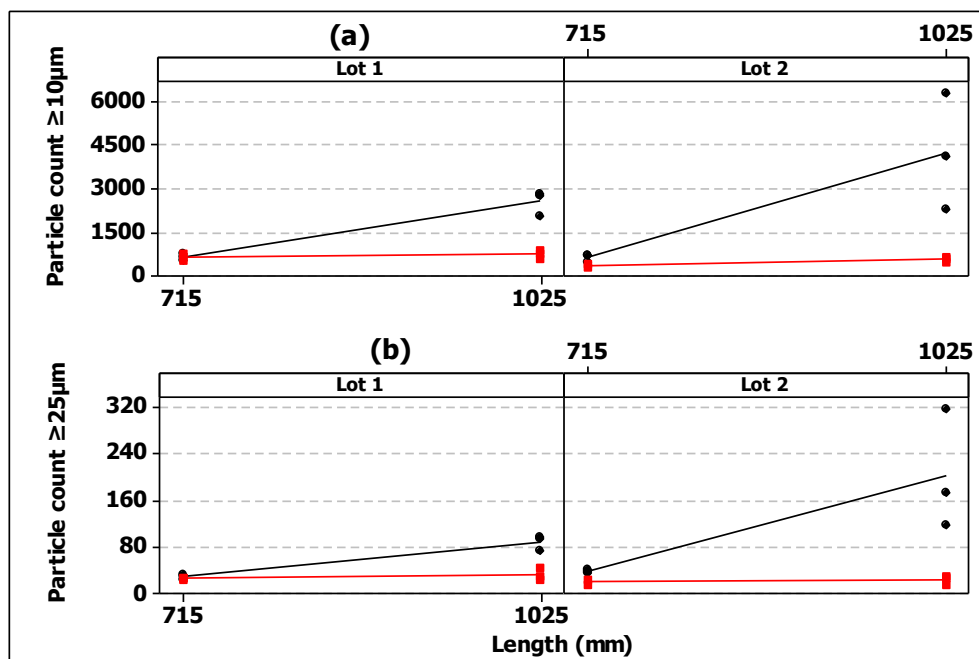


Figure 223 (a) $\geq 10 \mu\text{m}$ and (b) $\geq 25 \mu\text{m}$ particle counts taken (in red) prior to tracking devices through a curved section of the track model at 715 mm and then (in black) after the devices had been advanced through the serpentine curves to 1,025 mm.

7.12 Track material

The simulated use beaker method described in section 0, is carried out using a track model fabricated with PTFE tubing. However, borosilicate glass was selected for the CLP methods. PTFE has a lower coefficient of friction than glass, and as result it is easier to track SDS devices through PTFE than glass. To investigate if this difference in frictional force has any effect on particle counts, devices from the same batch were tracked through both materials. A PTFE track fixture was created for the CLP apparatus, the curvature of the track model was kept the same as the glass track model. Devices from 4 different batches were tracked in multiplate and the particle counts are provided in Figure 224.

Appendix 1

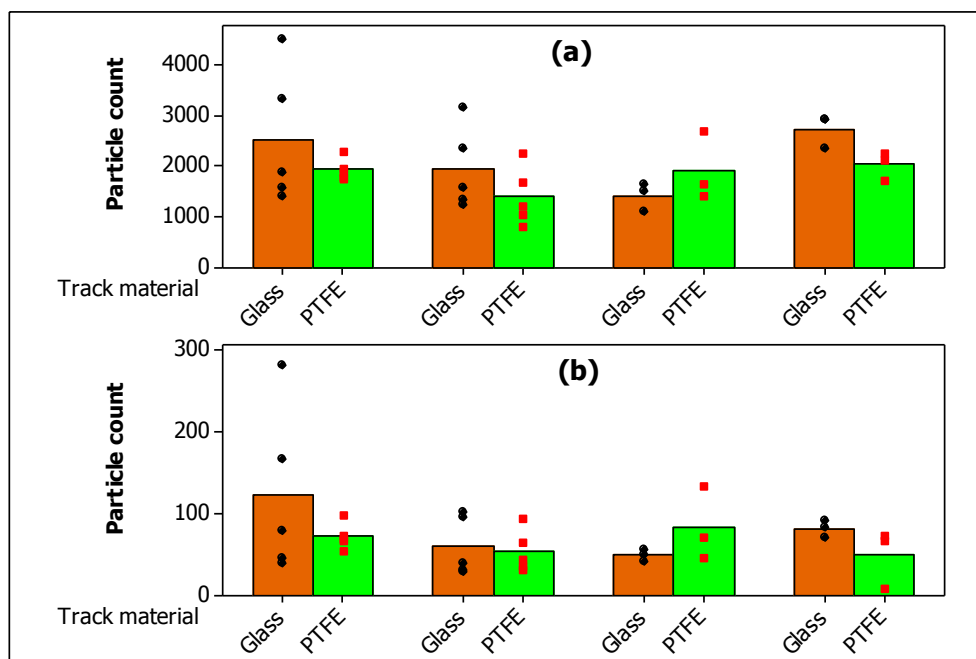


Figure 224 Comparison of (a) $\geq 10 \mu\text{m}$ and (b) $\geq 25 \mu\text{m}$ particle counts gathered using a PTFE model (in green) compared to a glass model (in orange) using 4 separate batches (lots) of SDS devices. The number of devices tested for Lot 1 and lot 2 was 5, and for Lot 3 and Lot 4 was 3 devices.

Of the 4 batches investigated, 3 displayed higher particulate levels after tracking through glass and 1 had higher particle levels after PTFE. The mean particle counts for both materials did not differ very significantly and remained within the range of individual measurements for all devices tested. The difference in particle count is likely due to unit to unit variation and not due to the material through which it is tracked.

7.13 Equipment design to deal with sources of measurement error in light obscuration

Common sources of measurement error that may contribute to additional particle counts when using LO fall into three categories[36]:

- 1) Air bubbles
- 2) Environmental contamination.
- 3) Non-water soluble liquids.

The CLP and DLP equipment has been designed to reduce the impact of the air bubbles and environmental contamination noise on particulate measurements. However it is not possible to remove the impact of non-water soluble liquids, such as silicone and other colloids. The standard approach to overcome non-water soluble liquids is to use the

Appendix 1

alternative particle enumeration method of light microscopy[36]. Procedural steps taken to reduce measurement error while executing tests have been detailed in the test method and associated work instructions.

7.13.1 Air bubbles

The LO detector used to count and size particulate matter cannot differentiate between air bubbles and other particulate matter [36], therefore it is important to mitigate against the introduction of air bubbles to the detector during the particulate test procedure. In general air bubbles can be formed in the following ways: by turbulent flow, cavitation in a flow of water through a tube, or they can be introduced by test devices. A number of design features in the equipment have been implemented to address air bubble generation by cavitation and turbulence. Introduction of air from test devices (catheters) has been addressed by describing preventative steps in the test procedures. Air bubbles that do form in the system are dissipated in the mixing chamber, where they travel to the top of the water in the mixing chamber and are expelled to the air.

The circulation loop of the DLP equipment operates at a relatively high flow rate of approximately 350 mL/min, this is required to keep large particles ($\geq 50 \mu\text{m}$) in suspension. In the circulation loop the water is pumped through a series of vessels that vary in internal diameter e.g. the 3.0 mm ASTM tortuous track transitions to the 8mm peristaltic pump tubing. If the flow of water moves from a vessel of small diameter to a vessel of larger diameter, bubbles may be formed.

It is suspected that the formation of bubbles is by cavitation, where bubbles form in a solution after a sudden decrease in pressure[122–124]. The pressure in a liquid decreases due to, for example, the contraction of the tube in which the liquid flows. When the pressure in the liquid decreases below its saturation pressure, vapour bubbles form and grow in the liquid. Such bubbles are called cavitation bubbles; refer to Figure 225 for a diagram of this effect. When the pressure in the liquid is above the saturation pressure, the bonds between the molecules in the liquid are strong. These strong bonds prevent the molecules from moving away from each other. Therefore, the liquid cannot vaporise. Decreased pressure in the liquid increases the mean distances between the molecules and this weakens the intermolecular bonds. When the pressure decreases below the saturation pressure, the thermal motion of the molecules breaks these bonds.

Appendix 1

As a result, some volumes of the liquid change into vapour, creating cavitation bubbles. This effect is readily observed when the flow rate of the water is increased through the circulation loop, which increases the pressure drop at transitions in vessel diameters. The air bubbles will manifest themselves when the particle count from a previously blanked system steadily increases over time.

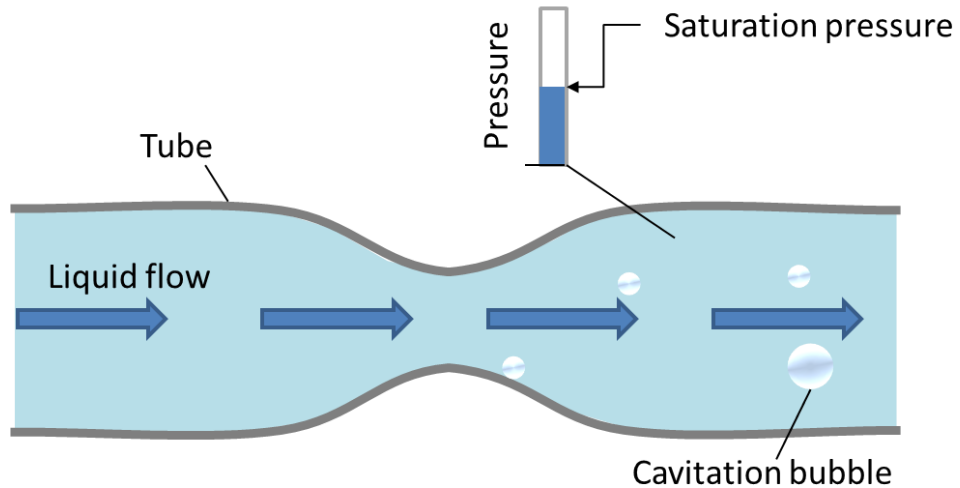


Figure 225 Formation of cavitation bubbles in a flowing liquid downstream from a point of constriction in a tube.

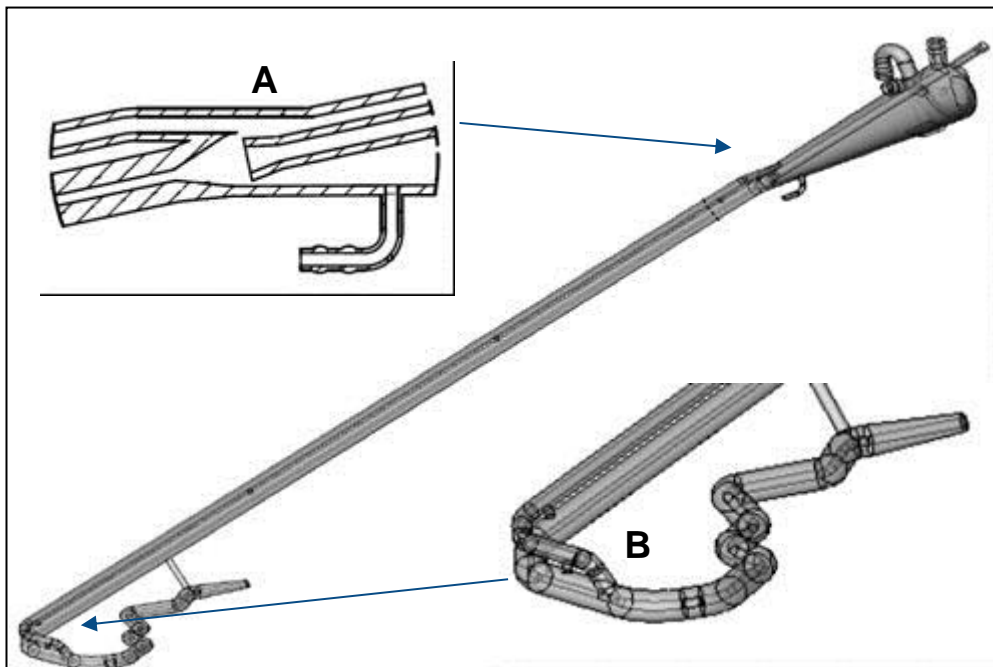


Figure 226 Twin capillary bifurcation designed to reduce bubble formation. (A) The flow is split between 2 capillaries on leaving the mixing chamber, one capillary is used to track the SDS device, it is necessary that this capillary has a maximum diameter of 3.0 mm to provide support for the SDS and prevent it from kinking. (B) The capillaries are recombined at the aortic arch of the track model, at this point the tracking capillary is widened to 3.5mm for the coronary artery model in accordance with FDA guidance [10].

Appendix 1

Cavitation bubble formation has been suppressed in the DLP equipment by designing a bifurcation to divide the water flow around constrictions and by tapering the transition in diameter over a long section of tubing to gradually decrease the pressure. Figure 226 illustrates the division in flow used on a test sample fixture.

7.13.2 Environmental contamination

The introduction of particulate matter from the environment is a possible source of additional particles that may add to sample counts. In order to reduce the contribution of environmental contamination the following controls are implemented:

- 1) The test equipment is housed in a laminar airflow hood that uses HEPA filtered air to maintain a particle free environment for the test.
- 2) The test equipment is a closed system with only two small access points open to the environment for addition of devices and reference particles. The small size of these openings limits the risk of extraneous particles making their way into the test equipment.
- 3) Thorough cleaning routines for the equipment are provided for analysts in controlled procedure documents.
- 4) Prior to each measurement the level of particulate matter is measured in the water to establish if the equipment is clean. No more than 10 particles $\geq 10 \mu\text{m}$ are allowed per 10 mL of water, and no more than 2 particles $\geq 25 \mu\text{m}$ are allowed per 10 mL of water.

These steps ensure that the test equipment and its environment do not introduce excessive particles to the sample measurements.